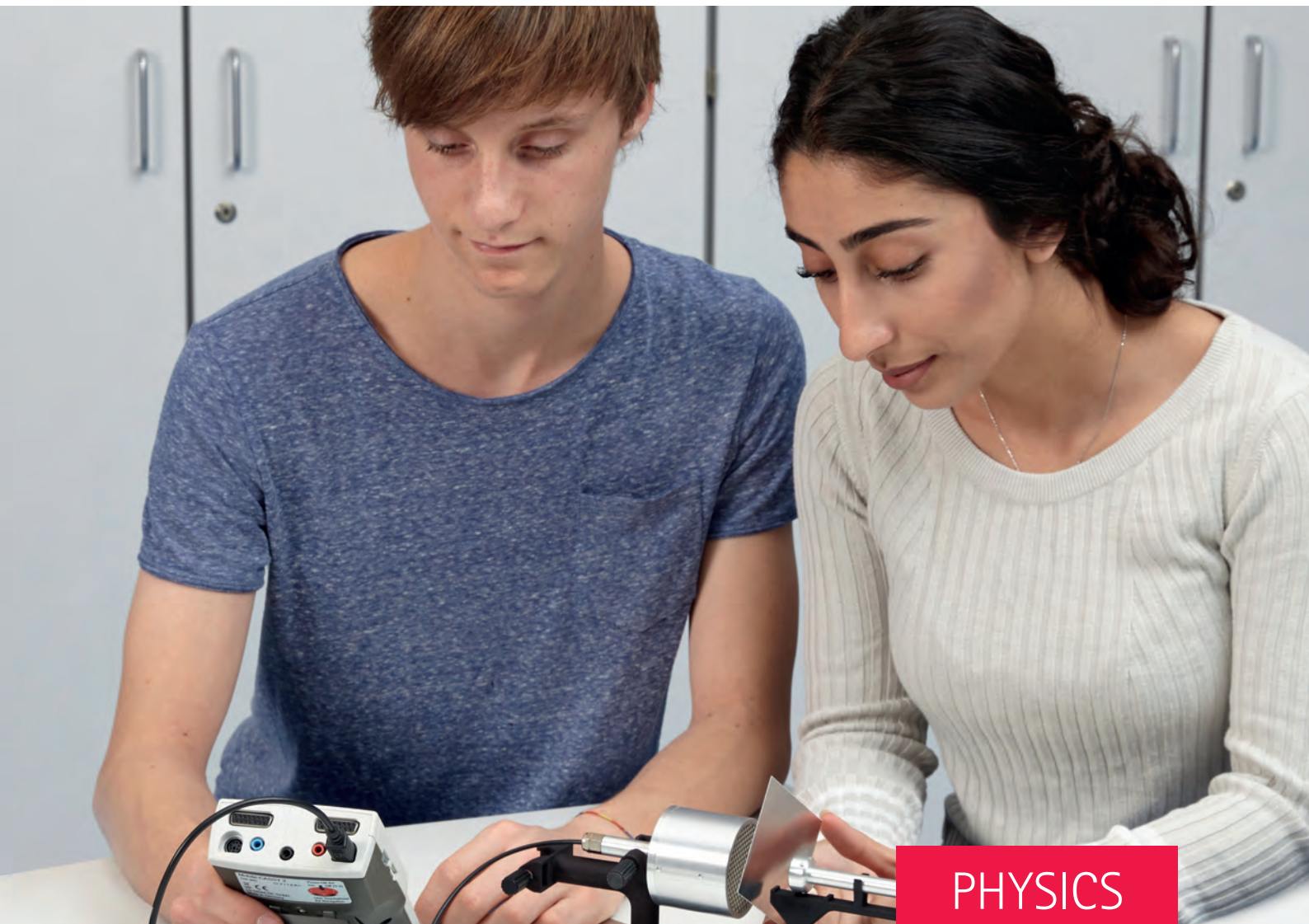# LEYBOLD®

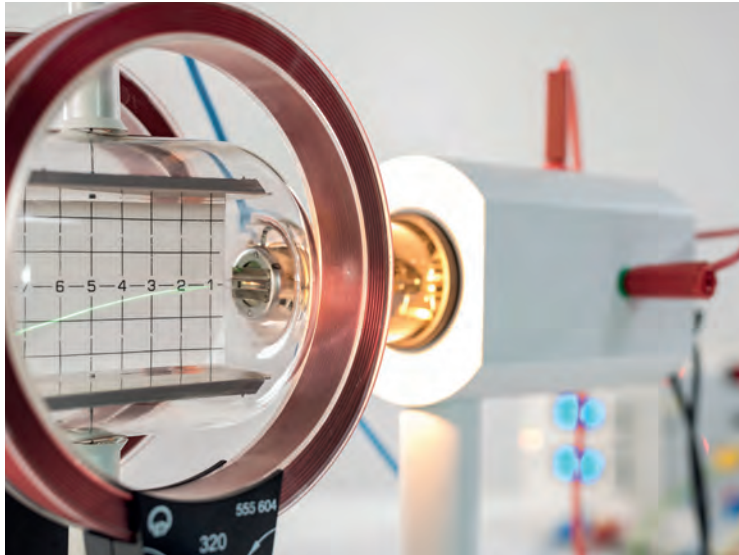## PHYSICS EXPERIMENTS

- ■ MECHANICS
- ■ HEAT
- ■ ELECTRICITY
- ■ ELECTRONICS
- ■ OPTICS
- ■ ATOMIC AND NUCLEAR PHYSICS
- ■ SOLID-STATE PHYSICS

LD DIDACTIC

PHYSICS EXPERIMENTS
IN TRUSTED LEYBOLD QUALITY

Experiments have become an indispensable part of education. Indispensable because the combination of theoretical knowledge with experimental learning sessions ensures sustainable and successful learning.

We provide a wide range of high-quality experiments from all areas of physics. Our proven LEYBOLD quality guarantees durability and safety during the complete experiment setup.

MORE THAN
500 EXPERIMENTS
IN VARIOUS
PHYSICS RANGES
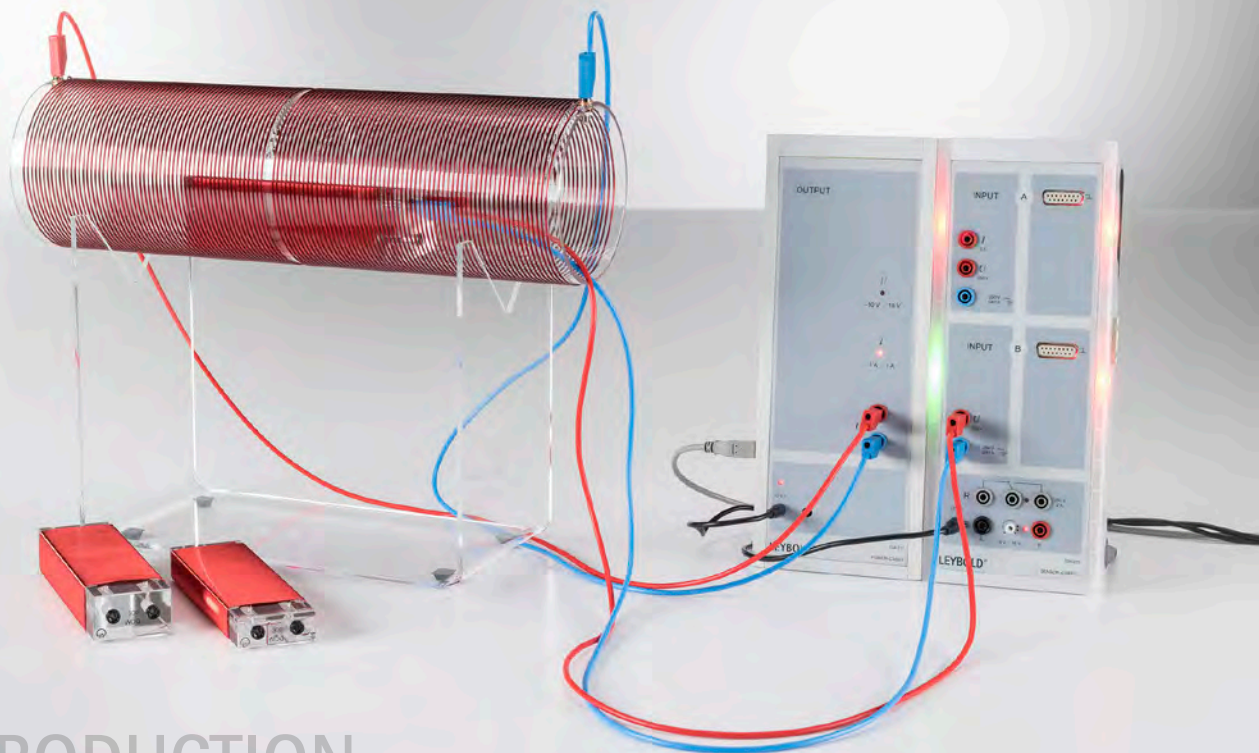
These are available in several versions (e.g. with or without PC support) which can be adapted to the time requirements and student's level of knowledge. The experiments are supported by instructions, which include clear step by step guidance, sample measurements and safety advices.

We will advise you personally and demonstrate our experiments for you.

Have fun experimenting!

FURTHER EXPERIMENTS
ARE AVAILABLE AT
OUR WEBSITE UNDER
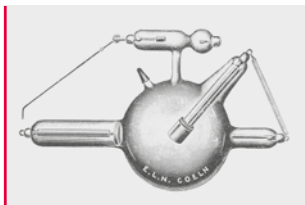
WWW.LEYBOLD-SHOP.COM

INTRODUCTION

EXPERIMENTS

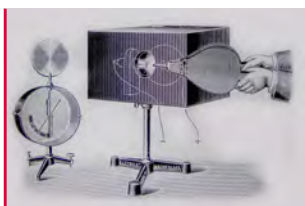LEYBOLD®

LD DIDACTIC GROUP
EXPERIMENTATION IS OUR PASSION

TRADITION AND INNOVATION

1896

1929

1968

1980

2004

X-ray apparatus

EXPERIMENTS FOR STUDENTS AND DEMONSTRATION FOR MORE THAN 170 YEARS

THE SECRET OF SUCCESS IS THE MIX OF THEORY & PRACTICE

Experimentation has always been a core competence of scientists and ensures to really understand physic phenomena.

The planning, carrying out and recording of experiments is an important element of a well-founded education in science. In order to reinforce newly acquired knowledge, experiments must be well matched to the theory.

A COMPETITIVE ADVANTAGE IN A HIGHLY COMPETITIVE WORLD

We believe in the importance of education as a fundamental driver of personal, national and global development. In a highly specialized world, knowledge has become a decisive factor: Skilled personnel are in greater demand than ever. Investing in the practical training of your students, you equip them with important science skills that the labor market requires.

THE PASSION FOR TEACHING EQUIPMENT IS IN OUR DNA

The LD DIDACTIC Group is a leading global manufacturer of high quality teaching and training system. From the very beginning in 1850 we at LEYBOLD concentrate on how to make academic content understandable and tangible for students at different levels of education. Therefore we are proud that for generations our training and educational systems have made a significant contribution to knowledge transfer in natural sciences.

However, for more than 170 years of experience we have found that you can achieve a lot when keeping pace with customer needs: we continuously challenge ourselves to preserve our high quality standards and develop our products and services in line with changing curricula and new technologies.

2021

LEYBOLD®

THE X-RAY APPARATUS – ALWAYS STATE OF THE ART
A perfect example for the spirit of innovation at LD DIDACTIC

Already one year after the discovery of the X-rays LD DIDACTIC offered the first equipment for this new topic of physics. During the time, the device was improved in handling, performance and safety. The newest generation supplies even digital teaching such as fully digital imaging techniques as well as live data distribution to the mobile devices of the students during the experiment.

LD DIDACTIC
THE BETTER CHOICE

Over 100,000 schools, colleges & universities in more than 80 countries trust our solutions, including top universities such as Harvard, Oxford, Cambridge, Stanford, Yale, Toronto, Tsinghua & Singapore.

YOU BENEFIT
170 YEARS EXPERIENCE, BASED ON EDUCATION SYSTEM IN GERMANY

YOU RECEIVE
INDIVIDUAL END-TO-END SOLUTION

YOU PROVIDE
RELEVANT AND EASY-TO-USE SOLUTIONS TO STUDENTS

YOU GAIN
KNOWLEDGE (CURRICULUM CONSULTING, LECTURER TRAINING)

YOU REALIZE
SUCCESSFUL AND SUSTAINABLE LEARNING OUTCOMES

YOU ENSURE
FUTURE-READY WITH INNOVATIONS (DIGITAL EDUCATION)

YOU GET PREMIUM QUALITY
YOU GET ...

YOU GET ...

GERMAN ENGINEERING

- Developed and designed in Germany
- Quality management certified to ISO 9001
- Highly specialized development team with didactic background

RELIABLE AND REWARDING

- Robust materials and stable constructions, worlwide recognized
- Great return on investment and carefree due to long lifetime
- Real life components for a true insight into future work
- Modular system allows replenishment of single items
- Easy to maintain materials (e.g. cleaning)
- Responsibly produced products

PERFECT FOR STUDENTS

- Composition of the experiment set-ups are perfectly matched
- Students can set up and conduct experiments independently
- Sturdy, easy to use and secure for students hands
- Tried and tested in everyday life in schools, colleges and universities

PHYSICS EXPERIMENTS
HIGHLIGHTS

Explore more than 500 experiment set-ups ready-to-use and covering all relevant topics within the world of Physics. Developed in close cooperation with teachers, professors and students around the world, the collection matches all international curricular and can be used for bachelor and master courses.

All experiment set-ups are special tailor-made compilations including all necessary equipment, state-of-the-art measurement technology and software. Within our broad experiment spectrum there are some that are special and unique.

MECHANICS
AERO- AND HYDRODYNAMICS

WIND TUNNEL
P1.8.7.4

- Powerful device in a reasonable size for teaching lab
- Motivation by application (e.g. airplane wing)
- Suitable for models made in a 3D printer

PAGE 56

HEAT
HEAT TRANSFER

THERMAL CONDUCTIVITY
P2.2.1.2

- Learning thermal conductivity at everday situation of house insulation
- Different measurement techniques in comparison
- Students have the possibilities to design their own materials and test it on their insulation qualities

PAGE 62

ELECTRICITY
ELECTROMAGNETIC OSCILLATIONS AND WAVES

DECIMETER WAVE SYSTEM
P3.7.2.2

- Macroscopic experience of wave phenomena of electromagnetic waves
- Polarization and change of wavelength in different dieletrics
- Application of data transmission

PAGE 119

ATOMIC AND NUCLEAR PHYSICS
NUCLEAR PHYSICS

RUTHERFORD SCATTERING
P6.5.2.1

- Didactic set-up, e.g. direct measurement of counting rate versus scattering scale
- Simple and safe handling
- Instruction sheet with detailed sample measurement results
- Crucial experiment in understand matter

PAGE 223

SOLID-STATE PHYSICS
CONDUCTION PHENOMENA
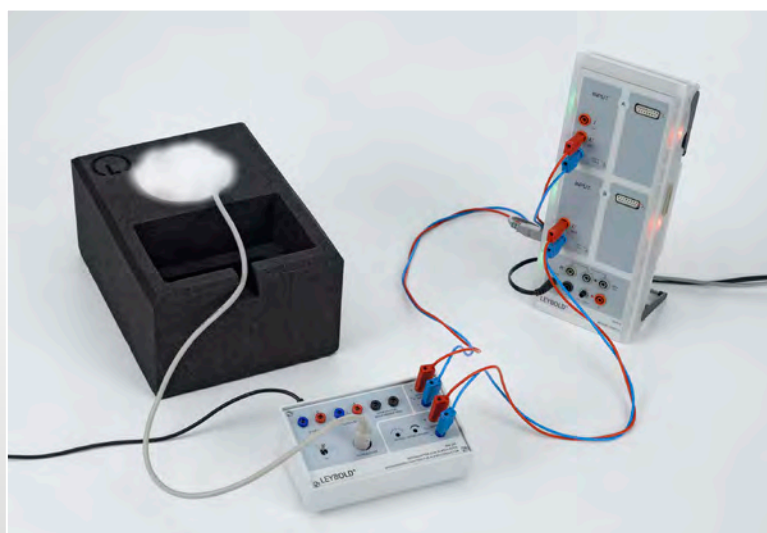
SUPERCONDUCTIVITY
P7.2.6.1

- Simple set-up for examination of the superconductivity and the Curie temperature
- Easy handling: just add liquid nitrogen and start measuring
- Compatible to nearly all interface systems

PAGE 242

LEYBOLD®

LEYBOLD X-RAY SYSTEM

SAFE X-RAY APPARATUS WITH TUBE CHANGING TECHNOLOGY

TOTALLY 100 % SAFE

The LEYBOLD X-ray system sets new standards and offers incredible options in students education in its 6th generation starting back in 1896.

- German institutional approved safety for usage at schools and universities
- Wide range of applications based on 6 different exchangeable tubes, e.g. iron, silver and gold
- Amazing resolution and intensity
- Individual configuration to your needs due to the modular structure
- Intuitive, clear operation with the "One button – one function" principle
- Built-in large LED display and extra scintillation screen
- Large volume tomography possible (8 x 8 x 8 cm)

BASIC EQUIPMENT

X-RAY APPARATUS

The X-ray apparatus is available in two variants - as a basic apparatus or as a complete apparatus with a Mo tube, goniometer and NaCl monocrystal. If you wish to use other tubes, the X-ray basic apparatus is the most flexible solution.

You can extend the X-ray apparatus with a drawer for your accessories irrespective of this.

GONIOMETER

No matter whether you are interested in Bragg spectra, X-ray energy spectra or computed tomography, you will be happy with the precision and high resolution of the goniometer.

TUBES

In addition to the Mo tube, there are other tubes, which are more suitable for special areas of application, e.g. Cu tube for Debye-Scherrer diagrams, Ag tube for X-ray fluorescence due to its high energy K-lines, W or Au tubes for radiation and computed tomography due to their high intensity.

SOFTWARE

CASSY LAB 2 FOR X-RAY APPARATUS

CASSY Lab 2 is enabling comprehensive measurements and the display of diagrams like Bragg spectra.

The software also enables live distribution of the spectra during measurements to digital devices of students. Free formulas for arbitrary conversions of the recorded spectra, the support of the high resolution of the HD Accessory, X-ray and the integrated help functionality with experiment examples are just some outstanding features of CASSY Lab 2.
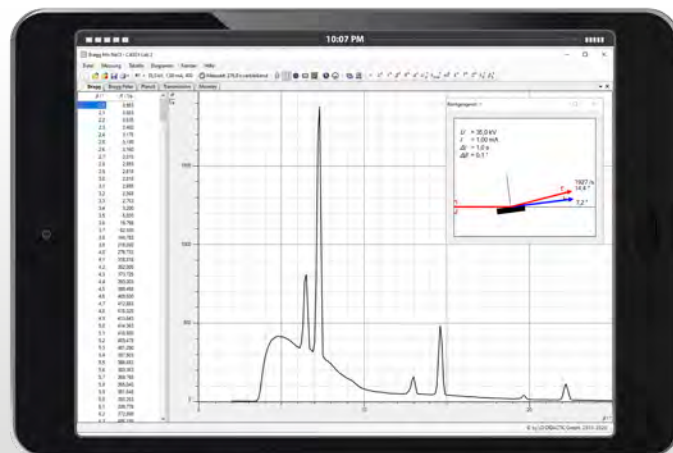
X-RAY ENERGY DETECTOR

The X-ray energy detector exposes energy-dispersive X-ray spectra with the CASSY system. Using the X-ray energy spectra, various chemical elements can be easily distinguished by means of their characteristic X-ray radiation and their mass fraction can also be determined. This also confirms the Compton effect.

COMPUTED TOMOGRAPHY MODULE

The X-ray apparatus has a laterally installed fluorescent screen, on which X-rays can be seen directly. The computed tomography module captures this visible X-ray image and the software provided there controls the rotation of the object in the X-ray apparatus through 360° and carries out the back projection of the X-ray image for the real-time 3D reconstruction.

BRAGG SPECTRA

With the complete apparatus with a Mo tube, you have everything you need for capturing your first Bragg spectrum. Other available monocrystals and/or X-ray tubes offer several possible variations.

COMPUTED TOMOGRAPHY PRO

If the resolution of the computed tomography module is insufficient, the X-ray image sensor provides the solution with its megapixel resolution and its 14-bit grey scale. With this, voxel resolutions up to an edge length of below 50 µm are possible. The X-ray image sensor also provides a comfortable and fast solution for Laue and Deybe-Scherrer diagrams.
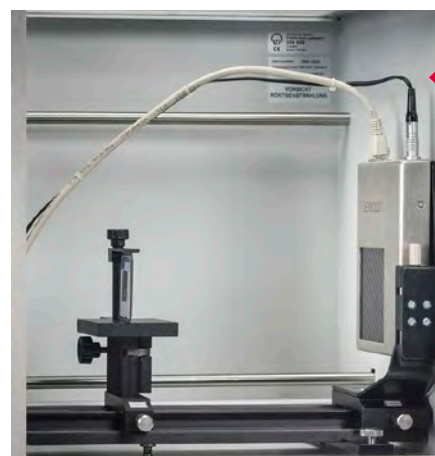
HD accessory

With the HD accessory consisting of a collimator and counter tube holder with narrow gaps and a new, high-resolution software, the angular resolution of the goniometer increases to 0.01°. Bragg spectra with a 4-fold resolution are possible with this.
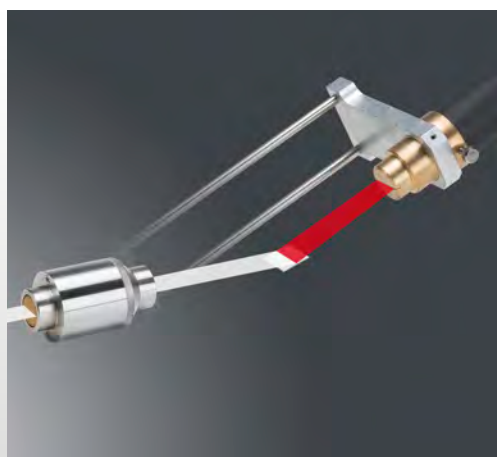
GOLD TUBE

The gold tube is the LEYBOLD tube with the highest intensity. It is particularly suitable for capturing X-ray images, Laue diagrams or computed tomograms.
In addition to the Tungsten tube, it is also the only tube whose Bragg spectra consist of L-lines.

LEYLAB

ONLINE-PORTAL FOR ORGANIZATION & MANAGEMENT OF EXPERIMENTS, DEVICES AND LITERATURE

LEYLAB

- Complete online portal
- Central organization & management of experiments and devices
- No installation needed
- For all platforms, tablets, smartphones, laptops or PCs
- Video tutorials included
- Access at anytime from anywhere

ANYTIME & ANYWHERE
EXPERIMENT COLLECTION

- Access to the whole LD experiments catalog with all the relevant information for every experiment
- Find desired experiment quickly and reliably
- Set-up own experiment collection
- Easily expand the LD experiments
- Easily create own, new experiments
- Intelligently link devices
- Additional documents are where you need them for the experiment
- Collection of all kinds of documents like PDFs, videos or links to websites or apps; can be shared with students
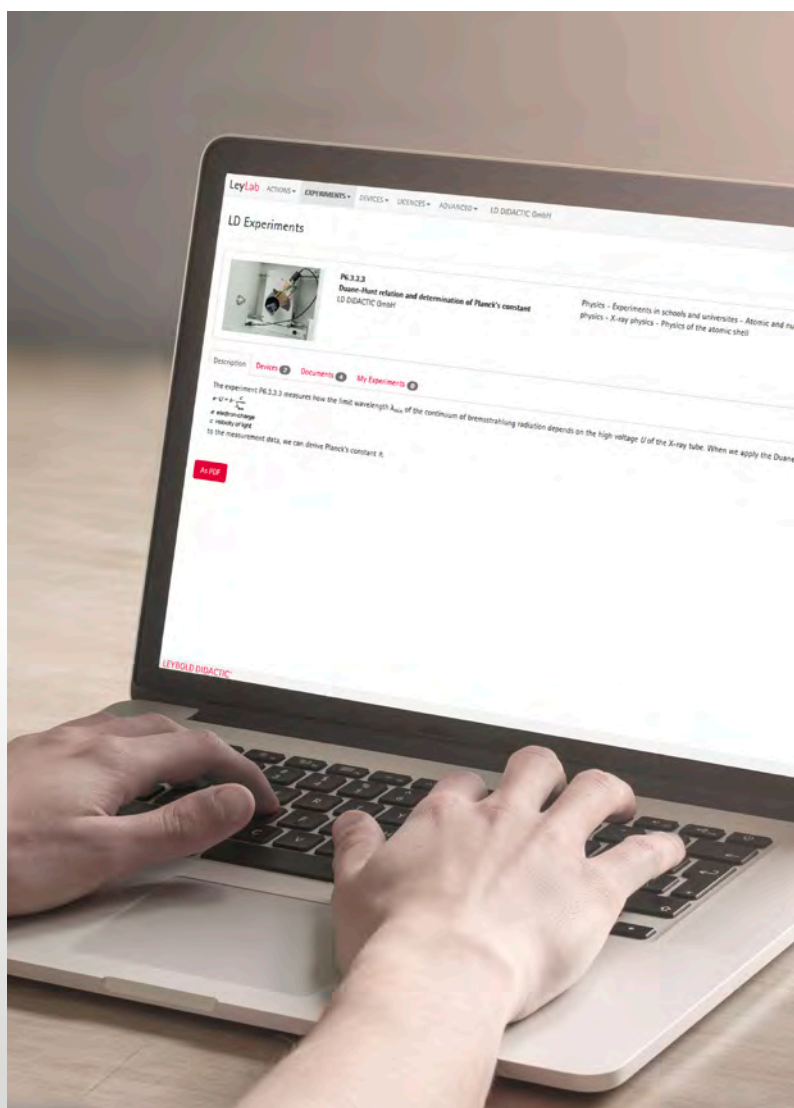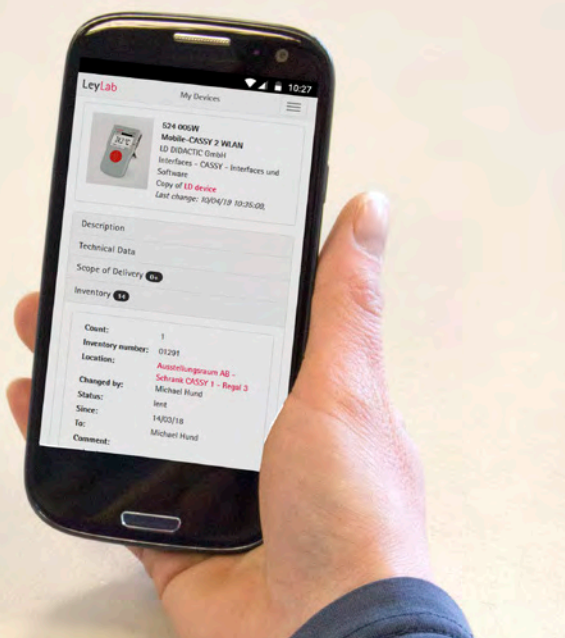
INVENTORY AT A GLANCE
DEVICE COLLECTION

- Direct overview of all available devices including quantity and storage location
- Save time searching for equipment
- Detailed information on every item
- Easy inventory of the complete collection
  - *LD devices and other manufacturers' devices*
  - *With bar code functionality*
- Clear inventory management with borrowing and return function

CENTRALLY AVAILABLE
LITERATURE

- Purchased LD literature will be visible at related experiment
- Can be easily shared with all students
- Own experiment instructions can be included

ALL IN ONE PLACE
LICENSE MANAGEMENT

- Manage all LD software and literature
- License codes are safely stored in the cloud, so they are not lost and can be used to install software on new hardware

SHARE INFORMATION
GUEST ACCESS & COLLABORATION

- Third party access to LeyLab is possible
- Collaborate with colleagues
- User administration with different access levels
- Share information with other lecturers from other institutes
- Enables a centralized organisation (e.g. by ministry) of many institutes and therefore a more efficient use of equipment, documents, etc.)
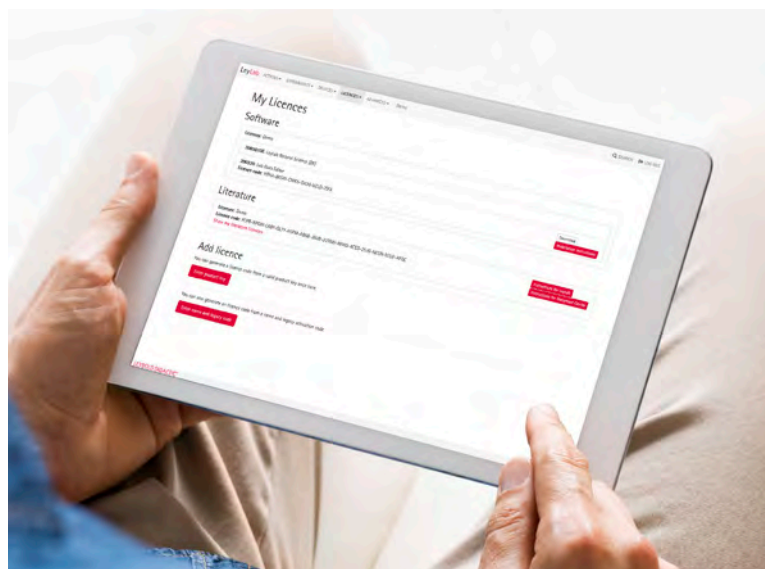
LEYLAB – ONLINE PORTAL

- School/college/university license
- For any number of users
- Unlimited inventory of devices & experiments
- Account can be deleted completely at any time
- Numerous experiment instructions are additionally available

200 310	LeyLab (License code)

http:www.leybold-shop.com/200310

EXPERIMENT INSTRUCTIONS
PERFECT SUPPORT FOR YOU AND YOUR STUDENTS

Our experiment instructions are easy to use, to distribute and to integrate into your teaching. They are tailored to requirements, curriculum-compliant and intuitive.

TIME-SAVING
PREPARATION

- LeyLab contains all purchased LD experiment instructions, can be accessed from anywhere
- All information is available directly on the experiment - literature, needed devices and location, extra information
- List of conductable experiments with existing devices can be downloaded
- Experiment instructions contains detailed accompanying information with experiment objectives, evaluation and further information
- Easy sharing of experiment instruction
- Free-of-charge online updates of experiment instructions in LeyLab
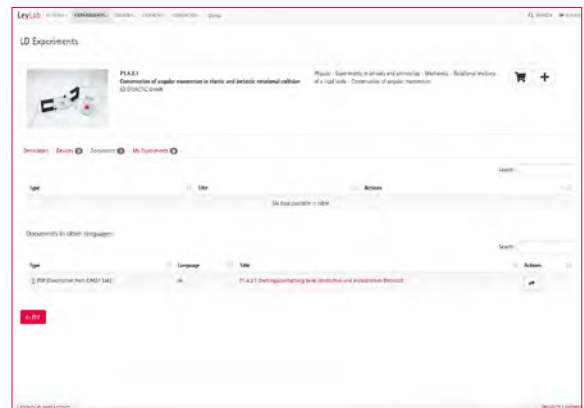
EASY-TO-USE AND FUNCTIONAL
EXPERIMENTING

- Clearly structured worksheets with hints and illustrations
- Step-by-step guide to perform experiment and warning notices for safe experimentation
- Real example measurement results and diagrams for students own monitoring

DISTRIBUTION

- Share experiment instruction in LeyLab with all students
- Via QR code on-site or online classes
- Via link per e-mail, learning platforms or online classes
- Via PDF file per e-Mail, learning platforms or online classes

EXPERIMENT INSTRUCTIONS

Experiment descriptions from all areas of physics for advanced secondary level or for practical exercises in colleges and universities.

- Product key for online use in LeyLab
- Complete package of all experiment instructions within this catalog

| 597 310 | LIT: Physics leaflets, digital (product key) |

http:www.leybold-shop.com/597310

LAB DOCS EDITOR
CREATE YOUR OWN DIGITAL EXPERIMENT INSTRUCTIONS

Lab Docs Editor is an easy-to-use tool that revolutionizes the editing of experiment instructions. Without any knowledge of HTML, the Lab Docs Editor allows the creation of digital and interactive experiment instructions.

- Create instruction & assignments; integrate & adapt interactive diagrams and tables; add text and response fields
- Insert images, vector graphics, hyperlink, etc.
- Prepare and create material lists
- Create formulas in LaTeX syntax

| 200 320 | Lab Docs Editor |

http:www.leybold-shop.com/200320

CASSY – THE SYSTEM
DATA LOGGING & MEASUREMENT

BASIC UNITS
WITH OR WITHOUT PC
& WLAN OPTION

1.

$+$

SENSORS
FOR ALL
MEASURING TASKS

2.

$+$

SOFTWARE
DATA ACQUISITION,
ANALYZING & EVALUATION

3.

WITH WIFI
MOBILE-CASSY 2

*ALSO WITH
WIFI ADAPTER*
SENSOR-CASSY 2

POCKET-CASSY 2

- For all teaching & training situations and requirements
- Easy use
- Fast & precise recording of data acquisition
- Wide choice
- Libraries for MATLAB and LabVIEW available free of charge

- More than 50 CASSY sensors
- Compatible across the CASSY system
- Measurement data acquisition of more than 50 measured quantities
- Automatic detection
- Existing sensors can be integrated

- Intuitively usable, all-round user-friendly software
- Interpretation & evaluation of the measured values
- Integrated experiment examples or own configurations
- Saving and sharing of measured values

CASSY – ALWAYS THE RIGHT SOLUTION

Whether you want to record the measured data from the experiments with or without a computer, or even want to include tablets in your digital class, CASSY has been developed for every need and can be flexibly expanded. You will always find the right combination of measuring device, sensor and measuring software for your specific requirements.

Detailed information on CASSY sensors

ENTIRE EXPERIMENT SET-UPS WITH MATCHING MEASURING DEVICES, SENSORS AND SOFTWARE

For each experiment, the recommended CASSY device and sensor is included in the experiment set-up for ideal data logging of the specific experiment.

With our selection of the measuring equipment for each single experiment we make sure that the devices perfectly meet the requirements of the measurement ranges and the measurement accuracy with no overpowering. While designing and testing every experiment set-up, we furthermore include factors such as technical conditions and ease of use for students into consideration.

If you want to acquire several experiments for your laboratory, we will be happy to advise you on how to optimize the measuring system.

YOU GET EXPERIMENT SET-UPS THAT PERFECTLY WORK!

Basic device		No. of sensor sockets	No. of channels for simultaneous measurement	Inte-grated relais	Integrated ability to measure	Inte-grated display	Data storage in the unit	Computer interface	Supported sensor types	Software support
	Sensor-CASSY 2 (524 013)	2	4	YES	U, I	NO	NO	USB, WiFi adapter	CASSY sensors S	CASSY App CASSY Lab 2 MATLAB LabVIEW
	Mobile-CASSY 2 WiFi (524 005W)	2	3	NO	U, I, P, E & temperature	YES	YES	Integrated WiFi, USB, standalone	CASSY sensors S, CASSY sensors M	CASSY App CASSY Lab 2 MATLAB LabVIEW
	Pocket-CASSY 2 Bluetooth (524 018)	1	1	NO	NONE	NO	NO	Bluetooth, USB	CASSY sensors S	CASSY App CASSY Lab 2 MATLAB LabVIEW
	Universal measurement instrument physics (531 835)	1	1	NO	NONE	YES	NO	USB, standalone	-	CASSY Lab 2 MATLAB LabVIEW

CASSY LAB 2

PROVEN SOFTWARE FOR RECORDING & EVALUATING MEASUREMENT DATA FROM ALL CASSY DEVICES

- Supports all CASSY devices and sensors
- Including measurement server for the distribution of live measurements, table and diagram as well as measurement files on tablets or smartphones, etc.
- One licence for use on any number of PCs in a school, college or university
- Automatic detection and display of all CASSYs, sensors and sensor boxes
- Automatic loading of typical experiment parameters
- Operable experiment examples included

- Manual or automatic recording of measured values
- Measurement data can be displayed in the form of analog/digital instruments, tables and/or graphs (also simultaneously, with user-definable axis assignment)
- Powerful evaluation functions including various fits (straight line, parabola, hyperbola, exponential function, free fitting), integrals, diagram labelling, calculation of user-definable formulas, differentiation, integration, Fourier transforms
- Using a QR code, students can follow measurement directly on their smartphone/tablet and then evaluate the measured data

THE LD SOLUTION
MUCH MORE THAN HARDWARE

LD SOLUTION
DETAILED INDIVIDUAL OFFER

LD SOLUTION
CONSULTING

LD SOLUTION
FINANCE

LD SOLUTION
LECTURER ACADEMY TRAINING

LD SOLUTION
PRODUCTION AND QUALITY CONTROL

LD SOLUTION
AFTER SALES SUPPORT

LD SOLUTION
INSTALLATION AND TRAINING ON SITE

LD

SOLUTION OFFER

LEYBOLD DIDACTIC ACADEMY

THE PATH TO TEACHING EXCELLENCE

CUSTOMIZED

TRAINING PROGRAMS TO ENSURE SUSTAINABLE FACILITIES AND RESOURCES

LDA LEYBOLD DIDACTIC ACADEMY

- Specialized training programs for teachers, lecturers and trainers
- Methodological, didactic and technical training
- Content and training focus is chosen on requirements
- Practical work is central point, incl. whole process to perform experiments
- Organization & maintenance of equipment
- Seminar has external parts at well-known schools, universities and institutions
- Insights into German didactic standards and trends
- Comprehensive guides and seminar documentation
- Possibility to achieve qualification to train other teachers, lecturers or trainers

REFERENCE PROJECT MEXICO

The university **"Universidad Autónoma del Estado de Hidalgo"** achieved a higher educational level for teachers in implementing experiments in classes through practical lab work and theory. They also obtained sustainable know-how in lab management and the all related work flow processes.

The seminar took place in the labs at LEYBOLD, the University of Cologne and an extracurricular place of learning.

WWW.LD-DIDACTIC.COM

LEYBOLD®

XVII

HOW TO USE THIS CATALOG
STRUCTURE OF THE PAGE

Subject

Subsection

Topic
of experiment set-up(s)

Experiment(s)
Each experiment is identified by a P - for Physics - and a four-digit number

Picture
shows one experiment, number of experiment is placed in brackets

Short description
of the topic and experiment(s)

Recommended CASSY device
marked in red

Equipment list
of each experiment

Experiment results
or additional picture(s) of experiment set-up(s)

CASSY marking
to quickly recognize the integration of CASSY devices

MECHANICS
TRANSLATIONAL MOTIONS OF A MASS POINT

ONE-DIMENSIONAL MOTIONS ON THE LINEAR AIR TRACK

P1.3.3.4
Path-time and velocity-time diagrams of straight motion - Recording and evaluating with CASSY

P1.3.3.5
Uniformly accelerated motion with reversal of direction - Recording and evaluating with CASSY

P1.3.3.6
Kinetic energy of a uniformly accelerated mass - Recording and evaluating with CASSY

Path-time and velocity-time diagrams of straight motion - Recording and evaluating with CASSY (P1.3.3.4)

Cat. No.	Description	P1.3.3.4	P1.3.3.5	P1.3.3.6
337 501	Air track	1	1	1
337 53	Air supply	1	1	1
667 8231	Power controller	1	1	1
337 462	Combination light barrier	1	1	1
524 013	Sensor-CASSY 2	1	1	1
524 220	CASSY Lab 2	1	1	1
524 074	Timer S	1	1	1
501 16	Multi-core cable, 6-pole, 1.5 m	1	1	1
501 46	Connecting leads 19 A, 100 cm, red/blue, pair	1		
	additionally required: PC with Windows XP/Vista/7/8/10 (x86 or x64)	1	1	1

The advantage of studying linear translational motions on the linear air track is that interference factors such as frictional forces and moments of inertia of wheels do not occur.

The computer-assisted measurement system CASSY is particularly suitable for simultaneously measuring transit time t, path s, velocity v and acceleration o of a slider on the linear air track. The linear motion of the slider is transmitted to the motion sensing element by means of a lightly tensioned thread; the signals of the motion sensing element are matched to the CASSY measuring inputs by the Timer S. The PC supports significantly the evaluation of the measured data. Alternatively the measured data can be exported in table format to external data evaluation.

The object of the experiment P1.3.3.4 is to study uniform and uniformly accelerated motions on the horizontally aligned linear air track.

In the experiment P1.3.3.5 the patch, velocity and acceleration of a slider is record, which moves uphill on an inclined plane, then stops, moves downhill, reflected elastically at the lower end and oscillated several times back and forth.

The experiment P1.3.3.6 records the kinetic energy

$$E = \frac{m}{2} \cdot v^2$$

of a uniformly accelerated slider of the mass m as a function of the time and compares it with the work

$$W = F \cdot s$$

which the accelerating force F has performed. This verifies the relationship

$$E(t) = W(t)$$

Path-time, velocity-time and acceleration-time diagram (P1.3.3.4)

CASSY®

P1 MECHANICS

P1 MECHANICS

P.1.1.1.2

P.1.1.1.1

P.1.1.1.3

MEASURING LENGTHS

P1.1.1.1
Using a caliper gauge with vernier

P1.1.1.2
Using a micrometer screw

P1.1.1.3
Using a spherometer to determine bending radii
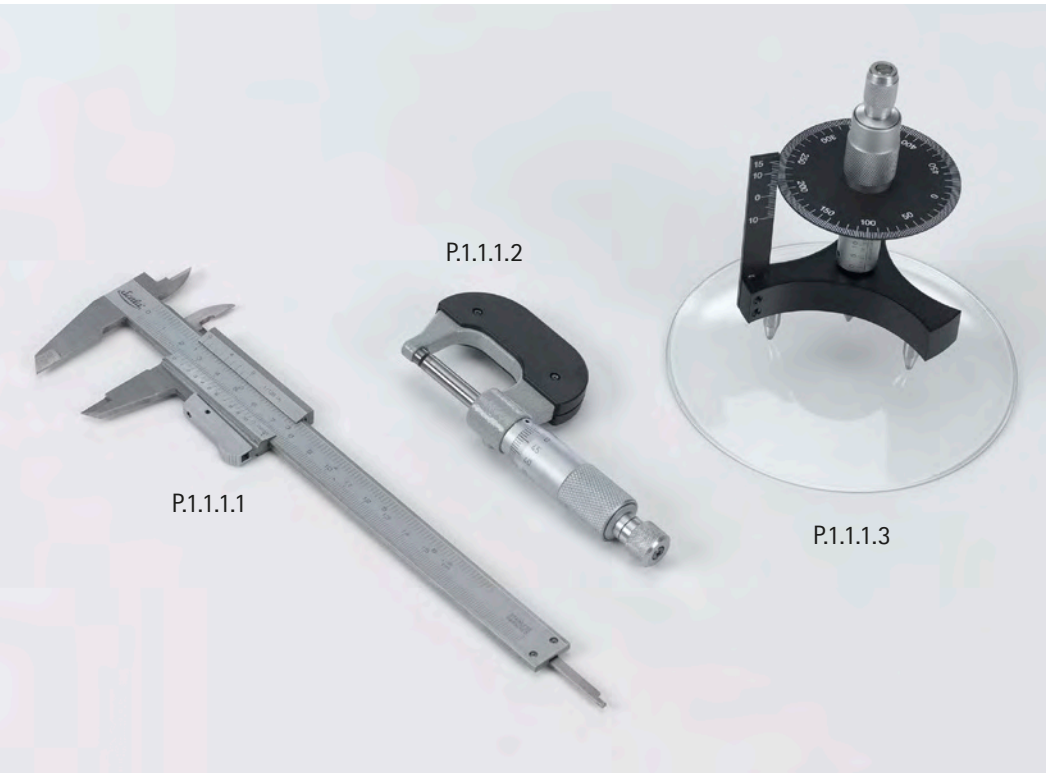
Using a spherometer to determine bending radii (P1.1.1.3)

Cat. No.	Description	P1.1.1.1	P1.1.1.2	P1.1.1.3
311 54	Precision vernier callipers	1		
311 83	Precision micrometer		1	
550 35	Copper resistance wire, 0.2 mm diam., 100 m		1	
550 39	Brass resistance wire, 0.5 mm diameter, 50 m		1	
311 86	Spherometer			1
460 291	Plane mirror, 11.5 cm x 10 cm			1
662 092	Cover slips			1
664 154	Watch glass dish 80 mm Ø			1
664 157	Watch glass dish 125 mm Ø			1

The caliper gauge, micrometer screw and spherometer are precision measuring instruments; their use is practiced in hands on measuring exercises.

In the experiment P1.1.1.1, the caliper gauge is used to determine the outer and inner dimensions of a test body. The vernier scale of the caliper gauge increases the reading accuracy to 1/20 mm.

Different wire gauges are measured in the experiment P1.1.1.2. In this exercise a fundamental difficulty of measuring becomes apparent, namely that the measuring process changes the measurement object. Particularly with soft wire, the measured results are too low because the wire is deformed by the measurement.

The experiment P1.1.1.3 determines the bending radii R of watch-glasses using a spherometer. These are derived on the basis of the convexity height h at a given distance r between the feet of the spherometer, using the formula

$$R = \frac{r^2}{2h} + \frac{h}{2}$$
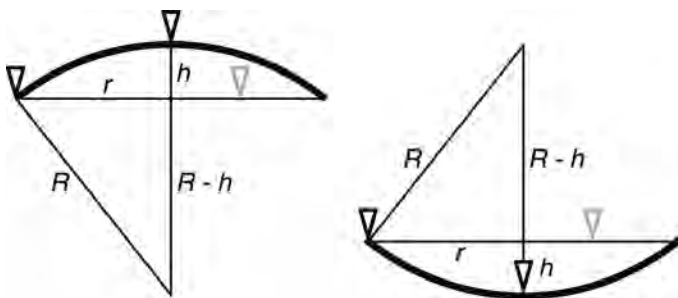
Vertical section through the measuring configuration with spherometer
Left: object with convex surface, Right: Object with concaves surface (P1.1.1.3)

MEASURING VOLUME AND DENSITY

P1.1.2.1
Determining the volume and density of solids

P1.1.2.2
Determining the density of liquids using the plumb bob

P1.1.2.3
Determining the density of liquids using the pycnometer according to Gay-Lussac

P1.1.2.4
Determining the density of air

Determining the density of air (P1.1.2.4)

Cat. No.	Description	P1.1.2.1	P1.1.2.2	P1.1.2.3	P1.1.2.4
362 04	Overflow vessel	1			
590 08	Measuring cylinder 100 ml	1			
590 06	Plastic beaker	1			
309 48	Fishing line	1			
311 54	Precision vernier callipers	1			
315 05	Single-pan suspension balance 311	1		1	1
352 52	Steel balls, 30 mm, set of 6	1			
361 63	Cubes (2x) and ball (1x)	1			
590 33	Gauge blocks, set of 2	1			
309 42	Colouring, red, 10 g	1			
362 025	Plumb bob		1		
315 011	Hydrostatic balance		1		
315 31	Set of weights, 10 mg to 200 g		1		
382 21	Stirring thermometer -10...+110 °C		1	1	
665 754	Measuring cylinder 100 ml, with plastic base		2	2	
671 9720	Ethanol, denaturated, 1 l		1	1	
666 145	Gay-Lussac pycnometer, 50 ml			1	
379 07	Sphere with 2 stopcocks, glass, 1 l				1
667 072	Support ring for round flask, 250 ml, cork				1
375 58	Hand vacuum pump				1

Depending on the respective aggregate state of a homogeneous substance, various methods are used to determine its density

$$\rho = \frac{m}{V}$$

m: mass, V: volume

The mass and volume of the substance are usually measured separately.

To determine the density of solid bodies, a weighting is combined with a volume measurement. The volumes of the bodies are determined from the volumes of liquid which they displace from an overflow vessel. In the experiment P1.1.2.1, this principle is tested using regular bodies for which the volumes can be easily calculated from their linear dimensions.

To determine the density of liquids, the plumb bob is used in the experiment P1.1.2.2. The measuring task is to determine the densities of water-ethanol mixtures. The Plumb bob determines the density from the buoyancy of a body of known volume in the test liquid.

To determine the density of liquids, the pyknometer according to Gay-Lussac is used in the experiment P1.1.2.3. The measuring task is to determine the densities of water-ethanol mixtures. The pyknometer is a pear-shaped bottle in which the liquid to be investigated is filled for weighing. The volume capacity of the pyknometer is determined by weighing with a liquid of known density (e.g. water).

In the experiment P1.1.2.4, the density of air is determined using a sphere of known volume with two stop-cocks. The weight of the enclosed air is determined by finding the difference between the overall weight of the air-filled sphere and the empty weight of the evacuated sphere.
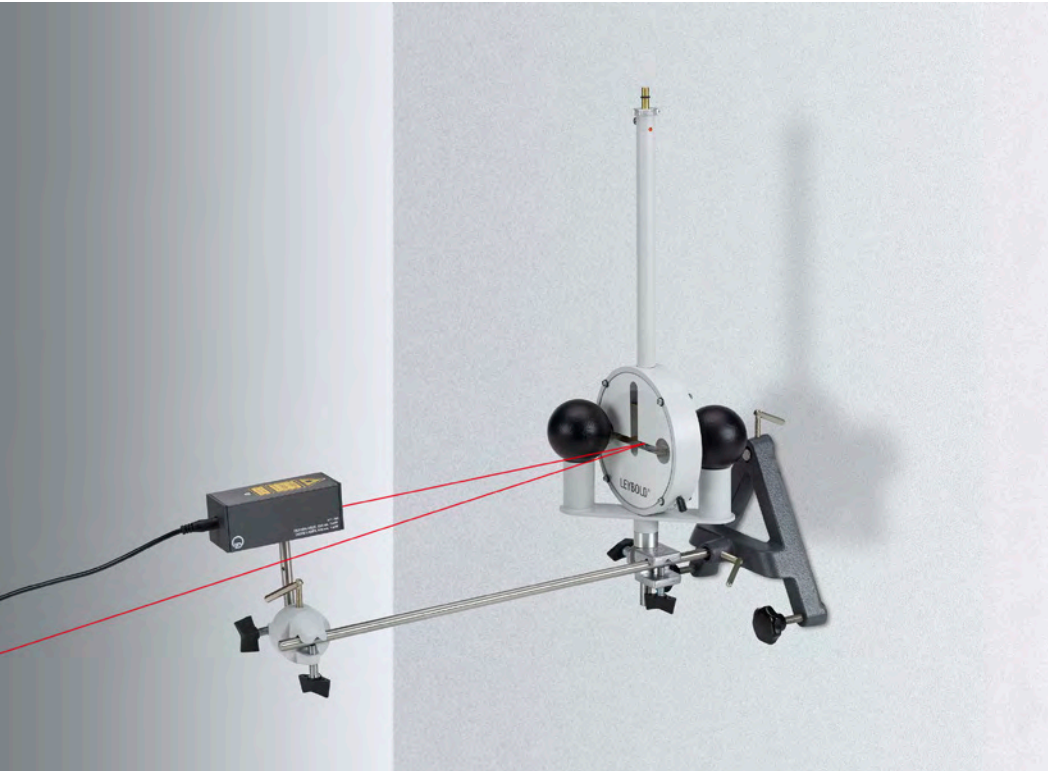
P1.1.3.1
Determining the gravitational constant with the gravitation torsion balance according to Cavendish - Measuring the excursion with a light pointer

P1.1.3.2
Determining the gravitational constant with the gravitation torsion balance according to Cavendish
- Recording the excursion and evaluating the measurement with the IR position detector and PC

Determining the gravitational constant with the gravitation torsion balance according to Cavendish - Measuring the excursion with a light pointer (P1.1.3.1)

Cat. No.	Description	P1.1.3.1	P1.1.3.2
332 101	Gravitation torsion balance	1	1
471 791	Diode laser, 635 nm, 1 mW	1	
313 27	Hand-held stop-watch, 60s/0.2s	1	
311 78	Tape measure 2 m / 1 mm	1	
300 02	Stand base, V-shaped, small	1	
301 03	Rotatable clamp	1	
301 01	Leybold multiclamp	1	
300 42	Stand rod, 47 cm, 12 mm diam.	1	
332 11	IR position detector		1
460 32	Optical bench with standardised profile, 1 m		1
460 373	Optics rider, 60/50		1
460 374	Optics rider, 90/50		1
300 41	Stand rod, 25 cm, 12 mm Ø		1
	additionally required: PC with Windows XP/Vista/7/8/10 (x86 or x64)		1
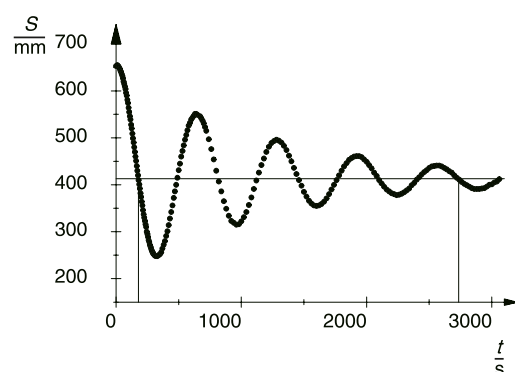
The heart of the gravitation torsion balance according to Cavendish is a light-weight beam horizontally suspended from a thin torsion band and having a lead ball with the mass m_2 = 15 g at each end. These balls are attracted by the two large lead spheres with the mass m_1 = 1.5 kg. Although the attractive force

$$F = G \cdot \frac{m_1 \cdot m_2}{r^2}$$

r: distance between sphere midpoints

is less than 10^{-9} N, it can be detected using the extremely sensitive torsion balance. The motion of the small lead balls is observed and measured using a light pointer. Using the curve over time of the motion, the mass m_1 and the geometry of the arrangement, it is possible to determine the gravitational constant G using either the end-deflection method or the acceleration method.

In the end-deflection method, a measurement error of less than 5 % can be achieved through careful experimenting. The gravitational force is calculated from the resting position of the elastically suspended small lead balls in the gravitational field of the large spheres and the righting moment of the torsion band. The righting moment is determined dynamically using the oscillation period of the torsion pendulum.

The acceleration method requires only about 1 min. observation time. The acceleration of the small balls by the gravitational force of the large spheres is measured, and the position of the balls as a function of time is registered.

In the experiment P1.1.3.1, the light pointer is a laser beam which is reflected in the concave reflector of the torsion balance onto a scale. Its position on the scale is measured manually point by point as a function of time.

The IR position detector (IRPD) enables automatic measurement of the motion of the lead balls in the gravitation torsion balance. The four IR diodes of the IRPD emit an infrared beam; the concave mirror on the torsion pendulum reflects this beam onto a row of 32 adjacent phototransistors. A microcontroller switches the four IR diodes on in sequence and then determines which phototransistor is illuminated each time. The primary S range of illumination is determined from the individual measurements. The IRPD is supplied complete with the demo version of CASSY Lab, for direct measurement and evaluation of the experiment P1.1.3.2 using a computer with Windows XP or higher. The system offers a choice of either the end-deflection or the acceleration method for measuring and evaluating.

Oscillations of the gravitation torsion balance around the final equilibrium position SII (P1.1.3.1)

STATIC EFFECTS OF FORCES

P1.2.1.1
Expansion of a helical spring

P1.2.1.2
Bending of a leaf spring

P1.2.1.1   P1.2.1.2

Expansion of a helical spring (P1.2.1.1)

Cat. No.	Description	P1.2.1.1	P1.2.1.2
352 07	Helical spring 10 N/m	1	
352 08	Helical spring 25 N/m	1	
340 85	Weights, each 50 g, set of 6	1	1
301 21	Stand base MF	2	2
301 27	Stand rod 50 cm, 10 mm Ø	2	2
301 26	Stand rod 25 cm, 10 mm Ø	1	1
301 25	Support block	1	
311 78	Tape measure 2 m / 1 mm	1	1
301 29	Pointer, pair	1	1
340 811	Plug-in axle	1	
352 051	Leaf spring		1
666 615	Universal bosshead		1
686 50	Metal plate		1
309 48	Fishing line		1

Forces can be recognized by their effects. Thus, static forces can e.g. deform a body. It becomes apparent that the deformation is proportional to the force acting on the body when this force is not too great.

The experiment P1.2.1.1 shows that the extension s of a helical spring is directly proportional to the force F_s. Hooke's law applies:

$$F_s = -D \cdot s$$

D: spring constant

The experiment P1.2.1.2 examines the bending of a leaf spring arrested at one end in response to a known force generated by hanging weights from the free end. Here too, the deflection is proportional to the force acting on the leaf spring.
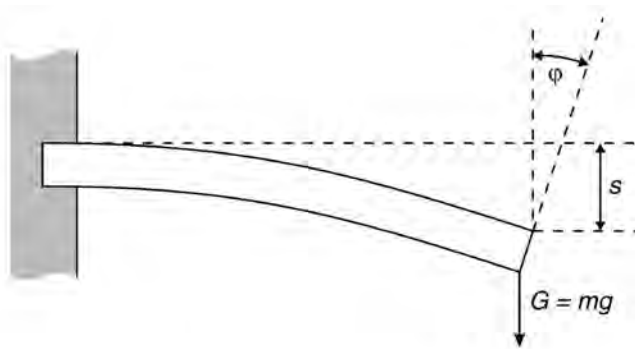
Schematic diagram of bending a leaf spring (P1.2.1.2)

Composition and resolution of forces (P1.2.2.1)

FORCE AS VECTOR

P1.2.2.1
Composition and resolution of forces
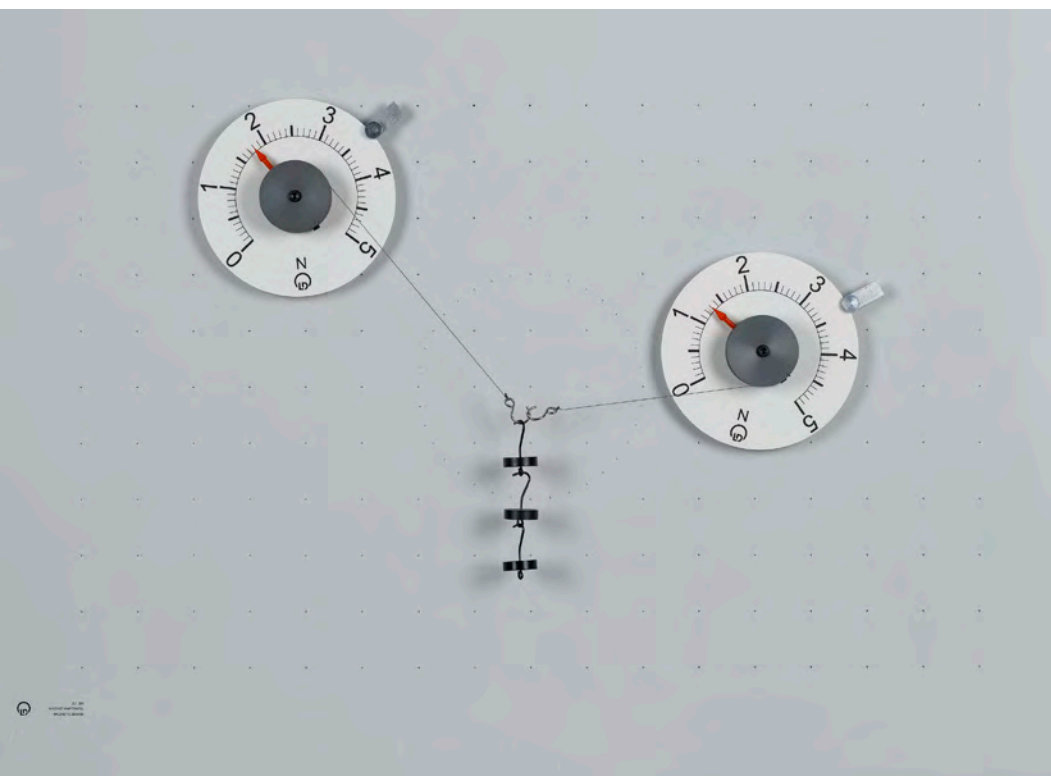
Cat. No.	Description	P1.2.2.1
301 301	Adhesive magnetic board	1
314 215	Circular dynamometer, 5 N	2
301 331	Magnetic base with hook	1
352 08	Helical spring 25 N/m	1
311 78	Tape measure 2 m / 1 mm	1
342 63	Weight 50 g	5
301 01	Leybold multiclamp	4
686 50	Metal plate	4
300 44	Stand rod, 100 cm, 12 mm diam.	2
301 07	Simple bench clamp	2

The nature of force as a vectorial quantity can be easily and clearly verified in experiments on the adhesive magnetic board. The point of application of all forces is positioned at the midpoint of the angular scale on the adhesive magnetic board, and all individual forces and the angles between them are measured. The underlying parallelogram of forces can be graphically displayed on the adhesive magnetic board to facilitate understanding.

In experiment P1.2.2.1, a force F is compensated by the spring force of two dynamometers arranged at angles α_1 and α_2 with respect to F. The component forces F_1 and F_2 are determined as a function of α_1 and α_2. This experiment verifies the relationships

$$F = F_1 \cdot \cos\alpha_1 + F_2 \cdot \cos\alpha_2$$

and

$$0 = F_1 \cdot \sin\alpha_1 + F_2 \cdot \sin\alpha_2$$
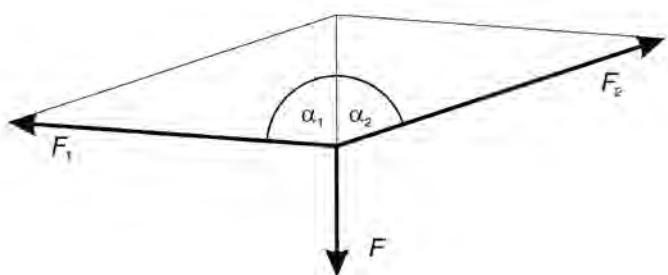
Parallelogram of forces (P1.2.2.1)

LEVER

P1.2.3.1
One-sided and two-sided lever

P1.2.3.2
Wheel and axle as a lever with unequal sides

Wheel and axle as a lever with unequal sides (P1.2.3.2)

Cat. No.	Description	P1.2.3.1	P1.2.3.2
342 60	Lever, 1 m	1	
342 63	Weight 50 g	12	8
314 45	Spring balance, 2 N	1	1
314 46	Spring balance, 5 N	1	1
300 02	Stand base, V-shaped, small	1	1
300 42	Stand rod, 47 cm, 12 mm diam.	1	1
301 01	Leybold multiclamp	1	1
342 75	Multiple pulley and moment disc		1

In physics, the law of levers forms the basis for all forms of mechanical transmission of force. This law can be explained using the higher-level concept of equilibrium of angular momentum.

The experiment P1.2.3.1 examines the law of levers:

$$F_1 \cdot x_1 = F_2 \cdot x_2$$

for one-sided and two-sided levers. The object is to determine the force F_1 which maintains a lever in equilibrium as a function of the load F_2, the load arm x_2 and the power arm x_1.

The experiment P1.2.3.2 explores the equilibrium of angular momentum using a wheel and axle. This experiment broadens the understanding of the concepts force, power arm and line of action, and explicitly proves that the absolute value of the angular momentum depends only on the force and the distance between the axis of rotation and the line of action.

One-sided and two-sided lever (P1.2.3.1)

BLOCK AND TACKLE

P1.2.4.1
Fixed pulley, loose pulley and block and tackle as simple machines

Fixed pulley, loose pulley and block and tackle as simple machines (P1.2.4.1)

Cat. No.	Description	P1.2.4.1
340 911	Pulley Ø 50 mm, plug-in	2
340 921	Pulley Ø 100 mm, plug-in	2
340 930	Pulley bridge	2
340 811	Plug-in axle	1
340 851	Weight, 50 g	4
340 87	Load hook	1
340 89	Coupling plug 4 mm	1
314 04	Support clip, for plugging in	2
314 01	Dynamometer, tension and compression, 1.5 N	1
314 02	Dynamometers, tension and compression, 3 N	1
311 78	Tape measure 2 m / 1 mm	1
301 29	Pointer, pair	1
686 51	Cord	1
667 017	Scissors 125 mm, round-ended	1
301 21	Stand base MF	2
301 25	Support block	2
666 615	Universal bosshead	1
301 26	Stand rod 25 cm, 10 mm Ø	1
301 27	Stand rod 50 cm, 10 mm Ø	2

The fixed pulley, loose pulley as well as block and tackle are classic examples of simple machines. Experiments with these machines represent the most accessible introduction to the concept of work in mechanics.

In the experiment P1.2.4.1, the experiments like block and tackle are set up on the lab bench using a stand base MF. The pulleys are mounted virtually friction-free in bearings.

MECHANICS
FORCES

INCLINED PLANE

P1.2.5.1
Inclined plane: force along the plane and force normal to the plane

P1.2.5.2
Determining the coefficient of static friction using the inclined plane
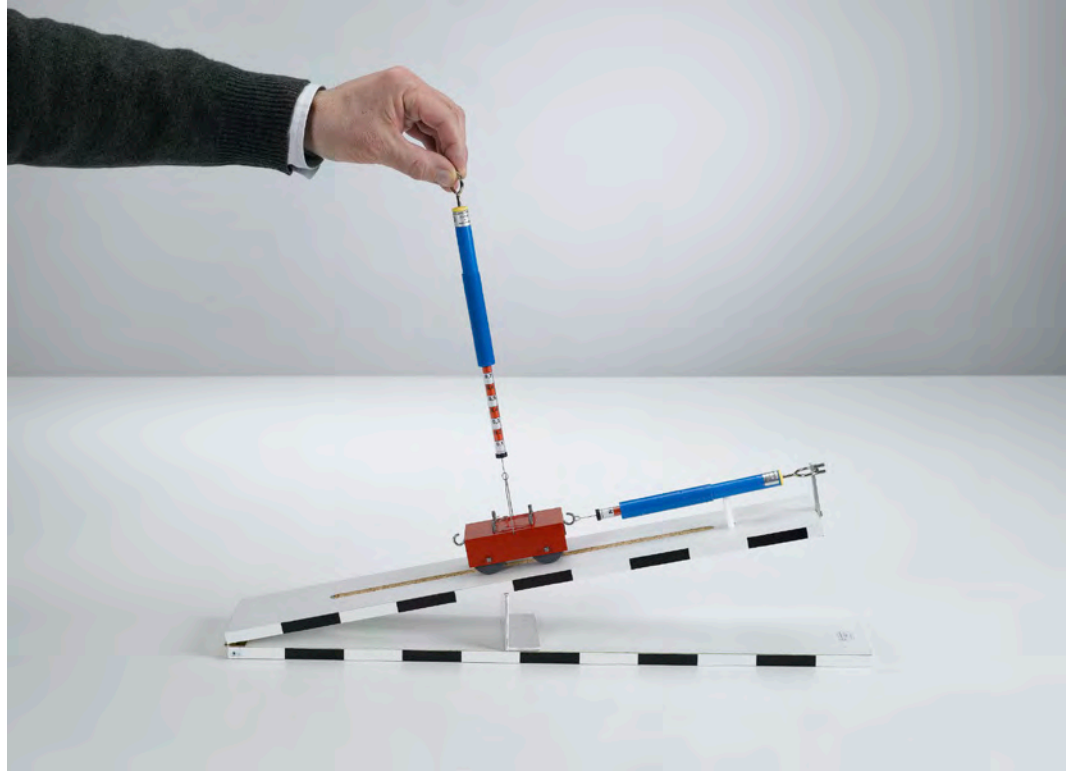
Inclined plane: force along the plane and force normal to the plane (P1.2.5.1)

Cat. No.	Description	P1.2.5.1	P1.2.5.2
341 21	Inclined plane	1	1
314 141	Precision dynamometer, 1 N	1	
342 10	Wooden blocks for friction experiments, pair		1
311 78	Tape measure 2 m / 1 mm		1

The motion of a body on an inclined plane can be described most easily when the force exerted by the weight G on the body is vectorially decomposed into a force F_1 along the plane and a force F_2 normal to the plane. The force along the plane acts parallel to a plane inclined at an angle α, and the force normal to the plane acts perpendicular to the plane. For the absolute values of the forces, we can say:

$$F_1 = G \cdot \sin\alpha \ \text{ and } \ F_2 = G \cdot \cos\alpha$$

This decomposition is verified in the experiment P1.2.5.1. Here, the two forces F_1 and F_2 are measured for various angles of inclination α using precision dynamometers.

The experiment P1.2.5.2 uses the dependency of the force normal to the plane on the angle of inclination for quantitative determination of the coefficient of static friction μ of a body. The inclination of a plane is increased until the body no longer adheres to the surface and begins to slide. From the equilibrium of the force along the plane and the coefficient of static friction

$$F_1 = \mu \cdot F_2 \ \text{ we can derive } \ \mu = \tan\alpha$$
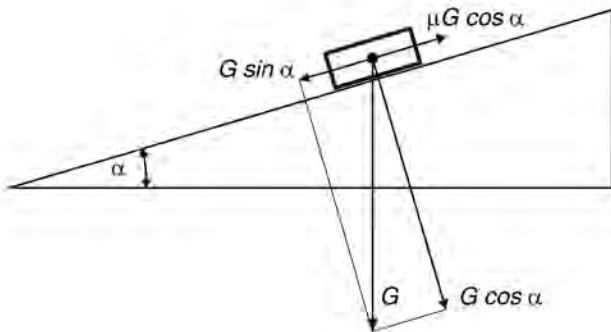
Calculating the coefficient of static friction (P1.2.5.2)

10 WWW.LD-DIDACTIC.COM

FRICTION

P1.2.6.1
Static friction, sliding friction and rolling friction

Static friction, sliding friction and rolling friction (P1.2.6.1)

Cat. No.	Description	P1.2.6.1
315 36	Set of weights, 0.1 kg to 2 kg	1
300 40	Stand rod, 10 cm, 12 mm diam.	6
314 47	Spring balance, 10 N	1
342 10	Wooden blocks for friction experiments, pair	1

In discussing friction between solid bodies, we distinguish between static friction, sliding friction and rolling friction. Static friction force is the minimum force required to set a body at rest on a solid base in motion. Analogously, sliding friction force is the force required to maintain a uniform motion of the body. Rolling friction force is the force which maintains the uniform motion of a body which rolls on another body.

To begin, the experiment P1.2.6.1 verifies that the static friction force F_H and the sliding friction force F_G are independent of the size of the contact surface and proportional to the resting force G on the base surface of the friction block. Thus, the following applies:

$$F_H = \mu_H \cdot G \quad \text{and} \quad F_G = \mu_G \cdot G$$

The coefficients μ_H and μ_G depend on the material of the friction surfaces. The following relationship always applies:

$$\mu_H > \mu_G$$

To distinguish between sliding and rolling friction, the friction block is placed on top of multiple stand rods laid parallel to each other. The rolling friction force F_R is measured as the force which maintains the friction block in a uniform motion on the rolling rods. The sliding friction force F_G is measured once more for comparison, whereby this time the friction block is pulled over the stand rods as a fixed base (direction of pull = direction of rod axes). This experiment confirms the relationship:

$$F_G > F_R$$
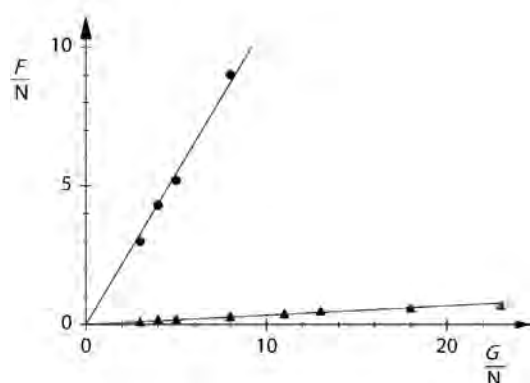
Comparison of sliding (point) and rolling friction (triangle) (P1.2.6.1)

LEYBOLD®

ONE–DIMENSIONAL MOTIONS ON FLETCHER'S TROLLEY

P1.3.2.1
Path-time diagram of straight motion - Recording the time with a counter

P1.3.2.2
Path-time diagram of straight motion - Recording and evaluating with CASSY

Path-time diagram of straight motion - Recording the time with a counter (P1.3.2.1)

Cat. No.	Description	P1.3.2.1	P1.3.2.2
337 130	Track, 1.5 m	1	1
337 110	Trolley	1	1
337 114	Additional weights, pair	1*	1*
315 411	Slotted mass hanger 10 g	1	1
315 417	Slotted weight 10 g	4	4
309 48	Fishing line	1	1
337 462	Combination light barrier	1	1
337 463	Holder for combination spoked wheel	1	
337 464	Combination spoked wheel	1	1
683 41	Holding magnet for track	1	1
336 25	Holding magnet adapter with a release mechanism	1	
575 471	Counter S	1	
501 16	Multi-core cable, 6-pole, 1.5 m	1	1
524 013	Sensor-CASSY 2		1
524 220	CASSY Lab 2		1
524 074	Timer S		1
501 46	Connecting leads 19 A, 100 cm, red/blue, pair		1
	additionally required: PC with Windows XP/Vista/7/8/10 (x86 or x64)		1

* additionally recommended

Fletcher's trolley is the classical experiment apparatus for investigating linear translational motions. The trolley has a ball bearing, his axles are spring-mounted and completely immersed in order to prevent being overloaded. The wheels are designed in such a way that the trolley centers itself on the track and friction at the wheel flanks is avoided.

Using extremely simple means, the experiment P1.3.2.1 makes the definition of the velocity v as the ratio of the path difference Δs and the corresponding time difference Δt directly accessible to the students. The path difference Δs is read off directly from a scale on the track. The electronic measurement of the time difference is started and stopped using a key and a light barrier. To enable investigation of uniformly accelerated motions, the trolley is connected to a thread which is laid over a pulley, allowing various weights to be suspended.

The experiment P1.3.2.2 looks at motion events which can be transmitted to the combination spoked wheel by means of a thin thread on Fletcher's trolley. The combination spoked wheel serves as an easy-running deflection pulley. The signals of the combination light barrier are recorded by the computer-assisted measuring system CASSY and converted to a path-time diagram. As this diagram is generated in real time while the experiment is running, the relationship between the motion and the diagram is extremely clear.
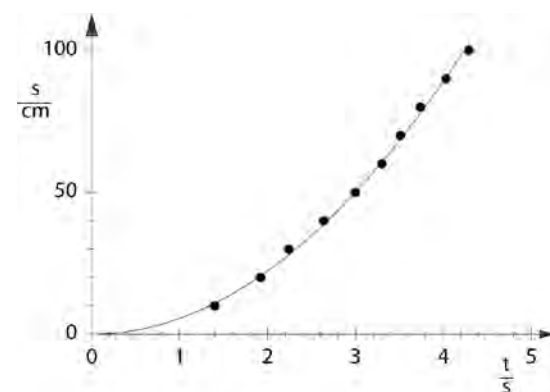
Path-time diagram of a linear motion (P1.3.2.1)

ONE–DIMENSIONAL MOTIONS ON FLETCHER'S TROLLEY

P1.3.2.5
Accelerated motions with an acceleration sensor

Accelerated motions with an acceleration sensor (P1.3.2.5)

Cat. No.	Description	P1.3.2.5
337 130	Track, 1.5 m	1
337 110	Trolley	1
337 114	Additional weights, pair	1
524 018	Pocket-CASSY 2 Bluetooth	1
524 019	Rechargeable battery for Pocket-CASSY 2 Bluetooth	1
524 0031	Bluetooth dongle	1
524 220	CASSY Lab 2	1
524 0424	3D acceleration sensor S	1
300 761	Support blocks, set of 6	1
	additionally required: PC with Windows XP/Vista/7/8/10 (x86 or x64)	1

In the experiment P1.3.2.5 the acceleration of a cart is recorded from within the system using a wireless, bluetooth connected and battery powered Pocket-CASSY equipped with a 3D acceleration sensor. The gravitational forces and accelerations are measured in different situations.

CASSY®

ONE-DIMENSIONAL MOTIONS ON THE LINEAR AIR TRACK

P1.3.3.4
Path-time and velocity-time diagrams of straight motion - Recording and evaluating with CASSY

P1.3.3.5
Uniformly accelerated motion with reversal of direction - Recording and evaluating with CASSY

P1.3.3.6
Kinetic energy of a uniformly accelerated mass - Recording and evaluating with CASSY

Path-time and velocity-time diagrams of straight motion - Recording and evaluating with CASSY (P1.3.3.4)

Cat. No.	Description	P1.3.3.4	P1.3.3.5	P1.3.3.6
337 501	Air track	1	1	1
337 53	Air supply	1	1	1
667 8231	Power controller	1	1	1
337 462	Combination light barrier	1	1	1
524 013	Sensor-CASSY 2	1	1	1
524 220	CASSY Lab 2	1	1	1
524 074	Timer S	1	1	1
501 16	Multi-core cable, 6-pole, 1.5 m	1	1	1
501 46	Connecting leads 19 A, 100 cm, red/blue, pair	1		1
	additionally required: PC with Windows XP/Vista/7/8/10 (x86 or x64)	1	1	1

The advantage of studying linear translational motions on the linear air track is that interference factors such as frictional forces and moments of inertia of wheels do not occur.

The computer-assisted measurement system CASSY is particularly suitable for simultaneously measuring transit time t, path s, velocity v and acceleration a of a slider on the linear air track. The linear motion of the slider is transmitted to the motion sensing element by means of a lightly tensioned thread; the signals of the motion sensing element are matched to the CASSY measuring inputs by the Timer S. The PC supports significantly the evaluation of the measured data. Alternatively the measured data can be exported in table format to external data evaluation.

The object of the experiment P1.3.3.4 is to study uniform and uniformly accelerated motions on the horizontally aligned linear air track.

In the experiment P1.3.3.5 the patch, velocity and acceleration of a slider is record, which moves uphill on an inclined plane, then stops, moves downhill, reflected elastically at the lower end and oscillated several times back and forth.

The experiment P1.3.3.6 records the kinetic energy

$$E = \frac{m}{2} \cdot v^2$$

of a uniformly accelerated slider of the mass m as a function of the time and compares it with the work

$$W = F \cdot s$$

which the accelerating force F has performed. This verifies the relationship

$$E(t) = W(t)$$

Path-time, velocity-time and acceleration-time diagram (P1.3.3.4)

CONSERVATION OF LINEAR MOMENTUM

P1.3.4.1
Energy and linear momentum in elastic and inelastic collision with Fletcher's trolleys – Measuring with two forked light barriers and CASSY

P1.3.4.6
Energy and linear momentum in elastic and inelastic collision with Fletcher's trolleys – Measuring with two forked light barriers and counter

Energy and linear momentum in elastic and inelastic collision with Fletcher's trolleys - Measuring with two forked light barriers and CASSY (P1.3.4.1)

Cat. No.	Description	P1.3.4.1	P1.3.4.6
337 130	Track, 1.5 m	1	1
337 110	Trolley	2	2
337 114	Additional weights, pair	1	1
337 112	Impact spring for track	1	1
337 462	Combination light barrier	2	2
524 013	Sensor-CASSY 2	1	
524 220	CASSY Lab 2	1	
524 074	Timer S	1	
501 16	Multi-core cable, 6-pole, 1.5 m	2	2
575 451	Counter P		1
	additionally required: PC with Windows XP/Vista/7/8/10 (x86 or x64)		

The use of a track makes superior quantitative results possible when verifying the conservation of linear momentum in an experiment.

In the experiment P1.3.4.1, the obscuration times Δt_i of two light barriers are measured, e.g. for two bodies on a linear track before and after elastic and inelastic collision. These experiments investigate collisions between a moving body and a body at rest, as well as collisions between two bodies in motion. The velocities

$$v_i = \frac{d}{\Delta t_i}$$

d: width of interrupter flags

the momentum values

$$p_i = m_i \cdot v_i$$

m_i: masses of bodies

and the energies

$$E_i = \frac{1}{2} \cdot m_i \cdot v_i^2$$

of the bodies before and after collision can be calculated and compared.

In the experiment P1.3.4.6, the obscuration times Δt_i of two light barriers are measured for two bodies on a track before and after elastic and inelastic collision. These experiments investigate collisions between a moving body and a body at rest, as well as collisions between two bodies in motion. The velocities

$$v_i = \frac{d}{\Delta t_i}$$

d: width of interrupter flags

the momentum values

$$p_i = m_i \cdot v_i$$

m_i: masses of bodies

and the energies

$$E_i = \frac{1}{2} \cdot m_i \cdot v_i^2$$

of the bodies before and after collision can be calculated and compared.

CONSERVATION OF LINEAR MOMENTUM

P1.3.4.5
Newton's third law and laws of collision – Recording and evaluating with two ultrasonic motion sensors and CASSY
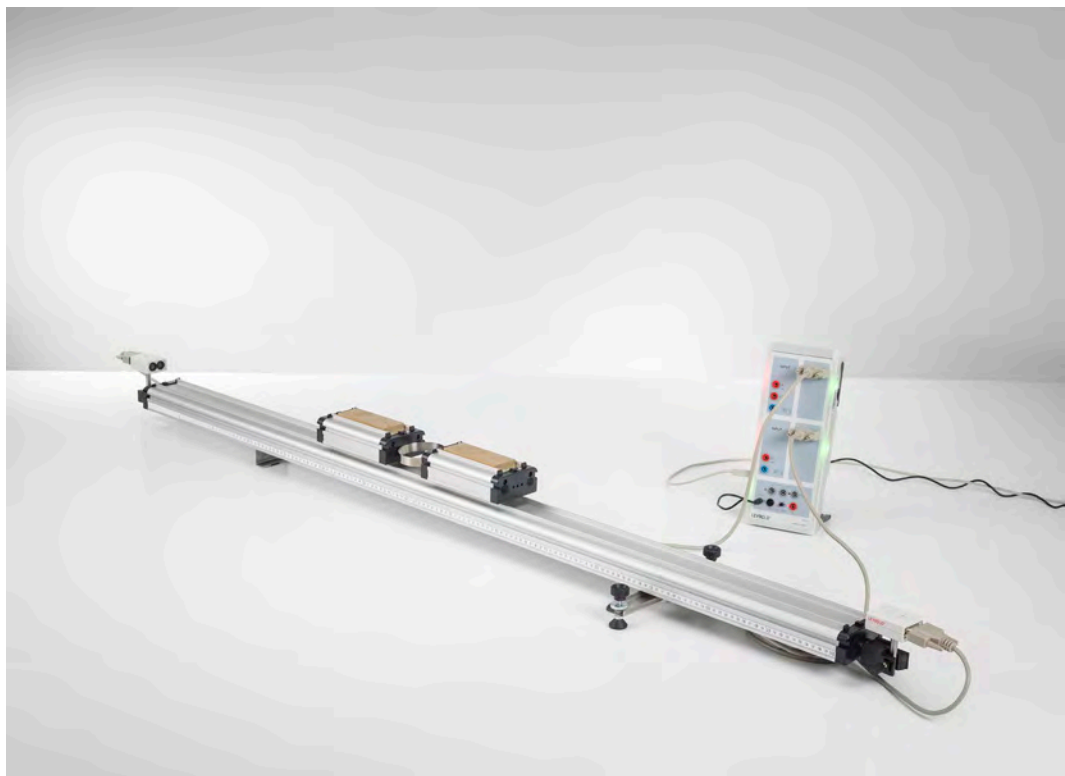
Newton's third law and laws of collision – Recording and evaluating with two ultrasonic motion sensors and CASSY (P1.3.4.5)

Cat. No.	Description	P1.3.4.5
337 130	Track, 1.5 m	1
337 110	Trolley	2
337 114	Additional weights, pair	1
337 473	Impact spring, soft	1
524 013	Sensor-CASSY 2	1
524 220	CASSY Lab 2	1
524 0701	Ultrasonic motion sensor S	2
501 11	Extension cable, 15 pin	2
301 25	Support block	2
340 89	Coupling plug 4 mm	4
	additionally required: PC with Windows XP/Vista/7/8/10 (x86 or x64)	1

The use of a track makes superior quantitative results possible when verifying the conservation of linear momentum in an experiment.

In the experiment P1.3.4.5 the way of the two trolleys are measured during an elastic or inelastic collision. This is done with two ultrasonic sensors. $v(t)$ and $a(t)$-diagrams are determined by the Sensor-CASSY. The forces $F_1(t)$ and $F_2(t)$ can be calculated from the accelerations $a_1(t)$ and $a_2(t)$ and the masses m_1 and m_2 of the trolleys. It is confirmed that $F_1(t) = -F_2(t)$ applies during the collision. It follows the conservation of momentum during the whole collision process:

$$\Delta p_1 + \Delta p_2 = \int F_1(t)dt + \int F_2(t)dt = \int (F_1(t) + F_2(t))dt = 0$$

In addition, the center of mass motion $s_3(t)$ is observed and it can be showed that the speed $v_3(t)$ of the center of gravity during the whole collision process is constant. This shows alternative the conservation of momentum during the whole collision process:

$$v_3 = \frac{m_1 \cdot v_1 + m_2 \cdot v_2}{m_1 + m_2} = \frac{p}{m_1 + m_2} = const.$$

CONSERVATION OF LINEAR MOMENTUM

P1.3.4.8
Energy and linear momentum in elastic and inelastic collision on the linear air track – Measuring with two forked light barriers and CASSY

P1.3.4.10
Rocket principle: conservation of momentum and reaction

Energy and linear momentum in elastic and inelastic collision on the linear air track – Measuring with two forked light barriers and CASSY (P1.3.4.8)

Cat. No.	Description	P1.3.4.8	P1.3.4.10
337 501	Air track	1	1
337 53	Air supply	1	1
667 8231	Power controller	1	1
337 46	Fork-type light barrier	2	
300 41	Stand rod, 25 cm, 12 mm Ø		1
300 42	Stand rod, 47 cm, 12 mm Ø		1
301 01	Leybold multiclamp		2
524 013	Sensor-CASSY 2	1	
524 005W	Mobile-CASSY 2 WiFi		1
524 220	CASSY Lab 2	1	
524 060	Force sensor S, ±1N		1
524 074	Timer S	1	
501 16	Multi-core cable, 6-pole, 1.5 m	1	
309 48	Fishing line	1	
	additionally required: PC with Windows XP/Vista/7/8/10 (x86 or x64)	1	

In the experiment P1.3.4.8, the obscuration times Δt_i of two light barriers are measured for two bodies on a linear track before and after elastic and inelastic collision. These experiments investigate collisions between a moving body and a body at rest, as well as collisions between two bodies in motion. The velocities

$$v_i = \frac{d}{\Delta t_i}$$

d: width of interrupter flags

the momentum values

$$p_i = m_i \cdot v_i$$

m_i: masses of bodies

and the energies

$$E_i = \frac{1}{2} \cdot m_i \cdot v_i^2$$

of the bodies before and after collision can be calculated and compared.

In the experiment P1.3.4.10, the recoil force on a jet slider is measured for different nozzle cross-sections using a sensitive dynamometer in order to investigate the relationship between repulsion and conservation of linear momentum.

FREE FALL

P1.3.5.1
Free fall: time measurement with the contact plate and the counter S
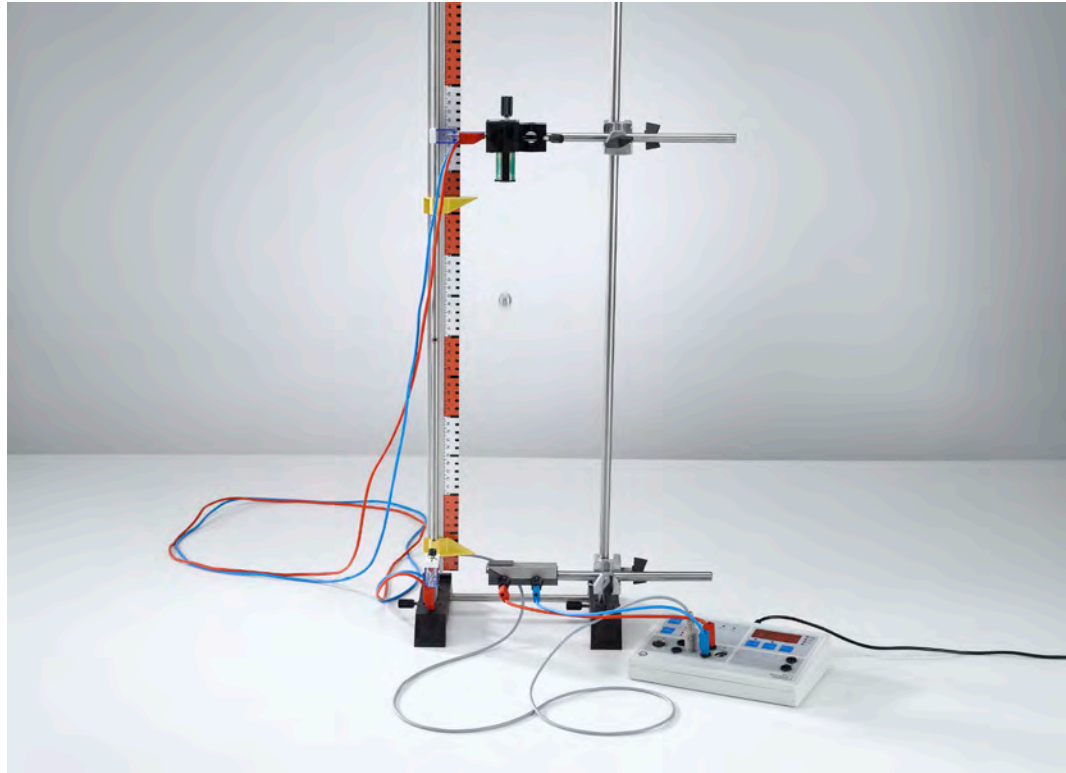
Free fall: time measurement with the contact plate and the counter S (P1.3.5.1)

Cat. No.	Description	P1.3.5.1
336 23	Contact plate, large	1
336 21	Holding magnet	1
336 25	Holding magnet adapter with a release mechanism	1
575 471	Counter S	1
301 21	Stand base MF	2
301 26	Stand rod 25 cm, 10 mm Ø	3
300 46	Stand rod, 150 cm, 12 mm diam.	1
301 01	Leybold multiclamp	2
311 23	Scale with pointers	1
501 25	Connecting lead, 32 A, 50 cm, red	1
501 26	Connecting lead, 32 A, 50 cm, blue	1
501 35	Connecting lead, 32 A, 200 cm, red	1
501 36	Connecting lead, 32 A, 200 cm, blue	1

To investigate free fall, a steel ball is suspended from an electromagnet. It falls downward with a uniform acceleration due to the force of gravity

$$F = m \cdot g$$

m: mass of ball, g: gravitational acceleration

as soon as the electromagnet is switched off. The friction of air can be regarded as negligible as long as the falling distance, and thus the terminal velocity, are not too great; in other words, the ball falls freely.

In the experiment P1.3.5.1, electronic time measurement is started as soon as the ball is released through interruption of the magnet current. After traveling a falling distance h, the ball falls on a contact plate, stopping the measurement of time t. The measurements for various falling heights are plotted as value pairs in a path-time diagram. As the ball is at rest at the beginning of timing, g can be determined using the relationship

$$h = \frac{1}{2}g \cdot t^2$$
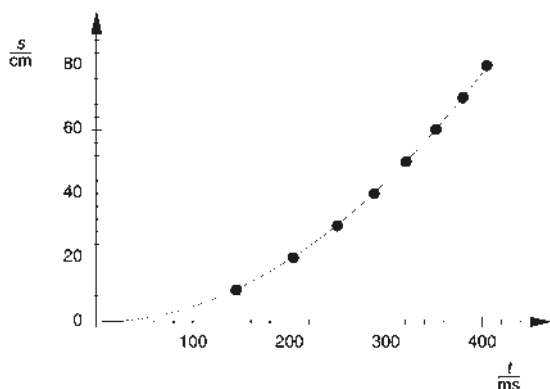
Path-time diagram of the free fall of the ball (P1.3.5.1)

Free fall: multiple measurements with the g ladder (P1.3.5.3)

FREE FALL

P1.3.5.3
Free fall: multiple measurements with the g ladder

Cat. No.	Description	P1.3.5.3
529 034	g ladder	1
337 46	Fork-type light barrier	1
501 16	Multi-core cable, 6-pole, 1.5 m	1
524 013	Sensor-CASSY 2	1
524 220	CASSY Lab 2	1
524 074	Timer S	1
	additionally required: PC with Windows XP/Vista/7/8/10 (x86 or x64)	1

The disadvantage of preparing a path-time diagram by recording the measured values point by point is that it takes a long time before the dependency of the result on experiment parameters such as the initial velocity or the falling height becomes apparent. Such investigations become much simpler when the entire measurement series of a path-time diagram is recorded in one measuring run using the computer.

In the experiment P1.3.5.3, a ladder with several rungs falls through a forked light barrier, which is connected to the CASSY computer interface device to measure the obscuration times. This measurement is equivalent to a measurement in which a body falls through multiple equidistant light barriers. The height of the falling body corresponds to the rung width. The measurement data are recorded and evaluated using CASSY Lab. The instantaneous velocities are calculated from the obscuration times and the rung width and displayed in a velocity-time diagram $v(t)$. The measurement points can be described by a straight line

$$v(t) = v_0 + g \cdot t$$

g: gravitational acceleration

whereby v_0 is the initial velocity of the ladder when the first rung passes the light barrier.

a1 = 9,805 m/s² ± 0,015 m/s²
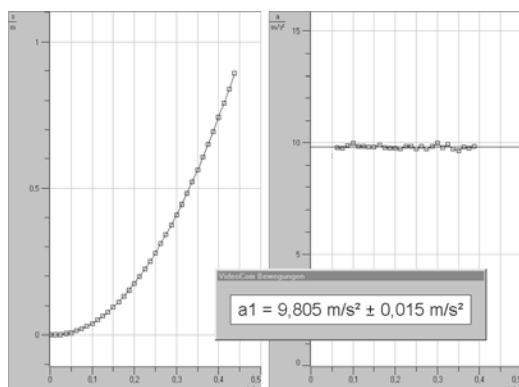
Path-time and acceleration-time diagrams of the falling body (P1.3.5.3)

LEYBOLD®

ANGLED PROJECTION

P1.3.6.1
Point-by-point recording of the projection parabola as a function of the speed and angle of projection

P1.3.6.2
Principle of superposing: comparison of inclined projection and free fall
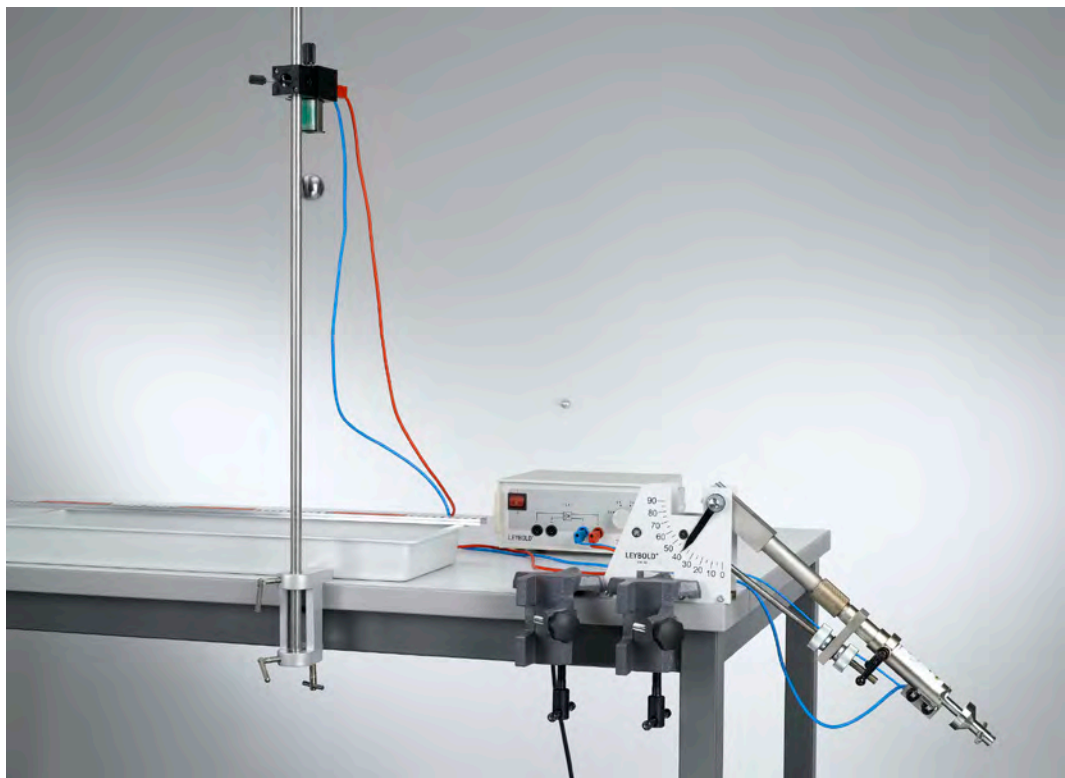
Principle of superposing: comparison of inclined projection and free fall (P1.3.6.2)

Cat. No.	Description	P1.3.6.1	P1.3.6.2
336 56	Projection apparatus, large	1	1
301 06	Bench clamp	2	2
311 78	Tape measure 2 m / 1 mm	1	
300 76	Laboratory stand II	1	
311 22	Vertical rule	1	
300 11	Saddle base	1	
649 42	Tray, 552 mm x 197 mm x 48 mm	1	1
688 108	Quartz sand, 1 kg	1	1
336 21	Holding magnet		1
521 231	Low-voltage power supply 3/6/9/12 V		1
311 02	Metal rule, 1 m		1
300 44	Stand rod, 100 cm, 12 mm diam.		1
301 07	Simple bench clamp		1
501 26	Connecting lead, 32 A, 50 cm, blue		1
501 35	Connecting lead, 32 A, 200 cm, red		1
501 36	Connecting lead, 32 A, 200 cm, blue		1

The trajectory of a ball launched at a projection angle α with a projection velocity v_0 can be reconstructed on the basis of the principle of superposing. The overall motion is composed of a motion with constant velocity in the direction of projection and a vertical falling motion. The superposition of these motions results in a parabola, whose height and width depend on the angle and velocity of projection.

The experiment P1.3.6.1 measures the trajectory of the steel ball point by point using a vertical scale. Starting from the point of projection, the vertical scale is moved at predefined intervals; the two pointers of the scale are set so that the projected steel ball passes between them. The trajectory is a close approximation of a parabola. The observed deviations from the parabolic form may be explained through friction with the air.

In the experiment P1.3.6.2, a second ball is suspended from a holding magnet in such a way that the first ball would strike it if propelled in the direction of projection with a constant velocity. Then, the second ball is released at the same time as the first ball is projected. We can observe that, regardless of the launch velocity v_0 of the first ball, the two balls collide; this provides experimental confirmation of the principle of superposing.
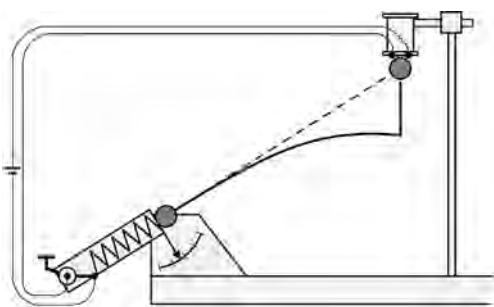
Schematic diagram comparing angled projection and free fall (P1.3.6.2)
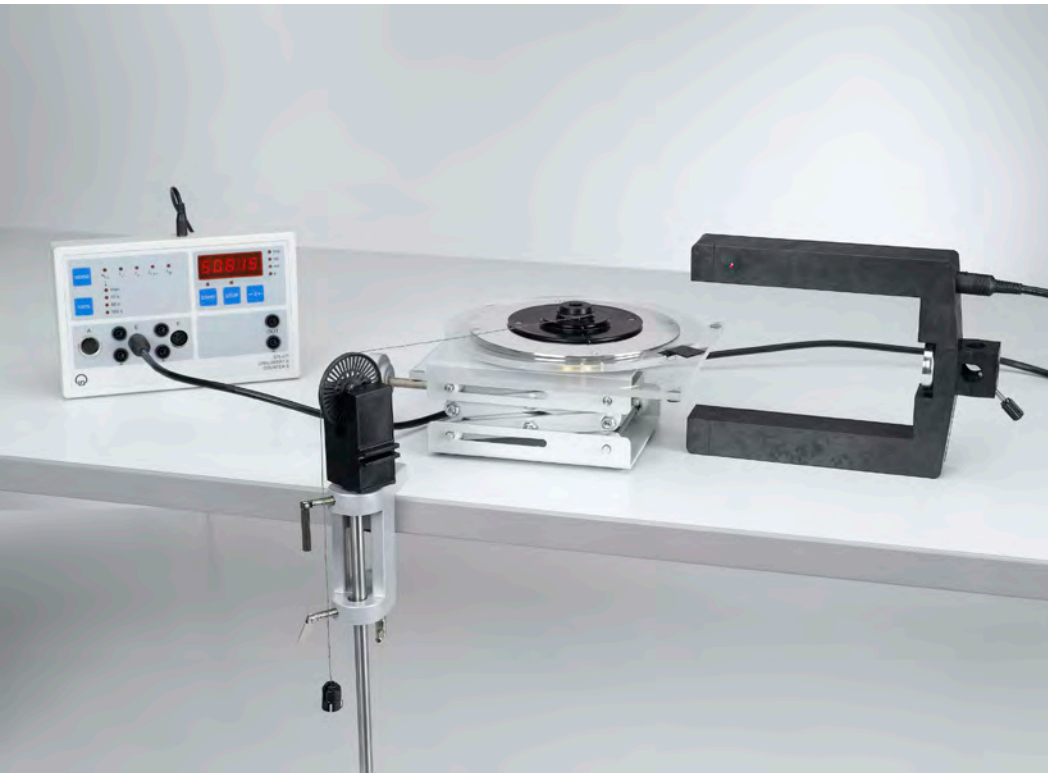
ROTATIONAL MOTIONS

P1.4.1.1
Path-time diagrams of rotational motions - Time measurement with the counter

P1.4.1.2
Path-time diagrams of rotational motions - Recording and evaluating with CASSY

Path-time diagrams of rotational motions - Time measurement with the counter (P1.4.1.1)

Cat. No.	Description	P1.4.1.1	P1.4.1.2
347 23	Rotation model	1	1
337 46	Fork-type light barrier	1	
575 471	Counter S	1	
501 16	Multi-core cable, 6-pole, 1.5 m	1	1
300 76	Laboratory stand II	1	1
301 07	Simple bench clamp	1	1
337 462	Combination light barrier		1
524 013	Sensor-CASSY 2		1
524 220	CASSY Lab 2		1
524 074	Timer S		1
336 21	Holding magnet		1
300 41	Stand rod, 25 cm, 12 mm Ø		1
300 11	Saddle base		1
501 46	Connecting leads 19 A, 100 cm, red/blue, pair		1
	additionally required: PC with Windows XP/Vista/7/8/10 (x86 or x64)		1

The low-friction Plexiglas disk of the rotation model is set in uniform or uniformly accelerated motion for quantitative investigations of rotational motions. Forked light barriers are used to determine the angular velocity; their light beams are interrupted by a 10° flag mounted on the rotating disk. When two forked light barriers are used, measurement of time t can be started and stopped for any angle φ (optional possible). This experiment determines the mean velocity

$$\omega = \frac{\varphi}{t}$$

If only one forked light barrier is available, the obscuration time Δt is measured, which enables calculation of the instantaneous angular velocity

$$\omega = \frac{10°}{\Delta t}$$

In the experiment P1.4.1.1, the angular velocity ω and the angular acceleration α are recorded analogously to acceleration in translational motions. Both uniform and uniformly accelerated rotational motions are investigated. The results are graphed in a velocity-time diagram $\omega(t)$. In the case of a uniformly accelerated motion of a rotating disk initially at rest, the angular acceleration can be determined from the linear function

$$\omega = \alpha \cdot t$$

The topic of the experiment P1.4.1.2 are homogeneous and constantly accellerated rotational motions, which are studied on the analogy of homogeneous and constantly accellerated translational motions.

The use of the computer-assisted measured-value recording system CASSY facilitates the study of uniform and uniformly accellerated rotational motions. A thread stretched over the surface of the rotation model transmits the rotational motion to the motion sensing element whose signals are adapted to the measuring inputs of CASSY by a box.

CONSERVATION OF ANGULAR MOMENTUM

P1.4.2.1
Conservation of angular momentum in elastic and inelastic rotational collision

Conservation of angular momentum in elastic and inelastic rotational collision (P1.4.2.1)

Cat. No.	Description	P1.4.2.1
347 23	Rotation model	1
524 431	Light barrier M	2
524 005W	Mobile-CASSY 2 WiFi	1

Torsion impacts between rotating bodies can be described analogously to one-dimensional translational collisions when the axes of rotation of the bodies are parallel to each other and remain unchanged during the collision. This condition is reliably met when carrying out measurements using the rotation model. The angular momentum is specified in the form

$$L = I \cdot \omega$$

I: moment of inertia, ω: angular velocity

The principle of conservation of angular momentum states that for any torsion impact of two rotating bodies, the quantity

$$L = I_1 \cdot \omega_1 + I_2 \cdot \omega_2$$

before and after impact remains the same.

The experiment P1.4.2.1 investigate the nature of elastic and inelastic torsion impact. Using two light barriers and the measuring system CASSY, the obscuration times of two interrupter flags are registered as a measure of the angular velocities before and after torsion impact.

CASSY®

Centrifugal force of an orbiting body - Measuring with the central force apparatus and CASSY (P1.4.3.3)

Cat. No.	Description	P1.4.3.3
524 068	Centrifugal force apparatus S	1
521 491	AC/DC power supply 0...12 V/3 A	1
524 013	Sensor-CASSY 2	1
524 220	CASSY Lab 2	1
524 074	Timer S	1
337 46	Fork-type light barrier	1
501 16	Multi-core cable, 6-pole, 1.5 m	1
301 06	Bench clamp	1
300 02	Stand base, V-shaped, small	1
300 40	Stand rod, 10 cm, 12 mm diam.	1
501 46	Connecting leads 19 A, 100 cm, red/blue, pair	1
	additionally required: PC with Windows XP/Vista/7/8/10 (x86 or x64)	1

The centrifugal force apparatus S enables experimental investigation of the centrifugal force F as a function of the rotating mass m, the distance r of the mass from the centre of rotation and the angular velocity ω, thus making it possible to confirm the relation

$$F = m \cdot \omega^2 \cdot r$$

r: radius of orbit, ω: angular velocity

for the centrifugal force.

In the centrifugal force apparatus S, the centrifugal force F acting on a rotating mass m is transmitted via a lever with ball-and-socket joint and a push pin in the axis of rotation to a leaf spring, whose deflection is measured electrically by means of a bridge-connected strain gauge. In the measuring range relevant for the experiment, the deformation of the leaf spring is elastic and thus proportional to the force F.

In the experiment P1.4.3.3, the relationship

$$F \propto \omega^2$$

is derived directly from the parabolic shape of the recorded curve $F(\omega)$. To verify the proportionalities

$$F \propto r, \quad F \propto m$$

curves are recorded and evaluated for different orbit radii r and various masses m.
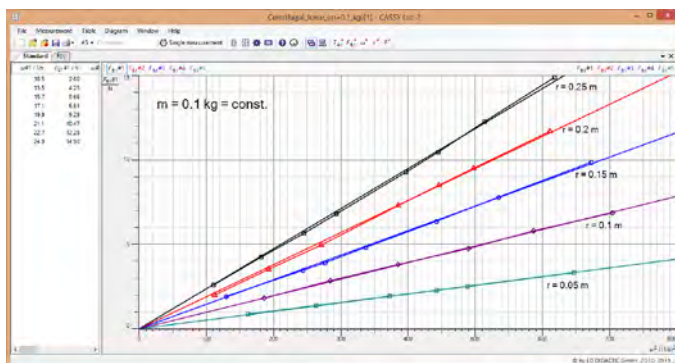
Centrifugal force of an orbiting body – Measuring with the central force apparatus and CASSY (P1.4.3.3)

MOTIONS OF A GYROSCOPE

P1.4.4.3
Precession and nutation of a gyroscope

Precession and nutation of a gyroscope (P1.4.4.3)

Cat. No.	Description	P1.4.4.3
348 20	Gyroscope	1
342 63	Weight 50 g	2
524 082	Rotary motion sensor S	1
337 468	Reflection light barrier	1
590 021	Double spring clip	1
524 074	Timer S	1
524 013	Sensor-CASSY 2	1
524 220	CASSY Lab 2	1
	additionally required: PC with Windows XP/Vista/7/8/10 (x86 or x64)	1

Gyroscopes generally execute extremely complex motions, as the axis of rotation is supported at only one point and changes directions constantly. We distinguish between the precession and the nutation of a gyroscope.

The aim of the experiment P1.4.4.3 is to investigate the precession of a gyroscope. The precession frequency f_P is measured by means of the rotary motion sensor S, the rotary frequency f of the gyroscope disk by means of the reflection light barrier, each in combination with CASSY. The dependance of the precession frequency f_P on the applied force, i.e. the torque M and the rotary frequency f is determined quantitatively. The relationship

$$\omega_P = \frac{M}{I} \cdot \frac{1}{\omega}$$

applies for the corresponding angular frequencies ω_P and ω and for a known moment of inertia I of the gyroscope around its axis of symmetry.

The nutation of a force-free gyroscope is investigated, too. The nutation frequency f_N is measured by means of the rotary motion sensor S, the rotary frequency f of the gyroscope disk by means of the reflextion light barrier, each in combination with CASSY. The dependance of the nutation frequency f_N on the rotary frequency f is determined quantitatively. The relationship

$$\omega_N = \frac{I \cdot \omega}{I_\perp}$$

applies for the corresponding angular frequencies ω_N and ω and for known moments of inertia I of the gyroscope around its axis of symmetry (rotational axis of the gyroscope disk) and $I_\perp$ around the pivotal point (point of support) of the axis.

P.1.4.5.2

P.1.4.5.3

P.1.4.5.1

Definition of moment of inertia (P1.4.5.1)

MOMENT OF INERTIA

P1.4.5.1
Definition of moment of inertia

P1.4.5.2
Moment of inertia and body shape

P1.4.5.3
Confirming Steiner's theorem

Cat. No.	Description	P1.4.5.1	P1.4.5.2	P1.4.5.3
347 801	Torsion axle	1	1	1
300 02	Stand base, V-shaped, small	1	1	1
313 27	Hand-held stop-watch, 60s/0.2s	1	1	1
347 81	Cylinders for torsion axle, set		1	
347 82	Sphere for the torsion axle		1	
347 83	Circular disc for the torsion axle			1

For any rigid body whose mass elements m_i are at a distance of r_i from the axis of rotation, the moment of inertia is

$$I = \sum_i m_i \cdot r_i^2$$

For a particle of mass m in an orbit with the radius r, we can say

$$I = m \cdot r^2$$

The moment of inertia is determined from the oscillation period of the torsion axle on which the test body is mounted and which is elastically joined to the stand via a helical spring. The system is excited to harmonic oscillations. For a known directed angular quantity D, the oscillation period T can be used to calculate the moment of inertia of the test body using the equation

$$I = D \cdot \left(\frac{T}{2\pi} \right)^2$$

In the experiment P1.4.5.1, the moment of inertia of a "mass point" is determined as a function of the distance r from the axis of rotation. In this experiment, a rod with two weights of equal mass is mounted transversely on the torsion axle. The centers of gravity of the two weights have the same distance r from the axis of rotation, so that the system oscillates with no unbalanced weight.

The experiment P1.4.5.2 compares the moments of inertia of a hollow cylinder, a solid cylinder and a solid sphere. This measurement uses two solid cylinders with equal mass but different radii. Additionally, this experiment examines a hollow cylinder which is equal to one of the solid cylinders in mass and radius, as well as a solid sphere with the same moment of inertia as one of the solid cylinders.

The experiment P1.4.5.3 verifies Steiner's law using a flat circular disk. Here, the moments of inertia I_A of the circular disk are measured for various distances a from the axis of rotation, and compared with the moment of inertia I_S around the axis of the center of gravity. This experiment confirms the relationship

$$I_A - I_S = M \cdot a^2$$

Confirming Steiner's theorem (P1.4.5.3)

CONSERVATION OF ENERGY

P1.4.6.1
Maxwell's wheel

P1.4.6.2
Maxwell's wheel – Recording and evaluating with ultrasonic motion sensor

Maxwell's wheel (P1.4.6.1)

Cat. No.	Description	P1.4.6.1	P1.4.6.2
331 22	Maxwell's wheel	1	1
337 46	Fork-type light barrier	1	
501 16	Multi-core cable, 6-pole, 1.5 m	1	
575 471	Counter S	1	
336 25	Holding magnet adapter with a release mechanism	1	
311 23	Scale with pointers	1	1
300 11	Saddle base	1	1
301 25	Support block	1	
301 21	Stand base MF	2	2
301 27	Stand rod 50 cm, 10 mm Ø	2	3
300 44	Stand rod, 100 cm, 12 mm diam.	2	2
301 01	Leybold multiclamp	4	7
524 0701	Ultrasonic motion sensor S		1
501 11	Extension cable, 15 pin		1
524 005W	Mobile-CASSY 2 WiFi		1

The law of conversation of energy states that the total amount of energy in an isolated system remains constant over time. Within this system the energy can change form, for instance potential in kinetic energy. In the daily experience (also during experiments) energy apparently is lost. The reason for this is a change to an energy form which is not considered like the friction.

Experiment P1.4.6.1 is used to examine the conservation of energy at the Maxwell's wheel. During the experiment potential energy E_{pot} is transformed to kinetic energy E_{kin} due a translational motion (E_{trans}) and a rotational motion (E_{rot}). For different heights times and velocities are measured. From the data one can determine the inertia of the Maxwell's wheel. With a known inertia, one can calculate the gravitational acceleration.

In the experiment P1.4.6.2 the conservation of energy at the Maxwell's wheel is studied. The position and velocity, required for calculation of kinetic energy, is measured with an ultrasonic motion sensor.

SIMPLE AND COMPOUND PENDULUM

P1.5.1.1
Determining the gravitational acceleration with a simple pendulum

P1.5.1.7
Determination of gravitational acceleration with a simple pendulum – Measuring with light barrier

Determination of gravitational acceleration with a simple pendulum - Measuring with light barrier (P1.5.1.7)

Cat. No.	Description	P1.5.1.1	P1.5.1.7
340 851	Weight, 50 g	3	3
686 51	Cord	1	1
314 04	Support clip, for plugging in	1	1
311 78	Tape measure 2 m / 1 mm	1	1
LDS 00001	Stopwatch, digital	1	
301 21	Stand base MF	2	2
301 26	Stand rod 25 cm, 10 mm Ø	1	1
301 27	Stand rod 50 cm, 10 mm Ø	1	1
301 25	Support block	1	1
524 005W	Mobile-CASSY 2 WiFi		1
524 431	Light barrier M		1
688 808	Stand rod, 10 x 223 mm, with thread M6		1
300 02	Stand base, V-shaped, small		1

A simple, or "mathematic" pendulum is understood to be a point-shaped mass m suspended on a massless thread with the length s. For small deflections, it oscillates under the influence of gravity with the period

$$T = 2\pi \cdot \sqrt{\frac{s}{g}}$$

Thus, a mathematic pendulum could theoretically be used to determine the gravitational acceleration g precisely through measurement of the oscillation period and the pendulum length.

In the experiment P1.5.1.1, a weight on a cord is used to determine the gravitational acceleration. As the mass of the weight is much greater than that of the cord on which it is suspended, this pendulum can be considered to be a close approximation of a mathematic pendulum. Multiple oscillations are recorded to improve measuring accuracy. For gravitational acceleration, the error then depends essentially on the accuracy with which the length of the pendulum is determined.

In the experiment P1.5.1.7, a weight on a cord is used to determine the gravitational acceleration. As the mass of the weight is much greater than that of the cord on which it is suspended, this pendulum can be considered to be a close approximation of a mathematic pendulum. The measurement is done with a light barrier and CASSY. The error of the gravitational acceleration then depends essentially on the accuracy with which the length of the pendulum is determined.

SIMPLE AND COMPOUND PENDULUM

P1.5.1.3
Oscillations of a rod pendulum and determination of the acceleration due to gravity on earth
– Measuring with rotary motion sensor

P1.5.1.6
Pendulum with changeable acceleration due to gravity (variable g-pendulum)

Oscillations of a rod pendulum and determination of the acceleration due to gravity on earth – Measuring with rotary motion sensor (P1.5.1.3)

Cat. No.	Description	P1.5.1.3	P1.5.1.6
346 20	Physical pendulum	1	1
524 005W	Mobile-CASSY 2 WiFi	1	
524 082	Rotary motion sensor S	1	1
301 21	Stand base MF	2	2
301 26	Stand rod 25 cm, 10 mm Ø	1	2
524 013	Sensor-CASSY 2		1
524 220	CASSY Lab 2		1
301 27	Stand rod 50 cm, 10 mm Ø		1
301 01	Leybold multiclamp		1
	additionally required: PC with Windows XP/Vista/7/8/10 (x86 or x64)		1

In the case of a physical pendulum, one considers the mass distribution of a rigid body. The calculation of the period of oscillation T is based on the moment of inertia J around the suspension point, the mass m and the distance s of the suspension point from the center of mass.

$$T = 2\pi \cdot \sqrt{\frac{J}{mgs}}$$

The reduced pendulum length l_R is the length of a mathematical pendulum of the same oscillation period. Often the reduced pendulum length cannot be determined with the desired accuracy because the exact determination of the moment of inertia or the center of gravity is difficult. In the case of the reversion pendulum, the mass distribution is changed so that the oscillation periods for the two axes of rotation are the same. As a result, it is clear that the reduced pendulum length l_R corresponds to the distance between the two axes of rotation and is therefore known very accurately.

In the experiment P1.5.1.3, the oscillation of a rod pendulum, i.e. an simple physical pendulum is investigated. Using the rotary motion sensor S the oscillation of the pendulum is recorded as a function of time. Angle $\alpha(t)$, velocity $\omega(t)$ and acceleration $a(t)$ are compared. In addition, the effective length of the pendulum is determined from the measured oscillation period T. The dependance of the period T on the amplitude A of a oscillation is investigated. For small deflections the oscillation of an pendulum is approximately harmonic and the period is independant from the amplitude. For high deflections this approximation is no longer satisfied: the higher the amplitude is the larger the period. The rod pendulum is applied as reversible pendulum. The value of the acceleration due to gravity is determined. The pendulum is set up at two pivot points at opposite sides of the rod. The position of two sliding weights influences the period. When the pendulum is properly adjusted, it oscillates on both edges with the same period T. The effective pendulum length l_r corresponds to the distance d between the two pivot points. The acceleration due to gravity is calculated form the effective pendulum length l_r and the period T.

In the experiment P1.5.1.6, a pendulum with variable acceleration due to gravity (variable g pendulum) is assembled and investigated. The oscillation plane is tilted. Therefore, the acceleration due to gravity is reduced. This leads to different oscillation periods depending on the tilt. In the experiment the dependance of the period on the tilt angle is determined. Additionally, the acceleration due to gravity on different celestial bodies is simulated.

CASSY®

Oscillations of a spring pendulum and determination of oscillation period as a function of the oscillating mass – Measuring with CASSY (P1.5.2.1)

HARMONIC OSCILLATIONS

P1.5.2.1
Oscillations of a spring pendulum and determination of oscillation period as a function of the oscillating mass – Measuring with CASSY

Cat. No.	Description	P1.5.2.1
352 10	Helical spring, 3 N/m	1
342 63	Weight 50 g	5
336 21	Holding magnet	1
337 462	Combination light barrier	1
337 464	Combination spoked wheel	1
524 074	Timer S	1
501 16	Multi-core cable, 6-pole, 1.5 m	1
524 013	Sensor-CASSY 2	1
524 220	CASSY Lab 2	1
300 01	Stand base, V-shaped, large	1
300 41	Stand rod, 25 cm, 12 mm Ø	1
300 46	Stand rod, 150 cm, 12 mm diam.	1
301 01	Leybold multiclamp	2
301 08	Clamp with hook	1
309 48	Fishing line	1
501 46	Connecting leads 19 A, 100 cm, red/blue, pair	1
	additionally required: PC with Windows XP/Vista/7/8/10 (x86 or x64)	1

When a system is deflected from a stable equilibrium position, oscillations can occur. An oscillation is considered harmonic when the restoring force F is proportional to the deflection x from the equilibrium position.

$$F = D \cdot x$$

D: directional constant

The oscillations of a spring pendulum are often used as a classic example of this.

In the experiment P1.5.2.1, the harmonic oscillations of a spring pendulum are recorded as a function of time using the motion transducer and the computer-assisted measured value recording system CASSY. In the evaluation, the oscillation quantities path x, velocity v and acceleration a are compared on the screen. These can be displayed either as functions of the time t or as a phase diagram. The experiment records and evaluates the oscillations of a spring pendulum for various suspended masses m. The relationship

$$T = 2\pi \cdot \sqrt{\frac{D}{m}}$$

for the oscillation period is verified.

TORSION PENDULUM

P1.5.3.1
Free rotational oscillations
– Measuring with a hand-held stopclock

P1.5.3.2
Forced rotational oscillations
– Measuring with a hand-held stopclock
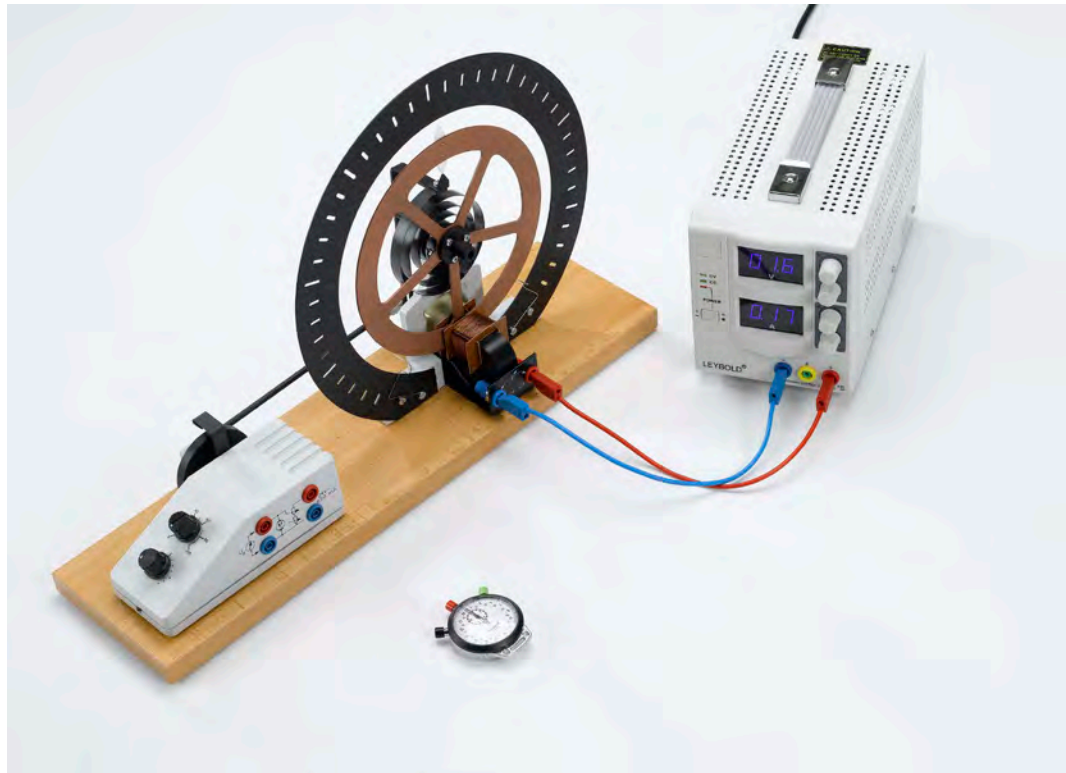
Free rotational oscillations - Measuring with a hand-held stopclock (P1.5.3.1)

Cat. No.	Description	P1.5.3.1	P1.5.3.2
346 00	Torsion pendulum	1	1
521 546	DC Power Supply 0...16 V/0...5 A	1	1
313 27	Hand-held stop-watch, 60s/0.2s	1	1
501 46	Connecting leads 19 A, 100 cm, red/blue, pair	1	2
562 793	Plug-in power supply for torsion pendulum		1
531 120	Multimeter LDanalog 20		1

The torsion pendulum according to Pohl can be used to investigate free or forced harmonic rotational oscillations. An electromagnetic eddy current brake damps these oscillations to a greater or lesser extent, depending on the set current. The torsion pendulum is excited to forced oscillations by means of a motor-driven eccentric rod.

The aim of the experiment P1.5.3.1 is to investigate free harmonic rotational oscillations of the type

$$\varphi(t) = \varphi_0 \cdot \cos\omega t \cdot e^{-\delta \cdot t} \quad \text{where} \quad \omega = \sqrt{\omega_0^2 - \delta^2}$$

ω_0: characteristic frequency of torsion pendulum

To distinguish between oscillation and creepage, the damping constant Δ is varied to find the current I_0 which corresponds to the aperiodic limiting case. In the oscillation case, the angular frequency ω is determined for various damping levels from the oscillation period T and the damping constant Δ by means of the ratio

$$\left| \frac{\varphi_{n+1}}{\varphi_n} \right| = e^{-\delta \cdot \frac{T}{2}}$$

of two sequential oscillation amplitudes. Using the relationship

$$\omega^2 = \omega_0^2 - \delta^2$$

we can determine the characteristic frequency ω_0.

In the experiment P1.5.3.2, the torsion pendulum is excited to oscillations with the frequency ω by means of a harmonically variable angular momentum. To illustrate the resonance behavior, the oscillation amplitudes determined for various damping levels are plotted as a function of ω^2 and compared with the theoretical curve

$$\varphi_0 = \frac{M_0}{I} \cdot \frac{1}{\sqrt{\left(\omega^2 - \omega_0^2\right)^2 + \delta^2 \cdot \omega^2}}$$

I: moment of inertia of torsion pendulum
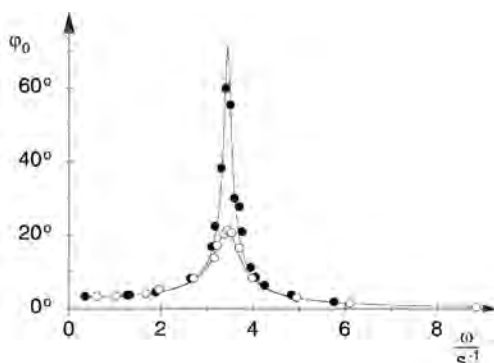
Resonance curves for two different damping constants (P1.5.3.2)

Free rotational oscillations - Recording with CASSY (P1.5.3.3)
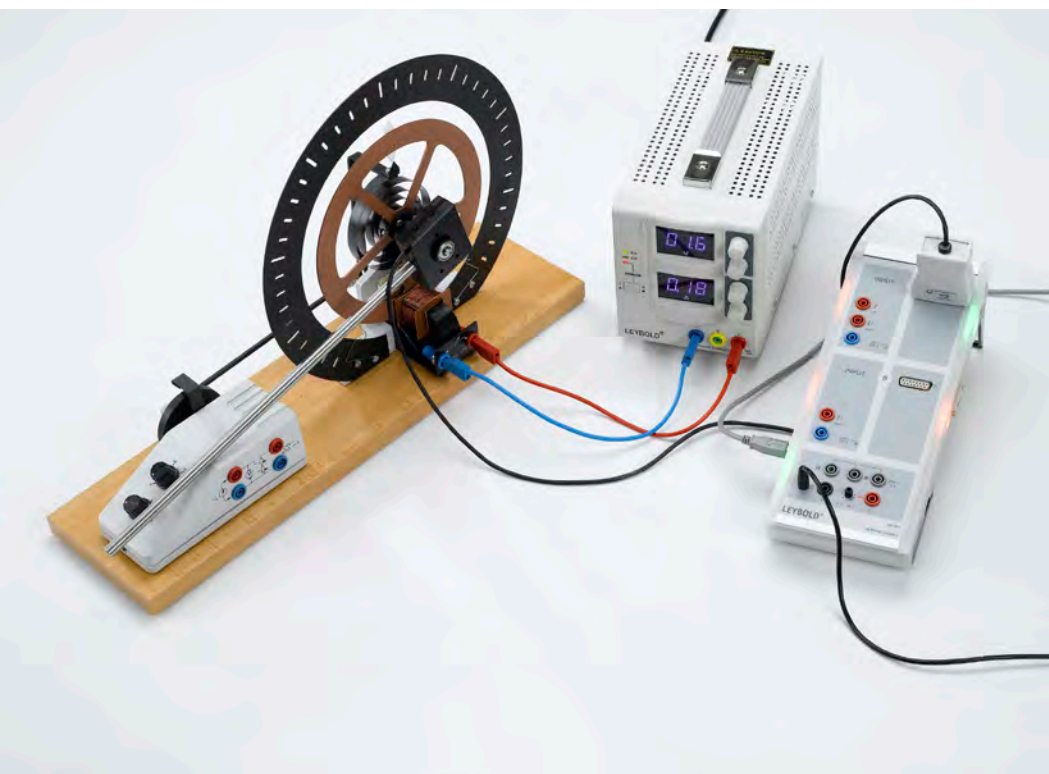
P1.5.3.3
Free rotational oscillations
– Recording with CASSY

P1.5.3.4
Forced harmonic and chaotic
rotational oscillations
– Recording with CASSY

Cat. No.	Description	P1.5.3.3	P1.5.3.4
346 00	Torsion pendulum	1	1
521 546	DC Power Supply 0...16 V/0...5 A	1	1
524 013	Sensor-CASSY 2	1	1
524 220	CASSY Lab 2	1	1
524 082	Rotary motion sensor S	1	1
501 46	Connecting leads 19 A, 100 cm, red/blue, pair	1	2
562 793	Plug-in power supply for torsion pendulum		1
531 120	Multimeter LDanalog 20		1
	additionally required: PC with Windows XP/Vista/7/8/10 (x86 or x64)	1	1

The computer-assisted CASSY measured-value recording system is ideal for recording and evaluating the oscillations of the torsion pendulum. The numerous evaluation options enable a comprehensive comparison between theory and experiment. Thus, for example, the recorded data can be displayed as path-time, velocity-time and acceleration-time diagrams or as a phase diagram (path-velocity diagram).

The aim of the experiment P1.5.3.3 is to investigate free harmonic rotational oscillations of the general type

$$\varphi(t) = (\varphi(0) \cdot \cos \omega t + \dot{\varphi}(0) \cdot \sin \omega t) \cdot e^{-\delta t}$$

$$\text{where } \omega = \sqrt{\omega_0^2 - \delta^2}$$

where ω_0: characteristic frequency of torsion pendulum

This experiment investigates the relationship between the initial deflection $\vartheta(0)$ and the initial velocity $\omega(0)$. In addition, the damping constant Δ is varied in order to find the current I_0 which corresponds to the aperiodic limiting case.

To investigate the transition between forced harmonic and chaotic oscillations, the linear restoring moment acting on the torsion pendulum is deliberately altered in the experiment P1.5.3.4 by attaching an additional weight to the pendulum. The restoring moment now corresponds to a potential with two minima, i.e. two equilibrium positions. When the pendulum is excited at a constant frequency, it can oscillate around the left minimum, the right minimum or back and forth between the two minima. At certain frequencies, it is not possible to predict when the pendulum will change from one minimum to another. The torsion pendulum is then oscillating in a chaotic manner.
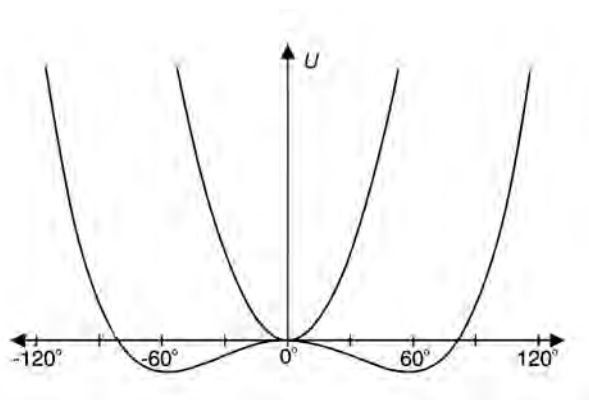
Potential energy of double pendulum with and without additional mass (P1.5.3.4)

COUPLING OF OSCILLATIONS

P1.5.4.1
Coupled pendulum - Measuring with a hand-held stopclock

Coupled pendulum - Measuring with a hand-held stopclock (P1.5.4.1)

Cat. No.	Description	P1.5.4.1
346 45	Double pendulum	1
300 02	Stand base, V-shaped, small	2
300 44	Stand rod, 100 cm, 12 mm diam.	2
300 42	Stand rod, 47 cm, 12 mm diam.	1
301 01	Leybold multiclamp	4
460 97	Metal rule, 0.5 m	1
313 27	Hand-held stop-watch, 60s/0.2s	1

Two coupled pendulums oscillate in phase with the angular frequency ω_+ when they are deflected from the equilibrium position by the same amount. When the second pendulum is deflected in the opposite direction, the two pendulums oscillate in phase opposition with the angular frequency ω_-. Deflecting only one pendulum generates a coupled oscillation with the angular frequency

$$\omega = \frac{\omega_+ + \omega_-}{2}$$

in which the oscillation energy is transferred back and forth between the two pendulums. The first pendulum comes to rest after a certain time, while the second pendulum simultaneously reaches its greatest amplitude. Then the same process runs in reverse. The time from one pendulum stand still to the next is called the beat period T_S. For the corresponding beat frequency, we can say

$$\omega_s = \omega_+ - \omega_-$$

The aim of the experiment P1.5.4.1 is to observe in-phase, phase-opposed and coupled oscillations. The angular frequencies ω_+, ω_-, ω_s and ω are calculated from the oscillation periods T_+, T_-, T_S and T measured using a stopclock and compared with each other.

Coupled pendulum – Recording and evaluating with CASSY (P1.5.4.4)

COUPLING OF OSCILLATIONS

P1.5.4.4
Coupled pendulum – Recording and evaluating with CASSY
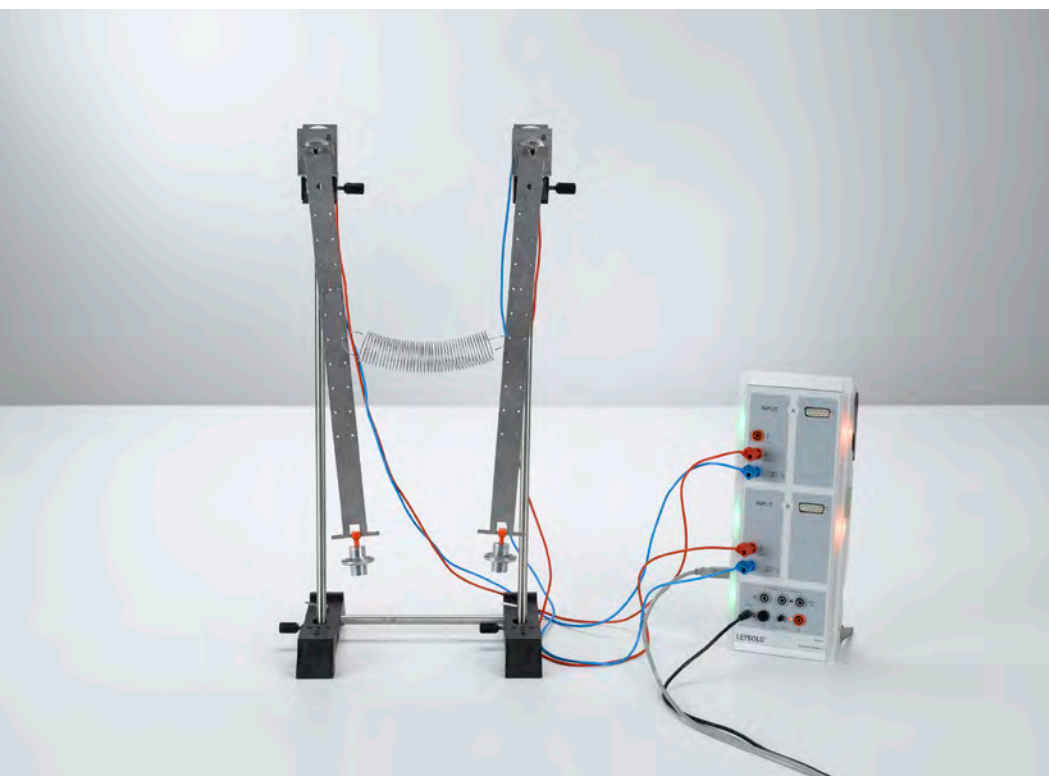
Cat. No.	Description	P1.5.4.4
346 03	Pendulums with axle, pair	1
340 85	Weights, each 50 g, set of 6	1
314 04	Support clip, for plugging in	2
352 10	Helical spring, 3 N/m	1
579 43	Motor and tachogenerator, STE 4/19/50	2
524 013	Sensor-CASSY 2	1
524 220	CASSY Lab 2	1
301 25	Support block	2
301 26	Stand rod 25 cm, 10 mm Ø	1
301 27	Stand rod 50 cm, 10 mm Ø	2
301 21	Stand base MF	2
501 46	Connecting leads 19 A, 100 cm, red/blue, pair	2
	additionally required: PC with Windows XP/Vista/7/8/10 (x86 or x64)	1

Two coupled pendulums swing in experiment P1.5.4.4 in phase with a frequency f_1 when they are deflected from the rest position by the same distance. When the second pendulum is deflected in the opposite direction, the two pendulums oscillate in opposing phase with the frequency f_2. Deflecting only one pendulum generates a coupled oscillation with the frequency

$$f_n = \frac{f_1 + f_2}{2}$$

in which oscillation energy is transferred back and forth between the two pendulums. The first pendulum comes to rest after a certain time, while the second pendulum simultaneously reaches its greatest amplitude. The time from one standstill of a pendulum to the next is called T_s. For the corresponding beat frequency, we can say

$$f_s = |f_1 - f_2|$$

CASSY®

TRANSVERSAL AND LONGITUDINAL WAVES

P1.6.1.3
Investigation of resonance vibrations of the leaf spring model and determination of the wavelength

P1.6.1.4
Production of standing waves on a string and determination of the wavelength

P1.6.1.5
Production of standing waves on a helical spring and determination of the wavelength

Production of standing waves on a helical spring and determination the wavelength (P1.6.1.5)

Cat. No.	Description	P1.6.1.3	P1.6.1.4	P1.6.1.5
346 54	Leaf spring resonance model	1		
587 09	Vibration generator	1	1	1
522 561	Function generator P	1	1	1
311 78	Tape measure 2 m / 1 mm	1	1	
501 33	Connecting lead, 32 A, 100 cm, black	2	2	2
309 50	Demonstration cord		1	
340 921	Pulley Ø 100 mm, plug-in		1	
683 10	Weight, 0.1 kg		1	
683 11	Weight, 0.2 kg		1	
300 01	Stand base, V-shaped, large		2	1
300 44	Stand rod, 100 cm, 12 mm diam.		2	1
301 01	Leybold multiclamp		2	3
301 25	Support block		1	
352 11	Helical spring, 2.7 N/m			1
311 22	Vertical rule			1
300 11	Saddle base			1
300 41	Stand rod, 25 cm, 12 mm Ø			1

A wave is formed when two coupled, oscillating systems sequentially execute oscillations of the same type. The wave can be excited e.g. as a transversal wave on an elastic string or as a longitudinal wave along a helical spring. The propagation velocity of an oscillation state - the phase velocity v - is related to the oscillation frequency f and the wavelength λ through the formula

$$v = \lambda \cdot f$$

When the string or the helical spring is fixed at both ends, reflections occur at the ends. This causes superposing of the "outgoing" and reflected waves. Depending on the string length s, there are certain frequencies at which this superposing of the waves forms stationary oscillation patterns – standing waves. The distance between two oscillation nodes or two antinodes of a standing wave corresponds to one half the wavelength. The fixed ends correspond to oscillation nodes. For a standing wave with n oscillation antinodes, we can say

$$s = n \cdot \frac{\lambda_n}{2}$$

This standing wave is excited with the frequency

$$f_n = n \cdot \frac{v}{2s}$$

In the experiment P1.6.1.3 the leaf spring model is stimulated with different frequencies f and thus examined for resonances. Hence the wavelength λ of the vibrations can be identified.

$$\lambda = \frac{c}{f}$$

c: propagation speed

In the experiment P1.6.1.4 a transversal wave is generated. By moving one end of a string up and down and keeping the other end fixed, a wave is created. The wave will be reflected at the fixed end and runs back on the string. For defined frequencies, certain points will being fixed (nodal) while others (antinodes) oscillate with high amplitude.

In the experiment P1.6.1.5, a longitudinal wave at a helical spring is observed. By moving one end up and down and the other end is fixed, reflects the wave there and runs back. Again for defined frequencies, certain points of the spring remain at rest while others oscillate.

Wavelength, frequency and phase velocity of travelling waves (P1.6.2.1)

Cat. No.	Description	P1.6.2.1	P1.6.2.2
401 20	Wave machine, basic module 1	2	2
401 22	Drive module for wave machine	1	1
401 23	Damping module for wave machine	1	
401 24	Brake unit for wave machine	2	2
521 231	Low-voltage power supply 3/6/9/12 V	1	1
726 890	DC-High Current Power Supply 1…32 V/0…20 A	1	1
313 27	Hand-held stop-watch, 60s/0.2s	1	1
311 78	Tape measure 2 m / 1 mm	1	1
501 451	Connecting leads, 19 A, 50 cm, black, pair	1	1
501 461	Connecting leads 19 A, 100 cm, black, pair	1	1
501 46	Connecting leads 19 A, 100 cm, red/blue, pair	1	1

The "modular wave machine" equipment set enables us to set up a horizontal torsion wave machine, while allowing the size and complexity of the setup within the system to be configured as desired. The module consists of 21 pendulum bodies mounted on edge bearings in a rotating manner around a common axis. They are elastically coupled on both sides of the axis of rotation, so that the deflection of one pendulum propagates through the entire system in the form of a wave.

The aim of the experiment P1.6.2.1 is to explicitly confirm the relationship

$$v = \lambda \cdot f$$

between the wavelength λ, the frequency f and the phase velocity v. A stopclock is used to measure the time t required for any wave phase to travel a given distance s for different wavelengths; these values are then used to calculate the phase velocity

$$v = \frac{s}{t}$$

The wavelength is then "frozen" using the built-in brake, to permit measurement of the wavelength λ. The frequency is determined from the oscillation period measured using the stopclock.

With the experiment P1.6.2.2 it is possible to demonstrate all significant phenomena pertaining to the propagation of linear transversal waves. In particular, these include the excitation of standing waves by means of reflection at a fixed or loose end.
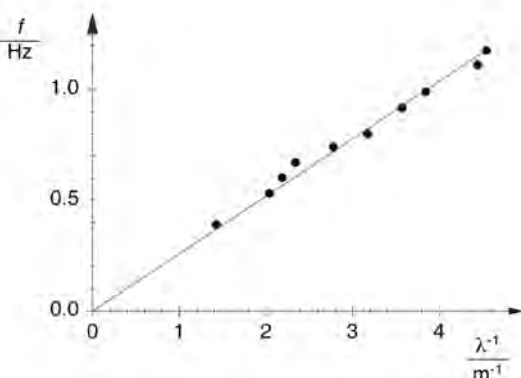
Relationship between the frequency and the wavelength of a propagating wave (P1.6.2.1)

CIRCULARLY POLARIZED WAVES

P1.6.3.1
Investigating circularly polarized string waves in the experiment setup according to Melde

P1.6.3.2
Determining the phase velocity of circularly polarized string waves in the experiment setup according to Melde

Investigating circularly polarized string waves in the experiment setup according to Melde (P1.6.3.1)

Cat. No.	Description	P1.6.3.1	P1.6.3.2
401 03	Vibrating string apparatus	1	1
311 78	Tape measure 2 m / 1 mm	1	1
451 281	Stroboscope		1
315 05	Single-pan suspension balance 311		1

The experiment setup according to Melde generates circularly polarized string waves on a string with a known length s using a motordriven eccentric. The tensioning force F of the string is varied until standing waves with the wavelength

$$\lambda_n = \frac{2s}{n}$$

n: **number of oscillation nodes**

appear.

In the experiment P1.6.3.1, the wavelengths λ_n of the standing string waves are determined for different string lengths s and string masses m at a fixed excitation frequency and plotted as a function of the respective tensioning force F_m. The evaluation confirms the relationship

$$\lambda \propto \sqrt{\frac{F}{m*}}$$

with the mass assignment

$$m* = \frac{m}{s}$$

m: **string mass,** s: **string length**

In the experiment P1.6.3.2, the same measuring procedure is carried out, but with the addition of a stroboscope. This is used to determine the excitation frequency f of the motor. It also makes the circular polarization of the waves visible in an impressive manner when the standing string wave is illuminated with light flashes which have a frequency approximating that of the standard wave. The additional determination of the frequency f enables calculation of the phase velocity c of the string waves using the formula

$$c = \lambda \cdot f$$

as well as quantitative verification of the relationship

$$c = \sqrt{\frac{F}{m*}}$$
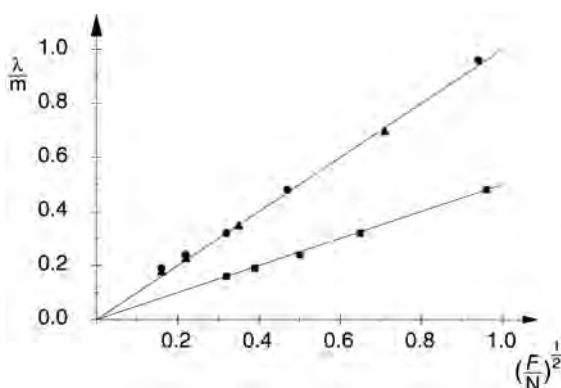
Wavelength λ of string waves as a function of the tension force F, the string length s and string density $m*$ (P1.6.3.1)

Exciting circular and straight water waves (P1.6.4.1)

PROPAGATION OF WATER WAVES

P1.6.4.1
Exciting circular and straight water waves

P1.6.4.2
Huygens' principle in water waves

P1.6.4.3
Propagation of water waves in two different depths

P1.6.4.4
Refraction of water waves

P1.6.4.5
Doppler effect in water waves

P1.6.4.6
Reflection of water waves at a straight obstacle

P1.6.4.7
Reflection of water waves at curved obstacles

Cat. No.	Description	P1.6.4.1	P1.6.4.2	P1.6.4.3	P1.6.4.4–7
401 501	Ripple tank D	1	1	1	1
LDS 00001	Stopwatch, digital	1			
311 78	Tape measure 2 m / 1 mm	1		1	

Fundamental concepts of wave propagation can be explained particularly clearly using water waves, as their propagation can be observed with the naked eye.

The experiment P1.6.4.1 investigates the properties of circular and straight waves. The wavelength λ is measured as a function of each excitation frequency f and these two values are used to calculate the wave velocity

$$v = f \cdot \lambda$$

The aim of the experiment P1.6.4.2 is to verify Huygens' principle. In this experiment, straight waves strike an edge, a narrow slit and a grating. We can observe a change in the direction of propagation, the creation of circular waves and the superposing of circular waves to form one straight wave.

The experiments P1.6.4.3 and P1.6.4.4 aim to study the propagation of water waves in different water depths. A greater water depth corresponds to a medium with a lower refractive index n. At the transition from one "medium" to another, the law of refraction applies:

$$\frac{\sin\alpha_1}{\sin\alpha_2} = \frac{\lambda_1}{\lambda_2}$$

α_1, α_2: angles with respect to axis of incidence in zone 1 and 2

λ_1, λ_2: wavelength in zone 1 and 2

A prism, a biconvex lens and a biconcave lens are investigated as practical applications for water waves.

The experiment P1.6.4.5 observes the Doppler effect in circular water waves for various speeds u of the wave exciter.

The experiments P1.6.4.6 and P1.6.4.7 examine the reflection of water waves. When straight and circular waves are reflected at a straight wall, the "wave beams" obey the law of reflection. When straight waves are reflected by curved obstacles, the originally parallel wave rays travel in either convergent or divergent directions, depending on the curvature of the obstacle. We can observe a focusing to a focal point, respectively a divergence from an apparent focal point, just as in optics.
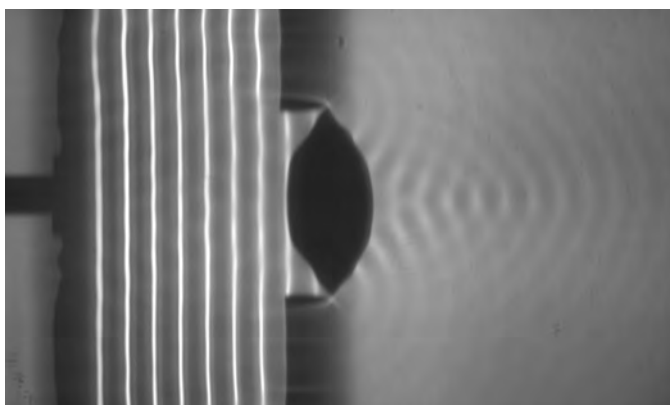
Convergent beam path behind a biconvex lens (P1.6.4.4)

LEYBOLD®

INTERFERENCE OF WATER WAVES

P1.6.5.1
Two-beam interference of water waves

P1.6.5.2
Lloyd's experiment on water waves

P1.6.5.3
Diffraction of water waves at a slit and at an obstacle

P1.6.5.4
Diffraction of water waves at a multiple slit

P1.6.5.5
Standing water waves in front of a reflecting barrier

Two-beam interference of water waves (P1.6.5.1)

Cat. No.	Description	P1.6.5.1–4	P1.6.5.5
401 501	Ripple tank D	1	1
311 78	Tape measure 2 m / 1 mm		1

Experiments on the interference of waves can be carried out in an easily understandable manner, as the diffraction objects can be seen and the propagation of the diffracted waves observed with the naked eye.

In the experiment P1.6.5.1, the interference of two coherent circular waves is compared with the diffraction of straight waves at a double slit. The two arrangements generate identical interference patterns.

The experiment P1.6.5.2 reproduces Lloyd's experiment on generating two-beam interference. A second wave coherent to the first is generated by reflection at a straight obstacle. The result is an interference pattern which is equivalent to that obtained for two-beam interference with two discrete coherent exciters.

In the experiment P1.6.5.3, a straight wave front strikes slits and obstacles of various widths. A slit which has a width of less than the wavelength acts like a point-shaped exciter for circular waves. If the slit width is significantly greater than the wavelength, the straight waves pass the slit essentially unaltered. Weaker, circular waves only propagate in the shadow zones behind the edges. When the slit widths are close to the wavelength, a clear diffraction pattern is formed with a broad main maximum flanked by lateral secondary maxima. When the waves strike an obstacle, the two edges of the obstacle act like excitation centers for circular waves. The resulting diffraction pattern depends greatly on the width of the obstacle.

The object of the experiment P1.6.5.4 is to investigate the diffraction of straight water waves at double, triple and multiple slits which have a fixed slit spacing d. This experiment shows that the diffraction maxima become more clearly defined for an increasing number n of slits. The angles at which the diffraction maxima are located remain the same.

The experiment P1.6.5.5 demonstrates the generation of standing waves by means of reflection of water waves at a wall arranged parallel to the wave exciter. The standing wave demonstrates points at regular intervals at which the crests and troughs of the individual traveling and reflected waves cancel each other out. The oscillation is always greatest at the midpoint between two such nodes.
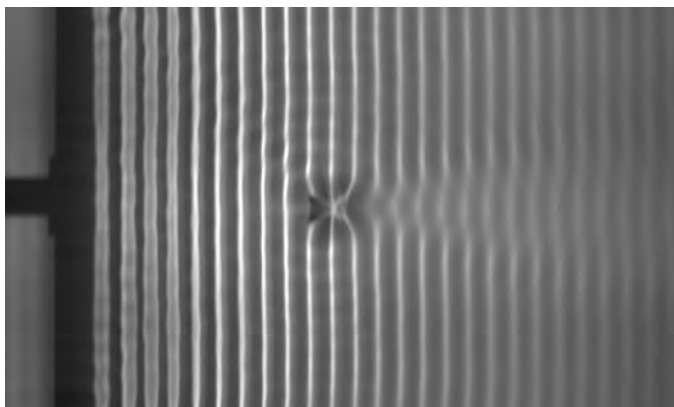
Diffraction of water waves at a narrow obstacle (P1.6.5.3)

SOUND WAVES

P1.7.1.2
Acoustic beats
– Displaying on the oscilloscope

P1.7.1.3
Acoustic beats
– Recording with CASSY

Acoustic beats - Recording with CASSY (P1.7.1.3)

Cat. No.	Description	P1.7.1.2	P1.7.1.3
414 72	Resonance tuning forks, pair	1	1
586 26	Multi-purpose microphone	1	1
575 302	Oscilloscope 30 MHz, digital, PT1265	1	
575 35	Adapter, BNC/4 mm, 2-pole	1	
300 11	Saddle base	1	1
524 013	Sensor-CASSY 2		1
524 220	CASSY Lab 2		1
	additionally required: PC with Windows XP/Vista/7/8/10 (x86 or x64)		1

Acoustics is the study of sound and all its phenomena. This discipline deals with both the generation and the propagation of sound waves.

The experiment P1.7.1.2 demonstrates the wave nature of sound. Here, acoustic beats are investigated as the superposing of two sound waves generated using tuning forks with slightly different frequencies f_1 and f_2 . The beat signal is received via a microphone and displayed on the oscilloscope. By means of further (mis-) tuning of one tuning fork by moving a clamping screw, the beat frequency

$$f_s = f_2 - f_1$$

is increased, and the beat period (i. e. the interval between two nodes of the beat signal)

$$T_S = \frac{1}{f_S}$$

is reduced.

In the experiment P1.7.1.3, the acoustic beats are recorded and evaluated via the CASSY computer interface device. The individual frequencies f_1 and f_2, the oscillation frequency f and the beat frequency f_S are determined automatically and compared with the calculated values

$$f = \frac{f_1 + f_2}{2}$$
$$f_s = f_2 - f_1$$

OSCILLATIONS OF A STRING

P1.7.2.1
Determining the oscillation frequency of a string as a function of the string length and tension
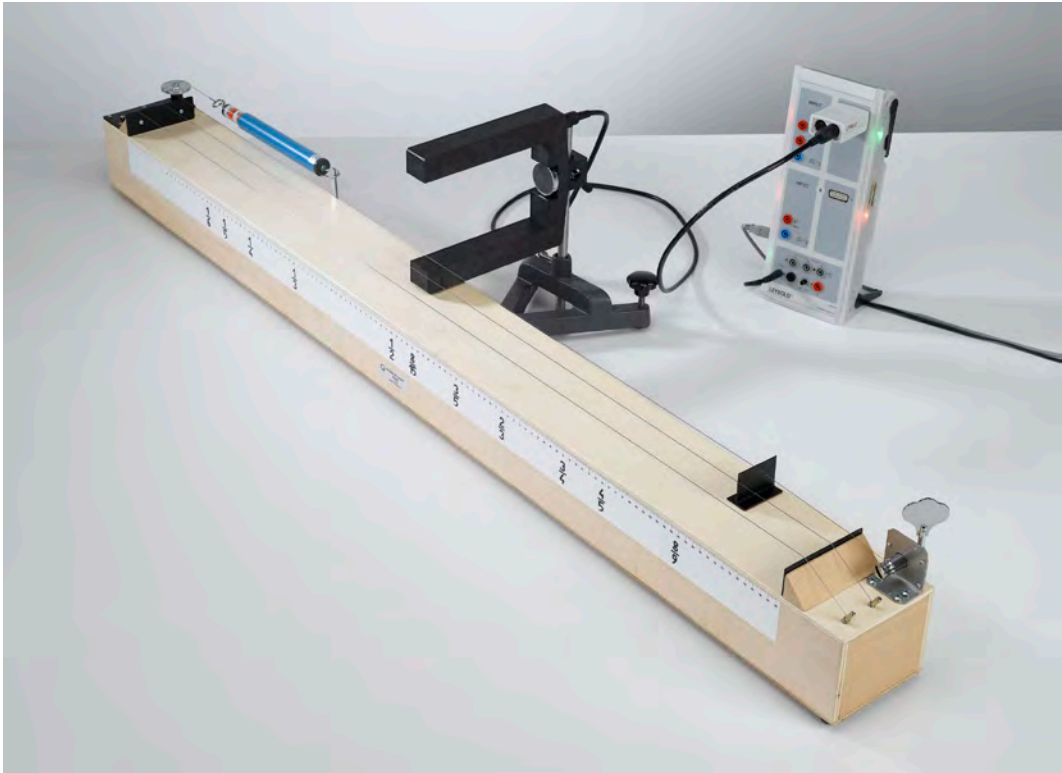
Determining the oscillation frequency of a string as a function of the string length and tension (P1.7.2.1)

Cat. No.	Description	P1.7.2.1
414 01	Monochord	1
314 201	Precision dynamometer, 100.0 N	1
524 013	Sensor-CASSY 2	1
524 220	CASSY Lab 2	1
524 074	Timer S	1
337 46	Fork-type light barrier	1
501 16	Multi-core cable, 6-pole, 1.5 m	1
300 02	Stand base, V-shaped, small	1
300 41	Stand rod, 25 cm, 12 mm Ø	1
	additionally required: PC with Windows XP/Vista/7/8/10 (x86 or x64)	1

In the fundamental oscillation, the string length s of an oscillating string corresponds to half the wavelength. Therefore, the following applies for the frequency of the fundamental oscillation:

$$f = \frac{c}{2s}$$

where the phase velocity c of the string is given by

$$c = \sqrt{\frac{F}{A \cdot \rho}}$$

F: tensioning force, A: area of cross-section, ρ: density

In the experiment P1.7.2.1, the oscillation frequency of a string is determined as a function of the string length and tensioning force. The measurement is carried out using a forked light barrier and the computer-assisted measuring system CASSY, which is used here as a high-resolution stop-clock. The aim of the evaluation is to verify the relationships

$$f \propto \sqrt{F}$$

and

$$f \propto \frac{1}{s}$$
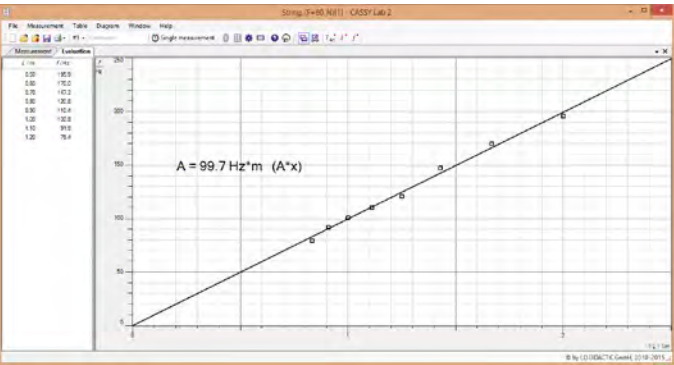
Frequency f as a function of the string length s (P1.7.2.1)

Kundt's tube: determining the wavelength of sound with the cork-powder method (P1.7.3.1)

Cat. No.	Description	P1.7.3.1	P1.7.3.2
413 01	Kundt's tube	1	
460 97	Metal rule, 0.5 m	1	
586 26	Multi-purpose microphone		1
587 08	Broad-band speaker		1
522 621	Function generator S 12		1
587 66	Reflection plate		1
300 11	Saddle base		3
311 78	Tape measure 2 m / 1 mm		1
531 120	Multimeter LDanalog 20		1
501 46	Connecting leads 19 A, 100 cm, red/blue, pair		1

Just like other waves, reflection of sound waves can produce standing waves in which the oscillation nodes are spaced at

$$d = \frac{\lambda}{2}$$

Thus, the wavelength λ of sound waves can be easily measured at standing waves.

The experiment P1.7.3.1 investigates standing waves in Kundt's tube. These standing waves are revealed in the tube using cork powder which is stirred up in the oscillation nodes. The distance between the oscillation nodes is used to determine the wavelength λ.

In the experiment P1.7.3.2, standing sound waves are generated by reflection at a barrier. This setup uses a function generator and a loudspeaker to generate sound waves in the entire audible range. A microphone is used to detect the intensity minima, and the wavelength λ is determined from their spacings.

Determining the wavelength of standing sound waves (P1.7.3.2)

MECHANICS
ACOUSTICS

WAVELENGTH AND VELOCITY OF SOUND

P1.7.3.3
Determining the velocity of sound in air as a function of the temperature

P1.7.3.4
Determining the velocity of sound in gases
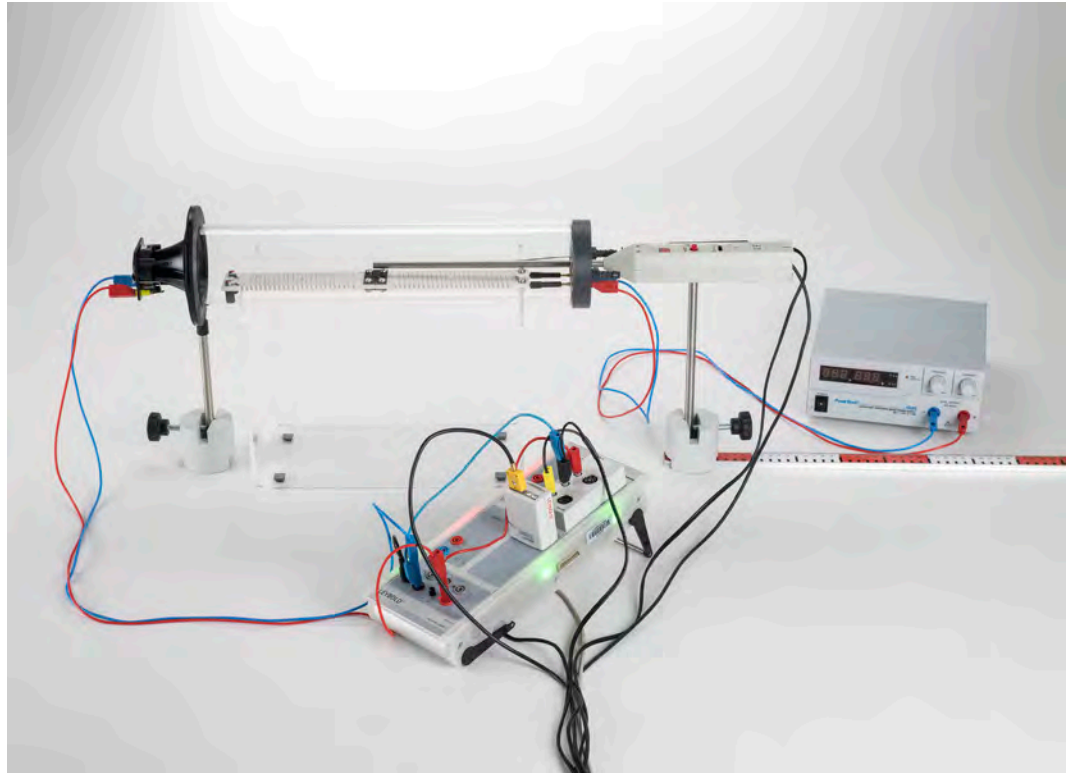
Determining the velocity of sound in air as a function of the temperature (P1.7.3.3)

Cat. No.	Description	P1.7.3.3	P1.7.3.4
413 60	Apparatus for sound velocity	1	1
516 249	Stand for tubes and coils	1	1
587 07	Tweeter	1	1
586 26	Multi-purpose microphone	1	1
524 013	Sensor-CASSY 2	1	1
524 220	CASSY Lab 2	1	1
524 034	Timer box	1	1
524 0673	NiCr-Ni adapter S, type K	1	
529 676	Temperature probe, NiCr-Ni, 1.5 mm, type K	1	
726 890	DC-High Current Power Supply 1...32 V/0...20 A	1	
300 11	Saddle base	2	2
460 97	Metal rule, 0.5 m	1	1
501 44	Connecting leads, 19 A, 25 cm, red/blue, pair	1	1
501 46	Connecting leads 19 A, 100 cm, red/blue, pair	2	1
660 999	Minican pressurised gas canister, carbon dioxide		1
660 984	Minican pressurised gas canister, helium		1
660 985	Minican pressurised gas canister, neon		1
660 980	Fine regulating valve for minican gas canisters		1
667 194	Silicone tubing 7 mm Ø, 1 m		1
604 481	Rubber tubing, 1 m x 4 mm diam., DIN 12865		1
604 510	Tubing connector, 4...15 mm		1
	additionally required: PC with Windows XP/Vista/7/8/10 (x86 or x64)	1	1

Sound waves demonstrate only slight dispersion, i.e. group and phase velocities demonstrate close agreement for propagation in gases. Therefore, we can determine the velocity of sound c as simply the propagation speed of a sonic pulse. In ideal gases, we can say

$$c = \sqrt{\frac{p \cdot \kappa}{\rho}} \quad \text{where} \quad \kappa = \frac{C_p}{C_V}$$

p: pressure, ρ: density, κ: adiabatic coefficient
C_p, C_V: specific heat capacities

The experiment P1.7.3.3 measures the velocity of sound in the air as a function of the temperature ϑ and compares it with the linear function resulting from the temperature-dependency of pressure and density

$$c(\vartheta) = c(0) + 0.6 \cdot \frac{\vartheta}{°C} \frac{m}{s}$$

The value $c(0)$ determined using a best-fit straight line and the literature values $p(0)$ and $\rho(0)$ are used to determine the adiabatic coefficient κ of air according to the formula

$$\kappa = \frac{c(0)^2 \cdot \rho(0)}{p(0)}$$

The experiment P1.7.3.4 determines the velocity of sound c in carbon dioxide and in the inert gases helium and neon. The evaluation demonstrates that the great differences in the velocities of sound of gases are essentially due to the different densities of the gases. The differences in the adiabatic coefficients of the gases are comparatively small.

Determining the velocity of sound in solids (P1.7.3.5)

Cat. No.	Description	P1.7.3.5
413 651	Metal rods, 1.5 m, set of 3	1
300 46	Stand rod, 150 cm, 12 mm diam.	1
587 251	Rochelle salt crystal (piezo-electric element)	1
524 013	Sensor-CASSY 2	1
524 220	CASSY Lab 2	1
301 07	Simple bench clamp	1
501 35	Connecting lead, 32 A, 200 cm, red	1
501 36	Connecting lead, 32 A, 200 cm, blue	1
	additionally required: PC with Windows XP/Vista/7/8/10 (x86 or x64)	1

In solid bodies, the velocity of sound is determined by the modulus of elasticity E and the density ρ. For the velocity of sound in a long rod, we can say

$$c = \sqrt{\frac{E}{\rho}}$$

In the case of solids, measurement of the velocity of sound thus yields a simple method for determining the modulus of elasticity.

The object of the experiment P1.7.3.5 is to determine the velocity of sound in aluminum, copper, brass and steel rods. This measurement exploits the multiple reflections of a brief sound pulse at the rod ends. The pulse is generated by striking the top end of the rod with a hammer, and initially travels to the bottom. The pulse is reflected several times in succession at the two ends of the rod, whereby the pulses arriving at one end are delayed with respect to each other by the time Δt required to travel out and back. The velocity of sound is thus

$$c = \frac{2s}{\Delta t}$$

s: length of rod

To record the pulses, the bottom end of the rod rests on a piezoelectric element which converts the compressive oscillations of the sound pulse into electrical oscillations. These values are recorded using the CASSY system for computer-assisted measured-value recording.

REFLECTION OF ULTRASONIC WAVES

P1.7.4.1
Reflection of planar ultrasonic waves at a plane surface

P1.7.4.2
Principle of an echo sounder

Reflection of planar ultrasonic waves at a plane surface (P1.7.4.1)

Cat. No.	Description	P1.7.4.1	P1.7.4.2
416 002	Ultrasonic transmitter	1	1
416 003	Ultrasonic receiver	1	1
416 014	Generator, 40 kHz	1	1
416 015	AC amplifier	1	1
389 242	Acoustic concave mirror	1	
416 020	Sensor holder for concave mirror	1	
575 302	Oscilloscope 30 MHz, digital, PT1265	1	1
575 24	Screened cable, BNC/4 mm	1	2
460 310	Optical bench, S1 profile, 1 m	2	
460 3151	Swivel joint with protactor scale and clamp	1	
460 3113	Clamp rider with clamp 105/65	2	
587 66	Reflection plate	1	1
300 40	Stand rod, 10 cm, 12 mm diam.	1	
301 27	Stand rod 50 cm, 10 mm Ø	1	
300 41	Stand rod, 25 cm, 12 mm Ø	1	
666 615	Universal bosshead	1	
361 051	Bull's eye spirit level, 14 mm diam.	1	
311 78	Tape measure 2 m / 1 mm	1	
300 42	Stand rod, 47 cm, 12 mm diam.		1
300 11	Saddle base		3
311 02	Metal rule, 1 m		1

The ultrasonic waves are generated by the mechanical oscillations of a piezoelectric body in the transducer. By the same token, ultrasonic waves excite mechanical oscillations in the piezoelectric body.

The aim of the experiment P1.7.4.1 is to confirm the law of reflection "angle of incidence = angle of reflection" for ultrasonic waves. In this setup, an ultrasonic transducer as a point-type source is set up in the focal point of a concave reflector, so that flat ultrasonic waves are generated. The flat wave strikes a plane surface at an angle of incidence α and is reflected there. The reflected intensity is measured at different angles using a second transducer. The direction of the maximum reflected intensity is defined as the angle of reflection β.

The experiment P1.7.4.2 utilizes the principle of an echo sounder to determine the velocity of sound in the air, as well as to determine distances. An echo sounder emits pulsed ultrasonic signals and measures the time at which the signal reflected at the boundary surface is received. For the sake of simplicity, the transmitter and receiver are set up as nearly as possible in the same place. When the velocity of sound c is known, the time difference t between transmission and reception can be used in the relationship

$$c = \frac{2s}{t}$$

to determine the distance s to the reflector or, when the distance is known, the velocity of sound.
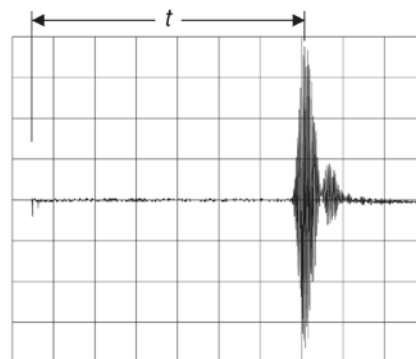
Echo sounder signal (P1.7.4.2)

INTERFERENCE OF ULTRASONIC WAVES

P1.7.5.1
Beating of ultrasonic waves

P1.7.5.2
Interference of two ultrasonic beams

P1.7.5.3
Diffraction of ultrasonic waves at a single slit

P1.7.5.4
Diffraction of ultrasonic waves at a double slit, a multiple slit and a grating

Beating of ultrasonic waves (P1.7.5.1)

Cat. No.	Description	P1.7.5.1	P1.7.5.2	P1.7.5.3	P1.7.5.4
416 002	Ultrasonic transmitter	2	2	1	1
416 003	Ultrasonic receiver	1	1	1	1
416 015	AC amplifier	1	1	1	1
416 014	Generator, 40 kHz	2	1	1	1
575 302	Oscilloscope 30 MHz, digital, PT1265	1			
575 24	Screened cable, BNC/4 mm	1			
300 11	Saddle base	3	2		
311 902	Rotating platform with motor drive		1	1	1
524 013	Sensor-CASSY 2		1	1	1
524 220	CASSY Lab 2		1	1	1
524 031	Current source box		1	1	1
521 546	DC Power Supply 0...16 V/0...5 A		1	1	1
501 031	Connecting lead, protected, 8 m, screened		1	1	1
311 78	Tape measure 2 m / 1 mm		1	1	
300 01	Stand base, V-shaped, large		1	1	1
300 02	Stand base, V-shaped, small		1	1	1
300 41	Stand rod, 25 cm, 12 mm Ø		1	1	1
300 42	Stand rod, 47 cm, 12 mm diam.		1	1	1
301 01	Leybold multiclamp		1	1	1
500 424	Connecting lead 19 A, 50 cm, black		1	1	1
501 46	Connecting leads 19 A, 100 cm, red/blue, pair		2	2	2
416 020	Sensor holder for concave mirror			1	1
416 021	Frame with holder			1	1
416 030	Grating and slit for ultrasonics experiments			1	1
389 242	Acoustic concave mirror			1	1
	additionally required: PC with Windows XP/Vista/7/8/10 (x86 or x64)		1	1	1

Experiments on the interference of waves can be carried out in a comprehensible manner using ultrasonic waves, as the diffraction objects are visible with the naked eye. In addition, it is not difficult to generate coherent sound beams.

In the experiment P1.7.5.1, beating of ultrasonic waves is investigated using two transducers which are operated using slightly different frequencies f_1 and f_2. The signal resulting from the superposing of the two individual signals is interpreted as an oscillation with the periodically varying amplitude

$$A(t) \sim \cos\left(\pi \cdot (f_2 - f_1) \cdot t\right)$$

The beat frequency f_S determined from the period T_S between two beat nodes and compared with the difference $f_2 - f_1$.

In the experiment P1.7.5.2, two identical ultrasonic transducers are operated by a single generator. These transducers generate two coherent ultrasonic beams which interfere with each other. The interference pattern corresponds to the diffraction of flat waves at a double slit when the two transducers are operated in phase. The measured intensity is thus greatest at the diffraction angles α where

$$\sin\alpha = n \cdot \frac{\lambda}{d} \quad \text{where} \quad n = 0, \pm 1, \pm 2, \ldots$$

λ: wavelength, d: spacing of ultrasonic transducers

The experiments P1.7.5.3 and P1.7.5.4 use an ultrasonic transducer as a point-shaped source in the focal point of a concave reflector. The flat ultrasonic waves generated in this manner are diffracted at a single slit, a double slit and a multiple slit. An ultrasonic transducer and the slit are mounted together on the turntable for computer-assisted recording of the diffraction figures. This configuration measures the diffraction at a single slit for various slit widths b and the diffraction at multiple slits and gratings for different numbers of slits N.

CASSY®

ACOUSTIC DOPPLER EFFECT

P1.7.6.1
Investigating the Doppler effect with ultrasonic waves

P1.7.6.2
Investigating the Doppler effect with ultrasonic waves - Recording and evaluating with CASSY
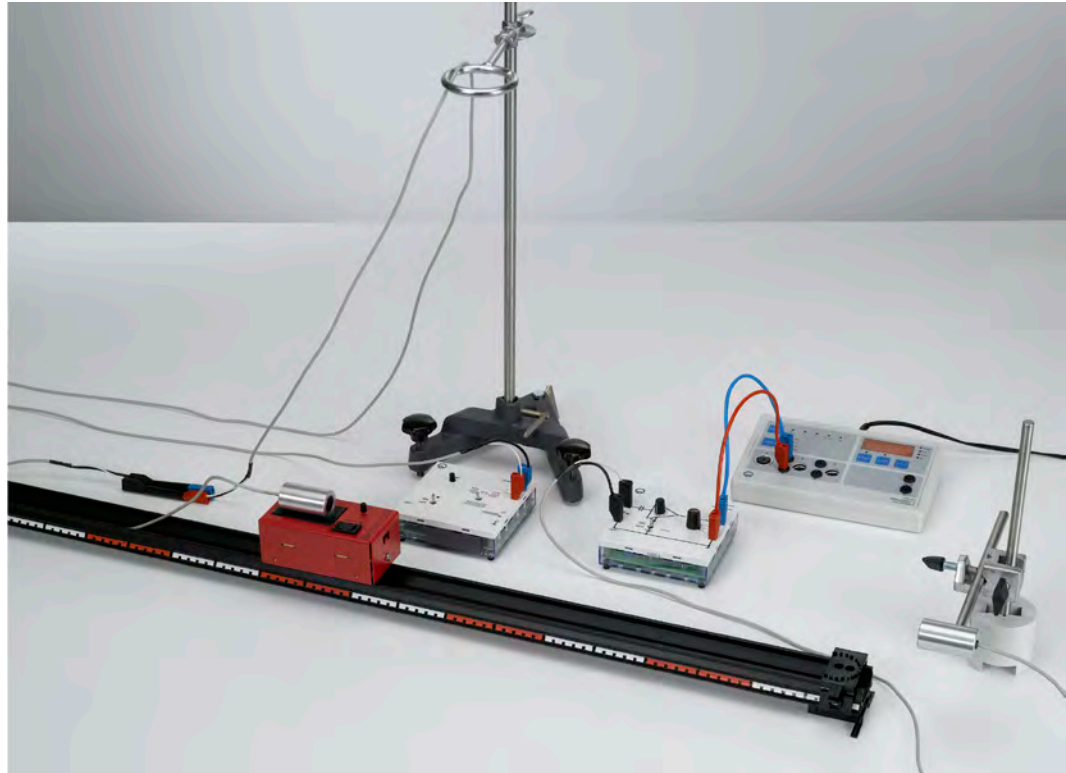
Investigating the Doppler effect with ultrasonic waves (P1.7.6.1)

Cat. No.	Description	P1.7.6.1	P1.7.6.2
416 002	Ultrasonic transmitter	1	1
416 003	Ultrasonic receiver	1	1
416 015	AC amplifier	1	1
416 014	Generator, 40 kHz	1	1
501 031	Connecting lead, protected, 8 m, screened	1	1
501 644	Two-way adapters, black, set of 6	1	1
685 44	Battery 1.5 V (AA)	2	2
337 07	Trolley with electric drive	1	1
460 81	Precision metal rail, 100 cm	2	2
460 85	Rail connector	1	1
460 88	Feet for metal rails, pair	1	1
460 95	Clamp rider	2	2
416 031	Accessories for acoustic Doppler effect	1	1
575 471	Counter S	1	
575 302	Oscilloscope 30 MHz, digital, PT1265	1	
575 24	Screened cable, BNC/4 mm	1	
313 27	Hand-held stop-watch, 60s/0.2s	1	
300 02	Stand base, V-shaped, small	1	2
300 11	Saddle base	1	1
300 41	Stand rod, 25 cm, 12 mm Ø	1	1
300 43	Stand rod, 75 cm, 12 mm diam.	1	1
301 01	Leybold multiclamp	1	2
608 100	Stand ring with clamp, 70 mm diam.	1	1
501 46	Connecting leads 19 A, 100 cm, red/blue, pair	1	1
524 013	Sensor-CASSY 2		1
524 220	CASSY Lab 2		1
524 034	Timer box		1
524 073	Laser motion sensor S		1
300 40	Stand rod, 10 cm, 12 mm diam.		1
	additionally required: PC with Windows XP/Vista/7/8/10 (x86 or x64)		1

The change in the observed frequency for a relative motion of the transmitter and receiver with respect to the propagation medium is called the acoustic Doppler effect. If the transmitter with the frequency f_0 moves at a velocity v relative to a receiver at rest, the receiver measures the frequency

$$f = \frac{f_0}{1 - \dfrac{v}{c}}$$

c: velocity of sound

If, on the other hand, the receiver moves at a velocity v relative to a transmitter at rest, we can say

$$f = f_0 \cdot \left(1 + \frac{v}{c}\right)$$

The change in the frequeny $f - f_0$ is proportional to the frequency f_0. Investigation of the acoustic Doppler effect on ultrasonic waves thus suggests itself.

In the experiment P1.7.6.1, two ultrasonic transducers are used as the transmitter and the receiver. One transducer is mounted on a measuring trolley with electric drive, while the other transducer is at rest on the lab bench. The frequency of the received signal is measured using a digital counter. To determine the speed of the transducer in motion, the time Δt which the measuring trolley requires to traverse the measuring distance is measured using a stopclock.

In the experiment P1.7.6.2, two ultrasonic transducers are used as the transmitter and the receiver. One transducer is mounted on a measuring trolley with electric drive, while the other transducer is at rest on the lab bench. The frequency of the received signal is measured using a high-resolution digital counter inside the CASSY. The Sensor-CASSY 2 in conjunction with the laser motion sensor S measures the speed of the transducer in motion.
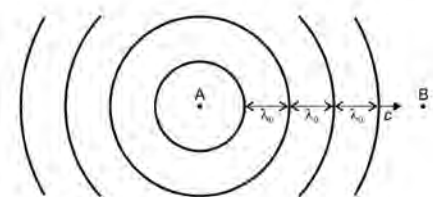
Propagation of sound with the sound source and the observer at rest (P1.7.6.1)

Fourier analysis of an electric oscillator circuit (P1.7.7.3)
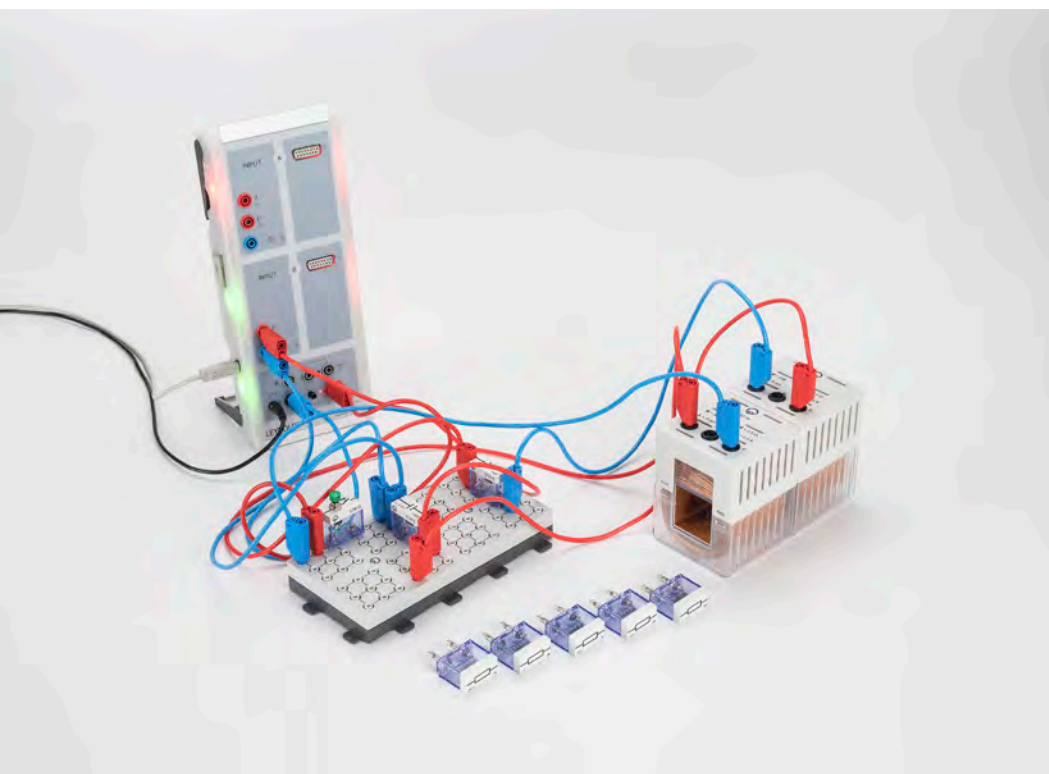
FOURIER ANALYSIS

P1.7.7.1
Investigating fast Fourier transforms: simulation of Fourier analysis and Fourier synthesis

P1.7.7.2
Fourier analysis of the periodic signals of a function generator

P1.7.7.3
Fourier analysis of an electric oscillator circuit

P1.7.7.4
Fourier analysis of sounds

Cat. No.	Description	P1.7.7.1	P1.7.7.2	P1.7.7.3	P1.7.7.4
524 220	CASSY Lab 2	1	1	1	1
522 621	Function generator S 12		1		
524 013	Sensor-CASSY 2			1	1	1
501 45	Connecting lead 19 A, 50 cm, red/blue, pair		1		
562 14	Coil, 500 turns			2	
578 15	Capacitor, 1 µF, STE 2/19			2	
579 10	Push button (NO), STE 2/19			1	
577 19	Resistor, 1 Ω, STE 2/19			1	
577 20	Resistor, 10 Ω, STE 2/19			1	
577 21	Resistor 5.1 Ohm, STE 2/19			1	
577 23	Resistor, 20 Ω, STE 2/19			1	
577 32	Resistor 100 Ohm, STE 2/19			1	
576 81	Plug-in board safety socket, 20/10			1	
500 621	Safety connecting lead 50 cm, red			4	
500 622	Safety connecting lead 50 cm, blue			4	
524 059	Microphone S				1
	additionally required: PC with Windows XP/Vista/7/8/10 (x86 or x64)	1	1	1	1

Fourier analysis and synthesis of sound waves are important tools in acoustics. Thus, for example, knowing the harmonics of a sound is important for artificial generation of sounds or speech.

The experiments P1.7.7.1 and 1.7.7.2 investigate Fourier transforms of periodic signals which are either numerically simulated or generated using a function generator.

In the experiment P1.7.7.3, the frequency spectrum of coupled electric oscillator circuits is compared with the spectrum of an uncoupled oscillator circuit. The Fourier transform of the uncoupled, damped oscillation is a Lorentz curve

$$L(f) = L_0 \cdot \frac{\gamma^2}{(f - f_0)^2 + \gamma^2}$$

in which the width increases with the ohmic resistance of the oscillator circuit. The Fourier-transformed signal of the coupled oscillator circuits shows the split into two distributions lying symmetrically around the uncoupled signal, with their spacing depending on the coupling of the oscillator circuits.

The aim of the experiment P1.7.7.4 is to conduct Fourier analysis of sounds having different tone colors and pitches. As examples, the vowels of the human voice and the sounds of musical instruments are analyzed. The various vowels of a language differ mainly in the amplitudes of the harmonics. The fundamental frequency f_0 depends on the pitch of the voice. This is approx. 200 Hz for high-pitched voices and approx. 80 Hz for low-pitched voices. The vocal tone color is determined by variations in the excitation of the harmonics. The audible tones of musical instruments are also determined by the excitation of harmonics.
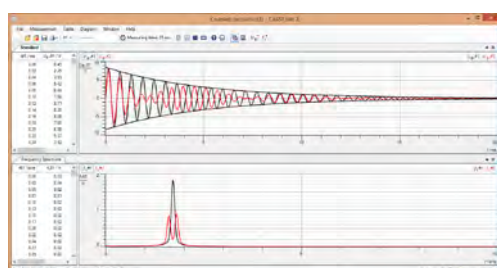
Coupled oscillator circuit with its Fourier transform (P1.7.7.3)

ULTRASOUND IN MEDIA

P1.7.8.1
Determination of the velocity of sound in liquids – standing ultrasonic waves as optical grating

Determination of the velocity of sound in liquids - standing ultrasonic waves as optical grating (P1.7.8.1)

Cat. No.	Description	P1.7.8.1
417 11	Ultrasound generator, 4 MHz	1
460 32	Optical bench with standardised profile, 1 m	1
460 374	Optics rider, 90/50	5
471 791	Diode laser, 635 nm, 1 mW	1
460 02	Lens in frame, f=50 mm	1
460 25	Prism table	1
477 02	Plate glass cell (cuvette), 50 x 100 x 50 mm	1
460 380	Cantilever arm	1
382 35	Thermometer, -10...+50 °C/0.1 K	1
300 41	Stand rod, 25 cm, 12 mm Ø	1
301 01	Leybold multiclamp	1
441 531	Screen	1
675 3410	Water, pure, 5 l	1
672 1210	Glycerin, 99 %, 250 ml	1
671 9740	Ethanol, denaturated, 250 ml	1
673 5700	Sodium chloride 250 g	1

Todays acousto-optic modulators are important building parts for telecommunication and rely on the interaction of sound and light in media. Density variations created by ultrasound are used as diffraction gratings.

Experiment P1.7.8.1 measures the wavelength of a standing ultrasound wave in different liquids. The local variation of density in the liquid is made visible on screen by geometrical projection.

In addition the experiment demonstrates the classic Debye-Sears-Effect, i.e. the diffraction of laser light by a phase grating created by ultrasound in a liquid. This is the basic principle of an acusto-optic modulator.
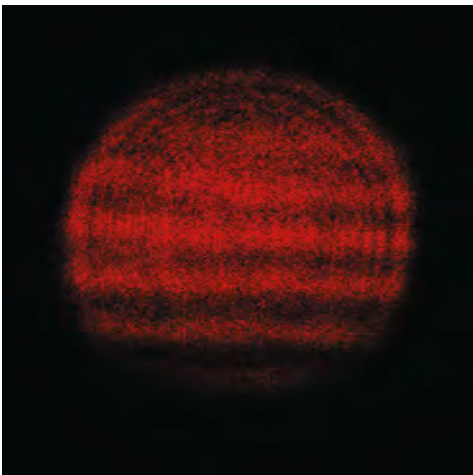
Projection of a standing wave pattern in water (P1.7.8.1)

Confirming Archimedes' principle (P1.8.2.1)

BOUYANCY

P1.8.2.1
Confirming Archimedes' principle

P1.8.2.2
Measuring the buoyancy as a function of the immersion depth

Cat. No.	Description	P1.8.2.1	P1.8.2.2
362 02	Archimedes' cylinder	1	1
315 011	Hydrostatic balance	1	
315 31	Set of weights, 10 mg to 200 g	1	
664 111	Beaker, DURAN, 100 ml, tall	1	
664 113	Beaker, DURAN, 250 ml, tall	1	1
672 1210	Glycerin, 99 %, 250 ml	1	1
671 9720	Ethanol, denaturated, 1 l	1	1
314 141	Precision dynamometer, 1 N		1
311 78	Tape measure 2 m / 1 mm		1

Archimedes' principle states that the buoyancy force F acting on any immersed body corresponds to the weight G of the displaced liquid.

The experiment P1.8.2.1 verifies Archimedes' principle. In this experiment, a hollow cylinder and a solid cylinder which fits snugly inside it are suspended one beneath the other on the beam of a balance. The deflection of the balance is compensated to zero. When the solid cylinder is immersed in a liquid, the balance shows the reduction in weight due to the buoyancy of the body in the liquid. When the same liquid is filled in the hollow cylinder the deflection of the balance is once again compensated to zero, as the weight of the filled liquid compensates the buoyancy.

In the experiment P1.8.2.2, the solid cylinder is immersed in various liquids to the depth h and the weight

$$G = \rho \cdot g \cdot A \cdot h$$

ρ: density, g: gravitational acceleration, A: cross-section

of the displaced liquid is measured as the buoyancy F using a precision dynamo-meter. The experiment confirms the relationship

$$F \sim \rho$$

As long as the immersion depth is less than the height of the cylinder, we can say:

$$F \sim h$$

At greater immersion depths the buoyancy remains constant.

Measuring the buoyancy as a fuction of the immersion depth (P1.8.2.2)

VISCOSITY

P1.8.3.1
Assembling a falling-ball viscosimeter to determine the viscosity of viscous fluids

Assembling a falling-ball viscosimeter to determine the viscosity of viscous fluids (P1.8.3.1)

Cat. No.	Description	P1.8.3.1
379 001	Guinea-and-feather apparatus	1
336 21	Holding magnet	1
352 54	Steel ball, 16 mm	1
336 25	Holding magnet adapter with a release mechanism	1
575 471	Counter S	1
510 48	Magnets, 35 mm Ø, pair	1
300 01	Stand base, V-shaped, large	1
300 41	Stand rod, 25 cm, 12 mm Ø	1
300 44	Stand rod, 100 cm, 12 mm diam.	1
301 01	Leybold multiclamp	1
301 11	Clamp with jaw clamp	1
311 78	Tape measure 2 m / 1 mm	1
672 1210	Glycerin, 99 %, 250 ml	6
590 08	Measuring cylinder 100 ml	1*
311 54	Precision vernier callipers	1*
OHC R221	Compact Balance CR221, 220 g : 0.1 g	1*

* additionally recommended

The falling-ball viscometer is used to determine the viscosity of liquids by measuring the falling time of a ball. The substance under investigation is filled in the vertical tube of the viscosimeter, in which a ball falls through a calibrated distance. The resulting falling time t is a measure of the dynamic viscosity η of the liquid according to the equation

$$\eta = K \cdot (\rho_1 - \rho_2) \cdot t$$

ρ_2: density of the liquid under study

whereby the constant K and the ball density ρ_1 may be read from the test certificate of a commercially available viscosimeter.

The object of the experiment P1.8.3.1 is to set up a falling-ball viscosimeter and to study this measuring method, using the viscosity of glycerine as an example.

WWW.LD-DIDACTIC.COM

Falling-ball viscosimeter: measuring the viscosity of sugar solutions as a function of the concentration (P1.8.3.2)

VISCOSITY

P1.8.3.2
Falling-ball viscosimeter: measuring the viscosity of sugar solutions as a function of the concentration

P1.8.3.3
Falling-ball viscosimeter: measuring the viscosity of Newtonian liquids as a function of the termperature

Cat. No.	Description	P1.8.3.2	P1.8.3.3
665 906	Höppler falling ball viscometer	1	1
313 27	Hand-held stop-watch, 60s/0.2s	1	1
666 7681	Circulation thermostat SC 100-S5P		1
667 194	Silicone tubing 7 mm Ø, 1 m		2
675 3410	Water, pure, 5 l		2

The experiment P1.8.3.2 investigates the relationship between viscosity and concentration using concentrated sugar solutions at room temperature.

In the experiment P1.8.3.3, the temperature regulation chamber of the viscosimeter is connected to a circulation thermostat to measure the dependency of the viscosity of a Newtonian fluid (e. g. olive oil) on the temperature.

VISCOSITY

P1.8.3.4
Hagen-Poiseuille Law

Hagen-Poiseuille Law (P1.8.3.4)

Cat. No.	Description	P1.8.3.4
665 195	Capillary tube, 300 mm x 5 mm, 0.4 mm diam.	1
665 196	Capillary tube, 300 mm x 8 mm, 2 mm diam.	1
665 205	Capillary tube, 300 mm x 8 mm, 0,8 mm diam.	1
667 510	Capillary tube	1
460 21	Holder for plug-in elements	1
590 02	Small clip plug	2
LDS 00001	Stopwatch, digital	1
382 21	Stirring thermometer -10...+110 °C	1
311 02	Metal rule, 1 m	1
362 05	Discharge vessel	1
665 752	Measuring cylinder 25 ml, with plastic base	1
608 160	Mohr clip, 50 mm	1
665 227	Connector, straight, 4 ... 8 mm diam.	1
667 194	Silicone tubing 7 mm Ø, 1 m	1
667 197	Silicone tubing, 4 mm diam., 1 m	1
300 01	Stand base, V-shaped, large	1
300 41	Stand rod, 25 cm, 12 mm Ø	1
300 44	Stand rod, 100 cm, 12 mm diam.	1
301 09	Bosshead S	2
648 01	Storage tray S8-FN	1
675 3400	Water, pure, 1 l	1
460 135	Ocular with scale	1*
460 317	Optical bench, S1 profile, 0.5 m	1*
460 312	Clamp rider with clamp 45/35	2*

* additionally recommended

For a Newtonian liquid (i.e. laminar case) the volume flow rate J and the pressure difference Δp are related by the Hagen-Poiseuille law:

$$J = \frac{\pi \cdot \Delta p \cdot r^4}{8 \cdot \eta \cdot L}$$

η: Viscosity of the liquid,

L: Length of the cappillary tube,

r: radius of the capillary tube

In the experiment P1.8.3.4 the Hagen-Poiseuille law can be verified by using several kind of capillary tubes and various effective level differences to get variant pressure difference.

Measuring the surface tension using the „break-away" method (P1.8.4.1)

SURFACE TENSION

P1.8.4.1
Measuring the surface tension using the „break-away" method

P1.8.4.2
Measuring the surface tension using the „break-away" method - Recording and evaluating with CASSY

Cat. No.	Description	P1.8.4.1	P1.8.4.2
367 46	Surface tension determination device	1	1
664 175	Crystallisation dish, 95 mm diam., 300 ml	1	1
314 111	Precision dynamometer, 0.1 N	1	
311 53	Vernier callipers	1	1
300 76	Laboratory stand II	1	1
300 02	Stand base, V-shaped, small	1	1
300 43	Stand rod, 75 cm, 12 mm diam.	1	
301 08	Clamp with hook	1	
671 9740	Ethanol, denaturated, 250 ml	1	1
675 3400	Water, pure, 1 l	1	1
524 060	Force sensor S, ±1N		1
524 005W	Mobile-CASSY 2 WiFi		1
300 42	Stand rod, 47 cm, 12 mm diam.		1
301 01	Leybold multiclamp		1

To determine the surface tension σ of a liquid, a metal ring is suspended horizontally from a precision dynamometer or a force sensor. The metal ring is completely immersed in the liquid, so that the entire surface is wetted. The ring is then slowly pulled out of the liquid, drawing a thin sheet of liquid behind it. The liquid sheet tears when the tensile force exceeds a limit value

$$F = \sigma \cdot 4\pi \cdot R$$

R: edge radius

The experiments P1.8.4.1 and P1.8.4.2 determines the surface tension of water and ethanol. It is shown that water has a particularly high surface tension in comparison to other liquids (literature value for water: 0.073 Nm^{-1}, for ethanol: 0.022 Nm^{-1}).

INTRODUCTORY EXPERIMENTS ON AERODYNAMICS

P1.8.5.1
Static pressure and determination of the volume flow with a Venturi tube – Measuring the pressure with the precision manometer

P1.8.5.3
Determining the wind speed with a Prandtl pressure probe – Measuring the pressure with the precision manometer

P1.8.5.4
Static pressure and determination of the volume flow with a Venturi tube – Measuring the pressure with a pressure sensor and CASSY

P1.8.5.6
Determining the wind speed with a Prandtl pressure probe – Measuring the pressure with a pressure sensor and CASSY

Static pressure and determination of the volume flow with a Venturi tube - Measuring the pressure with the precision manometer (P1.8.5.1)

Cat. No.	Description	P1.8.5.1	P1.8.5.3	P1.8.5.4	P1.8.5.6
373 041	Suction and pressure fan	1	1	1	1
373 091	Venturi tube with multimanoscope	1		1	
373 10	Precision manometer	1	1		
300 02	Stand base, V-shaped, small	2	1	1	
300 41	Stand rod, 25 cm, 12 mm Ø	1		1	
300 42	Stand rod, 47 cm, 12 mm diam.	1	1		
301 01	Leybold multiclamp	1		1	
391 151	Manometer fluid 100 ml	1	1		
373 13	Prandtl pressure probe		1		1
524 005W	Mobile-CASSY 2 WiFi			1	1
524 066	Pressure sensor S, ±70 hPa			1	1

The study of aerodynamics relies on describing the flow of air through a tube using the continuity equation and the Bernoulli equation. These state that regardless of the cross-section A of the tube, the volume flow

$$\dot{V} = v \cdot A$$

v: flow speed

and the total pressure

$$p_0 = p + p_s \quad \text{where} \quad p_s = \frac{\rho}{2} \cdot v^2$$

p: static pressure, p_s: dynamic pressure, ρ: density of air

remain constant as long as the flow speed remains below the speed of sound.

Note: In the experiments P1.8.5.1 and P1.8.5.3, the precision manometer is used to measure pressures. In addition to a pressure scale, it is provided with a further scale which indicates the flow speed directly when measuring with the pressure head sensor. In the experiments P1.8.5.4 and P1.8.5.6 the pressure is measured with a pressure sensor and recorded using the universal measuring instrument Mobile-CASSY.

In order to verify these two equations, the static pressure in a Venturi tube is measured for different cross-sections in the experiments P1.8.5.1 and P1.8.5.4. The static pressure decreases in the reduced cross-section, as the flow speed increases here. These experiments use the Venturi tube to measure the volume flow, too. Using the pressure difference $\Delta p = p_2 - p_1$ between two points with known cross-sections A_1 and A_2, we obtain

$$v_1 \cdot A_1 = \sqrt{\frac{2 \cdot \Delta p \cdot A_2^2}{\rho \cdot \left(A_2^2 - A_1^2\right)}}$$

The experiments P1.8.5.3 and P1.8.5.6 aims to determine flow speeds. Here, dynamic pressure (also called the "pressure head") is measured using the pressure head sensor according to *Prandtl* as the difference between the total pressure and the static pressure, and this value is used to calculate the speed at a known density ρ.

CASSY®

MEASURING AIR RESISTANCE

P1.8.6.1
Air resistance as a function of the wind speed and body shape
- Measuring the wind speed with the precision manometer

P1.8.6.3
Pressure curve on an airfoil profile
- Measuring the pressure with the precision manometer

P1.8.6.4
Air resistance as a function of the wind speed and body shape
- Measuring the wind speed with a pressure sensor and CASSY

P1.8.6.6
Pressure curve on an airfoil profile
- Measuring the pressure with a pressure sensor and CASSY

Air resistance as a function of the wind speed and body shape - Measuring the wind speed with the precision manometer (P1.8.6.1)

Cat. No.	Description	P1.8.6.1	P1.8.6.3	P1.8.6.4	P1.8.6.6
373 041	Suction and pressure fan	1	1	1	1
373 06	Open aerodynamics working section	1	1	1	1
373 071	Aerodynamics accessories 1	1		1	
373 075	Measurement trolley for wind tunnel	1		1	
373 14	Sector dynamometer, 0.65 N	1		1	
373 13	Prandtl pressure probe	1	1	1	1
373 10	Precision manometer	1	1		
300 02	Stand base, V-shaped, small	1	2	1	1
300 11	Saddle base	1		1	
300 43	Stand rod, 75 cm, 12 mm diam.	1			
391 151	Manometer fluid 100 ml	1	1		
373 70	Air foil model		1		1
300 42	Stand rod, 47 cm, 12 mm diam.		1	1	
524 005W	Mobile-CASSY 2 WiFi			1	1
524 066	Pressure sensor S, ±70 hPa			1	1

A flow of air exercises a force F_W on a body in the flow which is parallel to the direction of the flow; this force is called the air resistance. This force depends on the flow speed v, the cross-section A of the body perpendicular to the flow direction and the shape of the body. The influence of the body shape is described using the so-called drag coefficient c_W, whereby the air resistance is determined as:

$$F_w = c_w \cdot \frac{\rho}{2} \cdot v^2 \cdot A$$

Note: In the experiments P1.8.6.1 and P1.8.6.3, the precision manometer is used to measure pressures. In addition to a pressure scale, it is provided with a further scale which indicates the flow speed directly when measuring with the pressure head sensor. In the experiments P1.8.6.4 and P1.8.6.6 the pressure is measured with a pressure sensor and recorded using the universal measuring instrument Mobile-CASSY.

The experiments P1.8.6.1 and P1.8.6.4 examines the relationship between the air resistance and the flow speed using a circular disk. The flow speed is measured using a Prandtl pressure probe and the air resistance with a dynamometer. The experiment determines the drag coefficient c_w for various flow bodies with equal cross-sections.

The aim of the experiments P1.8.6.3 and P1.8.6.6 is to measure the static pressure p at various points on the underside of an airfoil profile. The measured curve not only illustrates the air resistance, but also explains the lift acting on the airfoil.

MEASUREMENTS IN A WIND TUNNEL

P1.8.7.1
Measurement of airfoils in a wind tunnel

P1.8.7.3
Verifying the Bernoulli equation
– Measuring with the precision manometer

P1.8.7.4
Verifying the Bernoulli equation
– Measuring with a pressure sensor and CASSY

Measurement of airfoils in a wind tunnel (P1.8.7.1)

Cat. No.	Description	P1.8.7.1	P1.8.7.3	P1.8.7.4
373 12	Wind tunnel	1	1	1
373 041	Suction and pressure fan	1	1	1
373 075	Measurement trolley for wind tunnel	1	1	1
373 08	Aerodynamics accessories 2	1		
373 14	Sector dynamometer, 0.65 N	1		
373 13	Prandtl pressure probe		1	1
373 10	Precision manometer		1	
391 151	Manometer fluid 100 ml		1	
524 005W	Mobile-CASSY 2 WiFi			1
524 066	Pressure sensor S, ±70 hPa			1

The wind tunnel provides a measuring configuration for quantitative experiments on aerodynamics that ensures an airflow which has a constant speed distribution with respect to both time and space. Among other applications, it is ideal for measurements on the physics of flight.

In the experiment P1.8.7.1, the air resistance f_W and the lift F_A of an airfoil are measured as a function of the angle of attack α of the airfoil against the direction of flow. In a polar diagram, F_W is graphed as a function of F_A with the angle of attack α as the parameter. From this polar diagram, we can read e.g. the optimum angle of attack. In the experiment, the students also perform comparable measurements on airfoils of their own design. The aim is to determine what form an airfoil must have to obtain the smallest possible quotient F_W / F_A at a given angle of attack α.

The experiments P1.8.7.3 and P1.8.7.4 verify the Bernoulli equation. The difference between the total pressure and the static pressure is measured as a function of the cross-section, whereby the cross-section of the wind tunnel is gradually reduced by means of a built-in ramp. If we assume that the continuity equation applies, the cross-section A provides a measure of the flow speed v due to

$$v = \frac{v_0 \cdot A_0}{A}$$

v_0: flow speed at cross-section A_0

The experiment verifies the following relationship, which follows from the Bernoulli equation:

$$\varnothing p \sim \frac{1}{A^2}$$

Verifying the Bernoulli equation - Measuring with a pressure sensor and Mobile-CASSY (P1.8.7.4)

CASSY®

P2 HEAT

P2 HEAT

THERMAL EXPANSION OF SOLIDS

P2.1.1.2
Thermal expansion of solids
– Measuring using the expansion apparatus

P2.1.1.3
Measuring the linear expansion of solids as a function of temperature

P2.1.1.4
Thermal expansion of solids
– Recording and evaluating with CASSY

Thermal expansion of solids - Measuring using the expansion apparatus (P2.1.1.2)

Cat. No.	Description	P2.1.1.2	P2.1.1.3	P2.1.1.4
381 341	Longitudinal expansion apparatus D	1	1	
361 152	Dial gauge with holder	1	1	
382 34	Thermometer, -10...+110 °C/0.2 K	1	1	1
303 28	Steam generator	1		
664 185	Petri dishes	1		
667 194	Silicone tubing 7 mm Ø, 1 m	1	2	1
666 7681	Circulation thermostat SC 100-S5P		1	
675 3410	Water, pure, 5 l		2	
381 332	Aluminium tube, 44 cm x 8 mm diam.			1
381 333	Iron tube, 44 cm x 8 mm diam.			1
667 2545	Rubber stopper with hole, 17...23 mm Ø			1
664 248	Erlenmeyer flask, Boro 3.3, 50 ml, narrow neck			1
665 226	Connector, straight, 6/8 mm Ø			1
686 53	Round tin with cap			1
524 013	Sensor-CASSY 2			1
524 220	CASSY Lab 2			1
524 082	Rotary motion sensor S			1
311 78	Tape measure 2 m / 1 mm			1
301 21	Stand base MF			2
301 27	Stand rod 50 cm, 10 mm Ø			2
301 09	Bosshead S			2
666 615	Universal bosshead			1
666 555	Universal clamp 0...80 mm			1
666 573	Stand ring with stem 100 mm Ø			1
666 685	Wire gauze 160 mm x 160 mm			1
666 711	Butane gas burner			1
666 712ET3	Butane cartridge, 190 g, set of 3			1
	additionally required: PC with Windows XP/Vista/7/8/10 (x86 or x64)			1

The relationship between the length s and the temperature ϑ of a solid body is approximately linear:

$$s = s_0 \cdot (1 + \alpha \cdot \vartheta)$$

s_0: length at 0 °C, ϑ: temperature in °C

The linear expansion coefficient α is determined by the material of the solid body. We can conduct measurements on this topic using e.g. thin tubes through which hot water or steam is flowing.

The experiment P2.1.1.2 measures the increase in length of various tube samples between room temperature and steam temperature using the expansion apparatus. The effective length s_0 of each tube can be defined as 200, 400 or 600 mm.

In the experiment P2.1.1.3, a circulation thermostat is used to heat the water, which flows through various tube samples. The expansion apparatus measures the change in the lengths of the tubes as a function of the temperature ϑ.

In the experiment P2.1.1.4, steam is channeled through different tube samples. The thermal expansion is measured with a rotary motion sensor.

THERMAL EXPANSION
OF LIQUIDS

P2.1.2.1
Determination of volumetric expansion coefficient of liquids

P2.1.2.2
Determination of volumetric expansion coefficient of liquids - Measuring with Mobile-CASSY

Determination of volumetric expansion coefficient of liquids - Measuring with Mobile-CASSY (P2.1.2.2)

Cat. No.	Description	P2.1.2.1	P2.1.2.2
382 15	Dilatometer	1	1
382 34	Thermometer, -10...+110 °C/0.2 K	1	
666 767	Hotplate, 1500 W, 180 mm Ø	1	1
664 104	Beaker, DURAN, 400 ml, squat	1	1
315 05	Single-pan suspension balance 311	1	1
300 02	Stand base, V-shaped, small	1	1
300 42	Stand rod, 47 cm, 12 mm diam.	1	1
301 01	Leybold multiclamp	2	2
666 555	Universal clamp 0...80 mm	2	2
671 9720	Ethanol, denaturated, 1 l	1	1
524 005W	Mobile-CASSY 2 WiFi		1

In general, liquids expand more than solids when heated. The relationship between the Volume V and the temperature ϑ of a liquid is approximately linear here:

$$V = V_0 \cdot \left(1 + \gamma \cdot \vartheta\right)$$

V_0: volume at 0 °C, ϑ: temperature in °C

When determining the volumetric expansion coefficient γ, it must be remembered that the vessel in which the liquid is heated also expands.

In the experiments P2.1.2.1 and P2.1.2.2 the volumetric expansion coefficients of water and ethanol are determined using a volume dilatometer made of glass. An attached riser tube with a known cross-section is used to measure the change in volume. i.e. the change in volume is determined from the rise height of the liquid.

In the experiment P2.1.2.2 the temperature is measured with a temperature sensor and Mobile-CASSY.

Determination of volumetric expansion coefficient of liquids (P2.1.2.1)

CASSY®

THERMAL ANOMALY OF WATER

P2.1.3.1
Investigation of the density maximum of water

P2.1.3.2
Investigation of the density maximum of water
– Measuring with Mobile-CASSY

Investigation of the density maximum of water – Measuring with Mobile-CASSY (P2.1.3.2)

| Cat. No.	Description	P2.1.3.1	P2.1.3.2
667 505	Anomaly of water apparatus	1	1
382 35	Thermometer, -10...+50 °C/0.1 K	1	
666 8451	Magnetic stirrer	1	1
602 725	Laboratory dish, 140 mm diam., 900 ml	1	1
665 009	Funnel PP 75 mm Ø	1	1
307 66	Tubing (rubber)	1	1
300 42	Stand rod, 47 cm, 12 mm diam.	1	1
666 555	Universal clamp 0...80 mm	1	1
301 01	Leybold multiclamp	1	1
300 02	Stand base, V-shaped, small	1	1
608 100	Stand ring with clamp, 70 mm diam.	1	1
524 005W	Mobile-CASSY 2 WiFi		1

When heated from a starting temperature of 0 °C, water demonstrates an important anomaly: it has a negative volumetric expansion coefficient up to 4 °C, i.e. it contracts when heated. After reaching zero at 4 °C, the volumetric expansion coefficient takes on a positive value. As the density corresponds to the reciprocal of the volume of a quantity of matter, water has a density maximum at 4 °C.

The experiment P2.1.3.1 verifies the density maximum of water by measuring the expansion in a vessel with riser tube. Starting at room temperature, the complete setup is cooled in a constantly stirred water bath to about 1 °C, or alternatively allowed to gradually reach the ambient temperature after cooling in an ice chest or refrigerator. The rise height h is measured as a function of the temperature ϑ. As the change in volume is very slight in relation to the total volume V_0, we obtain the density

$$\rho(\vartheta) = \rho(0°C) \cdot \left(1 - \frac{A}{V_0} \cdot h(\vartheta)\right)$$

A: cross-section of riser tube

The experiment P2.1.3.2 verifies the anomaly of water, too. Temperature is measured with a temperature sensor and Mobile-CASSY.
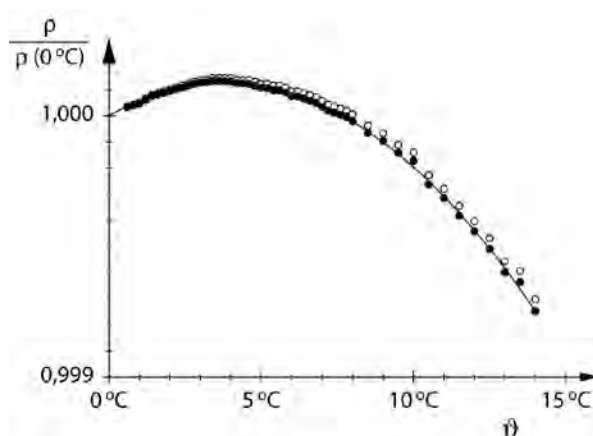
Relative density of water as a function of the temperature (P2.1.3.1-2)

THERMAL CONDUCTIVITY

P2.2.1.1
Determining the thermal conductivity of building materials using the single-plate method

P2.2.1.2
Determining the thermal conductivity of building materials using the heat flux plate principle

P2.2.1.3
Damping temperature fluctuations using multiple-layered walls

Determining the thermal conductivity of building materials using the single-plate method (P2.2.1.1)
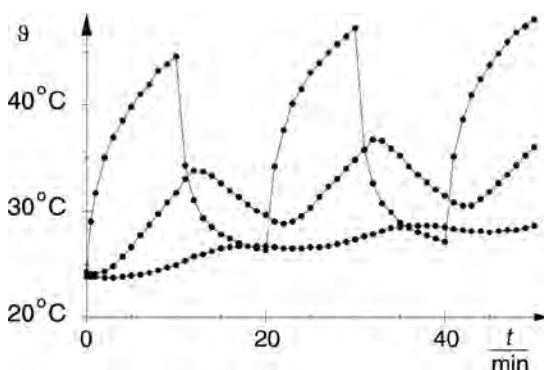
Cat. No.	Description	P2.2.1.1	P2.2.1.2	P2.2.1.3
389 29	Calorimetric chamber	1	1	1
389 30	Building materials for calorimetric chamber	1	1	1
726 890	DC-High Current Power Supply 1...32 V/0...20 A	1	1	1
524 013	Sensor-CASSY 2	1	1	1
524 220	CASSY Lab 2	1	1	1
524 0673	NiCr-Ni adapter S, type K	1	2	2
529 676	Temperature probe, NiCr-Ni, 1.5 mm, type K	2	3	3
500 98	Safety adapter sockets, black, set of 6	1	1	
500 624	Safety connecting lead 50 cm, black	2		2
500 644	Safety connecting lead, 100 cm, black	4	2	
450 641	Halogen lamp 12 V, 50/100W			1
450 63	Halogen bulb 12 V/100 W, G6.35			1
300 11	Saddle base			1
	additionally required: PC with Windows XP/Vista/7/8/10 (x86 or x64)	1	1	1

In the equilibrium state, the heat flow through a plate with the cross-section area A and the thickness d depends on the temperature difference $\vartheta_2 - \vartheta_1$ between the front and rear sides and on the thermal conductivity λ of the plate material:

$$\frac{\Delta Q}{\Delta t} = \lambda \cdot A \cdot \frac{\vartheta_2 - \vartheta_1}{d}$$

The object of the experiments P2.2.1.1 and P2.2.1.2 is to determine the thermal conductivity of building materials. In these experiments, sheets of building materials are placed in the heating chamber and their front surfaces are heated. The temperatures ϑ_1 and ϑ_2 are measured using temperature sensors. The heat flow is determined either from the electrical power of the hot plate or by measuring the temperature using a reference material with known thermal conductivity λ_0 which is pressed against the sheet of the respective building material from behind.

The experiment P2.2.1.3 demonstrates the damping of temperature variations by means of two-layer walls. The temperature changes between day and night are simulated by repeatedly switching a lamp directed at the outside surface of the wall on and off. This produces a temperature "wave" which penetrates the wall; the wall in turn damps the amplitude of this wave. This experiment measures the temperatures ϑ_A on the outer surface, ϑ_Z between the two layers and ϑ_I on the inside as a function of time.

Temperature variations in multi-layer walls (P2.2.1.3)

Efficiency of a solar collector (P2.2.2.1)

P2.2.2.1
Efficiency of a solar collector

Cat. No.	Description	P2.2.2.1
389 50	Solar collector	1
579 220	Water pump, STE 2/50	1
450 73	Halogen lamp 1000 W	1
521 491	AC/DC power supply 0...12 V/3 A	1
524 005W	Mobile-CASSY 2 WiFi	1
524 0673	NiCr-Ni adapter S, type K	1
529 676	Temperature probe, NiCr-Ni, 1.5 mm, type K	2
311 78	Tape measure 2 m / 1 mm	1
300 02	Stand base, V-shaped, small	2
300 41	Stand rod, 25 cm, 12 mm Ø	1
300 42	Stand rod, 47 cm, 12 mm diam.	1
300 43	Stand rod, 75 cm, 12 mm diam.	1
301 01	Leybold multiclamp	2
666 555	Universal clamp 0...80 mm	1
590 06	Plastic beaker	1
604 431	Silicone tubing, 5 mm diam., 1 m	1
604 432	Silicone tubing, 6 mm diam., 1 m	1
604 434	Silicone tubing, 8 mm diam., 1 m	1
665 226	Connector, straight, 6/8 mm Ø	1
501 46	Connecting leads 19 A, 100 cm, red/blue, pair	1

A solar collector absorbs radiant energy to heat the water flowing through it. When the collector is warmer than its surroundings, it loses heat to its surroundings through radiation, convection and heat conductivity. These losses reduce the efficiency

$$\eta = \frac{\Delta Q}{\Delta E}$$

i. e. the ratio of the emitted heat quantity ΔQ to the absorbed radiant energy ΔE.

In the experiment P2.2.2.1, the heat quantity ΔQ emitted per unit of time is determined from the increase in the temperature of the water flowing through the apparatus, and the radiant energy absorbed per unit of time is estimated on the basis of the power of the lamp and its distance from the absorber. The throughput volume of the water and the heat insulation of the solar collector are varied in the course of the experiment.

MIXING TEMPERATURES

P2.3.1.1
Mixing temperature of water

P2.3.1.2
Mixing temperature of water
– Measuring with Mobile-CASSY

Mixing temperature of water - Measuring with Mobile-CASSY (P2.3.1.2)

Cat. No.	Description	P2.3.1.1	P2.3.1.2
384 161	Cover for Dewar vessel	1	1
386 48	Dewar vessel calorimeter, 250 ml	1	1
382 34	Thermometer, -10...+110 °C/0.2 K	1	
315 23	Single-pan suspension balance 610 Tara	1	1
313 27	Hand-held stop-watch, 60s/0.2s	1	
666 767	Hotplate, 1500 W, 180 mm Ø	1	1
664 104	Beaker, DURAN, 400 ml, squat	2	2
524 005W	Mobile-CASSY 2 WiFi		1

When cold water with the temperature ϑ_1 is mixed with warm or hot water having the temperature ϑ_2, an exchange of heat takes place until all the water reaches the same temperature. If no heat is lost to the surroundings, we can formulate the following for the mixing temperature:

$$\vartheta_m = \frac{m_1}{m_1 + m_2}\vartheta_1 + \frac{m_2}{m_1 + m_2}\vartheta_2$$

m_1, m_2: mass of cold and warm water respectively

Thus the mixing temperature ϑ_m is equivalent to a weighted mean value of the two temperatures ϑ_1 and ϑ_2.

The use of the Dewar flask in the experiment P2.3.1.1 essentially prevents the loss of heat to the surroundings. This vessel has a double wall; the intermediate space is evacuated and the interior surface is mirrored. The water is stirred thoroughly to ensure a complete exchange of heat. This experiment measures the mixing temperature ϑ_m for different values for ϑ_1, ϑ_2, m_1 and m_2.

In the experiment P2.3.1.2 the different temperatures are measured with a temperature sensor and Mobile-CASSY.

HEAT CAPACITIES

P2.3.2.1
Determination of specific heat of solids

P2.3.2.2
Determination of specific heat of solids – Measuring with Mobile-CASSY

Determination of specific heat of solids – Measuring with Mobile-CASSY (P2.3.2.2)

Cat. No.	Description	P2.3.2.1	P2.3.2.2
384 161	Cover for Dewar vessel	1	1
386 48	Dewar vessel calorimeter, 250 ml	1	1
382 34	Thermometer, -10...+110 °C/0.2 K	1	
384 34	Heating apparatus	1	1
384 35	Copper shot, 200 g	1	1
384 36	Glass shot, 100 g	1	1
315 76	Lead shot, 200 g	1	1
315 23	Single-pan suspension balance 610 Tara	1	1
303 28	Steam generator	1	1
664 104	Beaker, DURAN, 400 ml, squat	1	1
667 194	Silicone tubing 7 mm Ø, 1 m	1	1
300 02	Stand base, V-shaped, small	1	1
300 42	Stand rod, 47 cm, 12 mm diam.	1	1
301 01	Leybold multiclamp	1	1
666 555	Universal clamp 0...80 mm	1	1
667 614	Heat protective gloves	1	1
524 005W	Mobile-CASSY 2 WiFi		1

When a body is heated or cooled, the absorbed heat capacity ΔQ is proportional to the change in temperature $\Delta \vartheta$ and to the mass m of the body:

$$\Delta Q = c \cdot m \cdot \Delta \vartheta$$

The proportionality factor c, the specific heat capacity of the body, is a quantity which depends on the respective material.

To determine the specific heat capacity in experiment P2.3.2.1, various materials in particle form are weighed, heated in steam to the temperature ϑ_1 and poured into a weighed-out quantity of water with the temperature ϑ_2. After careful stirring, heat exchange ensures that the particles and the water have the same temperature ϑ_m. The heat quantity released by the particles:

$$\Delta Q_1 = c_1 \cdot m_1 \cdot \left(\vartheta_1 \cdot \vartheta_m \right)$$

m_1: mass of particles

c_1: specific heat capacity of particles

is equal to the quantity absorbed by the water

$$\Delta Q_2 = c_2 \cdot m_2 \cdot \left(\vartheta_m \cdot \vartheta_2 \right)$$

m_2: mass of water

The specific heat capacity of water c_2 is assumed as a given. The temperature ϑ_1 corresponds to the temperature of the steam. Therefore, the specific heat quantity c_1 can be calculated from the measurement quantities ϑ_2, ϑ_m, m_1 and m_2.

In the experiment P2.3.2.2 the different temperatures are measured with a temperature sensor and Mobile-CASSY.

CONVERTING MECHANICAL ENERGY INTO HEAT

P2.3.3.1
Converting mechanical energy into heat energy – Recording and evaluating measured values manually

P2.3.3.2
Converting mechanical energy into heat energy – Recording and evaluating with CASSY

Converting mechanical energy into heat energy – Recording and evaluating measured values manually (P2.3.3.1)

Cat. No.	Description	P2.3.3.1	P2.3.3.2
388 00	Equivalent of heat, basic apparatus	1	1
388 01	Water calorimeter	1	1
388 02	Copper-block calorimeter	1	1
388 03	Aluminium-block calorimeter	1	1
388 04	Aluminium-block calorimeter, large	1	1
388 051	Thermometer for calorimeters, +15...35 °C/0.2 K	1	
388 24	Weight, 5 kg	1	1
524 013	Sensor-CASSY 2		1
524 220	CASSY Lab 2		1
524 074	Timer S		1
524 0673	NiCr-Ni adapter S, type K		1
529 676	Temperature probe, NiCr-Ni, 1.5 mm, type K		1
337 46	Fork-type light barrier		1
501 16	Multi-core cable, 6-pole, 1.5 m		1
300 02	Stand base, V-shaped, small		1
301 11	Clamp with jaw clamp		1
300 40	Stand rod, 10 cm, 12 mm diam.		1
300 41	Stand rod, 25 cm, 12 mm Ø		1
301 07	Simple bench clamp		1
	additionally required: PC with Windows XP/Vista/7/8/10 (x86 or x64)		1

Energy is a fundamental quantity of physics. This is because the various forms of energy can be converted from one to another and are thus equivalent to each other, and because the total energy is conserved in the case of conversion in a closed system.

Experiments P2.3.3.1 and P2.3.3.2 show the equivalence of mechanical and heat energy. A hand crank is used to turn various calorimeter vessels on their own axes, and friction on a nylon belt causes them to become warmer. The friction force is equivalent to the weight G of a suspended weight. For n turns of the calorimeter, the mechanical work is thus

$$W_n = G \cdot n \cdot \pi \cdot d$$

d: diameter of calorimeter

This results in an increase in the temperature of the calorimeter which corresponds to the specific heat capacity

$$Q_n = m \cdot c \cdot (\vartheta_n - \vartheta_0)$$

c: specific heat capacity, m: mass,

ϑ_n: temperature after n turns

To confirm the relationship

$$Q_n = W_n$$

the two quantities are plotted together in a diagram.

In the experiment P2.3.3.1 the measurement is conducted and evaluated manually point by point. The experiment P2.3.3.2 takes advantage of the computer-assisted measuring system CASSY.

CASSY®

CONVERTING ELECTRICAL ENERGY INTO HEAT

P2.3.4.1
Converting electrical energy into heat energy - Measuring with a voltmeter and an ammeter

P2.3.4.2
Converting electrical energy into heat energy - Measuring with the joule and wattmeter

P2.3.4.3
Converting electrical energy into heat energy - Measuring with CASSY

P2.3.4.4
Converting electrical energy into heat energy - Measuring with Mobile-CASSY

Converting electrical energy into heat energy - Measuring with Mobile-CASSY (P2.3.4.4)

Cat. No.	Description	P2.3.4.1	P2.3.4.2	P2.3.4.3	P2.3.4.4
384 20	Lid for 250 ml Dewar vessel with heater	1			
386 48	Dewar vessel calorimeter, 250 ml	1			
382 34	Thermometer, -10...+110 °C/0.2 K	1			
313 27	Hand-held stop-watch, 60s/0.2s	1			
664 103	Beaker, DURAN, 250 ml, squat	1			
665 755	Measuring cylinder 250 ml, with plastic base	1			
521 546	DC Power Supply 0...16 V/0...5 A	1			
501 28	Connecting lead, 32 A, 50 cm, black	1			
501 45	Connecting lead 19 A, 50 cm, red/blue, pair	1	1	1	1
388 02	Copper-block calorimeter		1	1	1
388 03	Aluminium-block calorimeter		1	1	1
388 04	Aluminium-block calorimeter, large		1	1	1
388 051	Thermometer for calorimeters, +15...35 °C/0.2 K		1		
388 06	Connecting leads, pair		1	1	1
531 831	Joule and wattmeter		1		
521 491	AC/DC power supply 0...12 V/3 A		1	1	1
524 013	Sensor-CASSY 2			1	
524 220	CASSY Lab 2			1	
524 0673	NiCr-Ni adapter S, type K			1	
529 676	Temperature probe, NiCr-Ni, 1.5 mm, type K			1	
524 005W	Mobile-CASSY 2 WiFi				1
	additionally required: PC with Windows XP/Vista/7/8/10 (x86 or x64)			1	

Just like mechanical energy, electrical energy can also be converted into heat. We can use e.g. a calorimeter vessel with a wire winding to which a voltage is connected to demonstrate this fact. When a current flows through the wire, Joule heat is generated and heats the calorimeter.

The supplied electrical energy

$$W(t) = U \cdot I \cdot t$$

is determined in the experiment P2.3.4.1 by measuring the voltage U, the current I and the time t. This results in a change in the temperature of the calorimeter which corresponds to the specific heat capacity

$$Q(t) = m \cdot c \cdot (\vartheta(t) - \vartheta(0))$$

c: specific heat capacity

m: mass

$\vartheta(t)$: temperature at time t

To confirm the equivalence

$$Q(t) = W(t)$$

the two quantities are plotted together in a diagram.

The supplied electrical energy is determined in the experiment P2.3.4.2 measured directly using the Joule and Wattmeter.

In the experiment P2.3.4.3, the equivalence of electrical energy E_{el} and thermal energy E_{th} is established experimentally. The supplied electrical energy E_{el} is converted into heat E_{th} in the heating coil (or heating spiral). This leads to a temperature rise in the calorimeter (or water, in which the heating spiral is immersed). As the current I and the temperature ϑ are measured simultaneously as functions of the time t, the constant voltage U being known, the two energy forms can be registered quantitatively in units of wattsecond (Ws) and Joule (J) so that their numerical equivalence can be demonstrated experimentally: $E_{el} = E_{th}$.

The supplied electrical energy is determined in the experiment P2.3.4.4 by measuring with the Mobile-CASSY.

CASSY®

LATENT HEAT AND VAPORIZATION HEAT

P2.4.1.1
Determination of specific vaporization heat of water

P2.4.1.2
Determination of specific latent heat of ice

P2.4.1.3
Determination of specific vaporization heat of water - Measuring with Mobile-CASSY

P2.4.1.4
Determination of specific latent heat of ice - Measuring with Mobile-CASSY

Determination of specific vaporization heat of water - Measuring with Mobile-CASSY (P2.4.1.3)

Cat. No.	Description	P2.4.1.1	P2.4.1.2	P2.4.1.3	P2.4.1.4
386 48	Dewar vessel calorimeter, 250 ml	1	1	1	1
384 17	Water separator	1		1	
382 34	Thermometer, -10...+110 °C/0.2 K	1	1		
315 23	Single-pan suspension balance 610 Tara	1	1	1	1
303 28	Steam generator	1		1	
667 194	Silicone tubing 7 mm Ø, 1 m	1		1	
664 104	Beaker, DURAN, 400 ml, squat	1	1	1	1
300 02	Stand base, V-shaped, small	1		1	
300 42	Stand rod, 47 cm, 12 mm diam.	1		1	
301 01	Leybold multiclamp	2		2	
666 555	Universal clamp 0...80 mm	2		2	
303 25	Immersion heater		1		1
590 06	Plastic beaker		1		1
524 005W	Mobile-CASSY 2 WiFi			1	1

When a substance is heated at a constant pressure, its temperature generally increases. When that substance undergoes a phase transition, however, the temperature does not increase even when more heat is added, as the heat is required for the phase transition. As soon as the phase transition is complete, the temperature once more increases with the additional heat supplied. Thus, for example, the specific evaporation heat Q_V per unit of mass is required for evaporating water, and the specific melting heat Q_S per unit of mass is required for melting ice.

To determine the specific evaporation heat Q_V of water, pure steam is fed into the calorimeter in the experiments P2.4.1.1 and P2.4.1.3, in which cold water is heated to the mixing temperature ϑ_m. The steam condenses to water and gives off heat in the process; the condensed water is cooled to the mixing temperature. The experiment measures the starting temperature ϑ_2 and the mass m_2 of the cold water, the mixing temperature ϑ_m and the total mass

$$m = m_1 + m_2$$

By comparing the amount of heat given off and absorbed, we can derive the equation

$$Q_V = \frac{m_1 \cdot c \cdot (\vartheta_m - \vartheta_1) + m_2 \cdot c \cdot (\vartheta_m - \vartheta_2)}{m_1}$$

$\vartheta_1 \approx 100$ °C, c: specific heat capacity of water

In the experiments P2.4.1.2 and P2.4.1.4, pure ice is filled in a calorimeter, where it cools water to the mixing temperature ϑ_m, in order to determine the specific melting heat. The ice absorbs the melting heat and melts into water, which warms to the mixing temperature. Analogously to the experiment P2.4.1.1, we can say for the specific melting heat:

$$Q_S = \frac{m_1 \cdot c \cdot (\vartheta_m - \vartheta_1) + m_2 \cdot c \cdot (\vartheta_m - \vartheta_2)}{m_1}$$

$\vartheta_1 = 0$ °C

In the experiments P2.4.1.1 and P2.4.1.2 the temperature is measured with a thermometer. In the experiments P2.4.1.3 and P2.4.1.4 the temperature is measured with the Mobile-CASSY and the corresponding temperature sensor.

CASSY®

Recording the vapor-pressure curve of water - Pressures up to 50 bar (P2.4.2.2)

MEASURING VAPOR PRESSURE

P2.4.2.1
Recording the vapor-pressure curve of water - Pressures up to 1 bar

P2.4.2.2
Recording the vapor-pressure curve of water - Pressures up to 50 bar

Cat. No.	Description	P2.4.2.1	P2.4.2.2
664 315	Double-necked, round-bottom flask	1	
665 305	Adapter	1	
667 186	Vacuum rubber tubing, 8 mm diam.	1	
665 255	Three-way valve, T-shaped, ST nozzles	1	
378 031	Hose nozzle, DN 16 KF	1	
378 045	Centering ring DN 16 KF	1	
378 050	Clamping ring, DN 10/16 KF	1	
378 701	Leybold high-vacuum grease	1	
524 013	Sensor-CASSY 2	1	
524 220	CASSY Lab 2	1	
524 065	Absolute pressure sensor S, 0...1500 hPa	1	
501 11	Extension cable, 15 pin	1	
688 808	Stand rod, 10 x 223 mm, with thread M6	1	
524 045	Temperature box, NiCr-Ni/NTC	1	
666 216	Temperature probe, NiCr-Ni, fast	1	
300 02	Stand base, V-shaped, small	1	
300 43	Stand rod, 75 cm, 12 mm diam.	1	
666 555	Universal clamp 0...80 mm	1	
301 01	Leybold multiclamp	3	
666 573	Stand ring with stem 100 mm Ø	1	
666 685	Wire gauze 160 mm x 160 mm	1	
666 711	Butane gas burner	1	1
666 712ET3	Butane cartridge, 190 g, set of 3	1	1
667 614	Heat protective gloves	1	1
385 16	High-pressure steam boiler		1
664 109	Beaker, DURAN, 25 ml, squat		1
300 01	Stand base, V-shaped, large		1
667 6131	Safety goggles for wearing over glasses		1
	additionally required: PC with Windows XP/Vista/7/8/10 (x86 or x64)	1	

The vapour pressure p of a liquid-vapor mixture in a closed system depends on the temperature T. Above the critical temperature, the vapor pressure is undefined. The substance is gaseous and cannot be liquefied no matter how high the pressure is. The increase in the vapor-pressure curve $p(T)$ is determined by several factors, including the molar evaporation heat q_v of the substance:

$$T \cdot \frac{dp}{dT} = \frac{q_v}{v_1 - v_2} \text{ (Clausius-Clapeyron)}$$

T: absolute temperature

v_1: molar volume of vapor

v_2: molar volume of liquid

As we can generally ignore v_2 and q_v hardly varies with T, we can derive a good approximation from the law of ideal gases:

$$\ln p = \ln p_0 - \frac{q_v}{R \cdot T}$$

In the experiment P2.4.2.1, the vapor pressure curve of water below the normal boiling point is recorded with the computer-assisted measuring system CASSY. The water is placed in a glass vessel, which was sealed beforehand while the water was boiling at standard pressure. The vapor pressure p is measured as a function of the temperature T when cooling and subsequently heating the system, respectively.

The high-pressure steam apparatus is used in the experiment P2.4.2.2 for measuring pressures of up to 50 bar. The vapor pressure can be read directly from the manometer of this device. A thermometer supplies the corresponding temperature. The measured values are recorded and evaluated manually point by point.

Recording the vapor-pressure curve of water - Pressures up to 1 bar (P2.4.2.1)
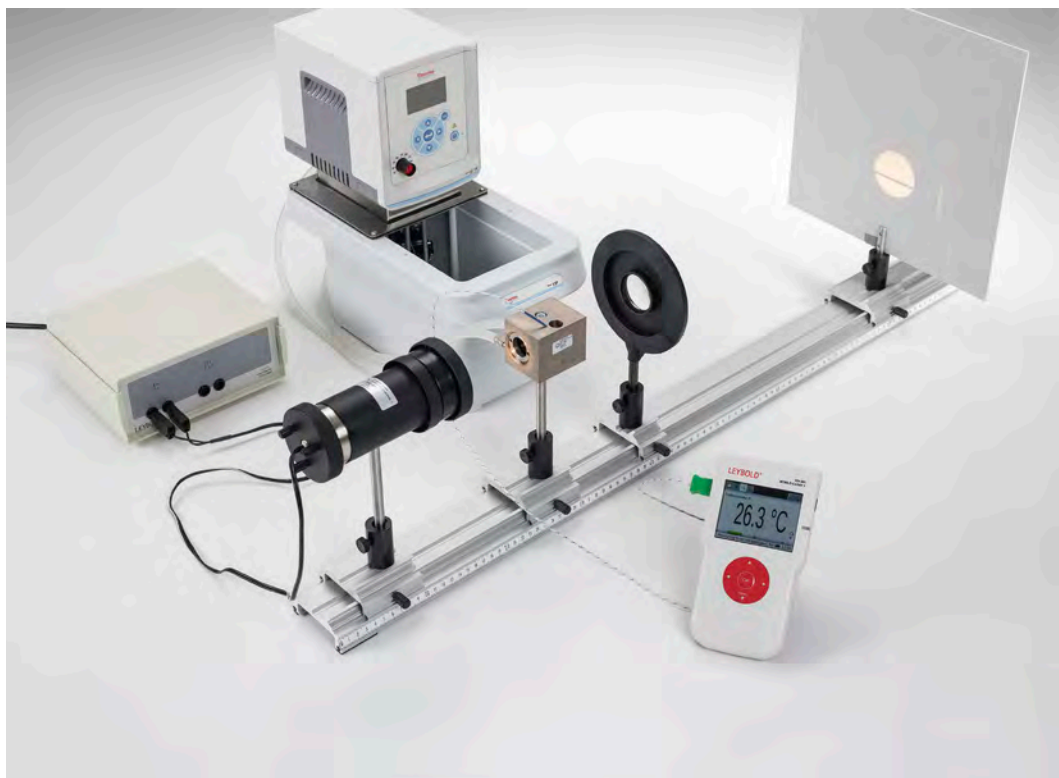
LEYBOLD®

CASSY®

CRITICAL TEMPERATURE

P2.4.3.1
Observing a mixture of liquid and gas at the critical point

P2.4.3.2
Observing a mixture of liquid and gas at the critical point – Measuring with Mobile-CASSY

Observing a mixture of liquid and gas at the critical point - Measuring with Mobile-CASSY (P2.4.3.2)

Cat. No.	Description	P2.4.3.1	P2.4.3.2
371 401	Pressure chamber for demonstrating the critical temperature	1	1
450 60	Lamp housing with cable	1	1
450 511	Bulbs, 6 V/30 W, E14, set of 2	1	1
460 20	Condenser with diaphragm holder	1	1
521 210	Transformer 6/12 V	1	1
460 03	Lens in frame, f=100 mm	1	1
460 310	Optical bench, S1 profile, 1 m	1	1
460 311	Clamp rider with clamp 45/65	2	2
460 312	Clamp rider with clamp 45/35	1	1
382 21	Stirring thermometer -10...+110 °C	1	
303 28	Steam generator	1	
667 194	Silicone tubing 7 mm Ø, 1 m	2	2
664 104	Beaker, DURAN, 400 ml, squat	1	
524 005W	Mobile-CASSY 2 WiFi		1
666 7681	Circulation thermostat SC 100-S5P		1
675 3410	Water, pure, 5 l		2

The critical point of a real gas is defined by the critical pressure p_c, the critical density ρ_c and the critical temperature T_C. Below the critical temperature, the substance is gaseous for a sufficiently great molar volume - it is termed a vapor - and is liquid at a sufficiently small molar volume. Between these extremes, a liquid-vapor mix exists, in which the vapor component increases with the molar volume. As liquid and vapor have different densities, they are separated in a gravitational field. As the temperature rises, the density of the liquid decreases and that of the vapor increases, until finally at the critical temperature both densities have the value of the critical density. Liquid and vapor mix completely, and the phase boundary disappears. Above the critical temperature, the substance is gaseous, regardless of the molar volume.

Experiments P2.4.3.1 and P2.4.3.2 investigate the behavior of sulfur hexafluoride (SF_6) close to the critical temperature. The critical temperature of this substance is T_C = 318.7 K and the critical pressure is p_c = 37.6 bar. The substance is enclosed in a pressure chamber designed so that hot water or steam can flow through the mantle. The dissolution of the phase boundary between liquid and gas while heating the substance, and its restoration during cooling, are observed in projection on the wall. As the system approaches the critical point, the substance scatters short-wave light particularly intensively; the entire contents of the pressure chamber appears red-brown. This critical opalescence is due to the variations in density, which increase significantly as the system approaches the critical point.

Note: The dissolution of the phase boundary during heating can be observed best when the pressure chamber is heated as slowly as possible.

The experiment is feasible with the steam generator and the measurement can be done with a thermometer. Or it is possible to use a circulation thermostat and the Mobile-CASSY with the temperature sensor.
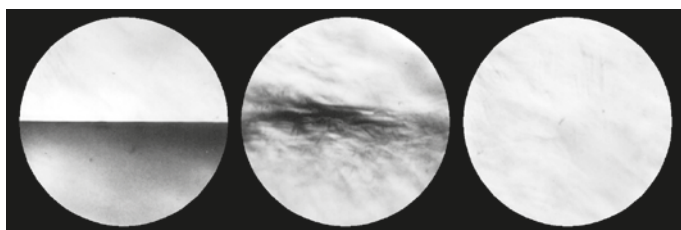
Contents of the pressure chamber: below, at the and above the critical temperatur (P2.4.3.1-2)

Pressure-dependency of the volume of a gas at a constant temperature (Boyle-Mariotte's law) (P2.5.2.1)

GAS LAWS

P2.5.2.1
Pressure-dependency of the volume of a gas at a constant temperature (Boyle-Mariotte's law)

P2.5.2.2
Temperature-dependency of the volume of a gas at a constant pressure (Gay-Lussac's law)

P2.5.2.3
Temperature-dependency of the pressure of a gas at a constant volume (Amontons' law)

Cat. No.	Description	P2.5.2.1	P2.5.2.2	P2.5.2.3
382 00	Gas thermometer	1	1	1
375 58	Hand vacuum pump	1	1	1
524 005W	Mobile-CASSY 2 WiFi	1	1	1
524 064	Pressure sensor S, ±2000 hPa	1		1
665 223ET10	Connector, T-shaped, 8 mm Ø, 10 pieces	1		1
300 02	Stand base, V-shaped, small	1	1	1
300 42	Stand rod, 47 cm, 12 mm diam.	1	1	1
301 11	Clamp with jaw clamp	2	2	2
666 767	Hotplate, 1500 W, 180 mm Ø		1	1
664 103	Beaker, DURAN, 250 ml, squat		1	1

The gas thermometer consists of a glass tube closed at the bottom end, in which a mercury stopper seals the captured air at the top. The volume of the air column is determined from its height and the cross-section of the glass tube. When the pressure at the open end is altered using a hand pump, this changes the pressure on the sealed side correspondingly. The temperature of the entire gas thermo-meter can be varied using a water bath.

In the experiment P2.5.2.1, the air column is maintained at a constant room temperature T. At an external pressure p_0, it has a volume of V_0 bounded by the mercury stopper. The pressure p in the air column is reduced by evacuating air at the open end, and the increased volume V of the air column is determined for different pressure values p. The evaluation confirms the relationship

$$p \cdot V = p_0 \cdot V_0 \quad \text{for} \quad T = \text{const. (Boyle-Mariotte's law)}$$

In the experiment P2.5.2.2, the gas thermometer is placed in a water bath of a specific temperature which is allowed to gradually cool. The open end is subject to the ambient air pressure, so that the pressure in the air column is constant. This experiment measures the volume V of the air column as a function of the temperature T of the water bath. The evaluation confirms the relationship

$$V \propto T \quad \text{for} \quad p = \text{const. (Gay-Lussac's law)}$$

In the experiment P2.5.2.3, the pressure p in the air column is constantly reduced by evacuating the air at the open end so that the volume V of the air column also remains constant as the temperature drops. This experiment measures the pressure p of the air column as a function of the temperature T of the water bath. The evaluation confirms the relationship

$$p \propto T \quad \text{for} \quad V = \text{const. (Amontons' law)}$$
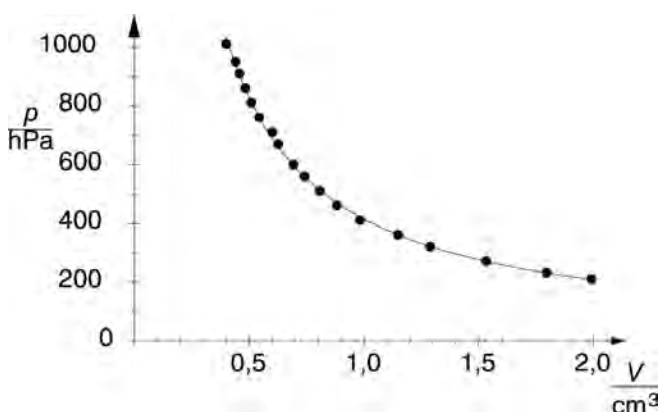
Pressure-dependency of the volume at a constant temperature (P2.5.2.1)

SPECIFIC HEAT OF GASES

P2.5.3.1
Determining the adiabatic exponent c_p/c_V of air according to Rüchardt

P2.5.3.2
Determining the adiabatic exponent c_p/c_V of various gases using the gas elastic resonance apparatus

Determining the adiabatic exponent c_p/c_V of air according to Rüchardt (P2.5.3.1)

Cat. No.	Description	P2.5.3.1	P2.5.3.2
371 051	Oscillation tube with Mariotte's bottle	1	
313 27	Hand-held stop-watch, 60s/0.2s	1	
317 20	Precision aneroid barometer	1	
590 06	Plastic beaker	1	
675 3120	Vaseline, 100 g	1	
371 07	Gas elastic resonance apparatus		1
531 120	Multimeter LDanalog 20		1
522 561	Function generator P		1
300 02	Stand base, V-shaped, small		1
660 980	Fine regulating valve for minican gas canisters		1
660 985	Minican pressurised gas canister, neon		1
660 999	Minican pressurised gas canister, carbon dioxide		1
665 255	Three-way valve, T-shaped, ST nozzles		1
667 194	Silicone tubing 7 mm Ø, 1 m		1
604 481	Rubber tubing, 1 m x 4 mm diam., DIN 12865		1
604 510	Tubing connector, 4...15 mm		1
500 422	Connecting lead 19 A, 50 cm, blue		1
501 46	Connecting leads 19 A, 100 cm, red/blue, pair		1

In the case of adiabatic changes in state, the pressure p and the volume V of a gas demonstrate the relationship

$$p \cdot V^\kappa = \text{const.}$$

whereby the adiabatic exponent is definid as

$$\kappa = \frac{c_p}{c_V}$$

i.e. the ratio of the specific heat capacities c_p and c_V of the respective gas.

The experiment P2.5.3.1 determines the adiabatic exponent of air from the oscillation period of a ball which caps and seals a gas volume in a glass tube, whereby the oscillation of the ball around the equilibrium position causes adiabatic changes in the state of the gas. In the equilibrium position, the force of gravity and the opposing force resulting from the pressure of the enclosed gas are equal. A deflection from the equilibrium position by Δx causes the pressure to change by

$$\Delta p = -\kappa \cdot p \cdot \frac{A \cdot \Delta x}{V}$$

A: cross-section of riser tube

which returns the ball to the equilibrium position. The ball thus oscillates with the frequency

$$f_0 = \frac{1}{2\pi} \cdot \sqrt{\frac{\kappa \cdot p \cdot A^2}{m \cdot V}}$$
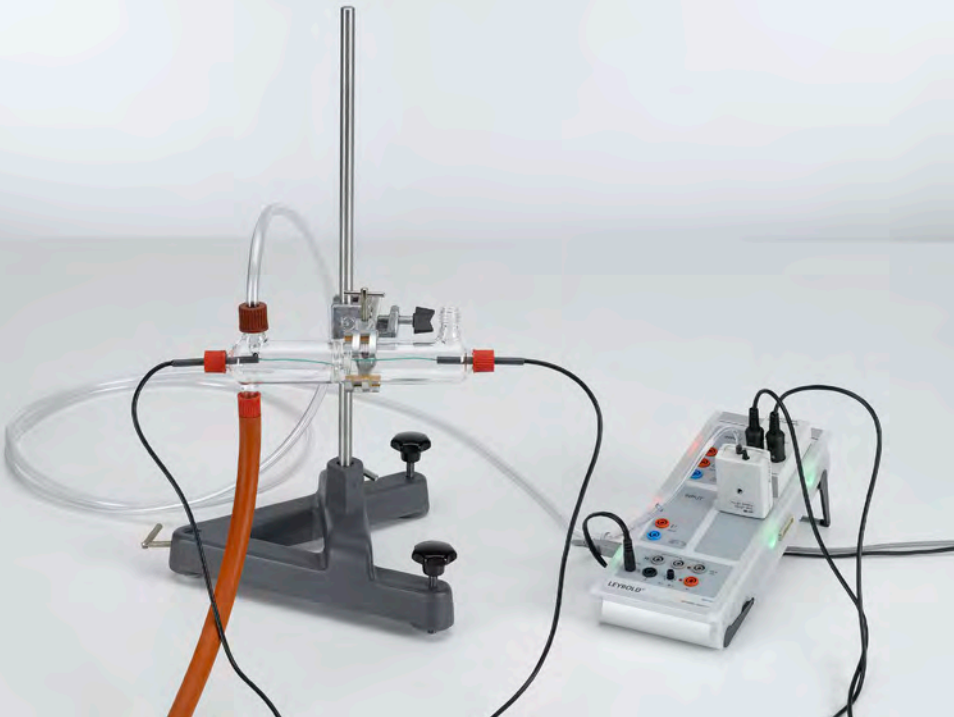
around its equilibrium position.

In the experiment P2.5.3.2, the adiabatic exponent is determined using the gas elastic resonance apparatus. Here, the air column is sealed by a magnetic piston which is excited to forced oscillations by means of an alternating electromagnetic field. The aim of the experiment is to find the characteristic frequency f_0 of the system, i.e. the frequency at which the piston oscillates with maximum amplitude. Other gases, such as carbon dioxide and nitrogen, can alternatively be used in this experiment.

Determining the adiabatic exponent c_p/c_V of various gases using the gas elastic resonance apparatus (P2.5.3.2)

Joule-Thomson effect (P2.5.4.1)

REAL GASES

P2.5.4.1
Joule-Thomson effect

Cat. No.	Description	P2.5.4.1
371 56	Joule-Thomson apparatus	1
524 013	Sensor-CASSY 2	1
524 220	CASSY Lab 2	1
524 045	Temperature box, NiCr-Ni/NTC	1
666 216	Temperature probe, NiCr-Ni, fast	2
524 064	Pressure sensor S, ±2000 hPa	1
667 186	Vacuum rubber tubing, 8 mm diam.	1
667 184	Tubing clamps 10...16 mm, set of 10	1
661 017	Pressure reducing valve for carbon dioxide, helium, argon	1
661 018	Pressure reducing valve for nitrogen	1
664 569	Open jaw spanner for gas canisters	1
661 0082	Carbon dioxide, compressed gas bottle, 2 l	1
661 0083	Nitrogen, compressed gas bottle, 2 l	1
661 021	Table rack for one compressed gas bottle 2 l	1
300 01	Stand base, V-shaped, large	1
300 42	Stand rod, 47 cm, 12 mm diam.	1
301 01	Leybold multiclamp	1
666 555	Universal clamp 0...80 mm	1
	additionally required: PC with Windows XP/Vista/7/8/10 (x86 or x64)	1

The Joule-Thomson effect occurs when a real gas or gas mixture undergoes a change in temperature by reduction of the pressure p. The strength and direction of the change in temperature is described by the Joule-Thomson coefficient μ:

$$\mu_{JT} = \left(\frac{\partial T}{\partial p} \right)_H$$

H : enthalpy = const.

In the experiment P2.5.4.1 the flowing gas is throttled through a membrane and expanded behind it. The volume occupied by the gas can increase behind the obstacle, so the average particle distance is increased. This causes a change in the temperature of the gas. The pressure and the temperature difference before and after the membrane is measured in this experiment.
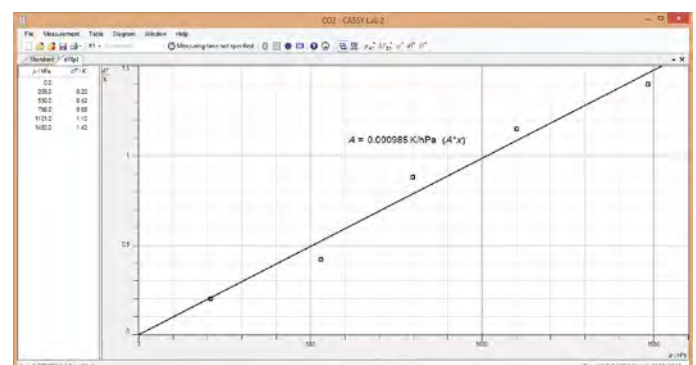
Temperature change against pressure (P2.5.4.1)

CASSY®

HOT–AIR ENGINE:
QUALITATIVE EXPERIMENTS

P2.6.1.5
Operating the hot-air engine P
as a thermal engine, heat pump
and a refrigerator

Operating the hot-air engine P as a thermal engine, heat pump and a refrigerator (P2.6.1.5)

Cat. No.	Description	P2.6.1.5
388 176	Hot-air engine P	1
303 22	Alcohol burner, metal	1
521 231	Low-voltage power supply 3/6/9/12 V	1
524 005W	Mobile-CASSY 2 WiFi	1
524 0673	NiCr-Ni adapter S, type K	1
666 1261	Temperature probe, NiCr-Ni, fast, type K	1
300 11	Saddle base	1
301 01	Leybold multiclamp	1
300 41	Stand rod, 25 cm, 12 mm Ø	1
590 13	Stand rod with bore holes	1
340 89	Coupling plug 4 mm	2
501 861	Crocodile-clips, polished, set of 6	1
501 46	Connecting leads 19 A, 100 cm, red/blue, pair	1

The hot-air engine (invented by *R. Stirling*, 1816) is the oldest thermal engine, along with the steam engine. In greatly simplified terms, its thermodynamic cycle consists of an isothermic compression at low temperature, an isochoric application of heat, an isothermic expansion at high temperature and an isochoric emission of heat. The displacement piston and the working piston are connected to a crankshaft via tie rods, whereby the displacement piston leads the working piston by 90°. When the working piston is at top dead center (a), the displacement piston is moving downwards, displacing the air into the electrically heated zone of the cylinder. Here, the air is heated, expands and forces the working piston downward (b). The mechanical work is transferred to the flywheel. When the working piston is at bottom dead center (c), the displacement piston is moving upwards, displacing the air into the water-cooled zone of the cylinder. The air cools and is compressed by the working cylinder (d). The flywheel delivers the mechanical work required to execute this process.

Depending on the direction of rotation of the crankshaft, the hot-air engine operates as either a heat pump or a refrigerating machine when its flywheel is externally driven. When the displacement piston is moving upwards while the working piston is at bottom dead center, it displaces the air in the top part of the cylinder. The air is then compressed by the working piston and transfers its heat to the cylinder head, i.e. the hot-air motor operates as a heat pump. When run in the opposite direction, the working piston causes the air to expand when it is in the top part of the cylinder, so that the air draws heat from the cylinder head; in this case the hot-air engine operates as a refrigerating machine.

The experiment P2.6.1.5 qualitatively investigates the operation of the hot-air engine P as a thermal engine. The hot-air engine P is a transparent model to show the basics of energy transformation. The hot-air engine P is driven by an alcohol burner and transforms via a small generator the mechanical energy into a voltage which can be measured. In addition, the operation of the hot-air engine P as a heat pump and a refrigerating machine is shown. By variing the speed of the electric motor, i.e. the mechanical power supplied to the hot-air engine P, the impact on heating or refrigerating power is observed.

Frictional losses in the hot-air engine (calorific determination) (P2.6.2.1)
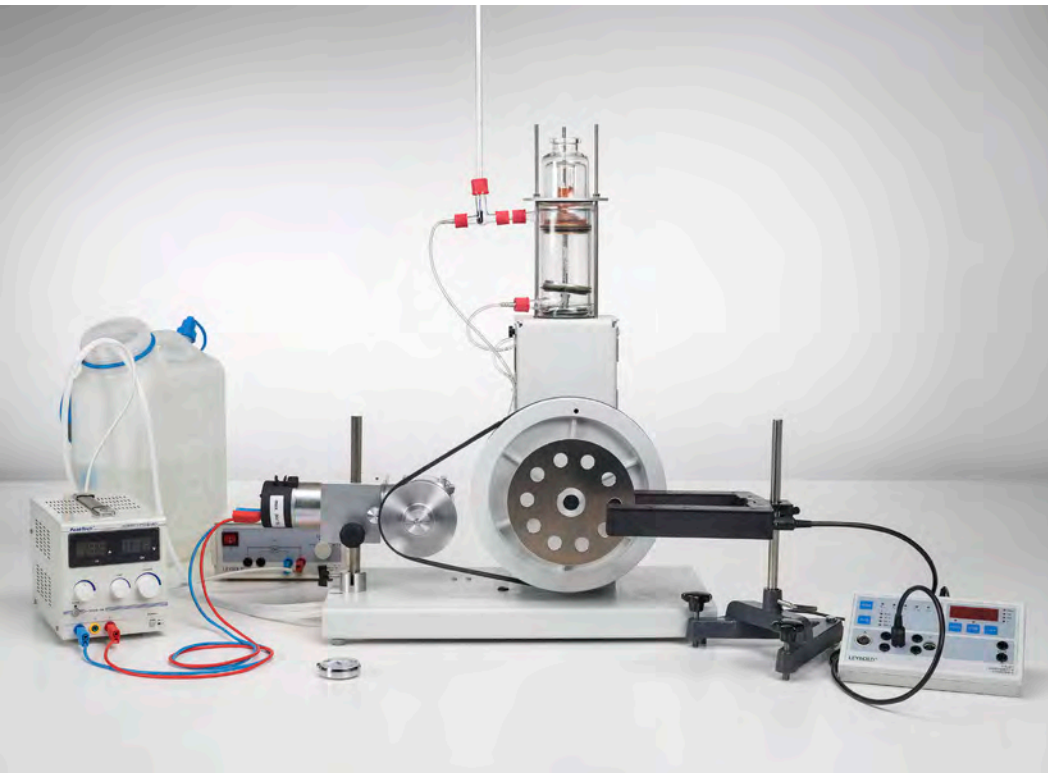
HOT-AIR ENGINE: QUANTITATIVE EXPERIMENTS

P2.6.2.1
Frictional losses in the hot-air engine (calorific determination)

P2.6.2.2
Determining the efficiency of the hot-air engine as a heat engine

P2.6.2.3
Determining the efficiency of the hot-air engine as a refrigerator

Cat. No.	Description	P2.6.2.1	P2.6.2.2	P2.6.2.3
388 182	Hot-air engine	1	1	1
388 221	Accessories for hot air engine for power measurement	1	1	1
347 38	Experiment motor 93 W	1		1
521 547	DC Power Supply 0...30 V/0...5 A	1		1
575 471	Counter S	1	1	1
337 46	Fork-type light barrier	1	1	1
501 16	Multi-core cable, 6-pole, 1.5 m	1	1	1
313 27	Hand-held stop-watch, 60s/0.2s	1	1	1
382 35	Thermometer, -10...+50 °C/0.1 K	1	1	1
300 02	Stand base, V-shaped, small	1	2	1
300 41	Stand rod, 25 cm, 12 mm Ø	1	1	1
590 06	Plastic beaker	1	1	1
500 641	Safety connecting lead, 100 cm, red	1		1
500 642	Safety connecting lead, 100 cm, blue	1		1
388 181	Immersion pump	1*	1*	1*
521 231	Low-voltage power supply 3/6/9/12 V	1*	1*	1*
667 194	Silicone tubing 7 mm Ø, 1 m	2*	2*	2*
604 313	Wide-mouthed can, 10 l	1*	1*	1*
562 11	U-core with yoke		1	
562 121	Clamping device with spring clip		1	
562 21	Mains coil, 500 turns		1	
562 18	Coil, 50 turns, extra-low voltage		1	
531 120	Multimeter LDanalog 20		1	
531 130	Multimeter LDanalog 30		1	
314 141	Precision dynamometer, 1 N		1	
300 42	Stand rod, 47 cm, 12 mm diam.		1	
300 51	Stand rod, right-angled		1	
301 01	Leybold multiclamp		2	
342 63	Weight 50 g		3	
501 45	Connecting lead 19 A, 50 cm, red/blue, pair		1	

Cat. No.	Description	P2.6.2.1	P2.6.2.2	P2.6.2.3
501 33	Connecting lead, 32 A, 100 cm, black		3	2
521 546	DC Power Supply 0...16 V/0...5 A			1

* additionally recommended

When the hot-air engine is operated as a heat engine, each engine cycle withdraws the amount of heat Q_1 from reservoir 1, generates the mechanical work W and transfers the difference $Q_2 = Q_1 - W$ to reservoir 2. The hot-air engine can also be made to function as a refrigerating machine while operated in the same rotational direction by externally applying the mechanical work W. In both cases, the work W_F converted into heat in each cycle through the friction of the piston in the cylinder must be taken into consideration.

Thermodynamic cycles are often described as a closed curve in a pV diagram (p: pressure, V: volume). The work added to or withdrawn from the system (depending on the direction of rotation) corresponds to the area enclosed by the curve.

In order to determine the work of friction W_F in the experiment P2.6.2.1, the temperature increase ΔT_F in the cooling water is measured while the hot-air engine is driven using an electric motor and the cylinder head is open.

The experiment P2.6.2.2 determines the efficiency

$$\eta = \frac{W}{W + Q_2}$$

of the hot-air engine as a heat engine. The mechanical work W exerted on the axle in each cycle can be calculated using the external torque N of a dynamometrical brake which brakes the hot-air engine to a speed f. The amount of heat Q_2 given off corresponds to a temperature increase ΔT in the cooling water.

The experiment P2.6.2.3 determines the efficiency

$$\eta = \frac{Q_2}{Q_1 - Q_2}$$

of the hot-air engine as a refrigerating machine. Here, the hot-air engine with closed cylinder head is driven using an electric motor and Q_1 is determined as the electrical heating energy required to maintain the cylinder head at the ambient temperature.

HOT–AIR ENGINE: QUANTITATIVE EXPERIMENTS

P2.6.2.4
pV diagram of the hot-air engine as a heat engine - Recording and evaluating with CASSY

pV diagram of the hot-air engine as a heat engine - Recording and evaluating with CASSY (P2.6.2.4)

Cat. No.	Description	P2.6.2.4
388 182	Hot-air engine	1
562 11	U-core with yoke	1
562 121	Clamping device with spring clip	1
562 21	Mains coil, 500 turns	1
562 18	Coil, 50 turns, extra-low voltage	1
524 013	Sensor-CASSY 2	1
524 220	CASSY Lab 2	1
524 082	Rotary motion sensor S	1
524 064	Pressure sensor S, ±2000 hPa	1
309 48	Fishing line	1
352 08	Helical spring 25 N/m	1
501 33	Connecting lead, 32 A, 100 cm, black	2
388 181	Immersion pump	1*
521 231	Low-voltage power supply 3/6/9/12 V	1*
667 194	Silicone tubing 7 mm Ø, 1 m	2*
604 313	Wide-mouthed can, 10 l	1*
	additionally required: PC with Windows XP/Vista/7/8/10 (x86 or x64)	1

* additionally recommended

When the hot-air engine is operated as a heat engine, each engine cycle withdraws the amount of heat Q_1 from reservoir 1, generates the mechanical work W and transfers the difference $Q_2 = Q_1 - W$ to reservoir 2. The hot-air engine can also be made to function as a refrigerating machine while operated in the same rotational direction by externally applying the mechanical work W. In both cases, the work W_F converted into heat in each cycle through the friction of the piston in the cylinder must be taken into consideration.

Thermodynamic cycles are often described as a closed curve in a pV diagram (p: pressure, V: volume). The work added to or withdrawn from the system (depending on the direction of rotation) corresponds to the area enclosed by the curve.

In the experiment P2.6.2.4, the pV diagram of the hot air engine as a heat engine is recorded using the computer-assisted measured value recording system CASSY. The pressure sensor measures the pressure p in the cylinder and a rotary motion sensor measures the position s, from which the volume is calculated, as a function of the time t. The measured values are displayed on the screen directly in a pV diagram. In the further evaluation, the mechanical work performed as piston friction per cycle

$$W = -\int p \cdot dV$$

and from this the mechanical power

$$P = W \cdot f$$

f: no-load speed

are calculated and plotted in a graph as a function of the no-load speed.
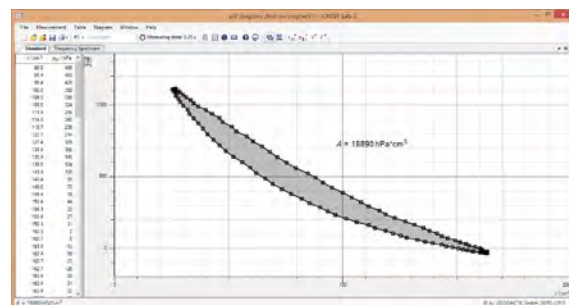
pV diagram of the hot air engine (P2.6.2.4)

Determining the efficiency of the heat pump as a function of the temperature differential (P2.6.3.1)

HEAT PUMP

P2.6.3.1
Determining the efficiency of the heat pump as a function of the temperature differential

P2.6.3.2
Investigating the function of the expansion valve of the heat pump

P2.6.3.3
Analyzing the cyclical process of the heat pump with the Mollier diagram

Cat. No.	Description	P2.6.3.1	P2.6.3.2	P2.6.3.3
389 521	Heat pump	1	1	1
531 831	Joule and wattmeter	1		1
524 005W	Mobile-CASSY 2 WiFi	1	1	1
524 0673	NiCr–Ni adapter S, type K	1	1	1
529 676	Temperature probe, NiCr–Ni, 1.5 mm, type K	2	2	3
313 12	Digital stop-watch	1	1	1

The heat pump extracts heat from a reservoir with the temperature T_1 through vaporization of a coolant and transfers heat to a reservoir with the temperature T_2 through condensation of the coolant. In the process, compression in the compressor (a–b) greatly heats the gaseous coolant. It condenses in the liquefier (c–d) and gives up the released condensation heat ΔQ_2 to the reservoir T_2. The liquefied coolant is filtered and fed to the expansion valve (e–f) free of bubbles. This regulates the supply of coolant to the vaporizer (g–h). In the vaporizer, the coolant once again becomes a gas, withdrawing the necessary evaporation heat ΔQ_1 from the reservoir T_1.

The aim of the experiment P2.6.3.1 is to determine the efficiency

$$\varepsilon = \frac{\Delta Q_2}{\Delta W}$$

of the heat pump as a function of the temperature differential $\Delta T = T_2 - T_1$. The heat quantity ΔQ_2 released is determined from the heating of water reservoir T_2, while the applied electrical energy ΔW is measured using the joule and watt-meter.

In the experiment P2.6.3.2, the temperatures T_f and T_h are recorded at the outputs of the expansion valve and the vaporizer. If the difference between these two temperatures falls below a specific limit value, the expansion valve chokes off the supply of coolant to the vaporizer. This ensures that the coolant in the vaporizer is always vaporized completely.

In the experiment P2.6.3.3, a Mollier diagram, in which the pressure p is graphed as a function of the specific enthalpy h of the coolant, is used to trace the energy transformations of the heat pump. The pressures p_1 and p_2 in the vaporizer and liquefier, as well as the temperatures T_a, T_b, T_e and T_f of the coolant are used to determine the corresponding enthalpy values h_a, h_b, h_e and h_f. This experiment also measures the heat quantities ΔQ_2 and ΔQ_1 released and absorbed per unit of time. This in turn is used to determine the amount of coolant Δm circulated per unit of time.
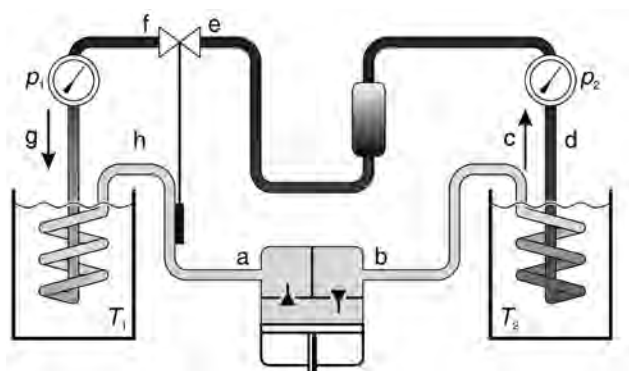
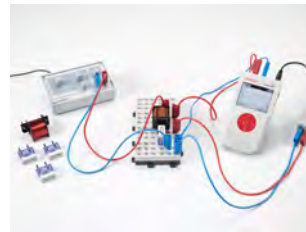Heat pump (389 521) with schematic diagram of all functional components (P2.6.3.1)

CASSY®

P3 ELECTRICITY

P3 ELECTRICITY

Basic electrostatics experiments with the electrometer amplifier (P3.1.1.2)

BASIC EXPERIMENTS ON ELECTROSTATICS

P3.1.1.2
Basic electrostatics experiments with the electrometer amplifier

Cat. No.	Description	P3.1.1.2
532 14	Electrometer amplifier	1
562 791	Plug-in power supply, 12 V AC	1
578 25	Capacitor, 1 nF, STE 2/19	1
578 10	Capacitor, 10 nF, STE 2/19	1
532 16	Connecting rod	1
531 120	Multimeter LDanalog 20	1
541 00	Friction rods, PVC and acrylic	1
541 22	Leather cloth	1
686 63	Polyethylene friction foils, set of 10	1
546 12	Faraday's cup	1
590 011	Clamping plug	1
542 51	Induction plate 8 cm x 4 cm	1
501 46	Connecting leads 19 A, 100 cm, red/blue, pair	1
500 424	Connecting lead 19 A, 50 cm, black	1
666 711	Butane gas burner	1*
666 712ET3	Butane cartridge, 190 g, set of 3	1*

* additionally recommended

The electrometer amplifier is an impedance converter with an extremely high-ohm voltage input ($\geq 10^{13}$ Ω) and a low-ohm voltage output (≤ 1 Ω). By means of capacitive connection of the input and using a Faraday's cup to collect charges, this device is ideal for measuring extremely small charges. Experiments on contact and friction electricity can be conducted with a high degree of reliability.

The experiment P3.1.1.2 investigates how charges can be separated through rubbing two materials together. It shows that one of the materials carries positive charges, and the other negative charges, and that the absolute values of the charges are equal. If we measure the charges of both materials at the same time, they cancel each other out. The sign of the charge of a material does not depend on the material alone, but also on the properties of the other material.
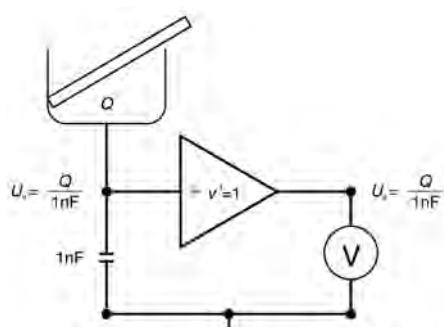
Measuring charges with the electrometer amplifier (P3.1.1.2)

LEYBOLD® 81

COULOMB'S LAW

P3.1.2.2
Confirming Coulomb's law
– Measuring with the force sensor

Confirming Coulomb's law - Measuring with the force sensor (P3.1.2.2)

Cat. No.	Description	P3.1.2.2
314 263	Bodies for electric charge, set	1
337 00	Trolley	1
460 82	Precision metal rail, 50 cm	1
460 95	Clamp rider	2
524 005W	Mobile-CASSY 2 WiFi	1
524 060	Force sensor S, ±1N	1
521 721	High-voltage power supply, 25 kV	1
501 051	Cable for high voltages, 1.5 m	1
590 13	Stand rod with bore holes	1
300 11	Saddle base	1
590 02	Small clip plug	1
532 14	Electrometer amplifier	1
562 791	Plug-in power supply, 12 V AC	1
578 25	Capacitor, 1 nF, STE 2/19	1
578 10	Capacitor, 10 nF, STE 2/19	1
546 12	Faraday's cup	1
590 011	Clamping plug	1
532 16	Connecting rod	1
300 02	Stand base, V-shaped, small	1
300 41	Stand rod, 25 cm, 12 mm Ø	1
301 01	Leybold multiclamp	1
501 45	Connecting lead 19 A, 50 cm, red/blue, pair	1
500 424	Connecting lead 19 A, 50 cm, black	1
501 42	Connecting lead 32 A, 100 cm, yellow/green	1
500 610	Safety connecting lead, 25 cm, yellow/green	1
500 640	Safety connecting lead, 100 cm, yellow/green	1

According to Coulomb's law, the force acting between two point-shaped electrical charges Q_1 and Q_2 at a distance r from each other can be determined using the formula

$$F = \frac{1}{4\pi\varepsilon_0} \cdot \frac{Q_1 \cdot Q_2}{r^2}$$

where $\varepsilon_0 = 8.85 \cdot 10^{-12} \frac{As}{Vm}$ (permittivity)

This force acts between two charged spheres when the distance r between the sphere midpoints is significantly greater than the sphere diameter, so that the uniform charge distribution on the spheres is undisturbed. In other words, the spheres in this geometry may be treated as points.

The coulomb force between two charged spheres can be determined using a sensitive force sensor. This device consists of two bending elements connected in parallel with four strain gauges in a bridge configuration; their electrical resistance changes when a load is applied. The change in resistance is proportional to the force acting on the instrument.

In the experiment P3.1.2.2, the force sensor is connected to a measuring instrument, which displays the measured force directly. No calibration is necessary. The coulomb force is measured as a function of the distance r between the sphere midpoints, the charge Q_1 of the first sphere and the charge Q_2 of the second sphere. The charges of the spheres are measured using an electrometer amplifier connected as a coulomb meter. The aim of the evaluation is to verify the proportionalities

$$F \propto \frac{1}{r^2}, \quad F \propto Q_1 \quad \text{and} \quad F \propto Q_2$$

and to calculate the permittivity ε_0.

ELECTRICITY
ELECTROSTATICS

COULOMB'S LAW

P3.1.2.3
Confirming Coulomb's law
– Recording and evaluating with CASSY

Confirming Coulomb's law - Recording and evaluating with CASSY (P3.1.2.3)

Cat. No.	Description	P3.1.2.3
314 263	Bodies for electric charge, set	1
337 00	Trolley	1
460 82	Precision metal rail, 50 cm	1
460 95	Clamp rider	2
524 013	Sensor-CASSY 2	1
524 220	CASSY Lab 2	1
524 060	Force sensor S, ±1N	1
524 082	Rotary motion sensor S	1
521 721	High-voltage power supply, 25 kV	1
501 051	Cable for high voltages, 1.5 m	1
590 13	Stand rod with bore holes	1
300 11	Saddle base	1
590 02	Small clip plug	1
532 14	Electrometer amplifier	1
562 791	Plug-in power supply, 12 V AC	1
578 25	Capacitor, 1 nF, STE 2/19	1
578 10	Capacitor, 10 nF, STE 2/19	1
531 120	Multimeter LDanalog 20	1
546 12	Faraday's cup	1
590 011	Clamping plug	1
532 16	Connecting rod	1
300 41	Stand rod, 25 cm, 12 mm Ø	1
300 02	Stand base, V-shaped, small	1
301 01	Leybold multiclamp	1
337 04	Driving weights, set	1
301 07	Simple bench clamp	1
309 48	Fishing line	1
501 45	Connecting lead 19 A, 50 cm, red/blue, pair	1
500 424	Connecting lead 19 A, 50 cm, black	1
501 43	Connecting lead 32 A, 200 cm, yellow/green	1

Cat. No.	Description	P3.1.2.3
500 610	Safety connecting lead, 25 cm, yellow/green	1
500 640	Safety connecting lead, 100 cm, yellow/green	1
	additionally required: PC with Windows XP/Vista/7/8/10 (x86 or x64)	1

For computer-assisted measuring of the coulomb force between two charged spheres, we can also connect the force sensor to the CASSY interface. A displacement sensor (Rotary motion sensor S) is additionally required to measure the distance between the charged spheres.

The experiment P3.1.2.3 utilizes the software CASSY Lab to record the values and evaluate them. The coulomb force is measured for different charges Q_1 and Q_2 as a function of the distance r. The charges of the spheres are measured using an electrometer amplifier connected as a coulomb meter. The aim of the evaluation is to verify the proportionality

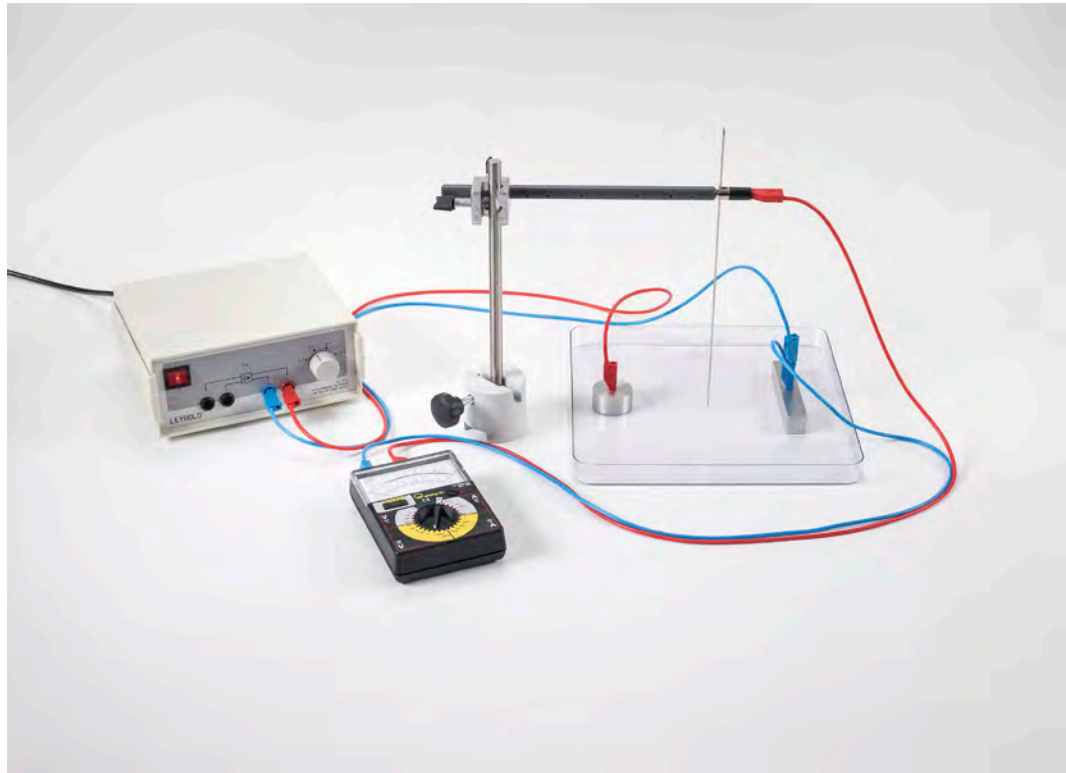$$F \propto \frac{1}{r^2}$$

and to calculate of the permittivity ε_0.

LEYBOLD® 83

FIELD LINES AND EQUIPOTENTIAL LINES

P3.1.3.1
Displaying lines of electric flux

P3.1.3.2
Displaying the equipotential lines of electric fields

Displaying the equipotential lines of electric fields (P3.1.3.2)

Cat. No.	Description	P3.1.3.1	P3.1.3.2
541 06	Electric field lines equipment set	1	
501 051	Cable for high voltages, 1.5 m	2	
521 70	High-voltage power supply, 10 kV	1	
MIK 74708	BMS SyncCam 8Mp	1*	
545 09	Electrolytic tank		1
501 861	Crocodile-clips, polished, set of 6		1
521 231	Low-voltage power supply 3/6/9/12 V		1
531 120	Multimeter LDanalog 20		1
686 66	Steel needle		1
590 011	Clamping plug		1
590 13	Stand rod with bore holes		1
300 41	Stand rod, 25 cm, 12 mm Ø		1
301 01	Leybold multiclamp		1
300 11	Saddle base		1
501 461	Connecting leads 19 A, 100 cm, black, pair		2
	additionally required: PC or device for image display	1	

* additionally recommended
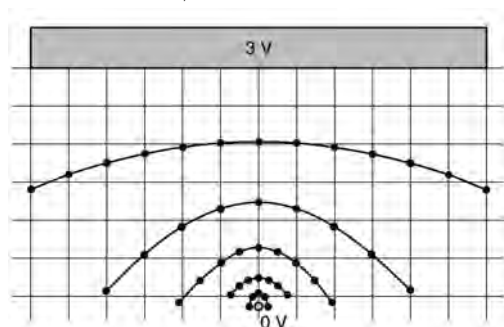
Measurement example: equipotential lines around a needle tip (P3.1.3.2)

The mutual force effect between electric charges can be described by an electric field. The electric field is also present even when it cannot be demonstrated through a force acting on a sample charge. A field is best described in terms of lines of electric flux, which follow the direction of electric field strength. The orientation of these lines of electric flux is determined by the spatial arrangement of the charges generating the field.

In a two-dimensional cross-section of an electric field, points of equal potential form a line. The direction of these isoelectric lines, just like the lines of electric flux, are determined by the spatial arrangement of the charges generating the field.

In the experiment P3.1.3.1, small particles in an oil-filled cuvette are used to illustrate the lines of electric flux. The particles align themselves in the electric field to form chains which run along the lines of electric flux. Four different pairs of electrodes are provided to enable electric fields with different spatial distributions to be generated; these electrode pairs are mounted beneath the cuvette, and connected to a high voltage source of up to 10 kV. The resulting patterns can be interpreted as the cross-sections of two spheres, one sphere in front of a plate, a plate capacitor and a spherical capacitor.

The experiment P3.1.3.2 measures the isoelectric lines for bodies with different charges. To do this, a voltage is applied to a pair of electrodes placed in an electrolytic tray filled with distilled water. An AC voltage is used to avoid potential shifts due to electrolysis at the electrodes. A voltmeter measures the potential difference between the 0 V electrode and a steel needle immersed in the water. To display the isoelectric lines, the points of equal potential difference are localized and drawn on graph paper. In this way, it is possible to observe and study two-dimensional sections through the electric field in a plate capacitor, a Faraday's cup, a dipole, an image charge and a slight curve.
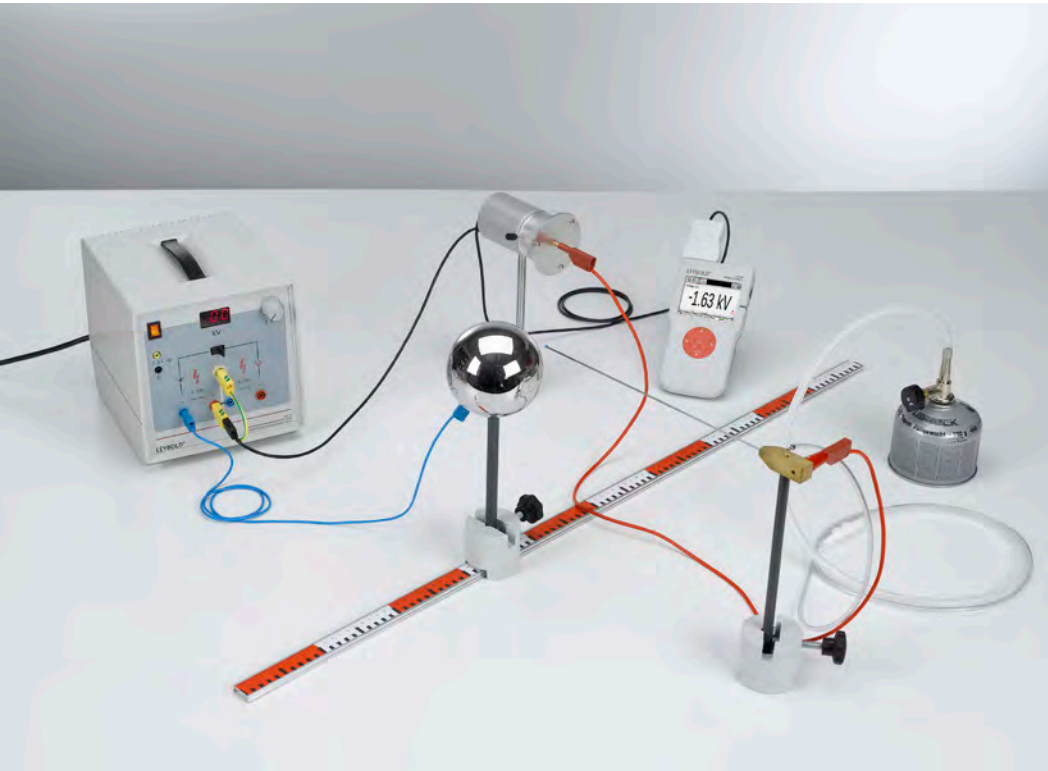
FIELD LINES AND EQUIPOTENTIAL LINES

P3.1.3.3
Measuring the potential inside a plate capacitor

P3.1.3.4
Measuring the potential around a charged sphere

Measuring the potential around a charged sphere (P3.1.3.4)

Cat. No.	Description	P3.1.3.3	P3.1.3.4
524 080	Electric field meter S	1	1
540 540	Accessories for electric field meter S	1	1
524 005W	Mobile-CASSY 2 WiFi	1	1
311 02	Metal rule, 1 m	1	1
521 70	High-voltage power supply, 10 kV	1	1
460 317	Optical bench, S1 profile, 0.5 m	1	
460 312	Clamp rider with clamp 45/35	2	
300 11	Saddle base	2	3
300 41	Stand rod, 25 cm, 12 mm Ø	2	
301 01	Leybold multiclamp	1	
500 600	Safety connection lead, 10 cm, yellow/green	1	1
500 621	Safety connecting lead 50 cm, red	1	
500 622	Safety connecting lead 50 cm, blue	1	1
500 641	Safety connecting lead, 100 cm, red	1	1
500 642	Safety connecting lead, 100 cm, blue	1	1
667 193	PVC tubing, 7 mm diam., 1 m	1	1
666 716	Valve for gas cartridge	1	1
666 715	Cartridge	1	1
543 021	Sphere on insulated stand rod		1
500 95	Safety adapter sockets, red, set of 6		1

Using a flame probe, the electric potential around a charged object can be investigated in all three dimensions and the equipotential surfaces can be determined.

In the experiment P3.1.3.3, the electric potential of a plate capacitor is investigated. The equipotential surfaces parallel to the capacitor plates are identified by measuring the electrical potential at different positions but with constant distance to the capacitor plates. In addition, the dependance of the variation of the electric potential on the distance to the capacitor plates is determined and used to calculate the electric field strength.

The aim of the experiment P3.1.3.4 is to investigate the electric potential around a charged sphere. The equipotential surfaces are concentric spherical shells around the charged sphere. They are identified by measuring the electrical potential at different positions but with constant distance to the surface of the sphere. In addition, the dependance of the variation of the electric potential on the distance to the surface of the sphere is determined and used to calculate the electric field strength.
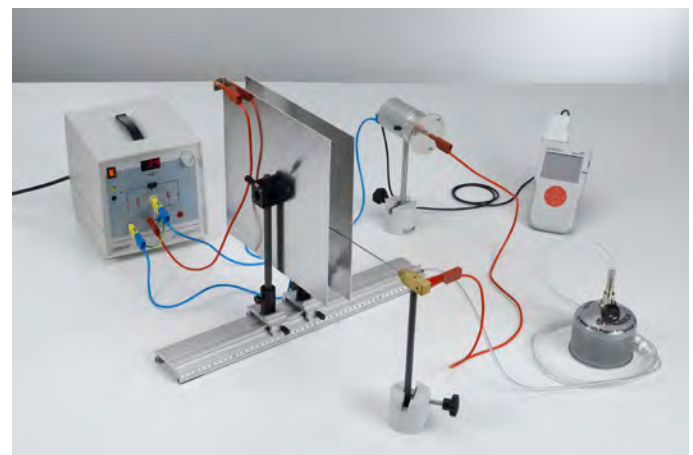
Measuring the potential inside a plate capacitor (P3.1.3.3)

EFFECTS OF FORCE IN AN ELECTRIC FIELD

P3.1.4.2
Kirchhoff's voltage balance: Measuring the force between two charged plates of a plate capacitor - Measuring with the force sensor

P3.1.4.3
Measuring the force between a charged sphere and a metal plate - Measuring with the force sensor

Kirchhoff's voltage balance: Measuring the force between two charged plates of a plate capacitor - Measuring with the force sensor (P3.1.4.2)

Cat. No.	Description	P3.1.4.2	P3.1.4.3
516 37	Electrostatics with current balance, accessories	1	1
516 31	Vertically adjustable stand	1	1
524 005W	Mobile-CASSY 2 WiFi	1	1
524 060	Force sensor S, ±1N	1	1
314 265	Support for conductor loops	1	1
521 70	High-voltage power supply, 10 kV	1	
300 02	Stand base, V-shaped, small	1	1
300 42	Stand rod, 47 cm, 12 mm diam.	1	1
301 01	Leybold multiclamp	1	1
500 98	Safety adapter sockets, black, set of 6	1	
500 610	Safety connecting lead, 25 cm, yellow/green	1	
500 620	Safety connecting lead 50 cm, yellow/green	1	
500 622	Safety connecting lead 50 cm, blue	2	
541 00	Friction rods, PVC and acrylic		1
541 22	Leather cloth		1
500 440	Connecting lead, 19 A, 100 cm, yellow/green		1

In a homogeneous electric field, the force F acting on an extended charged body is proportional to the total charge Q and the electric field strength E. Thus, the formula

$$F = Q \cdot E$$

applies.

In the experiment P3.1.4.2 a balance is set up in order to measure the force

$$F = \frac{1}{2} \cdot \varepsilon_0 \cdot \frac{U^2}{d^2} \cdot A$$

$$\text{where } \varepsilon_0 = 8.85 \cdot 10^{-12} \frac{As}{Vm} \text{ (permittivity)}$$

acting between the two charged plates of a plate capacitor. At a given area A, the measurement is conducted as a function of the plate distance d and the voltage U. The aim of the evaluation is to confirm the proportionalities

$$F \propto \frac{1}{d^2} \text{ and } F \propto U^2$$

and to determine the permittivity ε_0.

The experiment P3.1.4.3 consists of a practical investigation of the principle of the image charge. Here, the attractive force acting on a charged sphere in front of a metal plate is measured. This force is equivalent to the force of an equal, opposite charge at twice the distance $2d$. Thus, it is described by the formula

$$F = \frac{1}{4\pi\varepsilon_0} \cdot \frac{Q^2}{(2d)^2}$$

First, the force for a given charge Q is measured as a function of the distance d. The measurement is then repeated with half the charge. The aim of the evaluation is to confirm the proportionalities

$$F \propto \frac{1}{d^2} \text{ and } F \propto Q^2$$

EFFECTS OF FORCE IN AN ELECTRIC FIELD

P3.1.4.4
Measuring the force of an electric charge in a homogeneous electric field – Measuring with the force sensor

Measuring the force of an electric charge in a homogeneous electric field – Measuring with the force sensor (P3.1.4.4)

Cat. No.	Description	P3.1.4.4
544 22	Parallel plate capacitor	1
314 263	Bodies for electric charge, set	1
524 005W	Mobile-CASSY 2 WiFi	1
524 060	Force sensor S, ±1N	1
521 70	High-voltage power supply, 10 kV	1
541 00	Friction rods, PVC and acrylic	1
541 22	Leather cloth	1
590 02	Small clip plug	1
300 02	Stand base, V-shaped, small	1
300 42	Stand rod, 47 cm, 12 mm diam.	1
301 01	Leybold multiclamp	1
500 610	Safety connecting lead, 25 cm, yellow/green	1
500 640	Safety connecting lead, 100 cm, yellow/green	1
500 641	Safety connecting lead, 100 cm, red	1
500 642	Safety connecting lead, 100 cm, blue	1

The force in an electric field is measured using a force sensor connected to a measuring instrument. The force sensor consists of two bending elements connected in parallel with four strain gauges in a bridge configuration; their electrical resistance changes when a load is applied. The change in resistance is proportional to the force acting on the sensor. The measuring instrument displays the measured force directly.

In experiment P3.1.4.4 an electrostatic spoon is charged by a rubbed plastic rod. The electrostatic spoon is within the electric field of a plate capacitor and is aligned parallel to the plates. To verify the proportional relationship between the force and the field strength, the force F acting on the electrostatic spoon is measured at a known plate distance d as a function of the capacitor voltage U. The electric field E is determined using the equation

$$E = \frac{U}{d}$$

CASSY®

CHARGE DISTRIBUTIONS ON ELECTRICAL CONDUCTORS

P3.1.5.1
Investigating the charge distribution on the surface of electrical conductors

P3.1.5.2
Electrostatic induction with the hemispheres according to Cavendish

Electrostatic induction with the hemispheres according to Cavendish (P3.1.5.2)

Cat. No.	Description	P3.1.5.1	P3.1.5.2
543 071	Conical conductor on insulating stand	1	
546 12	Faraday's cup	2	
542 52	Test plate, 4 cm x 4 cm	1	
521 70	High-voltage power supply, 10 kV	1	1
501 051	Cable for high voltages, 1.5 m	1	1
532 14	Electrometer amplifier	1	1
562 791	Plug-in power supply, 12 V AC	1	1
578 25	Capacitor, 1 nF, STE 2/19	1	1
578 10	Capacitor, 10 nF, STE 2/19	1	1
531 120	Multimeter LDanalog 20	1	1
590 011	Clamping plug	1	
532 16	Connecting rod	1	1
540 52	Demonstration insulator	1	
501 861	Crocodile-clips, polished, set of 6	1	
300 11	Saddle base	1	3
500 610	Safety connecting lead, 25 cm, yellow/green	1	1
501 45	Connecting lead 19 A, 50 cm, red/blue, pair	1	1
500 424	Connecting lead 19 A, 50 cm, black	1	1
501 42	Connecting lead 32 A, 100 cm, yellow/green	1	1
543 021	Sphere on insulated stand rod		1
543 05	Cavendish hemispheres, pair		1
340 89	Coupling plug 4 mm		1
300 41	Stand rod, 25 cm, 12 mm Ø		2
301 01	Leybold multiclamp		2
590 13	Stand rod with bore holes		1

In static equilibrium, the interior of a metal conductor or a hollow body contains neither electric fields nor free electron charges. On the outer surface of the conductor, the free charges are distributed in such a way that the electric field strength is perpendicular to the surface at all points, and all points have equal potential.

In the experiment P3.1.5.1, an electric charge is collected from a charged hollow metal sphere using a charge spoon, and measured using a coulomb meter. It becomes apparent that the charge density is greater, the smaller the bending radius of the surface is. This experiment also shows that no charge can be taken from the interior of the hollow body.

The experiment P3.1.5.2 reconstructs a historic experiment first performed by Cavendish. A metal sphere is mounted on an insulated base. Two hollow hemispheres surround the sphere completely, but without touching it. When one of the hemispheres is charged, the charge distributes itself uniformly over both hemispheres, while the inside sphere remains uncharged. If the inside sphere is charged and then surrounded and contacted by the hemispheres, the two hemispheres again show equal charges, and the inside sphere is uncharged.

Determining the capacitance of a sphere in free space (P3.1.6.1)

P3.1.6.1
Determining the capacitance of a sphere in free space

P3.1.6.2
Determining the capacitance of a sphere in front of a metal plate

Cat. No.	Description	P3.1.6.1	P3.1.6.2
543 00	Set of 3 conducting spheres	1	1
521 70	High-voltage power supply, 10 kV	1	1
501 051	Cable for high voltages, 1.5 m	1	1
532 14	Electrometer amplifier	1	1
562 791	Plug-in power supply, 12 V AC	1	1
578 25	Capacitor, 1 nF, STE 2/19	1	1
578 10	Capacitor, 10 nF, STE 2/19	1	1
531 120	Multimeter LDanalog 20	1	1
546 12	Faraday's cup	1	1
590 011	Clamping plug	1	1
532 16	Connecting rod	1	1
590 13	Stand rod with bore holes	1	1
300 11	Saddle base	2	3
500 610	Safety connecting lead, 25 cm, yellow/green	1	1
501 45	Connecting lead 19 A, 50 cm, red/blue, pair	1	1
500 424	Connecting lead 19 A, 50 cm, black	1	1
501 43	Connecting lead 32 A, 200 cm, yellow/green	1	1
587 66	Reflection plate		1
501 861	Crocodile-clips, polished, set of 6		1
311 78	Tape measure 2 m / 1 mm		1
300 42	Stand rod, 47 cm, 12 mm diam.		1
501 33	Connecting lead, 32 A, 100 cm, black		1

The potential difference U of a charged conductor in an insulated mounting in free space with reference to an infinitely distant reference point is proportional to the charge Q of the body. We can express this using the relationship

$$Q = C \cdot U$$

and call C the capacitance of the body. Thus, for example, the capacitance of a sphere with the radius r in a free space is

$$C = 4\pi\varepsilon_0 \cdot r$$

because the potential difference of the charged sphere with respect to an infinitely distant reference point is

$$U = \frac{1}{4\pi\varepsilon_0} \cdot \frac{Q}{r}$$

where $\varepsilon_0 = 8.85 \cdot 10^{-12} \ \frac{As}{Vm}$ (permittivity)

The experiment P3.1.6.1 determines the capacitance of a sphere in a free space by charging the sphere with a known high voltage U and measuring its charge Q using an electrometer amplifier connected as a coulomb meter. The measurement is conducted for different sphere radii r. The aim of the evaluation is to verify the proportionalities

$$Q \propto U \text{ and } C \propto r$$

The experiment P3.1.6.2 shows that the capacitance of a body also depends on its environment, e.g. the distance to other earthed conductors. In this experiment, spheres with the radii r are arranged at a distance s from an earthed metal plate and charged using a high voltage U. The capacitance of the arrangement is now

$$C = 4\pi\varepsilon_0 \cdot r \cdot \left(1 + \frac{r}{2s} \right)$$

The aim of the evaluation is to confirm the proportionality between the charge Q and the potential difference U at any given distance s between the sphere and the metal plate.
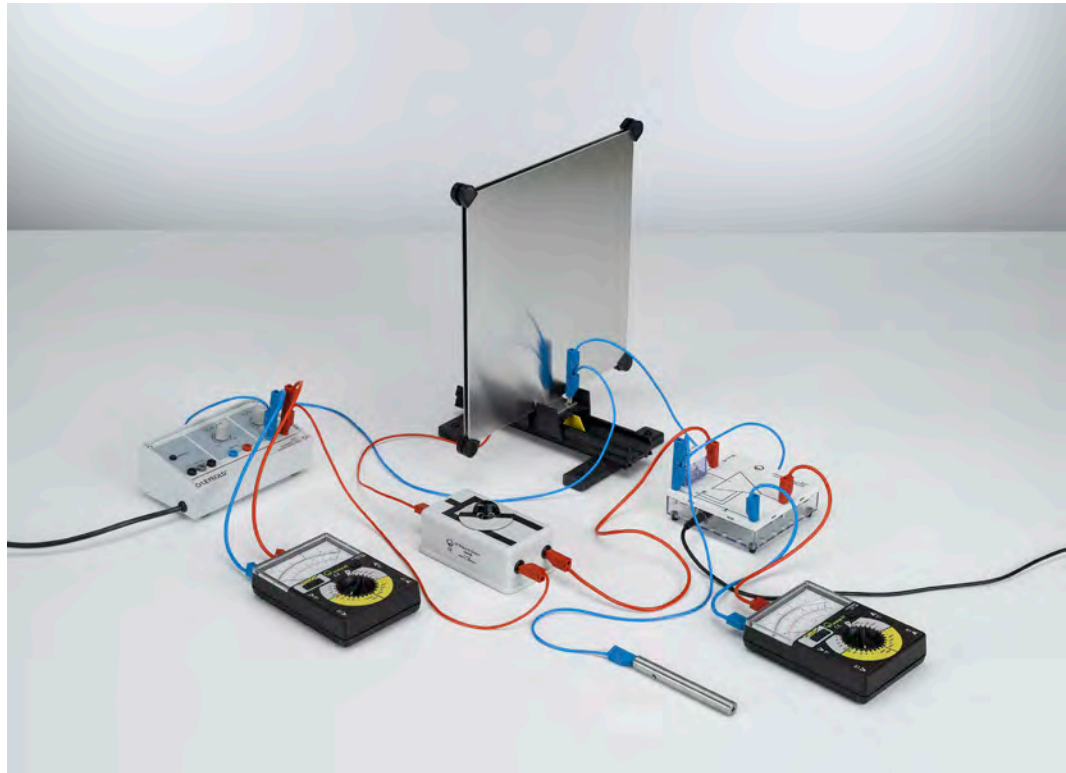
PLATE CAPACITOR

P3.1.7.1
Determining the capacitance of a plate capacitor - Measuring the charge with the electrometer amplifier

P3.1.7.2
Parallel and series connection of capacitors - Measuring the charge with the electrometer amplifier

Determining the capacitance of a plate capacitor - Measuring the charge with the electrometer amplifier (P3.1.7.1)

Cat. No.	Description	P3.1.7.1	P3.1.7.2
544 23	Capacitor assembly kit	1	1
522 27	Power supply, 450 V	1	1
504 48	Two-way switch	1	1
531 120	Multimeter LDanalog 20	2	2
532 14	Electrometer amplifier	1	1
578 10	Capacitor, 10 nF, STE 2/19	1	1
578 31	Capacitor, 0.1 µF, STE 2/19	1	1
532 16	Connecting rod	1	1
501 45	Connecting lead 19 A, 50 cm, red/blue, pair	4	5
501 46	Connecting leads 19 A, 100 cm, red/blue, pair	1	1

A plate capacitor is the simplest form of a capacitor. Its capacitance depends on the plate area A and the plate spacing d. The capacitance increases when an insulator with the dielectric constant ε_r is placed between the two plates. The total capacitance is

$$C = \varepsilon_r \varepsilon_0 \cdot \frac{A}{d}$$

where $\varepsilon_0 = 8.85 \cdot 10^{-12} \ \frac{As}{Vm}$ (permittivity)

In the experiment P3.1.7.1, this relationship is investigated using a demountable capacitor assembly with variable geometry. Capacitor plates with the areas $A = 40 \ cm^2$ and $A = 80 \ cm^2$ can be used, as well as various plate-type dielectrics. The distance can be varied in steps of one millimeter.

The experiment P3.1.7.2 determines the total capacitance C of the demountable capacitor with the two plate pairs arranged at a fixed distance and connected first in parallel and then in series, compares these with the individual capacitances C_1 and C_2 of the two plate pairs. The evaluation confirms the rela-tionship

$$C = C_1 + C_2$$

for parallel connection and

$$\frac{1}{C} = \frac{1}{C_1} + \frac{1}{C_2}$$

for serial connection.
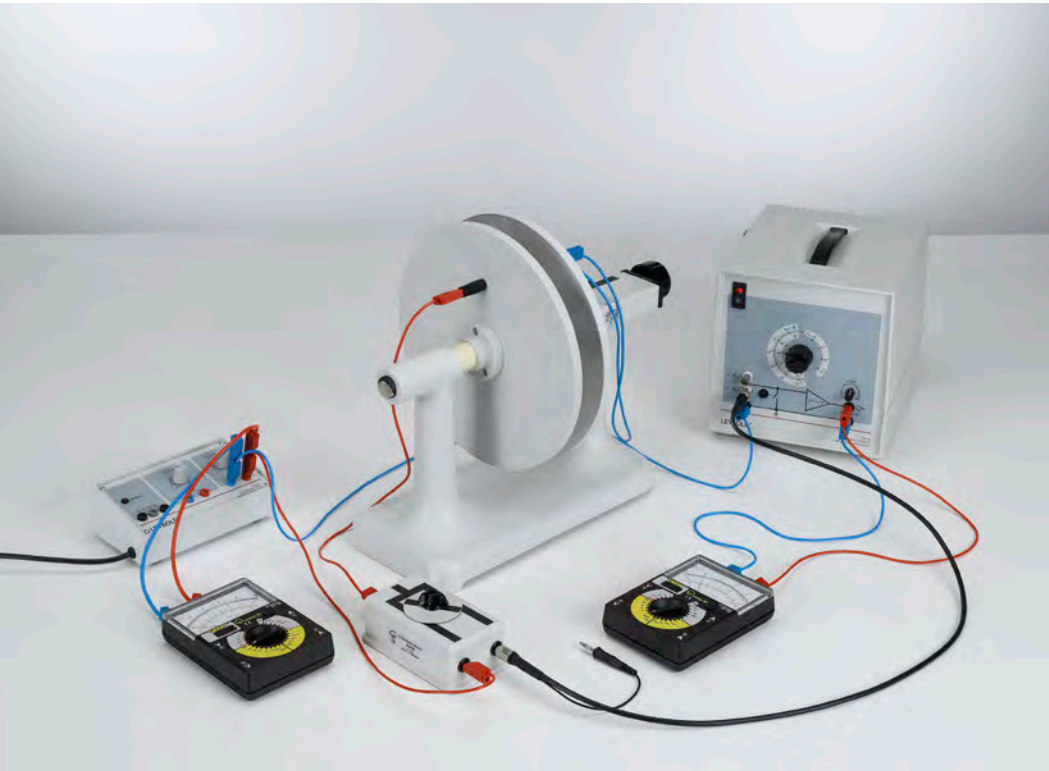
PLATE CAPACITOR

P3.1.7.3
Determining the capacitance of a plate capacitor - Measuring the charge with the I-measuring amplifier D

Determining the capacitance of a plate capacitor - Measuring the charge with the I-measuring amplifier D (P3.1.7.3)

Cat. No.	Description	P3.1.7.3
544 22	Parallel plate capacitor	1
522 27	Power supply, 450 V	1
504 48	Two-way switch	1
532 00	I-measuring amplifier D	1
531 183	Digital multimeter 3340	1
501 45	Connecting lead 19 A, 50 cm, red/blue, pair	3
501 46	Connecting leads 19 A, 100 cm, red/blue, pair	1

Calculation of the capacitance of a plate capacitor using the formula

$$C = \varepsilon_0 \cdot \frac{A}{d}$$

A: plate area

d: plate spacing

where $\varepsilon_0 = 8.85 \cdot 10^{-12} \ \frac{As}{Vm}$ (permittivity)

ignores the fact that part of the electric field of the capacitor extends beyond the edge of the plate capacitor, and that consequently a greater charge is stored for a specific potential difference between the two capacitors. For example, for a plate capacitor grounded on one side and having the area

$$A = \pi \cdot r^2$$

the capacitance is given by the formula

$$C = \varepsilon_0 \left(\frac{\pi \cdot r^2}{d} + 3.7724 \cdot r + r \cdot \ln\left(\frac{\pi r}{d} \right) + \ldots \right)$$

In the experiment P3.1.7.3, the capacitance C of a plate capacitor is measured as a function of the plate spacing d with the greatest possible accuracy. This experiment uses a plate capacitor with a plate radius of 13 cm and a plate spacing which can be continuously varied between 0 and 70 mm. The aim of the evaluation is to plot the measured values in the form

$$C = f\left(\frac{1}{d} \right)$$

and compare them with the values to be expected according to theory.

LEYBOLD®

PLATE CAPACITOR

P3.1.7.4
Measuring the electric field strength inside a plate capacitor

P3.1.7.5
Measuring the electric field strength inside a plate capacitor as a function of the dielectrics

P3.1.7.6
Measuring the electric field strength of a charged sphere in front of a conductive plate (image charge)

Measuring the electric field strength inside a plate capacitor (P3.1.7.4)

Cat. No.	Description	P3.1.7.4	P3.1.7.5	P3.1.7.6
524 080	Electric field meter S	1	1	1
540 540	Accessories for electric field meter S	1	1	1
524 005W	Mobile-CASSY 2 WiFi	1	1	1
521 70	High-voltage power supply, 10 kV	1		1
460 317	Optical bench, S1 profile, 0.5 m	1	1	
460 312	Clamp rider with clamp 45/35	2	2	
500 600	Safety connection lead, 10 cm, yellow/green	1		1
500 641	Safety connecting lead, 100 cm, red	1		1
500 642	Safety connecting lead, 100 cm, blue	1		1
531 120	Multimeter LDanalog 20		1	
522 27	Power supply, 450 V		1	
504 45	On-off switch, single pole		1	
500 421	Connecting lead 19 A, 50 cm, red		3	
500 422	Connecting lead 19 A, 50 cm, blue		1	
500 442	Connecting lead 19 A, 100 cm, blue		1	
543 021	Sphere on insulated stand rod			1
311 02	Metal rule, 1 m			1
300 11	Saddle base			2
500 95	Safety adapter sockets, red, set of 6			1

Using the electric field meter S the electric field strength E in a plate capacitor can be measured. The electric field strength depends on the applied voltage U and the distance d of the capacitor plates:

$$E = \frac{U}{d}$$

Alternatively, the electrical field strength E can be calculated from the charge Q on the capacitor plates:

$$E = \frac{Q}{\varepsilon_0 \cdot \varepsilon_r \cdot A}$$

Here, E depends on the area of the plates A and the permittivity ε_r of the material between the capacitor plates as well.

In the experiment P3.1.7.4 the dependance of the electric field strength E on the applied voltage U and the plate spacing d is determined. First, keeping the distance of the plates constant, the value of the applied voltage U is varied and the electric field strength is measured. Then, the voltage U is kept constant and the dependance of the electric field strength E on the plate spacing d is determined.

The aim of the experiment P3.1.7.5 is to investigate the influence of the permittivity ε_r on the field strength E. First, keeping the applied voltage U constant a dielectric (glass, plastics) is placed between the capacitor plates and the electric field strength is measured. Second, the charged capacitor is disconnected from the power supply. Then, the dielectric is removed and the field strength measured again.

In the experiment P3.1.7.6, the electric field strength on the surface of a conductive plate with distance r to a charged sphere is measured. The field gradient in front of the plate is equivalent to the case where instead of the plate a sphere with opposite charge is situated in twice the distance to the sphere (mirror or image charge). This leads to a doubling in field strength compared to a free-standing sphere.

Verifying Ohm's law and measuring specific resistances (P3.2.2.1)
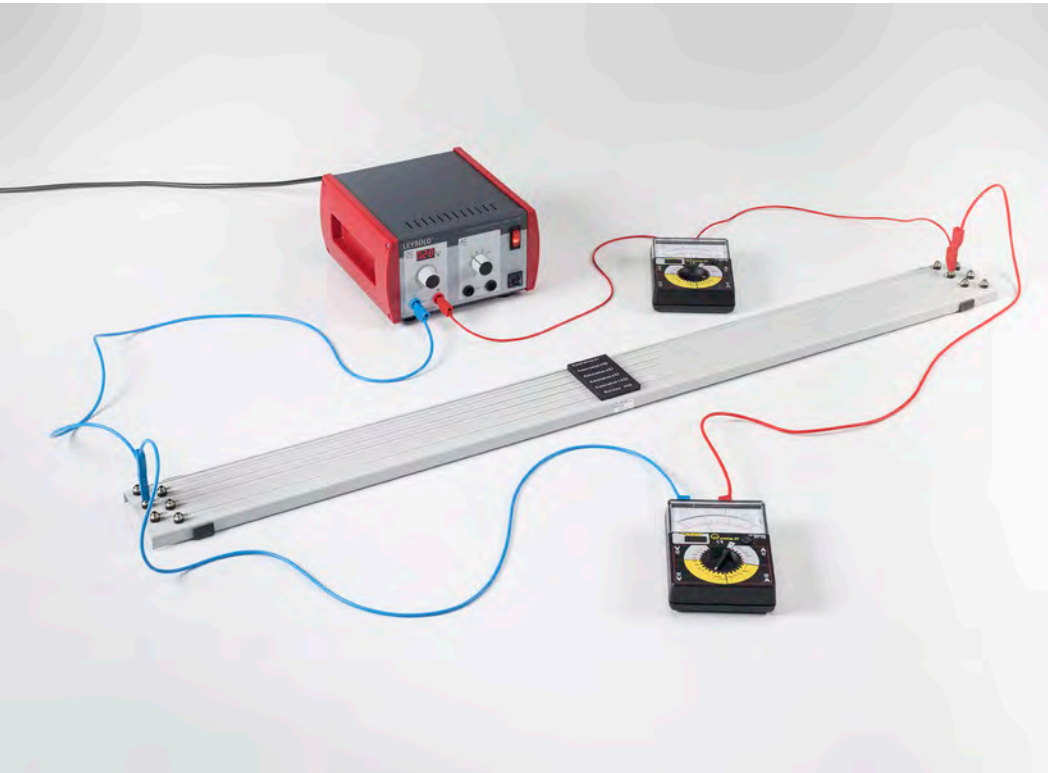
OHM'S LAW

P3.2.2.1
Verifying Ohm's law and measuring specific resistances

P3.2.2.2
Verifying Ohm's law
– Measuring with CASSY

Cat. No.	Description	P3.2.2.1	P3.2.2.2
550 57	Apparatus for resistance measurements	1	
521 487	AC/DC power supply PRO 0...12 V/3 A	1	
531 120	Multimeter LDanalog 20	2	
501 25	Connecting lead, 32 A, 50 cm, red	2	
501 30	Connecting lead, 32 A, 100 cm, red	1	
501 31	Connecting lead, 32 A, 100 cm, blue	2	
576 81	Plug-in board safety socket, 20/10		2
501 48	Bridging plugs STE 2/19, set of 10		1
567 18	Wrapping plate for wires		1
550 46	Chrome-nickel resistance wire, 0.25 mm diameter, 100 m		1
579 331	Plug-in holder STE		2
579 13	Toggle switch STE 2/19		1
577 32	Resistor 100 Ohm, STE 2/19		1
521 231	Low-voltage power supply 3/6/9/12 V		1
524 005W	Mobile-CASSY 2 WiFi		1
500 621	Safety connecting lead 50 cm, red		2
500 622	Safety connecting lead 50 cm, blue		2
500 624	Safety connecting lead 50 cm, black		1

In circuits consisting of metal conductors, Ohm's law

$$U = R \cdot I$$

represents a very close approximation of the actual circumstances. In other words, the voltage drop U in a conductor is proportional to the current I through the conductor. The proportionality constant R is called the resistance of the conductor. For the resistance, we can say

$$R = \rho \cdot \frac{s}{A}$$

ρ: resistivity of the conductor material

s: length of wire

A: cross-section of wire

The experiment P3.2.2.1 verifies the proportionality between the current and voltage for metal wires of different materials, thicknesses and lengths, and calculates the resistivity of each material.

The experiment P3.2.2.2 verifies the proportionality between the current and voltage for a metal wire using the CASSY system.

KIRCHHOFF'S LAWS

P3.2.3.1
Measuring current and voltage at resistors connected in parallel and in series

Measuring current and voltage at resistors connected in parallel and in series (P3.2.3.1)

Cat. No.	Description	P3.2.3.1
576 81	Plug-in board safety socket, 20/10	1
577 36	Resistor, 220 Ω, STE 2/19	1
577 38	Resistor, 330 Ω, STE 2/19	1
577 40	Resistor 470 Ohm, STE 2/19	1
577 44	Resistor 1 kOhm, STE 2/19	1
577 53	Resistor, 5.6 kΩ, STE 2/19	1
577 56	Resistor 10 kOhm, STE 2/19	1
577 68	Resistor, 100 kΩ, STE 2/19	1
501 48	Bridging plugs STE 2/19, set of 10	1
521 487	AC/DC power supply PRO 0...12 V/3 A	1
524 005W	Mobile-CASSY 2 WiFi	1
500 621	Safety connecting lead 50 cm, red	2
500 622	Safety connecting lead 50 cm, blue	2
500 624	Safety connecting lead 50 cm, black	1

Kirchhoff's laws are of fundamental importance in calculating the component currents and voltages in branching circuits. The so-called "nodal rule" (or junction rule) states that the sum of all currents flowing into a particular junction point in a circuit is equal to the sum of all currents flowing away from this junction point. The "mesh rule" (or loop rule) states that in a closed path the sum of all voltages through the loop in any arbitrary direction of flow is zero. Kirchhoff's laws are used to derive a system of linear equations which can be solved for the unknown current and voltage components.

The experiment P3.2.3.1 examines the validity of Kirchhoff's laws in circuits with resistors connected in parallel and in series. The result demonstrates that two resistors connected in series have a total resistance R

$$R = R_1 + R_2$$

while for parallel connection of resistors, the total resistance R is

$$\frac{1}{R} = \frac{1}{R_1} + \frac{1}{R_2}$$
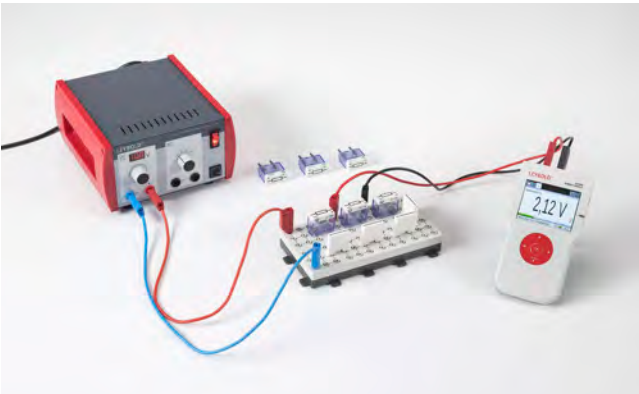
Measurement of current and voltage in a series connection (P3.2.3.1)

CASSY®
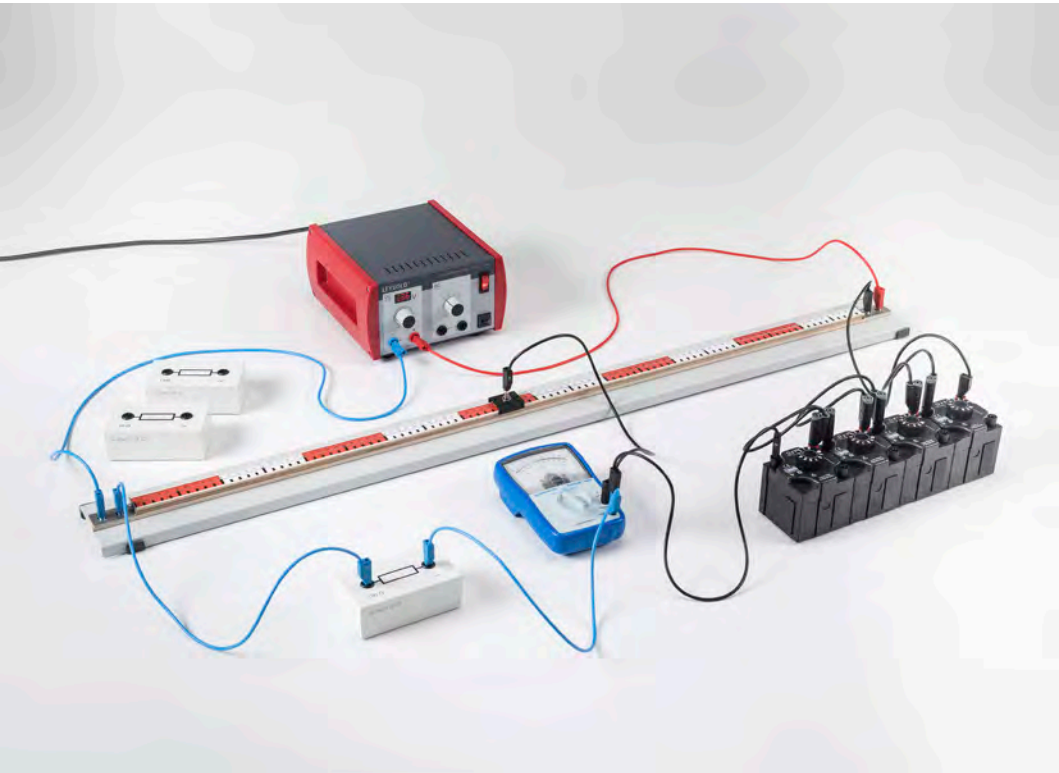
KIRCHHOFF'S LAWS

P3.2.3.4
Determining resistances using
a Wheatstone bridge

Determining resistances using a Wheatstone bridge (P3.2.3.4)

Cat. No.	Description	P3.2.3.4
536 02	Demonstration bridge	1
536 121	Measuring resistor, 10 Ω	1
536 131	Measuring resistor, 100 Ω	1
536 141	Measuring resistor, 1 kΩ	1
536 776	Decade resistor, 0...1 kΩ	1
536 777	Decade resistor, 0...100 Ω	1
536 778	Decade resistor, 0...10 Ω	1
536 779	Decade resistor, 0...1 Ω	1
521 487	AC/DC power supply PRO 0...12 V/3 A	1
531 131	Galvanometer PT 3204	1
501 26	Connecting lead, 32 A, 50 cm, blue	2
501 28	Connecting lead, 32 A, 50 cm, black	3
501 30	Connecting lead, 32 A, 100 cm, red	1
501 31	Connecting lead, 32 A, 100 cm, blue	1

In modern measuring practice, the bridge configuration developed in 1843 by *Ch. Wheatstone* is used almost exclusively.

In the experiment P3.2.3.4, a voltage U is applied to a 1 m long measuring wire with a constant cross-section. The ends of the wire are connected to an unknown resistor R_x and a variable resistor R arranged behind it, whose value is known precisely. A sliding contact divides the measuring wire into two parts with the lengths s_1 and s_2. The slide contact is connected to the node between R_x and R via an ammeter which is used as a zero indicator. Once the current has been regulated to zero, the relationship

$$R_x = \frac{s_1}{s_2} \cdot R$$

applies. Maximum accuracy is achieved by using a symmetrical experiment setup, i. e. when the slide contact over the measuring wire is set in the middle position so that the two sections s_1 and s_2 are the same length.
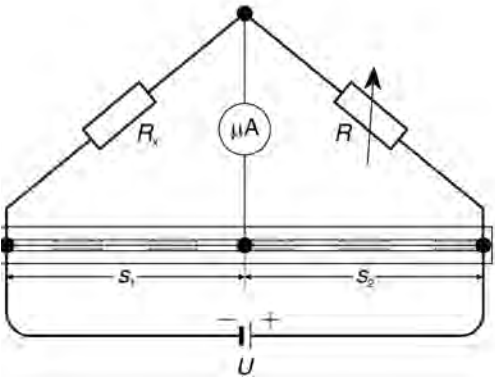
Circuit diagram of Wheatstone bridge (P3.2.3.4)

CIRCUITS WITH ELECTRICAL MEASURING INSTRUMENTS

P3.2.4.1
The ammeter as an ohmic resistor in a circuit

P3.2.4.2
The voltmeter as an ohmic resistor in a circuit

The ammeter as an ohmic resistor in a circuit (P3.2.4.1)

Cat. No.	Description	P3.2.4.1	P3.2.4.2
521 487	AC/DC power supply PRO 0...12 V/3 A	1	1
576 81	Plug-in board safety socket, 20/10	1	1
577 33	Resistor, 82 Ω, STE 2/19	3	
577 52	Resistor 4.7 kOhm, STE 2/19	1	1
531 110	Multimeter LDanalog 10	2	2
501 48	Bridging plugs STE 2/19, set of 10	1	
500 621	Safety connecting lead 50 cm, red	3	3
500 622	Safety connecting lead 50 cm, blue	3	3
577 75	Resistor, 680 kΩ, STE 2/19		1
577 71	Resistor, 220 kΩ, STE 2/19		1

One important consequence of Kirchhoff's laws is that the internal resistance of an electrical measuring instrument affects the respective current or voltage measurement. Thus, an ammeter increases the overall resistance of a circuit by the amount of its own internal resistance and thus measures a current value which is too low whenever the internal resistance is above a negligible level. A voltmeter measures a voltage value which is too low when its internal resistance is not great enough with respect to the resistance at which the voltage drop is to be measured.

In the experiment P3.2.4.1, the internal resistance of an ammeter is determined by measuring the voltage which drops at the ammeter during current measurement. It is subsequently shown that the deflection of the ammeter pointer is reduced by half, or that the current measuring range is correspondingly doubled, by connecting a second resistor equal to the internal resistance in parallel to the ammeter.

The experiment P3.2.4.2 determines the internal resistance of a voltmeter by measuring the current flowing through it. In this experiment, the measuring range is extended by connecting a second resistor with a value equal to the internal resistance to the voltmeter in series.

Determining the Faraday constant (P3.2.5.1)
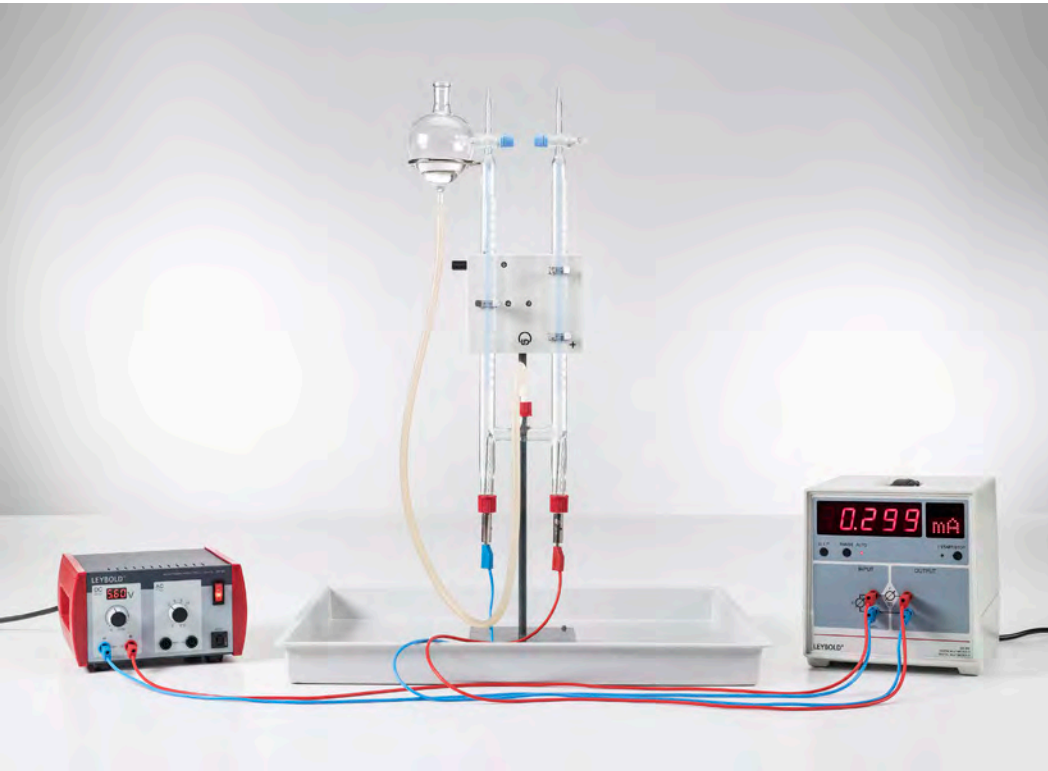
CONDUCTING ELECTRICITY BY MEANS OF ELECTROLYSIS

P3.2.5.1
Determining the Faraday constant

Cat. No.	Description	P3.2.5.1
664 350	Water electrolysis apparatus	1
382 35	Thermometer, -10...+50 °C/0.1 K	1
531 832	Digital multimeter P	1
521 487	AC/DC power supply PRO 0...12 V/3 A	1
501 45	Connecting lead 19 A, 50 cm, red/blue, pair	1
501 46	Connecting leads 19 A, 100 cm, red/blue, pair	1
649 45	Tray, 552 mm x 459 mm x 48 mm	1
674 7920	Sulfuric acid, diluted, approx. 2 N, 500 ml	1

In electrolysis, the processes of electrical conduction entails liberation of material. The quantity of liberated material is proportional to the transported charge Q flowing through the electrolyte. This charge can be calculated using the Faraday constant F, a universal constant which is related to the unit charge e by means of Avogadro's number N_A.

$$F = N_A \cdot e$$

When we insert the molar mass n for the material quantity and take the valence z of the separated ions into consideration, we obtain the relationship

$$Q = n \cdot F \cdot z$$

In the experiment P3.2.5.1, a specific quantity of hydrogen is produced in an electrolysis apparatus according to Hofmann to determine the Faraday constant. The valance of the hydrogen ions is $z = 1$. The molar mass n of the liberated hydrogen atoms is calculated using the laws of ideal gas on the basis of the volume V of the hydrogen collected at an external pressure p and room temperature T:

$$n = 2 \cdot \frac{pV}{RT}$$

$$\text{where } R = 8.314 \ \frac{\text{J}}{\text{mol} \cdot \text{K}} \ \text{(universal gas constant)}$$

At the same time, the electric work W is measured which is expended for electrolysis at a constant voltage U_0. The transported charge quantity is then

$$Q = \frac{W}{U_0}$$

BASIC EXPERIMENTS ON MAGNETOSTATICS

P3.3.1.1
Displaying lines of magnetic flux
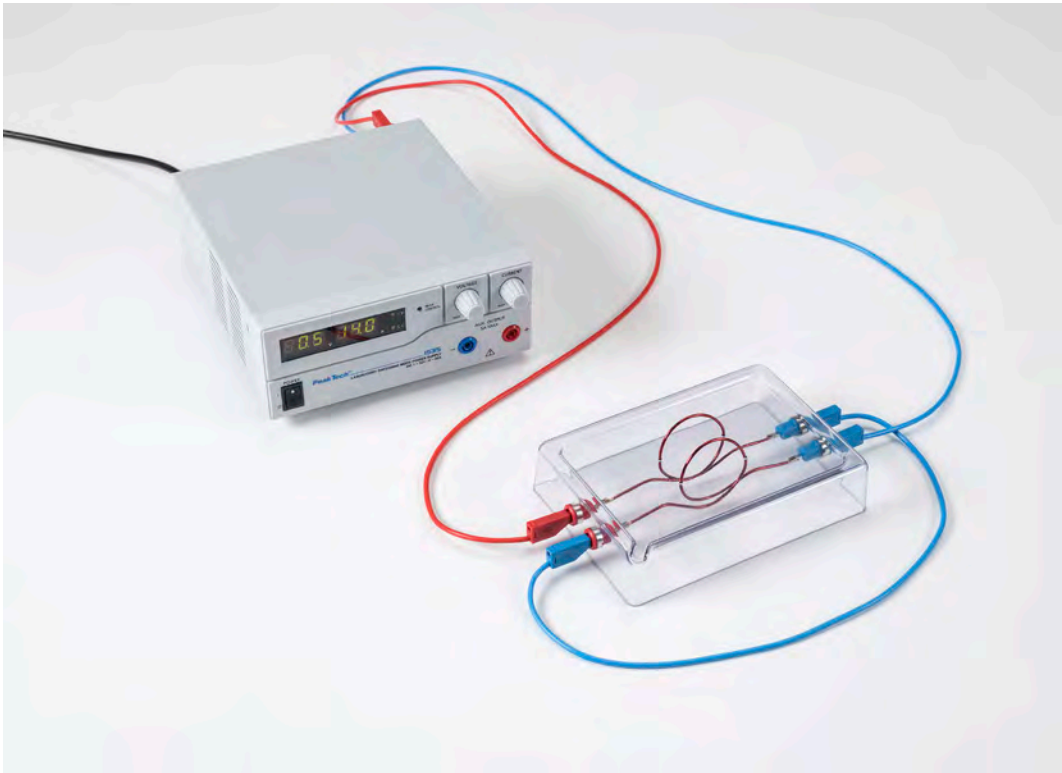
Displaying lines of magnetic flux (P3.3.1.1)

Cat. No.	Description	P3.3.1.1
560 701	Magnetic field demonstration set	1
726 890	DC-High Current Power Supply 1...32 V/0...20 A	1
501 26	Connecting lead, 32 A, 50 cm, blue	1
501 30	Connecting lead, 32 A, 100 cm, red	1
501 31	Connecting lead, 32 A, 100 cm, blue	1
MIK 74708	BMS SyncCam 8Mp	1*
	additionally required: PC or device for image display	1

* additionally recommended

Magnetostatics studies the spatial distribution of magnetic fields in the vicinity of permanent magnets and stationary currents as well as the force exerted by a magnetic field on magnets and currents. Basic experiments on this topic can be carried out without complex experiment setups.

In the experiment P3.3.1.1, magnetic fields are observed by spreading iron filings over a smooth surface so that they align themselves with the lines of magnetic flux. By this means it becomes possible to display the magnetic field of a straight conductor, the magnetic field of a conductor loop and the magnetic field of a coil.
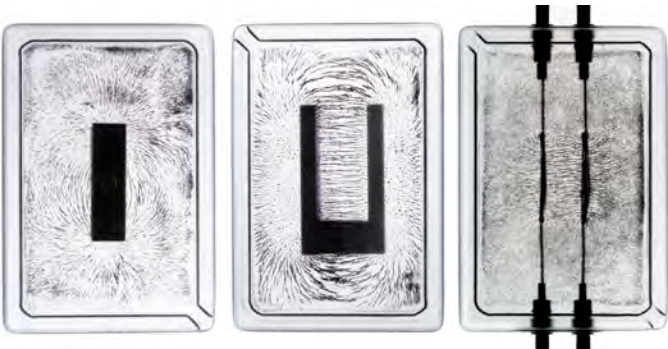

Displaying lines of magnetic flux (P3.3.1.1)

EFFECTS OF FORCE IN A MAGNETIC FIELD

P3.3.3.1
Measuring the force acting on current-carrying conductors in the field of a horseshoe magnet

P3.3.3.2
Measuring the force acting on current-carrying conductors in a homogeneous magnetic field - Recording with CASSY

Measuring the force acting on current-carrying conductors in the field of a horseshoe magnet (P3.3.3.1)

Cat. No.	Description	P3.3.3.1	P3.3.3.2
510 22	Large horseshoe magnet with yoke	1	
314 265	Support for conductor loops	1	1
516 34	Conductor loops for force measurement	1	1
726 890	DC-High Current Power Supply 1...32 V/0...20 A	1	1
524 005W	Mobile-CASSY 2 WiFi	1	
524 060	Force sensor S, ±1N	1	1
300 02	Stand base, V-shaped, small	1	1
300 42	Stand rod, 47 cm, 12 mm diam.	1	1
301 01	Leybold multiclamp	1	1
501 30	Connecting lead, 32 A, 100 cm, red	1	2
501 31	Connecting lead, 32 A, 100 cm, blue	1	2
562 11	U-core with yoke		1
562 14	Coil, 500 turns		2
562 25	Pole-shoe yoke		1
524 013	Sensor-CASSY 2		1
524 220	CASSY Lab 2		1
524 0431	30-A-Box		1
531 183	Digital multimeter 3340		1
521 487	AC/DC power supply PRO 0...12 V/3 A		1
501 26	Connecting lead, 32 A, 50 cm, blue		3
	additionally required: PC with Windows XP/Vista/7/8/10 (x86 or x64)		1

To measure the force acting on a current-carrying conductor in a magnetic field, conductor loops are attached to a force sensor. The force sensor contains two bending elements arranged in parallel with four strain gauges connected in a bridge configuration; their resistance changes in proportion to the force when a strain is applied. The force sensor is connected to the CASSY computer interface device. A 30 ampere box is recommended for current measurement.

In the experiment P3.3.3.1, the conductor loops are placed in the magnetic field of a horseshoe magnet. This experiment measures the force F as a function of the current I, the conductor length s and the angle α between the magnetic field and the conductor, and reveals the relationship

$$F = I \cdot s \cdot B \cdot \sin\alpha$$

In the experiment P3.3.3.2, a homogeneous magnetic field is generated using an electromagnet with U-core and pole-piece attachment. This experiment measures the force F as a function of the current I. The measurement results for various conductor lengths s are compiled and evaluated in a graph.

CASSY®

EFFECTS OF FORCE IN A MAGNETIC FIELD

P3.3.3.3
Measuring the force acting on current-carrying conductors in the magnetic field of an air coil – Recording with CASSY

P3.3.3.4
Basic measurements for the electrodynamic definition of the ampere
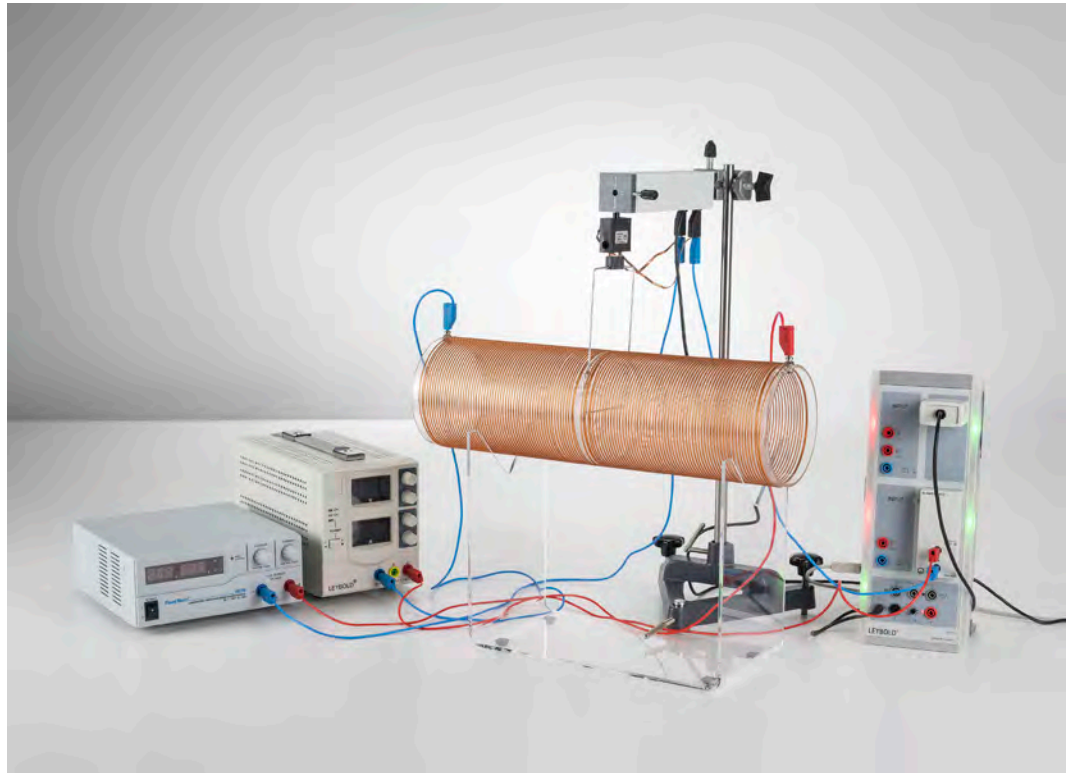
Measuring the force acting on current-carrying conductors in the magnetic field of an air coil – Recording with CASSY (P3.3.3.3)

Cat. No.	Description	P3.3.3.3	P3.3.3.4
314 265	Support for conductor loops	1	1
516 34	Conductor loops for force measurement	1	
516 244	Field coil, d = 120 mm	1	
516 249	Stand for tubes and coils	1	
524 013	Sensor-CASSY 2	1	
524 220	CASSY Lab 2	1	
524 0431	30-A-Box	1	
524 060	Force sensor S, ±1N	1	1
521 546	DC Power Supply 0...16 V/0...5 A	1	
726 890	DC-High Current Power Supply 1...32 V/0...20 A	1	1
300 02	Stand base, V-shaped, small	1	1
300 42	Stand rod, 47 cm, 12 mm diam.	1	1
301 01	Leybold multiclamp	1	1
501 26	Connecting lead, 32 A, 50 cm, blue	1	1
501 30	Connecting lead, 32 A, 100 cm, red	2	1
501 31	Connecting lead, 32 A, 100 cm, blue	2	1
516 33	Conductors for Ampere definition		1
516 31	Vertically adjustable stand		1
524 005W	Mobile-CASSY 2 WiFi		1
	additionally required: PC with Windows XP/Vista/7/8/10 (x86 or x64)	1	

To measure the force acting on a current-carrying conductor in a magnetic field, conductor loops are attached to a force sensor. The force sensor contains two bending elements arranged in parallel with four strain gauges connected in a bridge configuration; their resistance changes in proportion to the force when a strain is applied. The force sensor is connected to the CASSY computer interface device. A 30 ampere box is recommended for current measurement.

The experiment P3.3.3.3 uses an air coil to generate the magnetic field. The magnetic field is calculated from the coil parameters and compared with the values obtained from the force measurement.

The object of the experiment P3.3.3.4 is the former electrodynamic definition of the ampere. Here, the current is defined on the basis of the force exerted between two parallel conductors of infinite length which carry an identical current. When r represents the distance between the two conductors, the force per unit of length of the conductor is:

$$\frac{F}{s} = \mu_0 \cdot \frac{I_2}{2\pi \cdot r}$$

This experiment uses two conductors approx. 30 cm long, placed just a few millimeters apart. The forces F are measured as a function of the different current levels I and distances r.

CASSY®

Measuring the magnetic field for a straight conductor and on circular conductor loops (P3.3.4.1)

P3.3.4.1
Measuring the magnetic field for a straight conductor and on circular conductor loops

P3.3.4.2
Measuring the magnetic field of an air coil

P3.3.4.4
Measuring the magnetic field for a straight conductor and on circular conductor loops at small currents

P3.3.4.5
Measuring the magnetic field of an air coil at small currents

Cat. No.	Description	P3.3.4.1	P3.3.4.2	P3.3.4.4	P3.3.4.5
516 235	Current conductors, set of 4	1		1	
524 005W	Mobile-CASSY 2 WiFi	1	1	1	1
524 0381	Combi B sensor S	1			
501 11	Extension cable, 15 pin	1	1	1	1
726 890	DC-High Current Power Supply 1...32 V/0...20 A	1	1		
460 21	Holder for plug-in elements	1		1	
460 310	Optical bench, S1 profile, 1 m	1		1	
460 311	Clamp rider with clamp 45/65	1		1	
460 312	Clamp rider with clamp 45/35	1		1	
501 644	Two-way adapters, black, set of 6	1		1	
501 30	Connecting lead, 32 A, 100 cm, red	1	1	1	1
501 31	Connecting lead, 32 A, 100 cm, blue	1	1	1	1
516 242	Coil with variable number of turns per unit length		1		1
516 249	Stand for tubes and coils		1		1
524 0382	Axial B sensor S, ±1000 mT		1		
300 11	Saddle base		1		
524 0383	Axial B sensor S, ±0.3 mT			1	1
521 546	DC Power Supply 0...16 V/0...5 A			1	1
301 01	Leybold multiclamp			1	
300 42	Stand rod, 47 cm, 12 mm diam.			1	

In principle, it is possible to calculate the magnetic field of any current-carrying conductor using Biot and Savart's law. However, analytical solutions can only be derived for conductors with certain symmetries, e.g. for an infinitely long straight wire, a circular conductor loop and a cylindrical coil. Biot and Savart's law can be verified easily using these types of conductors.

In the experiments P3.3.4.1 and P3.3.4.4, the magnetic field of a long, straight conductor is measured for various currents I as a function of the distance r from the conductor. The result is a quantitative confirmation of the relationship

$$B = \frac{\mu_0}{2\pi} \cdot \frac{I}{r}$$

In addition, the magnetic fields of circular coils with different radii R are measured as a function of the distance x from the axis through the center of the coil. The measured values are compared with the values which are calculated using the equation

$$B = \frac{\mu_0}{2} \cdot \frac{I \cdot R^2}{\left(R^2 + x^2\right)^{\frac{3}{2}}}$$

The measurements in P3.3.4.1 are carried out using the combi B sensor. This device contains two Hall sensors for the field measurements. In experiment P3.3.4.4 a sensitive magnetic field sensor is used and the experiment is performed at low current levels.

The experiments P3.3.4.2 and P3.3.4.5 investigate the magnetic field of an air coil in which the length L can be varied for a constant number of turns N. For the magnetic field the relationship

$$B = \mu_0 \cdot I \cdot \frac{N}{L}$$

applies.
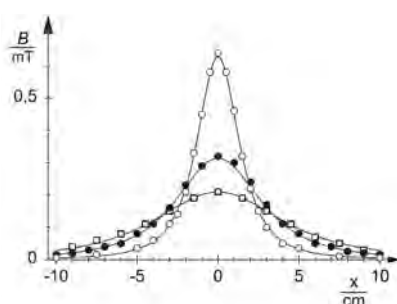
The magnetic field B of circular conductor loops with radius R as a function of the space coordinate x (P3.3.4.1).

BIOT–SAVART'S LAW

P3.3.4.3
Measuring the magnetic field of a pair of coils in the Helmholtz configuration

P3.3.4.6
Measuring the magnetic field of a pair of coils in the Helmholtz configuration at small currents

Measuring the magnetic field of a pair of coils in the Helmholtz configuration (P3.3.4.3)

Cat. No.	Description	P3.3.4.3	P3.3.4.6
555 604	Pair of Helmholtz coils	1	1
524 005W	Mobile-CASSY 2 WiFi	1	1
524 0382	Axial B sensor S, ±1000 mT	1	
501 11	Extension cable, 15 pin	1	1
521 546	DC Power Supply 0...16 V/0...5 A	1	1
460 310	Optical bench, S1 profile, 1 m	1	1
460 311	Clamp rider with clamp 45/65	1	1
460 312	Clamp rider with clamp 45/35	2	2
501 26	Connecting lead, 32 A, 50 cm, blue	1	1
501 30	Connecting lead, 32 A, 100 cm, red	1	1
501 31	Connecting lead, 32 A, 100 cm, blue	1	2
524 0383	Axial B sensor S, ±0.3 mT		1

In principle, it is possible to calculate the magnetic field of any current-carrying conductor using Biot and Savart's law. However, analytical solutions can only be derived for conductors with certain symmetries, e.g. for an infinitely long straight wire, a circular conductor loop and a cylindrical coil. Biot and Savart's law can be verified easily using these types of conductors.

The experiments P3.3.4.3 and P3.3.4.6 examine the homogeneity of the magnetic field in a pair of Helmholtz coils. The magnetic field along the axis through the coil centers is recorded in several measurement series; the spacing a between the coils is varied from measurement series to measurement series. When a is equal to the coil radius, the magnetic field is essentially independent of the location x on the coil axis.

Generating a voltage surge in a conductor loop with a moving permanent magnet (P3.4.1.1)

VOLTAGE IMPULSE

P3.4.1.1
Generating a voltage surge in a conductor loop with a moving permanent magnet

Cat. No.	Description	P3.4.1.1
510 12	Cylindrical bar magnets, pair	1
562 13	Coil, 250 turns	1
562 14	Coil, 500 turns	1
562 15	Coil, 1 000 turns	1
524 013	Sensor-CASSY 2	1
524 220	CASSY Lab 2	1
501 46	Connecting leads 19 A, 100 cm, red/blue, pair	1
	additionally required: PC with Windows XP/Vista/7/8/10 (x86 or x64)	1

Each change in the magnetic flux Φ through a conductor loop induces a voltage U, which has a level proportional to the change in the flux. Such a change in the flux is caused e. g. when a permanent magnet is moved inside a fixed conductor loop. In this case, it is common to consider not only the time-dependent voltage

$$U = -\frac{d\Phi}{dt}$$

but also the voltage surge

$$\int_{t_1}^{t_2} U(t)\,dt = \Phi(t_1) - \Phi(t_2)$$

This corresponds to the difference in the magnetic flux densities before and after the change.

In the experiment P3.4.1.1, the voltage surge is generated by manually inserting a bar magnet into an air coil, or pulling it out of a coil. The curve of the voltage U over time is measured and the area inside the curve is evaluated. This is always equal to the flux Φ of the permanent magnet inside the air coil independent of the speed at which the magnet is moved, i. e. proportional to the number of turns of the coil for equal coil areas.
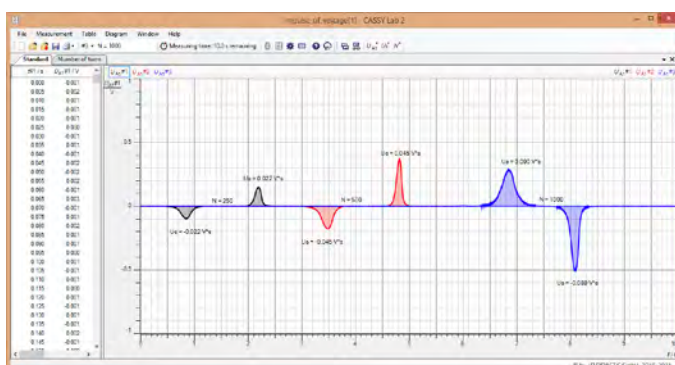
Induced voltages of a moving magnet (P3.4.1.1)

INDUCTION IN A MOVING CONDUCTOR LOOP

P3.4.2.1
Measuring the induction voltage in a conductor loop moved through a magnetic field

Measuring the induction voltage in a conductor loop moved through a magnetic field (P3.4.2.1)

Cat. No.	Description	P3.4.2.1
516 40	Induction apparatus with wire loops	1
510 48	Magnets, 35 mm Ø, pair	6
347 38	Experiment motor 93 W	1
521 547	DC Power Supply 0...30 V/0...5 A	1
524 005W	Mobile-CASSY 2 WiFi	1
524 0401	µV sensor S	1
500 641	Safety connecting lead, 100 cm, red	1
500 642	Safety connecting lead, 100 cm, blue	1

When a conductor loop with the constant width b is withdrawn from a homogeneous magnetic field B with the speed

$$v = \frac{dx}{dt}$$

the magnetic flux changes over the time dt by the value

$$d\Phi = -B \cdot b \cdot dx$$

This change in flux induces the voltage

$$U = B \cdot b \cdot v$$

in the conductor loop.

In the experiment P3.4.2.1, a slide on which induction loops of various widths are mounted is moved between the two pole pieces of a magnet. The object is to measure the induction voltage U as a function of the magnetic flux density B, the width b and the speed v of the induction loops. The aim of the evaluation is to verify the proportionalities

$$U \propto B, \ U \propto b, \ U \propto v$$
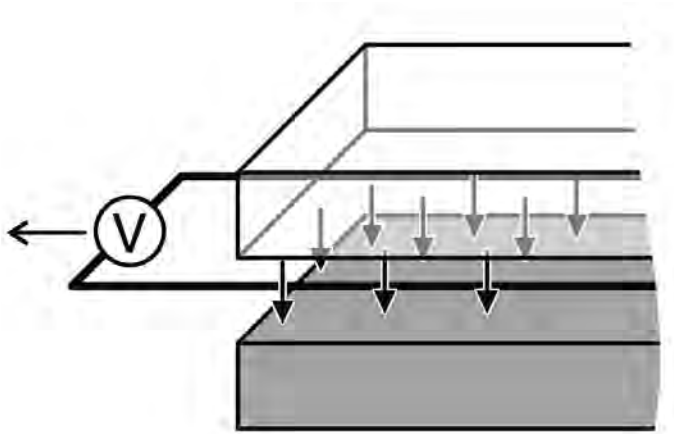
Induction voltage in a moved conductor loop (P3.4.2.1).

CASSY®

Measuring the induction voltage in a conductor loop for a variable magnetic field - with Power-CASSY as variable source of current (P3.4.3.2)

INDUCTION BY MEANS OF A VARIABLE MAGNETIC FIELD

P3.4.3.2
Measuring the induction voltage in a conductor loop for a variable magnetic field - with Power-CASSY as variable source of current
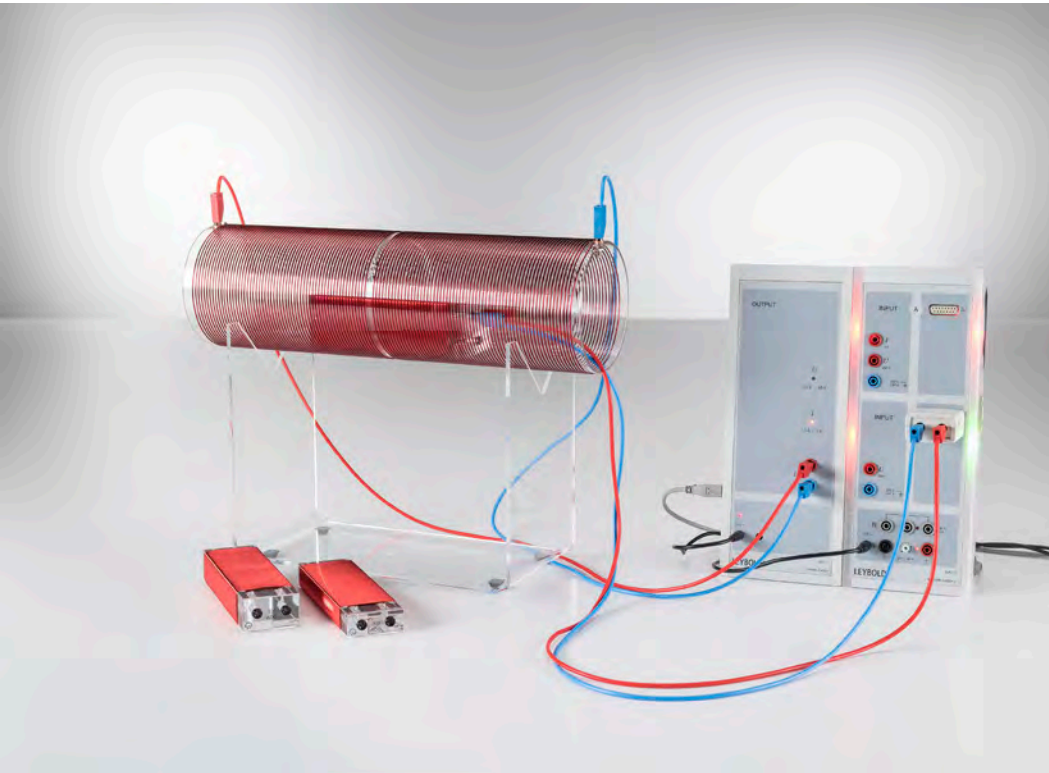
Cat. No.	Description	P3.4.3.2
516 249	Stand for tubes and coils	1
516 244	Field coil, d = 120 mm	1
516 241	Induction coils, set of 3	1
524 011USB	Power-CASSY USB	1
524 013	Sensor-CASSY 2	1
524 220	CASSY Lab 2	1
524 0401	µV sensor S	1
501 46	Connecting leads 19 A, 100 cm, red/blue, pair	2
	additionally required: PC with Windows XP/Vista/7/8/10 (x86 or x64)	1

A change in the homogeneous magnetic field B inside a coil with N_1 windings and the area A_1 over time induces the voltage

$$U = N_1 \cdot A_1 \cdot \frac{dB}{dt}$$

in the coil.

In the experiment P3.4.3.2, induction coils with different areas and numbers of turns are arranged in a cylindrical field coil through which alternating currents of various frequencies, amplitudes and signal forms flow. In the field coil, the currents generate the magnetic field

$$B = \mu_0 \cdot \frac{N_2}{L_2} \cdot I$$

$$\text{where } \mu_0 = 4\pi \cdot 10^{-7} \ \frac{\text{Vs}}{\text{Am}} \ (\text{permeablility})$$

and $I(t)$ is the time-dependent current level, N_2 the number of turns and L_2 the overall length of the coil. The curve over time $U(t)$ of the voltages induced in the induction coils is recorded using the CASSY system. This experiment explores how the voltage is dependent on the area and the number of turns of the induction coils, as well as on the frequency, amplitude and signal form of the exciter current.

TRANSFORMER

P3.4.5.1
Voltage and current transformation with a transformer

P3.4.5.2
Voltage transformation with a transformer under load

P3.4.5.3
Recording the voltage and current of a transformer under load as a function of time

Voltage and current transformation with a transformer (P3.4.5.1)

Cat. No.	Description	P3.4.5.1	P3.4.5.2	P3.4.5.3
562 801	Transformer for students' experiments	1	1	1
531 120	Multimeter LDanalog 20	2	2	
521 391	AC/DC power supply 0...24 V/5 A	1	1	
500 444	Connecting lead 19 A, 100 cm, black	6	7	6
537 34	Rheostat, 100 ohms		1	1
459 23	Acrylic glass screen on rod		1	
514 72	Shaker for iron filings		1	
514 73	Iron powder		1	
524 013	Sensor-CASSY 2			1
524 011USB	Power-CASSY USB			1
524 220	CASSY Lab 2			1
500 414	Connecting lead, 19 A, 25 cm, black			1
	additionally required: PC with Windows XP/Vista/7/8/10 (x86 or x64)			1

Voltage transformation with a transformer under load (P3.4.5.2)

Regardless of the physical design of the transformer, the voltage transformation of a transformer without load is determined by the ratio of the respective number of turns

$$\frac{U_2}{U_1} = \frac{N_2}{N_1} \ \left(\text{when } I_2 = 0\right)$$

The current transformation in short-circuit operation is inversely proportional to the ratio of the number of turns

$$\frac{I_2}{I_1} = \frac{N_2}{N_1}\left(\text{when } U_2 = 0\right)$$

The behavior of the transformer under load, on the other hand, depends on its particular physical design. This fact can be demonstrated using the transformer for students' experiments.

The aim of the experiment P3.4.5.1 is to measure the voltage transformation of a transformer without load and the current transformation of a transformer in short-circuit mode. At the same time, the difference between an isolating transformer and an autotransformer is demonstrated.

The experiment P3.4.5.2 examines the ratio between primary and secondary voltage in a "hard" and a "soft" transformer under load. In both cases, the lines of magnetic flux of the transformer are revealed using iron filings on a glass plate placed on top of the transformer.

In the experiment P3.4.5.3, the primary and secondary voltages and the primary and secondary currents of a transformer under load are recorded as time-dependent quantities using the CASSY system. The CASSY software determines the phase relationships between the four quantities directly and additionally calculates the time-dependent power values of the primary and secondary circuits.

TRANSFORMER

P3.4.5.4
Power transmission of a transformer
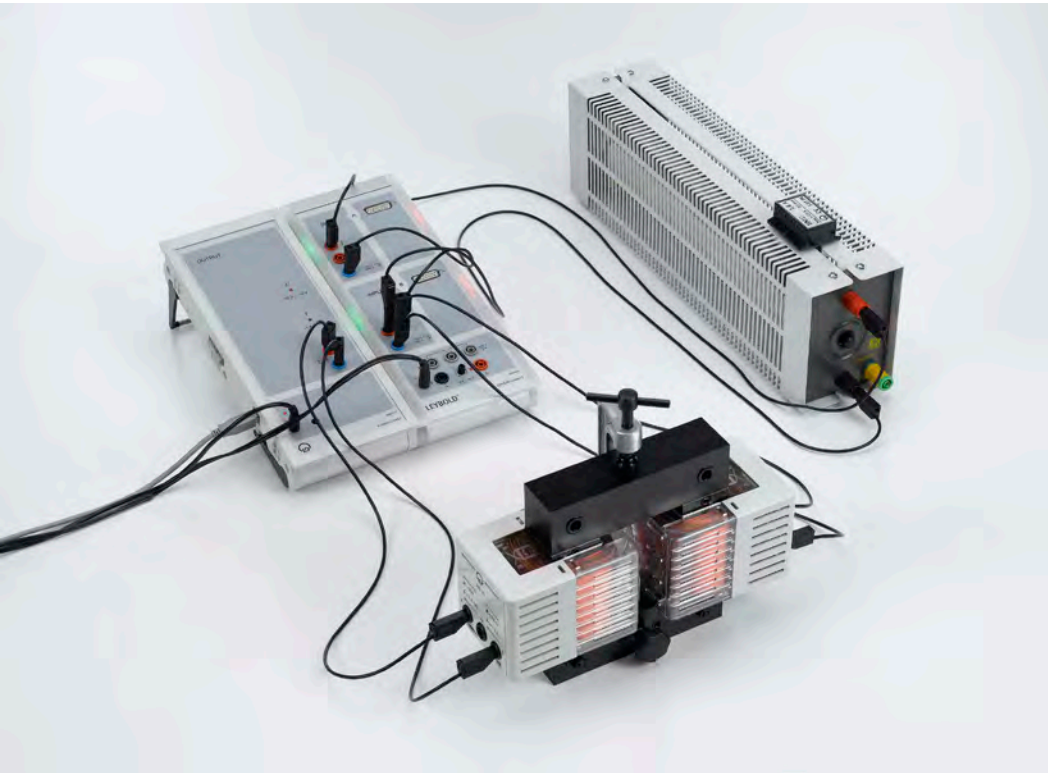
Power transmission of a transformer (P3.4.5.4)

Cat. No.	Description	P3.4.5.4
562 11	U-core with yoke	1
562 121	Clamping device with spring clip	1
562 13	Coil, 250 turns	2
524 013	Sensor-CASSY 2	1
524 011USB	Power-CASSY USB	1
524 220	CASSY Lab 2	1
537 34	Rheostat, 100 ohms	1
500 414	Connecting lead, 19 A, 25 cm, black	1
500 444	Connecting lead 19 A, 100 cm, black	6
	additionally required: PC with Windows XP/Vista/7/8/10 (x86 or x64)	1

As an alternative to the transformer for students' experiments, the demountable transformer with a full range of coils is available which simply slide over the arms of the U-core, making them easily interchangeable. The experiments described for the transformer for students' experiments (P3.4.5.1-3) can of course be performed just as effectively using the demountable transformer, as well as a number of additional experiments.

The experiment P3.4.5.4 examines the power transmission of a transformer. Here, the RMS values of the primary and secondary voltage and the primary and secondary current are measured on a variable load resistor $R = 0 - 100\ \Omega$ using the CASSY system. The phase shift between the voltage and current on the primary and secondary sides is determined at the same time. In the evaluation, the primary power P_1, the secondary power P_2 and the efficiency

$$\eta = \frac{P_2}{P_1}$$

are calculated and displayed in a graph as a function of the load resistance R.

CASSY®

MEASURING THE EARTH'S MAGNETIC FIELD

P3.4.6.2
Measuring the earth's magnetic field with a rotating induction coil and CASSY

Measuring the earth's magnetic field with a rotating induction coil and CASSY (P3.4.6.2)

Cat. No.	Description	P3.4.6.2
555 604	Pair of Helmholtz coils	1
348 22	Gyroscope axle	1
524 005W	Mobile-CASSY 2 WiFi	1
524 0401	µV sensor S	1
301 01	Leybold multiclamp	1
666 615	Universal bosshead	1
501 44	Connecting leads, 19 A, 25 cm, red/blue, pair	1

When a circular induction loop with N turns and a radius R rotates in a homogeneous magnetic field B around its diameter as its axis, it is permeated by a magnetic flux of

$$\Phi(t) = N \cdot \pi \cdot R^2 \cdot n(t) \cdot B$$

$n(t)$: normal vector of a rotating loop

If the angular velocity ω is constant, we can say that

$$\Phi(t) = N \cdot \pi \cdot R^2 \cdot B_\perp \cdot \cos \omega t$$

Where $B_\perp$ is the effective component of the magnetic field perpendicular to the axis of rotation. We can determine the magnetic field from the amplitude of the induced voltage

$$U_0 = N \cdot \pi \cdot R^2 \cdot B_\perp \cdot \omega$$

To achieve the maximum measuring accuracy, we need to use the largest possible coil.

In the experiment P3.4.6.2 the voltage $U(t)$ induced in the earth's magnetic field is measured in the rotating system and stored or transmitted wirelessly using the computer-based Mobile-CASSY measuring system. The amplitude and frequency of the recorded signals are used to calculate the horizontal component of the earth's magnetic field.

CASSY®

ELECTRIC GENERATORS

P3.5.2.1
Generating AC voltage using
a revolving-field generator and
a stationary-field generator

P3.5.2.2
Generating DC voltage using
a stationary-field generator

P3.5.2.3
Generating AC voltage using
a generator with electromagnetic
rotating pole (power-plant generator)

P3.5.2.4
Generating voltage with
an AC/DC generator (generator with
electromagnetic stationary pole)
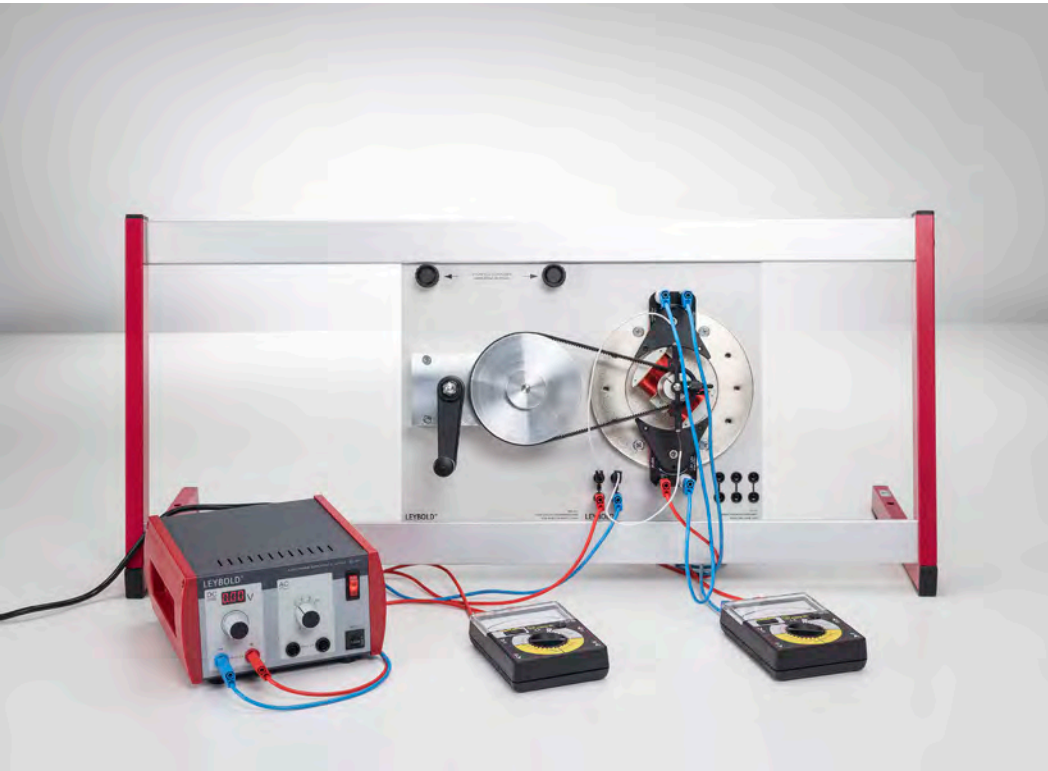
Generating AC voltage using a generator with electromagnetic rotating pole (power-plant generator) (P3.5.2.3)

Cat. No.	Description	P3.5.2.1	P3.5.2.2	P3.5.2.3	P3.5.2.4
563 480	ELM basic set	1	1	1	1
727 81	Basic machine unit	1	1	1	1
563 303	ELM hand-cranked gear	1	1	1	1
726 19	Panel frame SL85, single-level	1	1	1	1
531 120	Multimeter LDanalog 20	2	1	2	2
313 27	Hand-held stop-watch, 60s/0.2s	1			
537 36	Rheostat, 1000 ohms	1			
500 621	Safety connecting lead 50 cm, red	1		1	1
500 622	Safety connecting lead 50 cm, blue	1		1	1
500 641	Safety connecting lead, 100 cm, red	2	1	2	2
500 642	Safety connecting lead, 100 cm, blue	2	1	1	2
563 23	ELM three-pole rotor		1*		
575 302	Oscilloscope 30 MHz, digital, PT1265		1*		
575 24	Screened cable, BNC/4 mm		1*		
521 487	AC/DC power supply PRO 0...12 V/3 A			1	1

* additionally recommended

Electric generators exploit the principle of electromagnetic induction discovered by Faraday to convert mechanical into electrical energy. We distinguish between revolving-armature generators (excitation of the magnetic field in the stator, induction in the rotor) and revolving-field generators (excitation of the magnetic field in the rotor, induction in the stator).

Both types of generators are assembled in the experiment P3.5.2.1 using permanent magnets. The induced AC voltage U is measured as a function of the speed f of the rotor. Also, the electrical power P produced at a fixed speed is determined as a function of the load resistance R.

The experiment P3.5.2.2 demonstrates the use of a commutator to rectify the AC voltage generated in the rotor of a rotating-armature generator. The number of rectified half-waves per rotor revolution increases when the two-pole rotor is replaced with a threepole rotor.

The experiments P3.5.2.3 and P3.5.2.4 investigate generators which use electromagnets instead of permanent magnets. Here, the induced voltage depends on the excitation current of the magnetic field. The excitation current can be used to vary the generated power without changing the speed of the rotor or the frequency of the AC voltage. This principle is used in power-plant generators. In the AC/DC generator, the voltage can also be tapped via the commutator in rectified form.

LEYBOLD®

ELECTRIC MOTORS

P3.5.3.1
Experiments on DC motor
with two-pole rotor

P3.5.3.2
Experiments on DC motor
with three-pole rotor

P3.5.3.3
Experiments with a universal motor
in shunt connection

P3.5.3.4
Assembling an AC synchronous motor

Experiments with a universal motor in shunt connection (P3.5.3.3)

Cat. No.	Description	P3.5.3.1	P3.5.3.2	P3.5.3.3	P3.5.3.4
563 480	ELM basic set	1	1	1	1
727 81	Basic machine unit	1	1	1	1
726 19	Panel frame SL85, single-level	1	1	1	1
531 120	Multimeter LDanalog 20	2	2	2	
521 391	AC/DC power supply 0...24 V/5 A	1	1	1	1
451 281	Stroboscope	1	1	1	1
500 621	Safety connecting lead 50 cm, red	1	1	2	
500 622	Safety connecting lead 50 cm, blue	1	1	2	
500 641	Safety connecting lead, 100 cm, red	2	2	2	2
500 642	Safety connecting lead, 100 cm, blue	2	2	2	2
563 23	ELM three-pole rotor		1	1*	
314 151	Precision dynamometer, 2 N		1	1	
314 161	Precision dynamometer, 5 N		1	1	
309 50	Demonstration cord		1	1	
666 470	Holder with clamp, height-adjustable, CPS		1	1	
300 41	Stand rod, 25 cm, 12 mm Ø		1	1	
563 303	ELM hand-cranked gear				1
726 501	Safety socket plug-in board, 297 mm x 200 mm				1
579 13	Toggle switch STE 2/19				1
579 06	Lamp holder, E10, top, STE 2/19				1
505 181	Bulbs, 24 V/3 W, E10, set of 5				1

*additionally recommended

Electric motors exploit the force acting on current-carrying conductors in magnetic fields to convert electrical energy into mechanical energy. We distinguish between asynchronous motors, in which the rotor is supplied with AC or DC voltage via a commutator, and synchronous motors, which have no commutator, and whose frequencies are synchronized with the frequency of the applied voltage.

The experiment P3.5.3.1 investigates the basic function of an electric motor with commutator. The motor is assembled using a permanent magnet as stator and a two-pole rotor. The polarity of the rotor current determines the direction in which the rotor turns. This experiment measures the relationship between the applied voltage U and the no-load speed f_0.

The use of the three-pole rotor is the object of the experiment P3.5.3.2. The rotor starts turning automatically, as an angular momentum (torque) acts on the rotor for any position in the magnetic field. To record the torque curve $M(f)$, the speed f of the rotor is recorded as a function of a counter-torque M. In addition, the mechanical power produced is compared with the electrical power consumed.

The experiment P3.5.3.3 takes a look at the so-called universal motor, in which the stator and rotor fields are electrically excited. The stator and rotor coils are connected in series ("serieswound") or in parallel ("shunt-wound") to a common voltage source. This motor can be driven both with DC and AC voltage, as the torque acting on the rotor remains unchanged when the polarity is reversed. The torque curve $M(f)$ is recorded for both circuits. The experiment shows that the speed of the shuntwound motor is less dependent on the load than that of the series-wound motor.

In the experiment P3.5.3.4, the rotor coil of the AC synchronous motor is synchronized with the frequency of the applied voltage using a hand crank, so that the rotor subsequently continues running by itself.

THREE-PHASE MACHINES

P3.5.4.1
Experiments with a three-phase revolving-armature generator

P3.5.4.2
Experiments with a three-phase revolving-field generator

P3.5.4.3
Comparing star and delta connections on a three-phase generator

P3.5.4.4
Assembling synchronous and asynchronous three-phase motors
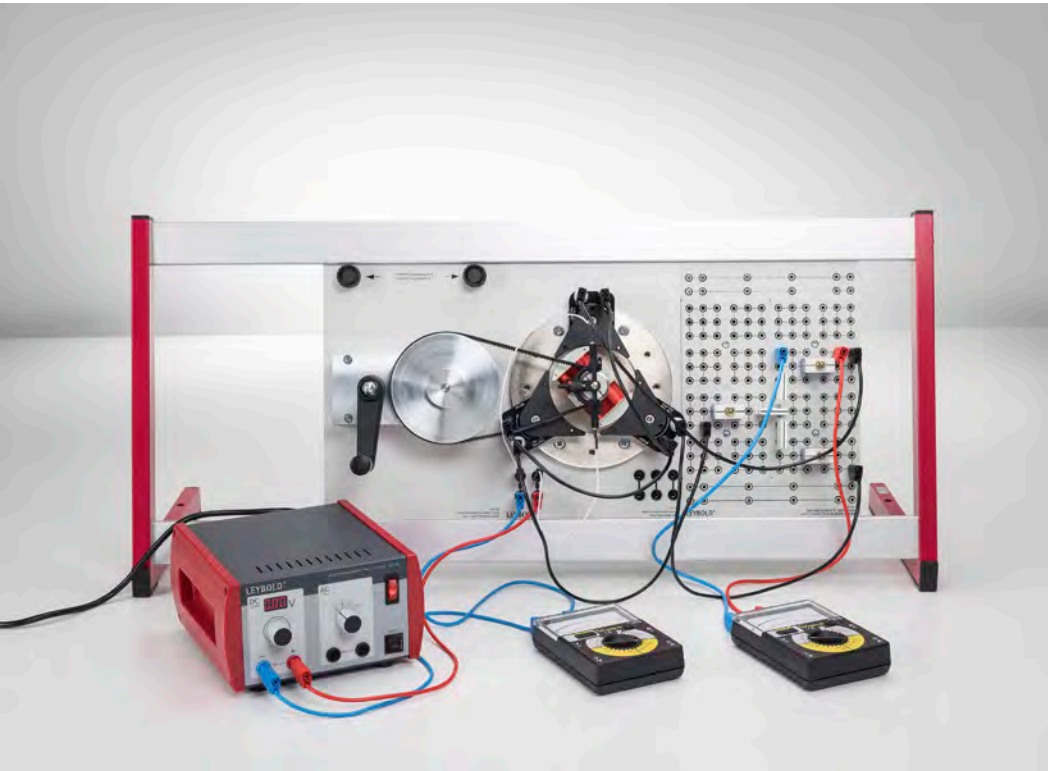
Comparing star and delta connections on a three-phase generator (P3.5.4.3)

Cat. No.	Description	P3.5.4.1	P3.5.4.2	P3.5.4.3	P3.5.4.4
563 480	ELM basic set	1	1	1	1
563 481	ELM supplementary set	1	1	1	1
727 81	Basic machine unit	1	1	1	1
563 303	ELM hand-cranked gear	1	1	1	
726 19	Panel frame SL85, single-level	1	1	1	1
531 120	Multimeter LDanalog 20	3	3	2	1
500 624	Safety connecting lead 50 cm, black	6	6	7	4
575 302	Oscilloscope 30 MHz, digital, PT1265	1*	1*		
575 24	Screened cable, BNC/4 mm	2*	2*		
313 27	Hand-held stop-watch, 60s/0.2s	1*	1*		
521 487	AC/DC power supply PRO 0...12 V/3 A		1	1	
500 621	Safety connecting lead 50 cm, red		1	3	1
500 622	Safety connecting lead 50 cm, blue		1	2	1
726 501	Safety socket plug-in board, 297 mm x 200 mm			1	
579 06	Lamp holder, E10, top, STE 2/19			3	
505 14	Bulbs, 6 V/3 W, E10, set of 10			1	
501 48	Bridging plugs STE 2/19, set of 10			1	
500 614	Safety connecting lead, 25 cm, black			3	3
563 12	ELM squirrel-cage rotor				1
521 291	Three-phase extra-low voltage transformer				1

* additionally recommended

In the real world, power is supplied mainly through the generation of three-phase AC, usually referred to simply as "threephase current". Consequently, three-phase generators and motors are extremely significant in actual practice. In principle, their function is analogous to that of AC machines. As with AC machines, we differentiate between revolving-armature and revolving-field generators, and between asynchronous and synchronous motors.

The simplest configuration for generating three-phase current, a revolving-armature generator which rotates in a permanent magnetic field, is assembled in the experiment P3.5.4.1 using a threepole rotor.

The experiment P3.5.4.2 examines the more common revolving-field generator, in which the magnetic field of the rotor in the stator coils is induced by phase-shifted AC voltages. In both cases, instruments for measuring current and voltage, and for observing the phase shift for a slowly turning rotor, are connected between two taps. For faster rotor speeds, the phase shift is measured using an oscilloscope.

In the experiment P3.5.4.3, loads are connected to the three-phase generator in star and delta configuration. In the star configuration, the relationship

$$\frac{U_{aa}}{U_{a0}} = \sqrt{3}$$

is verified for the voltages U_{aa} between any two outer conductors as well as U_{a0} between the outer and neutral conductors. For the currents I_1 flowing to the loads and the currents I_2 flowing through the generator coils in delta configuration, the result is

$$\frac{I_1}{I_2} = \sqrt{3}$$

The experiment P3.5.4.4 examines the behavior of asynchronous and synchronous machines when the direction of rotation is reversed.
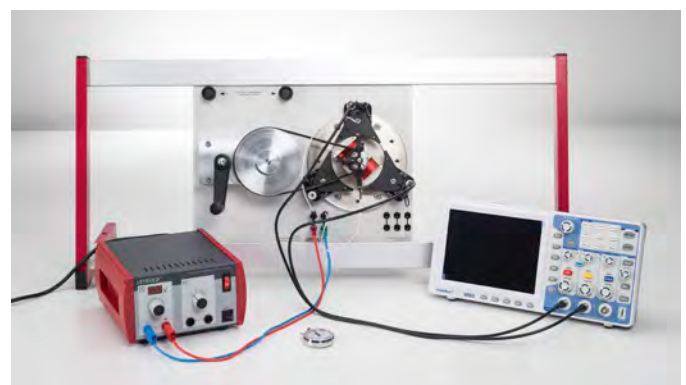
It can also be displayed with an oscilloscope (P3.5.4.2)

LEYBOLD®

ELECTRICITY
DC AND AC CIRCUITS

CIRCUIT WITH CAPACITOR

P3.6.1.1
Charging and discharging a capacitor when switching DC on and off

P3.6.1.2
Determining the capacitive reactance of a capacitor in an AC circuit

P3.6.1.3
Charging and discharging a capacitor when switching DC on and off
- Measuring with a multimeter

P3.6.1.4
Charging and discharging a capacitor when switching DC on and off
- Measuring with Mobile-CASSY

P3.6.1.5
Determining the capacitive reactance of a capacitor in an AC circuit
- Measuring with Mobile-CASSY
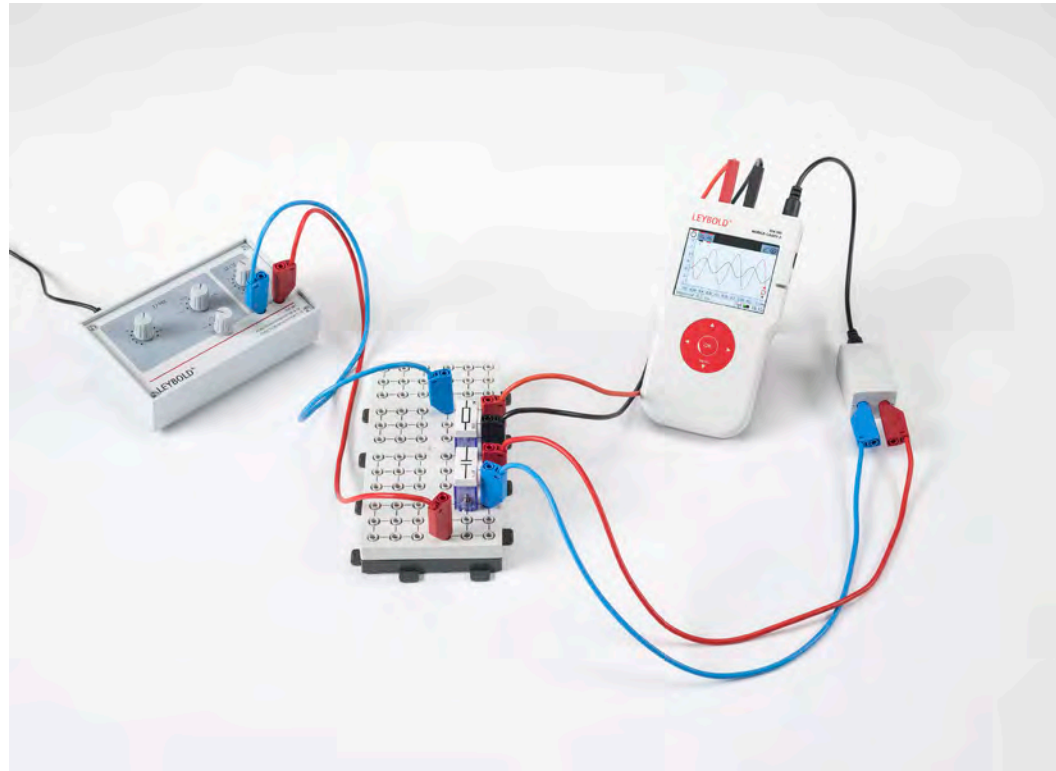
Determining the capacitive reactance of a capacitor in an AC circuit - Measuring with Mobile-CASSY (P3.6.1.5)

Cat. No.	Description	P3.6.1.1	P3.6.1.2	P3.6.1.3	P3.6.1.4	P3.6.1.5
576 81	Plug-in board safety socket, 20/10	1	1	1	1	1
578 15	Capacitor, 1 µF, STE 2/19	3	3		3	3
577 40	Resistor 470 Ohm, STE 2/19	1			1	
577 44	Resistor 1 kOhm, STE 2/19	1			1	
577 48	Resistor, 2.2 kΩ, STE 2/19	1			1	
522 621	Function generator S 12	1	1		1	1
575 302	Oscilloscope 30 MHz, digital, PT1265	1	1			
575 24	Screened cable, BNC/4 mm	2	2			
500 641	Safety connecting lead, 100 cm, red	1	1		3	3
500 642	Safety connecting lead, 100 cm, blue	1	1		2	2
577 19	Resistor, 1 Ω, STE 2/19		1			
577 20	Resistor, 10 Ω, STE 2/19		1			1
578 16	Capacitor, 4.7 µF, STE 2/19			1		
578 12	Capacitor, 10 µF, STE 2/50			1		
577 76	Resistor, 1 MΩ, STE 2/19			1		
582 81	Change-over switch STE 4/50			1		
501 48	Bridging plugs STE 2/19, set of 10			1		
521 487	AC/DC power supply PRO 0...12 V/3 A			1		
531 120	Multimeter LDanalog 20			1		
313 27	Hand-held stop-watch, 60s/0.2s			1		
500 621	Safety connecting lead 50 cm, red			2		
500 622	Safety connecting lead 50 cm, blue			2		
524 005W	Mobile-CASSY 2 WiFi				1	1
524 438	Voltage sensor M, ±30 V				1	1
500 644	Safety connecting lead, 100 cm, black				1	1

To investigate the behavior of capacitors in DC and AC circuits, the voltage U_C at a capacitor is measured using a two-channel oscilloscope, and the current I_C through the capacitor is additionally calculated from the voltage drop across a resistor R connected in series. Alternatively a Mobile-CASSY 2 is used. The circuits for conducting these measurements are assembled on a plug-in board using the STE plug-in system. A function generator is used as a voltage source with variable amplitude and variable frequency.

In the experiments P3.6.1.1 and P3.6.1.4, the function generator generates periodic square-wave signals which simulate switching a DC voltage on and off. In experiment P3.6.1.1 the square-wave signals are displayed on channel I of the oscilloscope, and the capacitor voltage or capacitor current is displayed on oscilloscope channel II, while in experiment P3.6.1.4 the current and voltage are recorded by Mobile-CASSY 2. The aim of the experiment is to determine the time constant

$$\tau = R \cdot C$$

for various capacitances C from the exponential curve of the respective charging or discharge current I_C.

In the experiments P3.6.1.2 and P3.6.1.5, an AC voltage with the amplitude U_0 and the frequency f is applied to a capacitor. The voltage $U_C(t)$ and the current $I_C(t)$ are displayed simultaneously on the oscilloscope or recorded by Mobile-CASSY 2. The experiment shows that in this circuit the current leads the voltage by 90°. In addition, the proportionality between the voltage amplitude U_0 and the current amplitude I_0 is confirmed, and for the proportionality constant

$$Z_C = \frac{U_0}{I_0}$$

the relationship

$$Z_C = -\frac{1}{2\pi f \cdot C}$$

is revealed.

In experiment P3.6.1.3 a large capacitor is charged and discharged with a long time constant and the process can be recorded with a multimeter and a stopclock.
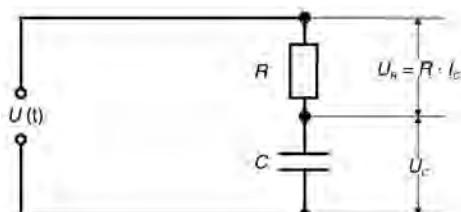
Schematic circuit diagram (P3.6.1.2+5)

Measuring the current in a coil when switching DC on and off - Measuring with Mobile-CASSY (P3.6.2.3)

CIRCUIT WITH COIL

P3.6.2.1
Measuring the current in a coil when switching DC on and off

P3.6.2.2
Determining the inductive reactance of a coil in an AC circuit

P3.6.2.3
Measuring the current in a coil when switching DC on and off - Measuring with Mobile-CASSY

P3.6.2.4
Determining the inductive reactance of a coil in an AC circuit - Measuring with Mobile-CASSY

Cat. No.	Description	P3.6.2.1	P3.6.2.2	P3.6.2.3	P3.6.2.4
576 81	Plug-in board safety socket, 20/10	1	1	1	1
590 84	Coil 1000 turns STE 2/50	2	2	2	2
577 19	Resistor, 1 Ω, STE 2/19	1	1		
577 20	Resistor, 10 Ω, STE 2/19	1	1	1	1
577 24	Resistor, 22 Ω, STE 2/19	1		1	
577 28	Resistor 47 Ohm, STE 2/19	1		1	
501 48	Bridging plugs STE 2/19, set of 10	1	1		
522 621	Function generator S 12	1	1	1	1
575 302	Oscilloscope 30 MHz, digital, PT1265	1	1		
575 24	Screened cable, BNC/4 mm	2	2		
500 641	Safety connecting lead, 100 cm, red	1	1	3	3
500 642	Safety connecting lead, 100 cm, blue	1	1	2	2
524 005W	Mobile-CASSY 2 WiFi			1	1
524 438	Voltage sensor M, ±30 V			1	1
500 644	Safety connecting lead, 100 cm, black			1	1

To investigate the behavior of coils in DC and AC circuits, the voltage U_L at a coil is measured using a two-channel oscilloscope, and the current I_L through the coil is additionally calculated from the voltage drop across a resistor R connected in series. Alternatively a Mobile-CASSY 2 can be used. The circuits for conducting these measurements are assembled on a plug-in board using the STE plug-in system for electricity/electronics. A function generator is used as a voltage source with variable amplitude and variable frequency.

In the experiments P3.6.2.1 and P3.6.2.3, the function generator generates periodic square-wave signals which simulate switching a DC voltage on and off. In experiment P3.6.2.1 the square-wave signals are displayed on channel I of the oscilloscope, and the coil voltage or coil current is displayed on oscilloscope channel II, while in experiment P3.6.2.3 the current and voltage are recorded by Mobile-CASSY 2. The aim of the experiment is to determine the time constant

$$\tau = \frac{L}{R}$$

for different inductances L from the exponential curve of the coil voltage U_L.

In the experiments P3.6.2.2 and P3.6.2.4, an AC voltage with the amplitude U_0 and the frequency f is applied to a coil. The voltage $U_L(t)$ and the current $I_L(t)$ are displayed simultaneously on the oscilloscope or recorded by Mobile-CASSY 2. The experiment shows that in this circuit the current lags behind the voltage by 90°. In addition, the proportionality between the voltage amplitude U_0 and the current amplitude I_0 is confirmed, and, for the proportionality constant

$$Z_L = \frac{U_0}{I_0}$$

the relationship

$$Z_L = 2\pi f \cdot L$$

is revealed.
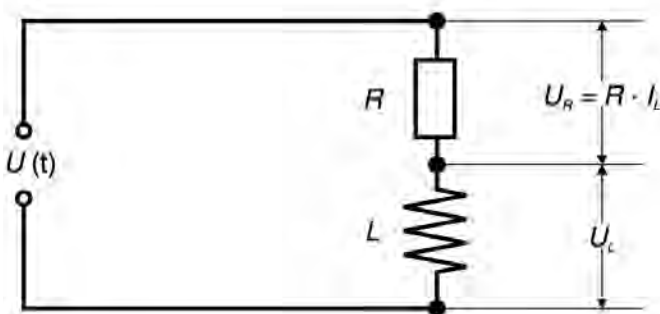
Schematic circuit diagram (P3.6.2.2+4)

CASSY®

IMPEDANCES

P3.6.3.1
Determining the impedance in circuits with capacitors and ohmic resistors

P3.6.3.2
Determining the impedance in circuits with coils and ohmic resistors

P3.6.3.3
Determining the impedance in circuits with capacitors and coils

P3.6.3.4
Determining the impedance in circuits with capacitors and ohmic resistors
- Measuring with Mobile-CASSY

P3.6.3.5
Determining the impedance in circuits with coils and ohmic resistors
- Measuring with Mobile-CASSY

P3.6.3.6
Determining the impedance in circuits with capacitors and coils
- Measuring with Mobile-CASSY
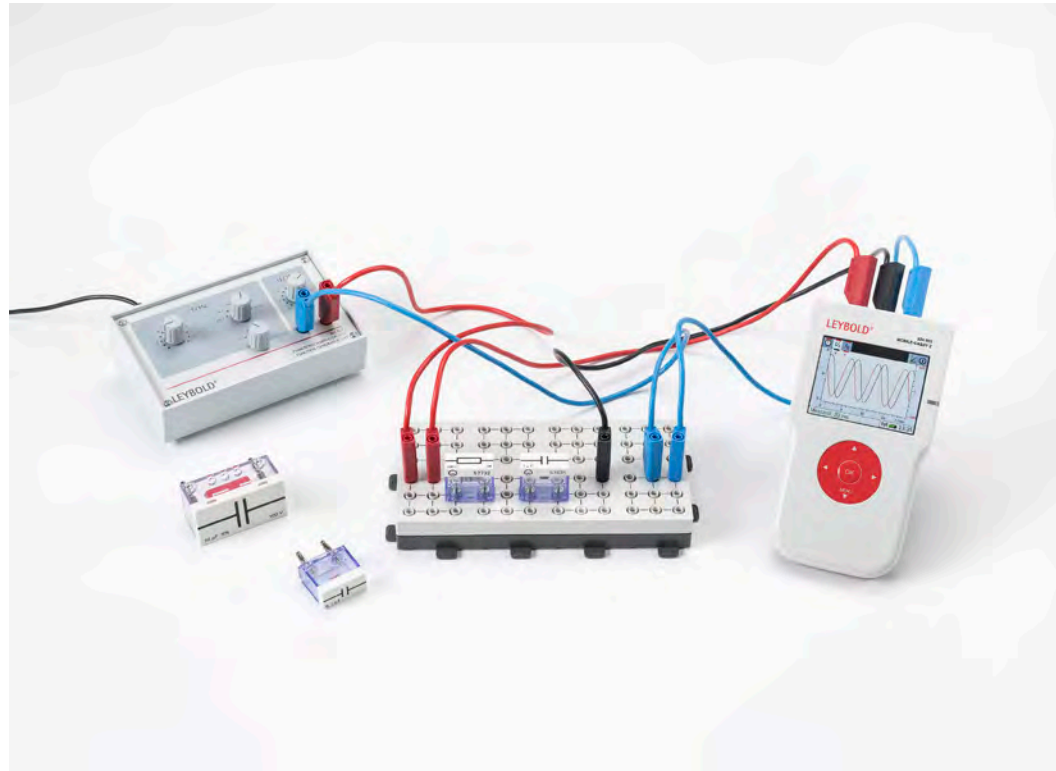
Determining the impedance in circuits with capacitors and ohmic resistors - Measuring with Mobile-CASSY (P3.6.3.4)

Cat. No.	Description	P3.6.3.1	P3.6.3.2	P3.6.3.3	P3.6.3.4	P3.6.3.5	P3.6.3.6
576 81	Plug-in board safety socket, 20/10	1	1	1	1	1	1
577 19	Resistor, 1 Ω, STE 2/19	1	1				
577 32	Resistor 100 Ohm, STE 2/19	1	1	1	1	1	1
578 12	Capacitor, 10 µF, STE 2/50	1			1		
578 15	Capacitor, 1 µF, STE 2/19	1		1	1		1
578 31	Capacitor, 0.1 µF, STE 2/19	1			1		
522 621	Function generator S 12	1	1	1	1	1	1
575 302	Oscilloscope 30 MHz, digital, PT1265	1	1	1			
575 24	Screened cable, BNC/4 mm	2	2	2			
500 641	Safety connecting lead, 100 cm, red	1	1	1	2	2	3
500 642	Safety connecting lead, 100 cm, blue	1	1	1	2	2	2
590 83	Coil 500 turns STE 2/50		1	1		1	1
590 84	Coil 1000 turns STE 2/50		1	1		1	1
577 20	Resistor, 10 Ω, STE 2/19			1			1
578 16	Capacitor, 4.7 µF, STE 2/19			1			1
524 005W	Mobile-CASSY 2 WiFi				1	1	1
500 644	Safety connecting lead, 100 cm, black				1	1	1
524 438	Voltage sensor M, ±30 V						1

The current $I(t)$ and the voltage $U(t)$ in an AC circuit are measured as time-dependent quantities using a dual-channel oscilloscope or a Mobile-CASSY 2. A function generator is used as a voltage source with variable amplitude U_0 and variable frequency f. The measured quantities are then used to determine the absolute value of the total impedance

$$Z = \frac{U_0}{I_0}$$

and the phase shift φ between the current and the voltage.

A resistor R is combined with a capacitor C in the experiments P3.6.3.1 and P3.6.3.4, and an inductor L in the experiments P3.6.3.2 and P3.6.3.5. These experiments confirm the relationship

$$Z_s = \sqrt{R^2 + Z_I^2} \text{ and } \tan\varphi_s = \frac{Z_I}{R}$$

with $Z_I = -\dfrac{1}{2\pi f \cdot C}$ resp. $Z_I = 2\pi f \cdot L$

for series connection and

$$\frac{1}{Z_P} = \sqrt{\frac{1}{R^2} + \frac{1}{Z_I^2}} \text{ and } \tan\varphi_P = \frac{R}{Z_I}$$

for parallel connection.

The experiments P3.6.3.3 and P3.6.3.6 examine the oscillator circuit as the series and parallel connection of capacitance and inductance. The total impedance of the series circuit

$$Z_s = 2\pi f \cdot L - \frac{1}{2\pi f \cdot C}$$

disappears at the resonance frequency

$$f_r = \frac{1}{2\pi \cdot \sqrt{LC}}$$

i.e. at a given current I the total voltage U at the capacitor and the coil is zero, because the individual voltages U_C and U_L are equal and opposite. For parallel connection, we can say

$$\frac{1}{Z_P} = \frac{1}{2\pi f \cdot L} - 2\pi f \cdot C$$

At the resonance frequency, the impedance of this circuit is infinitely great; in other words, at a given voltage U the total current I in the supply line is zero, as the two individual currents I_C and I_L are equal and opposed.
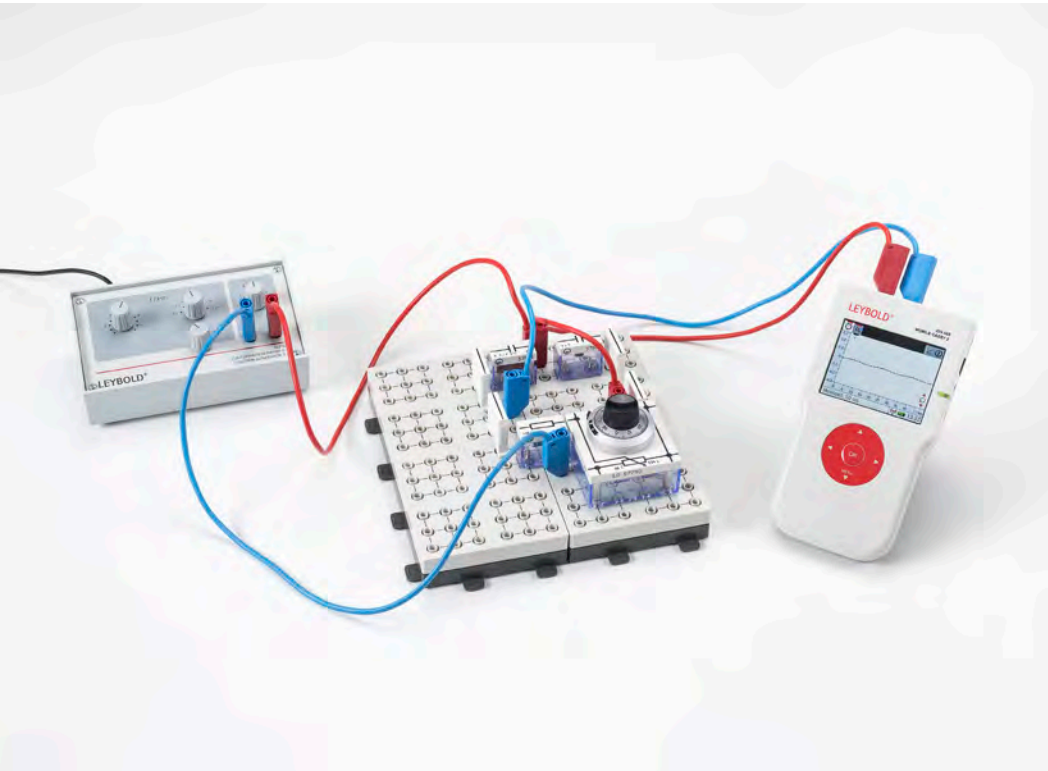
MEASURING–BRIDGE CIRCUITS

P3.6.4.1
Determining capacitive reactance with a Wien measuring bridge

P3.6.4.2
Determining inductive reactance with a Maxwell measuring bridge

P3.6.4.3
Determining capacitive reactance with a Wien measuring bridge
- Measuring with Mobile-CASSY

P3.6.4.4
Determining inductive reactance with a Maxwell measuring bridge
- Measuring with Mobile-CASSY

Determining capacitive reactance with a Wien measuring bridge - Measuring with Mobile-CASSY (P3.6.4.3)

Cat. No.	Description	P3.6.4.1	P3.6.4.2	P3.6.4.3	P3.6.4.4
576 81	Plug-in board safety socket, 20/10	2	2	2	2
577 32	Resistor 100 Ohm, STE 2/19	1	1	1	1
577 93	Potentiometer, 1 kΩ, 10-turn, STE 4/50	1	2	1	2
578 15	Capacitor, 1 µF, STE 2/19	1		1	
578 16	Capacitor, 4.7 µF, STE 2/19	1	1	1	1
575 302	Oscilloscope 30 MHz, digital, PT1265	1	1		
575 24	Screened cable, BNC/4 mm	1	1		
522 621	Function generator S 12	1	1	1	1
501 48	Bridging plugs STE 2/19, set of 10	1	1	1	1
500 621	Safety connecting lead 50 cm, red	1	1	2	2
500 622	Safety connecting lead 50 cm, blue	1	1	1	1
590 83	Coil 500 turns STE 2/50		1		1
590 84	Coil 1000 turns STE 2/50		1		1
524 005W	Mobile-CASSY 2 WiFi			1	1
500 624	Safety connecting lead 50 cm, black			1	1

The Wheatstone measuring bridge is one of the most effective means of measuring ohmic resistance in DC and AC circuits. Capacitive and inductive reactance can also be determined by means of analogous circuits. These measuring bridges consist of four passive bridge arms which are connected to form a rectangle, an indicator arm with a null indicator and a supply arm with the voltage source. Inserting variable elements in the bridge arm compensates the current in the indicator arm to zero. Then, for the component resistance values, the fundamental compensation condition

$$Z_1 = Z_2 \cdot \frac{Z_3}{Z_4}$$

applies, from which the measurement quantity Z_1 is calculated.

The experiments P3.6.4.1 and P3.6.4.3 investigate the principle of a Wien measuring bridge for measuring a capacitive reactance Z_1. In this configuration, Z_2 is a fixed capacitive reactance, Z_3 is a fixed ohmic resistance and Z_4 is a variable ohmic resistance. For zero compensation, the following applies regardless of the frequency of the AC voltage:

$$\frac{1}{C_1} = \frac{1}{C_2} \cdot \frac{R_3}{R_4}$$

An oscilloscope or Mobile-CASSY 2 can be used as a zero indicator.

In the experiments P3.6.4.2 and P3.6.4.4, a Maxwell measuring bridge is assembled to determine the inductive reactance Z_1. As the resistive component of Z_1 is also to be compensated, this circuit is somewhat more complicated. Here, Z_2 is a variable ohmic resistance, Z_3 is a fixed ohmic resistance and Z_4 is a parallel connection consisting of a capacitive reactance and a variable ohmic resistor. For the purely inductive component, the following applies with respect to zero compensation:

$$2\pi f \cdot L_1 = R_2 \cdot R_3 \cdot 2\pi f \cdot C_4$$

f: AC voltage frequency
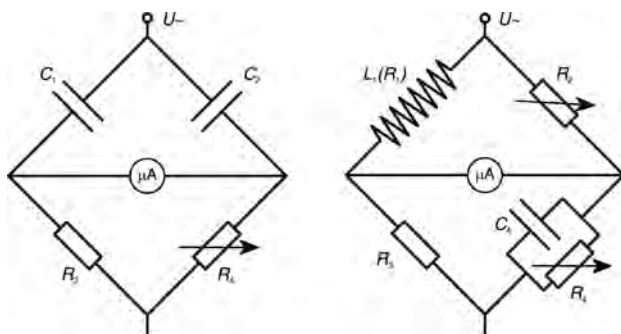
Schematic circuit diagramm: Wien measruing bridge (left) - Maxwell measuring bridge (right) (P3.6.4.1-4)

ELECTRICAL WORK AND POWER

P3.6.6.1
Determining the heating power of an ohmic load in an AC circuit as a function of the applied voltage

Determining the heating power of an ohmic load in an AC circuit as a function of the applied voltage (P3.6.6.1)

Cat. No.	Description	P3.6.6.1
384 21	Cover for calorimeter	1
384 22	Heating wire for calorimeter cover	1
384 52	Aluminium calorimeter	1
524 005W	Mobile-CASSY 2 WiFi	1
521 391	AC/DC power supply 0...24 V/5 A	1
590 06	Plastic beaker	1
501 28	Connecting lead, 32 A, 50 cm, black	4

The relationship between the power P at an ohmic resistance R and the applied voltage U can be expressed with the relationship

$$P = \frac{U^2}{R}$$

The same applies for AC voltage when P is the power averaged over time and U is replaced by the RMS value

$$U_{rms} = \frac{U_0}{\sqrt{2}}$$

U_0: amplitude of AC voltage

The relationship

$$P = U \cdot I$$

can also be applied to ohmic resistors in AC circuits when the direct current I is replaced by the RMS value of the AC

$$I_{rms} = \frac{I_0}{\sqrt{2}}$$

I_0: amplitude of AC

In the experiment P3.6.6.1, the electrical power of an immersion heater for extra-low voltage is determined from the Joule heat emitted per unit of time and compared with the applied voltage U_{rms}. This experiment confirms the relationship

$$P \propto U_{rms}^2$$

Determining the active and reactive power in AC circuits (P3.6.6.5)

ELECTRICAL WORK AND POWER

P3.6.6.3
Quantitative comparison of DC power and AC power in an incandescent lamp

P3.6.6.4
Determining the crest factors of various AC signal forms

P3.6.6.5
Determining the active and reactive power in AC circuits

Cat. No.	Description	P3.6.6.3	P3.6.6.4	P3.6.6.5
531 831	Joule and wattmeter	1	1	1
505 14	Bulbs, 6 V/3 W, E10, set of 10	1		
579 06	Lamp holder, E10, top, STE 2/19	2		
576 81	Plug-in board safety socket, 20/10	1		
521 487	AC/DC power supply PRO 0...12 V/3 A	1		
500 621	Safety connecting lead 50 cm, red	1		
500 622	Safety connecting lead 50 cm, blue	1		
500 641	Safety connecting lead, 100 cm, red	2		
500 642	Safety connecting lead, 100 cm, blue	2		
522 621	Function generator S 12		1	
536 131	Measuring resistor, 100 Ω		1	
575 302	Oscilloscope 30 MHz, digital, PT1265		1	1
575 24	Screened cable, BNC/4 mm		1	1
501 45	Connecting lead 19 A, 50 cm, red/blue, pair		2	1
521 391	AC/DC power supply 0...24 V/5 A			1
537 35	Rheostat, 330 ohms			1
517 021	Capacitor, 40 µF			1
562 11	U-core with yoke			1
562 121	Clamping device with spring clip			1
562 15	Coil, 1 000 turns			1
575 35	Adapter, BNC/4 mm, 2-pole			1
504 45	On-off switch, single pole			1
500 421	Connecting lead 19 A, 50 cm, red			2
501 46	Connecting leads 19 A, 100 cm, red/blue, pair			2

The electrical power of a time-dependent voltage $U(t)$ at any load resisance is also a function of time:

$$P(t) = U(t) \cdot I(t)$$

$I(t)$: time-dependent current through the load resistor

Thus, for periodic currents and voltages, we generally consider the power averaged over one period T. This quantity is often referred to as the active power P_W. It can be measured electronically for any DC or AC voltages using the joule and wattmeter.

In the experiment P3.6.6.3, two identical incandescent light bulbs are operated with the same electrical power. One bulb is operated with DC voltage, the other with AC voltage. The equality of the power values is determined directly using the joule and wattmeter, and additionally by comparing the lamp brightness levels. This equality is reached when the DC voltage equals the RMS value of the AC voltage.

The object of the experiment P3.6.6.4 is to determine the crest factors, i. e. the quotients of the amplitude U_0 and the RMS value U_{rms} for different AC voltage signal forms generated using a function generator by experimental means. The amplitude is measured using the joule and wattmeter connected to a PC. The RMS value is calculated from the power P measured at an ohmic resistor R using the joule and wattmeter according to the formula

$$U_{eff} = \sqrt{P \cdot R}$$

The experiment P3.6.6.5 measures the current I_{rms} through a given load and the active power P_W for a fixed AC voltage U_{rms}. To verify the relationship

$$P_w = U_{rms} \cdot I_{rms} \cdot \cos\varphi$$

the phase shift φ between the voltage and the current is additionally determined using an oscilloscope. This experiment also shows that the active power for a purely inductive or capacitive load is zero, because the phase shift is $\varphi = 90°$. The apparent power

$$P_s = U_{rms} \cdot I_{rms}$$

is also referred to as reactive power in this case.

LEYBOLD®

117

ELECTROMAGNETIC OSCILLATOR CIRCUIT

P3.7.1.1
Free electromagnetic oscillations
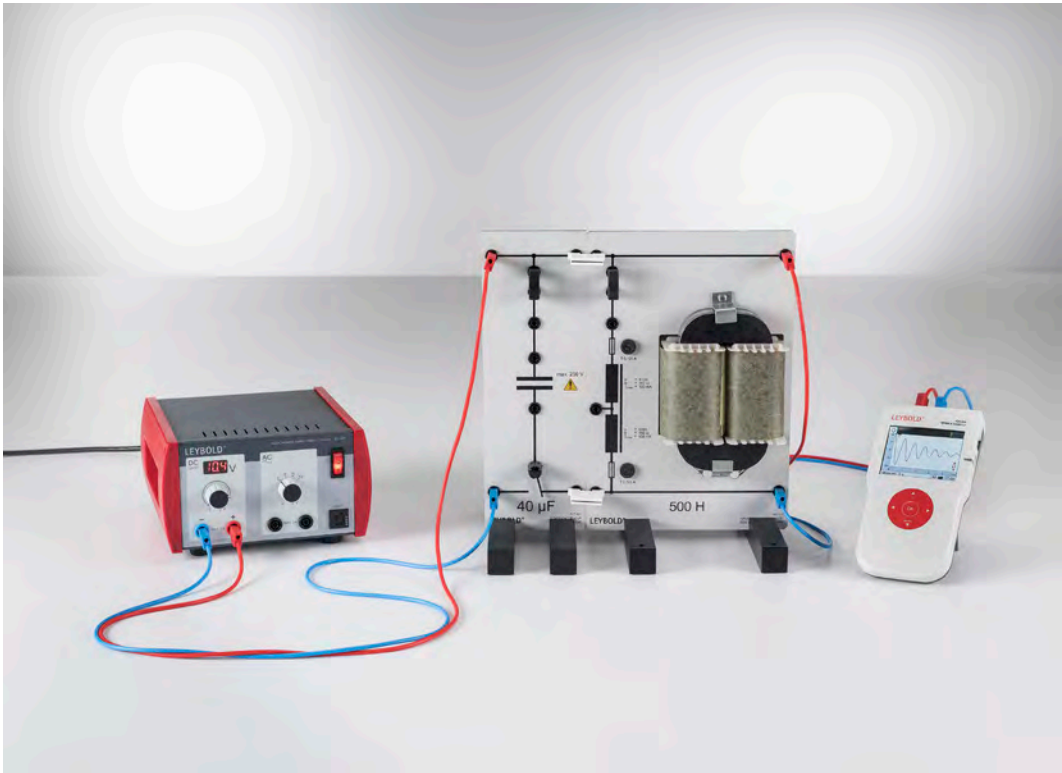
Free electromagnetic oscillations (P3.7.1.1)

Cat. No.	Description	P3.7.1.1
517 011	Coil with high inductance	1
517 021	Capacitor, 40 µF	1
301 339	Stand bases, pair	2
501 48	Bridging plugs STE 2/19, set of 10	1
521 487	AC/DC power supply PRO 0...12 V/3 A	1
524 005W	Mobile-CASSY 2 WiFi	1
500 641	Safety connecting lead, 100 cm, red	2
500 642	Safety connecting lead, 100 cm, blue	2

Electromagnetic oscillation usually occurs in a frequency range in which the individual oscillations cannot be seen with the naked eye. However, this is not the case in an oscillator circuit consisting of a high-capacity capacitor (C = 40 µF) and a high-inductance coil (L = 500 H). Here, the oscillation period is about 1 s, so that the voltage and current oscillations can be observed directly on a pointer instrument.

The experiment P3.7.1.1 investigates the phenomenon of free electromagnetic oscillations. The damping is so low that multiple oscillation periods can be observed and their duration measured. In the process, the deviations between the observed oscillation periods and those calculated using Thomson's equation

$$T = 2\pi \cdot \sqrt{L \cdot C}$$

are observed. These deviations can be explained by the current dependency of the inductance, as the permeability of the iron core of the coil depends on the magnetic field strength.
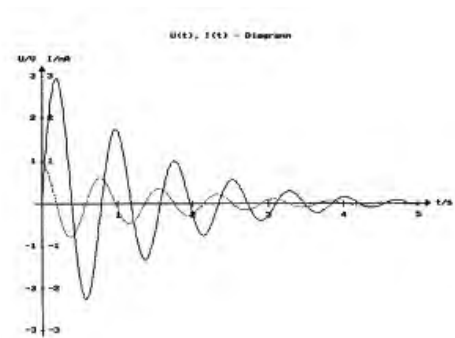
Damped electromagnetic oscillation in the 1 Hz range (P3.7.1.1)

Estimating the dielectric constant of water in the decimeter-wave range (P3.7.2.4)

DECIMETER-RANGE WAVES

P3.7.2.1
Radiation characteristic and polarization of decimeter waves

P3.7.2.2
Amplitude modulation of decimeter waves

P3.7.2.4
Estimating the dielectric constant of water in the decimeter-wave range

Cat. No.	Description	P3.7.2.1	P3.7.2.2	P3.7.2.4
587 551	UHF wave generator	1	1	1
531 110	Multimeter LDanalog 10	1		
300 11	Saddle base	2	3	1
501 38	Connecting lead, 32 A, 200 cm, black	2		
522 621	Function generator S 12		1	
532 20	AC/DC amplifier 30 W		1	
587 08	Broad-band speaker		1	
575 24	Screened cable, BNC/4 mm		1	
501 33	Connecting lead, 32 A, 100 cm, black			4
587 54	Dipoles in water tank			1

It is possible to excite electromagnetic oscillations in a straight conductor in a manner analogous to an oscillator circuit. An oscillator of this type emits electromagnetic waves, and their radiated intensity is greatest when the conductor length is equivalent to exactly one half the wavelength (we call this a $\lambda/2$ dipole). Experiments on this topic are particularly impressive with wavelengths in the decimeter range. We can best demonstrate the existence of such decimeter waves using a second dipole which also has the length $\lambda/2$, and from which the voltage is applied to an incandescent lamp or (via a high-frequency rectifier) to a measuring instrument.

The experiment P3.7.2.1 investigates the radiation characteristic of a $\lambda/2$ dipole for decimeter waves. Here, the receiver is aligned parallel to the transmitter and moved around the transmitter. In a second step, the receiver is rotated with respect to the transmitter in order to demonstrate the polarization of the emitted decimeter waves.

The experiment P3.7.2.2 deal with the transmission of audio-frequency signals using amplitude-modulated decimeter waves. In amplitude modulation a decimeter-wave signal

$$E(t) = E_0 \cdot \cos(2\pi \cdot f \cdot t)$$

is modulated through superposing of an audio-frequency signal $u(t)$ in the form

$$E_{AM}(t) = E_0 \cdot (1 + k_{AM} \cdot u(t)) \cdot \cos(2\pi \cdot f \cdot t)$$

k_{AM}: coupling coefficient

The experiment P3.7.2.4 demonstrates the dielectric nature of water. In water, decimeter waves of the same frequency propagate with a shorter wavelength than in air. Therefore, a receiver dipole tuned for reception of the wavelength in air is no longer adequately tuned when placed in water.

LEYBOLD®

PROPAGATION OF DECIMETER–RANGE WAVES ALONG LINES

P3.7.3.1
Determining the current and voltage maxima on a Lecher line

P3.7.3.2
Investigating the current and voltage on a Lecher line with a loop dipole

Determining the current and voltage maxima on a Lecher line (P3.7.3.1)

Cat. No.	Description	P3.7.3.1-2
587 551	UHF wave generator	1
587 56	Lecher system with accessories	1
311 78	Tape measure 2 m / 1 mm	1
300 11	Saddle base	3

E. Lecher (1890) was the first to suggest using two parallel wires for directional transmission of electromagnetic waves. Using such Lecher lines, as they are known today, electromagnetic waves can be transmitted to any point in space. They are measured along the line as a voltage $U(x,t)$ propagating as a wave, or as a current $I(x,t)$.

In the experiment P3.7.3.1, a Lecher line open at the wire ends and a shorted Lecher line are investigated. The waves are reflected at the ends of the wires, so that standing waves are formed. The current is zero at the open end, while the voltage is zero at the shorted end. The current and voltage are shifted by $\lambda/4$ with respect to each other, i. e. the wave antinodes of the voltage coincide with the wave nodes of the current. The voltage maxima are located using a probe with an attached incandescent lamp. An induction loop with connected incandescent lamp is used to detect the current maxima. The wavelength λ is determined from the intervals d between the current maxima or voltage maxima. We can say

$$d = \frac{\lambda}{2}$$

In the experiment P3.7.3.2, a transmitting dipole ($\lambda/2$ folded dipole) is attached to the end of the Lecher line. Subsequently, it is no longer possible to detect any voltage or current maxima on the Lecher line itself. A current maximum is detectable in the middle of the dipole, and voltage maxima at the dipole ends.

Current and voltage maxima on a Lecher line (P3.7.3.1)
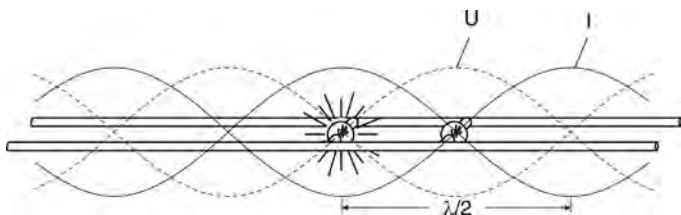
Diffraction of microwaves (P3.7.4.4)

MICROWAVES

P3.7.4.1
Directional characteristic and polarization of microwaves in front of a horn antenna

P3.7.4.2
Absorption of microwaves

P3.7.4.3
Interference of microwaves

P3.7.4.4
Diffraction of microwaves

P3.7.4.5
Refraction of microwaves

P3.7.4.6
Total reflection of microwaves

Cat. No.	Description	P3.7.4.1–2	P3.7.4.3	P3.7.4.4	P3.7.4.5	P3.7.4.6
737 01	Gunn oscillator	1	1	1	1	1
737 020	Gunn power supply with amplifier	1	1	1	1	1
737 21	Large horn antenna	1	1	1	1	1
737 35	Electric field probe	1	1	1	1	1
688 809	Stand rod 245 mm, 10 mm Ø, with thread M6	1	1	1	1	1
737 27	Physics microwave accessories I	1	1	1		
531 120	Multimeter LDanalog 20	1	1	1	1	1
300 11	Saddle base	2	2	4	2	1
501 022	BNC cable, 2 m	2	2	2	2	2
501 461	Connecting leads 19 A, 100 cm, black, pair	1	1	1	1	1
737 390	Set of Microwave Absorbers	1*	1*	1*	1*	1*
737 275	Physics microwave accessories II			1	1	1
311 78	Tape measure 2 m / 1 mm			1		
300 02	Stand base, V-shaped, small					1

*additionally recommended

Microwaves are electromagnetic waves in the wavelength range between 0.1 mm and 100 mm. They are generated e.g. in a cavity resonator, whereby the frequency is determined by the volume of the cavity resonator. An E-field probe is used to detect the microwaves; this device measures the parallel component of the electric field. The output signal of the probe is proportional to the square of the field strength, and thus to the intensity.

The experiment P3.7.4.1 investigates the orientation and polarization of the microwave field in front of a radiating horn antenna. Here, the field in front of the horn antenna is measured point by point in both the longitudinal and transverse directions using the E-field probe. To determine the polarization, a rotating polarization grating made of thin metal strips is used; in this apparatus, the electric field can only form perpendicular to the metal strips. The polarization grating is set up between the horn antenna and the E-field probe. This experiment shows that the electric field vector of the radiated microwaves is perpendicular to the long side of the horn radiator.

The experiment P3.7.4.2 deals with the absorption of microwaves. Working on the assumption that reflections may be ignored, the absorption in different materials is calculated using both the incident and the transmitted intensity. This experiment reveals a fact which has had a profound impact on modern cooking: microwaves are absorbed particularly intensively by water.

In the experiment P3.7.4.3, standing microwaves are generated by reflection at a metal plate. The intensity, measured at a fixed point between the horn antenna and the metal plate, changes when the metal plate is shifted longitudinally. The distance between two intensity maxima corresponds to one half the wavelength. Inserting a dielectric in the beam path shortens the wavelength.

The experiments P3.7.4.4 and P3.7.4.5 show that many of the properties of microwaves are comparable to those of visible light. The diffraction of microwaves at an edge, a single slit, a double slit and an obstacle are investigated. Additionally, the refraction of microwaves is demonstrated and the validity of Snell's law of refraction is confirmed.

The experiment P3.7.4.6 investigates total reflection of microwaves at media with lower refractive indices. We know from wave mechanics that the reflected wave penetrates about three to four wavelengths deep into the medium with the lower refractive index, before traveling along the boundary surface in the form of surface waves. This is verified in an experiment by placing an absorber (e.g. a hand) on the side of the medium with the lower refractive index close to the boundary surface and observing the decrease in the reflected intensity.

LEYBOLD®

PROPAGATION OF MICROWAVES ALONG LINES

P3.7.5.1
Guiding of microwaves along a
Lecher line

P3.7.5.2
Qualitative demonstration of
guiding of microwaves along
a metal waveguide

Guiding of microwaves along a Lecher line (P3.7.5.1)

Cat. No.	Description	P3.7.5.1	P3.7.5.2
737 01	Gunn oscillator	1	1
737 020	Gunn power supply with amplifier	1	1
737 21	Large horn antenna	1	1
737 35	Electric field probe	1	1
688 809	Stand rod 245 mm, 10 mm Ø, with thread M6	1	1
737 275	Physics microwave accessories II	1	
531 120	Multimeter LDanalog 20	1	1
300 11	Saddle base	2	1
501 022	BNC cable, 2 m	2	2
501 461	Connecting leads 19 A, 100 cm, black, pair	1	1
737 390	Set of Microwave Absorbers	1*	
737 27	Physics microwave accessories I		1

* additionally recommended

To minimize transmission losses over long distances, microwaves can also be transmitted along lines. For this application, metal waveguides are most commonly used; Lecher lines, consisting of two parallel wires, are less common.

Despite this, the experiment P3.7.5.1 investigates the guiding of microwaves along a Lecher line. The voltage along the line is measured using the E-field probe. The wavelengths are determined from the spacing of the maxima.

The experiment P3.7.5.2 demonstrates the guiding of microwaves along a hollow metal waveguide. First, the E-field probe is used to verify that the radiated intensity at a position beside the horn antenna is very low. Next, a flexible metal waveguide is set up and bent so that the microwaves are guided to the E-field probe, where they are measured at a greater intensity.

Directional characteristic of a helix antenna - Recording measured values manually (P3.7.6.1)

DIRECTIONAL CHARACTERISTIC OF DIPOLE RADIATION

P3.7.6.1
Directional characteristic of a helix antenna – Recording measured values manually

P3.7.6.2
Directional characteristic of a Yagi antenna – Recording measured values manually
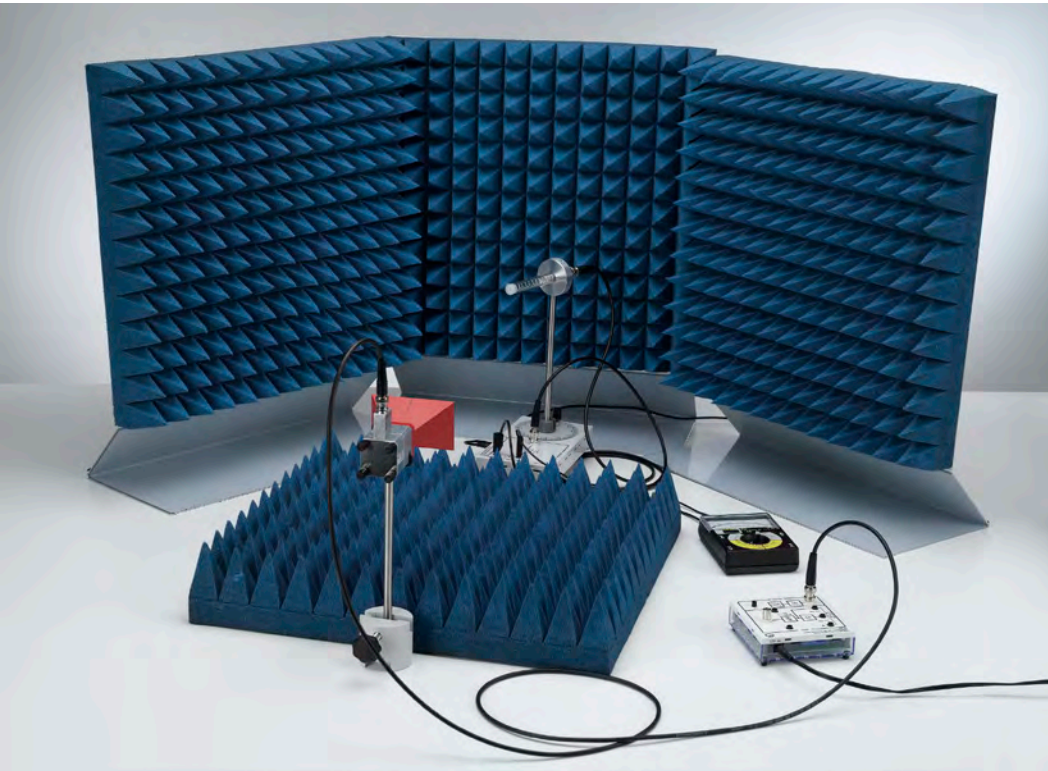
Cat. No.	Description	P3.7.6.1	P3.7.6.2
737 440	Helical Antenna Kit	1	
737 03	Coax Detector	1	
737 407	Antenna Stand with Amplifier	1	1
737 020	Gunn power supply with amplifier	1	1
737 01	Gunn oscillator	1	1
737 21	Large horn antenna	1	1
688 809	Stand rod 245 mm, 10 mm Ø, with thread M6	2	2
737 390	Set of Microwave Absorbers	1	1
531 120	Multimeter LDanalog 20	1	1
300 11	Saddle base	1	1
501 022	BNC cable, 2 m	1	1
575 24	Screened cable, BNC/4 mm	1	1
501 461	Connecting leads 19 A, 100 cm, black, pair	2	2
737 415	Set of wire antennas		1

Directional antennas radiate the greater part of their electromagnetic energy in a particular direction and/or are most sensitive to reception from this direction. All directional antennas require dimensions which are equivalent to multiple wavelengths. In the microwave range, this requirement can be fulfilled with an extremely modest amount of cost and effort. Thus, microwaves are particularly suitable for experiments on the directional characteristics of antennas.

In the experiment P3.7.6.1, the directional characteristic of a helical antenna is recorded. As the microwave signal is excited with a linearly polarizing horn antenna, the rotational orientation of the helical antenna (clockwise or counter-clockwise) is irrelevant. The measurement results are represented in the form of a polar diagram, from which the unmistakable directional characteristic of the helical antenna can be clearly seen.

In the experiment P3.7.6.2, a dipole antenna is expanded using parasitic elements to create a Yagi antenna, to improve the directional properties of the dipole arrangement. Here, a total of four shorter elements are placed in front of the dipole as directors, and a slightly longer element placed behind the dipole serves as a reflector. The directional factor of this arrangement is determined from the polar diagram.
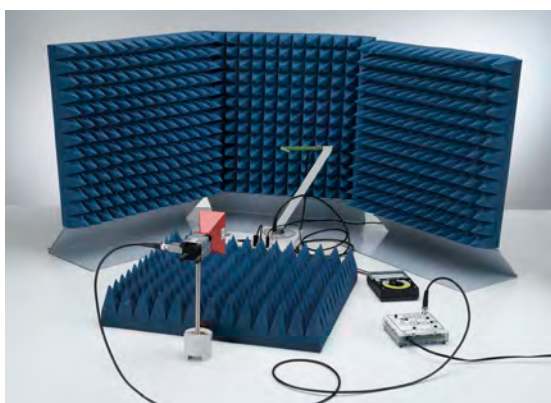
Directional characteristic of a Yagi antenna - Recording measured values manually (P3.7.6.2)

LEYBOLD®

MALTESE–CROSS TUBE

P3.8.3.1
Demonstrating the linear propagation of electrons in a field-free space

P3.8.3.2
Deflection of electrons in an axial magnetic field
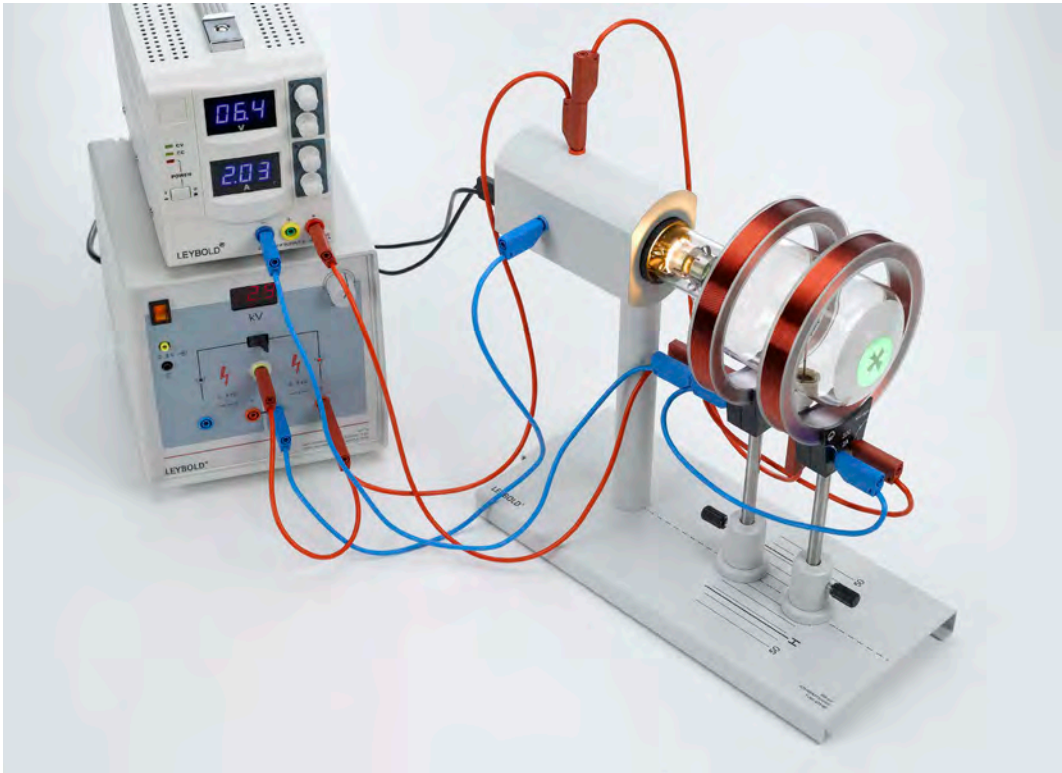
Deflection of electrons in an axial magnetic field (P3.8.3.2)

Cat. No.	Description	P3.8.3.1	P3.8.3.2
555 620	Maltese cross tube	1	1
555 600	Tube stand	1	1
521 70	High-voltage power supply, 10 kV	1	1
510 48	Magnets, 35 mm Ø, pair	1	
500 611	Safety connecting lead, 25 cm, red	1	1
500 621	Safety connecting lead 50 cm, red	1	2
500 641	Safety connecting lead, 100 cm, red	1	2
500 642	Safety connecting lead, 100 cm, blue	1	2
500 644	Safety connecting lead, 100 cm, black	2	2
555 604	Pair of Helmholtz coils		1
521 546	DC Power Supply 0…16 V/0…5 A		1
500 622	Safety connecting lead 50 cm, blue		1

In the Maltese cross tube, the electrons are accelerated by the anode to a fluorescent screen, where they can be observed as luminescent phenomena. A Maltese cross is arranged between the anode and the fluorescent screen, and its shadow can be seen on the screen. The Maltese cross has its own separate lead, so that it can be connected to any desired potential.

The experiment P3.8.3.1 confirms the linear propagation of electrons in a field-free space. In this experiment, the Maltese cross is connected to the anode potential and the shadow of the Maltese cross in the electron beam is compared with the light shadow. We can conclude from the observed coincidence of the shadows that electrons propagate in a straight line. The Maltese cross is then disconnected from any potential. The resulting space charges around the Maltese cross give rise to a repulsive potential, so that the image on the fluorescent screen becomes larger.

In the experiment P3.8.3.2 an axial magnetic field is applied using an electromagnet. The shadow cross turns and shrinks as a function of the coil current. When a suitable relationship between the high voltage and the coil current is set, the cross is focused almost to a point, and becomes larger again when the current is increased further. The explanation for this magnetic focusing may be found in the helical path of the electrons in the magnetic field.

Shadow of the maltese cross on the fluorescent screen (P3.8.3.1)
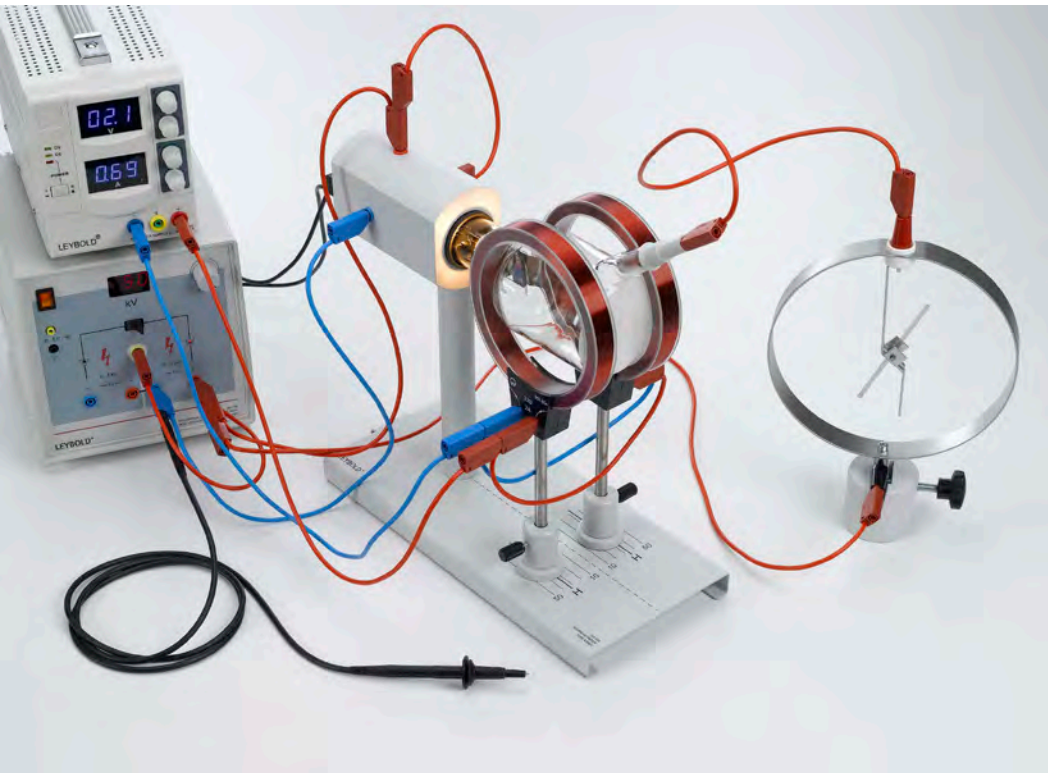
PERRIN TUBE

P3.8.4.1
Hot-cathode emission in a vacuum: determining the polarity and estimating the specific charge of the emitted charge carriers

Hot-cathode emission in a vacuum: determining the polarity and estimating the specific charge of the emitted charge carriers (P3.8.4.1)

Cat. No.	Description	P3.8.4.1
555 622	Perrin tube	1
555 600	Tube stand	1
555 604	Pair of Helmholtz coils	1
521 70	High-voltage power supply, 10 kV	1
521 546	DC Power Supply 0…16 V/0…5 A	1
540 091	Electroscope	1
300 11	Saddle base	1
501 051	Cable for high voltages, 1.5 m	1
500 611	Safety connecting lead, 25 cm, red	1
500 621	Safety connecting lead 50 cm, red	2
500 622	Safety connecting lead 50 cm, blue	1
500 641	Safety connecting lead, 100 cm, red	4
500 642	Safety connecting lead, 100 cm, blue	2
500 644	Safety connecting lead, 100 cm, black	2

In the Perrin tube, the electrons are accelerated through an anode with pin-hole diaphragm onto a fluorescent screen. Deflection plates are mounted at the opening of the pin-hole diaphragm for horizontal electrostatic deflection of the electron beam. A Faraday's cup, which is set up at an angle of 45° to the electron beam, can be charged by the electrons deflected vertically upward. The charge current can be measured using a separate connection.

In the experiment P3.8.4.1, the current through a pair of Helmholtz coils is set so that the electron beam is incident on the Faraday's cup of the Perrin tube. The Faraday's cup is connected to an electroscope which has been pre-charged with a known polarity. The polarity of the electron charge can be recognized by the direction of electroscope deflection when the Faraday's cup is struck by the electron beam. At the same time, the specific electron charge can be estimated. The following relationship applies:

$$\frac{e}{m} = \frac{2U_A}{(B \cdot r)^2} \quad U_A: \text{anode voltage}$$

The bending radius r of the orbit is predetermined by the geometry of the tube. The magnetic field B is calculated from the current I through the Helmholtz coils.

THOMSON TUBE

P3.8.5.1
Investigating the deflection of electrons in electrical and magnetic fields

P3.8.5.2
Assembling a velocity filter (Wien filter) to determine the specific electron charge
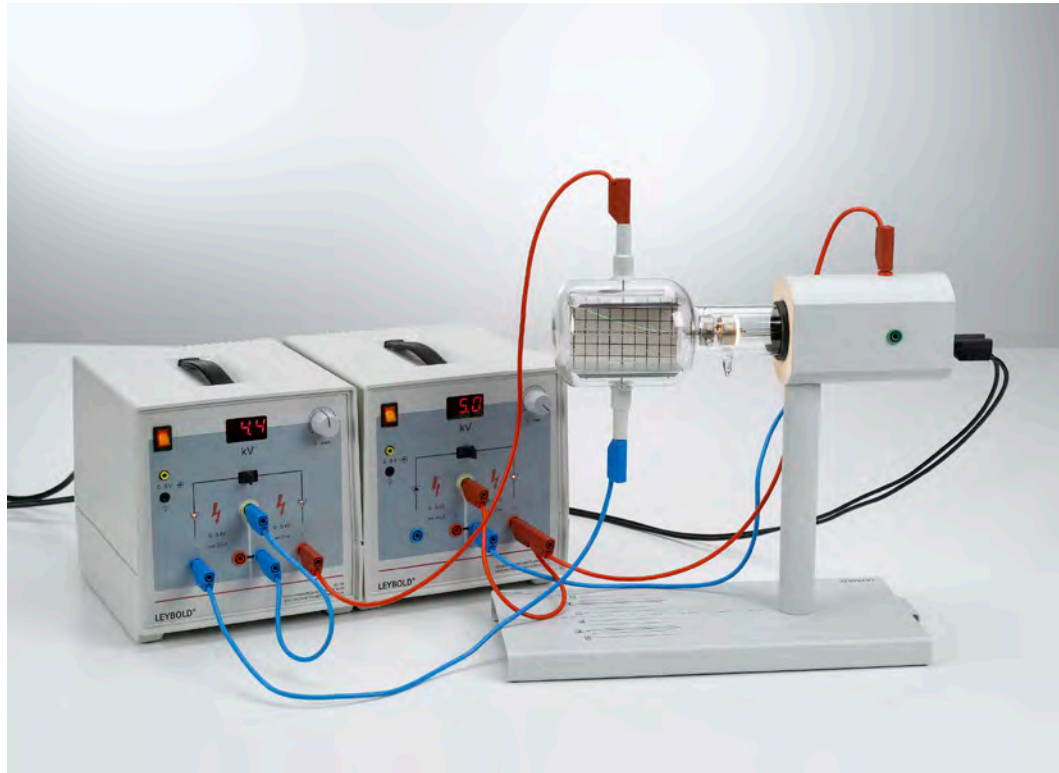
Investigating the deflection of electrons in electrical and magnetic fields (P3.8.5.1)

Cat. No.	Description	P3.8.5.1–2
555 624	Electron deflection tube	1
555 600	Tube stand	1
555 604	Pair of Helmholtz coils	1
521 70	High-voltage power supply, 10 kV	2
521 546	DC Power Supply 0...16 V/0...5 A	1
500 611	Safety connecting lead, 25 cm, red	2
500 621	Safety connecting lead 50 cm, red	1
500 622	Safety connecting lead 50 cm, blue	1
500 641	Safety connecting lead, 100 cm, red	2
500 642	Safety connecting lead, 100 cm, blue	4
500 644	Safety connecting lead, 100 cm, black	2

In the Thomson tube, the electrons pass through a slit behind the anode and fall glancingly on a fluorescent screen placed in the beam path at an angle. A plate capacitor is mounted at the opening of the slit diaphragm which can electrostatically deflect the electron beam vertically. In addition, Helmholtz coils can be used to generate an external magnetic field which can also deflect the electron beam.

The experiment P3.8.5.1 investigates the deflection of electrons in electric and magnetic fields. For different anode voltages U_A, the beam path of the electrons is observed when the deflection voltage U_P at the plate capacitor is varied. Additionally, the electrons are deflected in the magnetic field of the Helmholtz coils by varying the coil current I. The point at which the electron beam emerges from the fluorescent screen gives us the radius R of the orbit. When we insert the anode voltage in the following equation, we can obtain an experimental value for the specific electron charge

$$\frac{e}{m} = \frac{2U_A}{(B \cdot r)^2}$$

whereby the magnetic field B is calculated from the current I.

In the experiment P3.8.5.2, a velocity filter (Wien filter) is constructed using crossed electrical and magnetic fields. Among other things, this configuration permits a more precise determination of the specific electron charge. At a fixed anode voltage U_A, the current I of the Helmholtz coils and the deflection voltage U_P are set so that the effects of the electric field and the magnetic field just compensate each other. The path of the beam is then virtually linear, and we can say:

$$\frac{e}{m} = \frac{1}{2U_A} \cdot \left(\frac{U_P}{B \cdot d} \right)^2$$

d: plate spacing of the plate capacitor
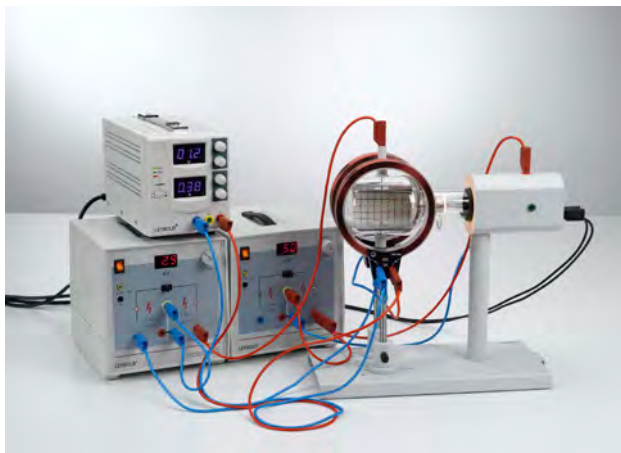
Assembling a velocity filter (Wien filter) to determine the specific electron charge (P3.8.5.2)

GAS DISCHARGE AT REDUCED PRESSURE

P3.9.2.1
Investigating spontaneous gas discharge in air as a function of pressure

Investigating spontaneous gas discharge in air as a function of pressure (P3.9.2.1)

Cat. No.	Description	P3.9.2.1
554 161	Discharge tube, canal rays	1
378 752	Rotary-vane vacuum pump D 2.5 E	1
378 023	Male ground joint, ST 19/26, DN 16 KF	1
378 015	Cross piece, DN 16 KF	1
378 050	Clamping ring, DN 10/16 KF	5
378 045	Centering ring DN 16 KF	5
378 777	Fine vacuum ball valve, DN 16 KF	1
378 776	Variable leak valve, DN 16 KF	1
378 5131	Pirani vacuum gauge with display	1
378 701	Leybold high-vacuum grease	1
521 70	High-voltage power supply, 10 kV	1
501 051	Cable for high voltages, 1.5 m	2
378 764	Exhaust filter AF 8	1*

* additionally recommended

Glow discharge is a special form of gas discharge. It maintains itself at low pressures with a relatively low current density, and is connected with spectacular luminous phenomena. Research into these phenomena provided fundamental insights into the structure of the atom.

In the experiment P3.9.2.1, a cylindrical glass tube is connected to a vacuum pump and slowly evacuated. A high voltage is applied to the electrodes at the end of the glass tube. No discharge occurs at standard pressure. However, when the pressure is reduced to a certain level, current flows, and a luminosity is visible. When the gas pressure is further reduced, multiple phases can be observed: First, a luminous "thread" joins the anode and the cathode. Then, a column of light extends from the anode until it occupies almost the entire space. A glowing layer forms on the cathode. The column gradually becomes shorter and breaks down into multiple layers, while the glowing layer becomes larger. The layering of the luminous zone occurs because after collision excitation, the exciting electrons must traverse an acceleration distance in order to acquire enough energy to re-excite the atoms. The spacing of the layers thus illustrates the free path length.

P4.1.5.5
Recording the characteristics of a field-effect
transistor with CASSY
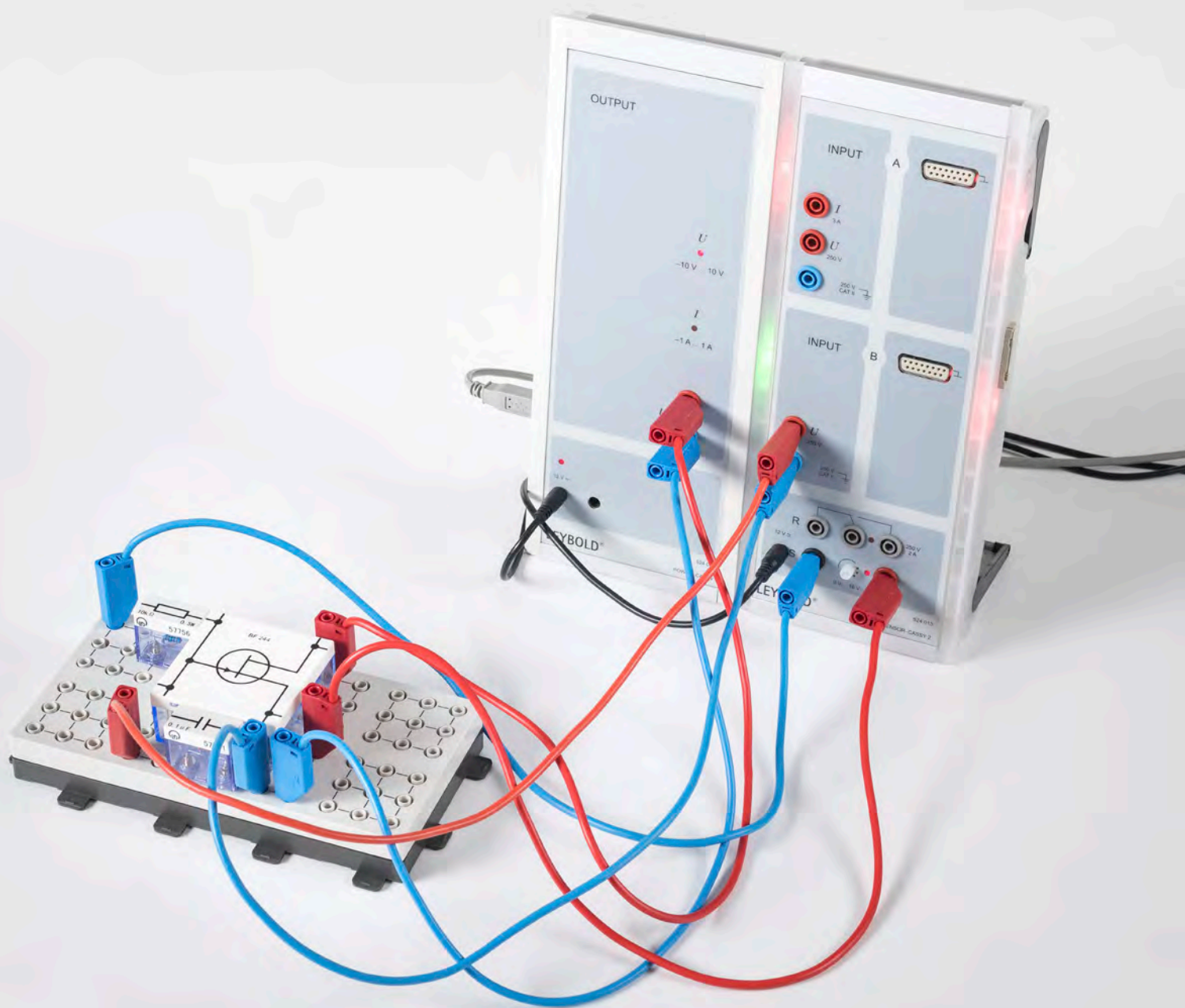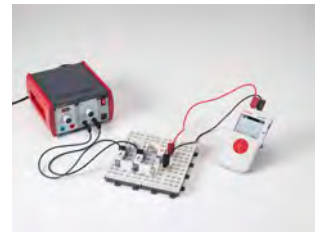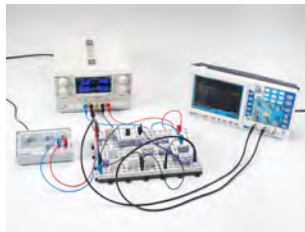
P4 ELECTRONICS

LEYBOLD®

129
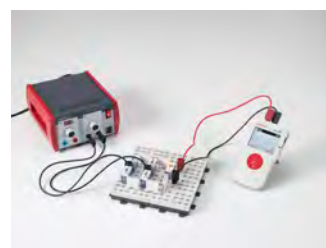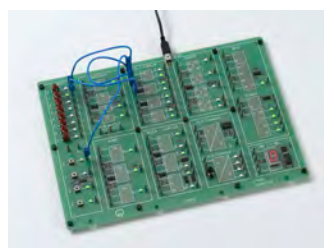
P4 ELECTRONICS

CURRENT AND VOLTAGE SOURCES

P4.1.1.1
Determining the internal resistance of a battery

P4.1.1.3
Recording the current-voltage characteristics of a solar battery as a function of the irradiance

Recording the current-voltage characteristics of a solar battery as a function of the irradiance (P4.1.1.3)

Cat. No.	Description	P4.1.1.1	P4.1.1.3
576 86	Monocell holder STE 2/50	1	
576 81	Plug-in board safety socket, 20/10	1	3
685 48	Mono cell 1.5 V (IEC R20)	1	
531 120	Multimeter LDanalog 20	2	2
537 32	Rheostat, 10 ohms	1	
500 614	Safety connecting lead, 25 cm, black	5	
578 63	Solar module, 2 V/0.3 A, STE 4/100		1
577 90	Potentiometer 220 Ohm, STE 4/50		1
501 48	Bridging plugs STE 2/19, set of 10		1
450 641	Halogen lamp 12 V, 50/100W		1
450 63	Halogen bulb 12 V/100 W, G6.35		1
726 890	DC-High Current Power Supply 1...32 V/0...20 A		1
300 01	Stand base, V-shaped, large		1
300 43	Stand rod, 75 cm, 12 mm diam.		1
301 01	Leybold multiclamp		1
500 621	Safety connecting lead 50 cm, red		2
500 622	Safety connecting lead 50 cm, blue		2
500 624	Safety connecting lead 50 cm, black		2

The voltage U_0 generated in a voltage source generally differs from the terminal voltage U measured at the connections as soon as a current I is drawn from the voltage source. A resistance R_i must therefore exist within the voltage source, across which a part of the generated voltage drops. This resistance is called the internal resistance of the voltage source.

The solar cell is a semiconductor photoelement in which irradiance is converted directly to electrical energy at the p-n junction. Often, multiple solar cells are combined to create a solar battery.

In the experiment P4.1.1.1, a rheostat as an ohmic load is connected to a battery to determine the internal resistance. The terminal voltage U of the battery is measured for different loads, and the voltage values are plotted over the current I through the rheostat. The internal resistance R_i is determined using the formula

$$U = U_0 - R_i \cdot I$$

by drawing a best-fit straight line through the measured values. A second diagram illustrates the power

$$P = U \cdot I$$

as a function of the load resistance. The power is greatest when the load resistance has the value of the internal resistance R_i.

In the experiment P4.1.1.3 the current-voltage characteristics of a solar battery are recorded for different irradiance levels. The irradiance is varied by changing the distance of the light source. The characteristic curves reveal the characteristic behavior. At a low load resistance, the solar battery supplies an approximately constant current. When it exceeds a critical voltage (which depends on the irradiance), the solar battery functions increasingly as a constant-voltage source.
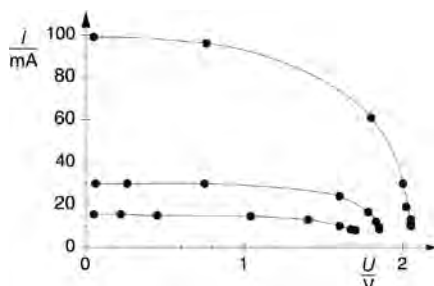
Current-voltage characteristics for different illuminance levels (P4.1.1.3)

SPECIAL RESISTORS

P4.1.2.1
Recording the current-voltage characteristic of an incandescent lamp

P4.1.2.2
Recording the current-voltage characteristic of a varistor

P4.1.2.3
Measuring the temperature-dependancy of PTC and NTC resistors

P4.1.2.4
Measuring the light-dependancy of photoresistors

Recording the current-voltage characteristic of an incandescent lamp (P4.1.2.1)

Cat. No.	Description	P4.1.2.1	P4.1.2.2	P4.1.2.3	P4.1.2.4
505 08	Bulbs, 12 V/3 W, E10, set of 10	1			
579 06	Lamp holder, E10, top, STE 2/19	1			
524 011USB	Power-CASSY USB	1			
524 220	CASSY Lab 2	1			
578 00	VDR resistor, STE 2/19		1		
576 81	Plug-in board safety socket, 20/10		1	1	
521 546	DC Power Supply 0...16 V/0...5 A		1	1	1
531 120	Multimeter LDanalog 20		2	2	1
500 621	Safety connecting lead 50 cm, red		2	2	
500 622	Safety connecting lead 50 cm, blue		2	2	
500 642	Safety connecting lead, 100 cm, blue		1	1	
578 06	PTC probe, 30 Ω, STE 2/19			1	
578 04	NTC probe, 4.7 kΩ, STE 2/19			1	
666 767	Hotplate, 1500 W, 180 mm Ø			1	
382 34	Thermometer, -10...+110 °C/0.2 K			1	
664 104	Beaker, DURAN, 400 ml, squat			1	
578 02	Photoresistor LDR 05, STE 2/19				1
579 05	Lamp holder E10, lateral, STE 2/19				1
505 131	Bulbs, 6 V/5 W, E10, set of 10				1
460 21	Holder for plug-in elements				2
521 210	Transformer 6/12 V				1
460 310	Optical bench, S1 profile, 1 m				1
460 312	Clamp rider with clamp 45/35				2
501 45	Connecting lead 19 A, 50 cm, red/blue, pair				2
500 422	Connecting lead 19 A, 50 cm, blue				1
	additionally required: PC with Windows XP/Vista/7/8/10 (x86 or x64)	1			

Many materials do not conduct voltage and current in proportion to one another. Their resistance depends on the current level. In technical applications, elements in which the resistance depends significantly on the temperature, the luminous intensity or another physical quantity are important.

In the experiment P4.1.2.1, the CASSY system is used to record the current-voltage characteristic of an incandescent lamp. As the incandescent filament heats up when current is applied, and its resistance depends on the temperature, different characteristic curves are generated when the current is switched on and off. The characteristic also depends on the rate of increase dU/dt of the voltage.

The experiment P4.1.2.2 records the current-voltage characteristic of a varistor (VDR voltage dependent resistor). Its characteristic is non-linear in its operating range. At higher currents, it enters the so-called "rise range", in which the ohmic component of the total resistance increases.

The aim of the experiment P4.1.2.3 is to measure the temperature characteristics of an NTC thermistor resistor and a PTC thermistor resistor. The respective measured values can be described using empirical equations in which only the rated value R_0, the reference temperature T_0 and a material constant appear as parameters.

The subject of the experiment P4.1.2.4 is the characteristic of a light-dependent resistor (LDR). Its resistance varies from approx. 100 Ω to approx. 10 MΩ, depending on the brightness. The resistance is measured as a function of the distance from an incandescent lamp which illuminates the light-dependent resistor.
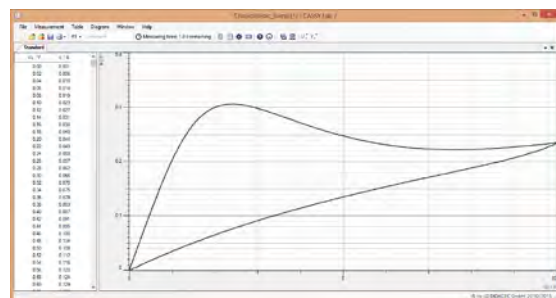
Current-voltage characteristic of the light bulb (P4.1.2.1)

Recording the current–voltage characteristics of light-emitting diodes (LED) (P4.1.3.3)
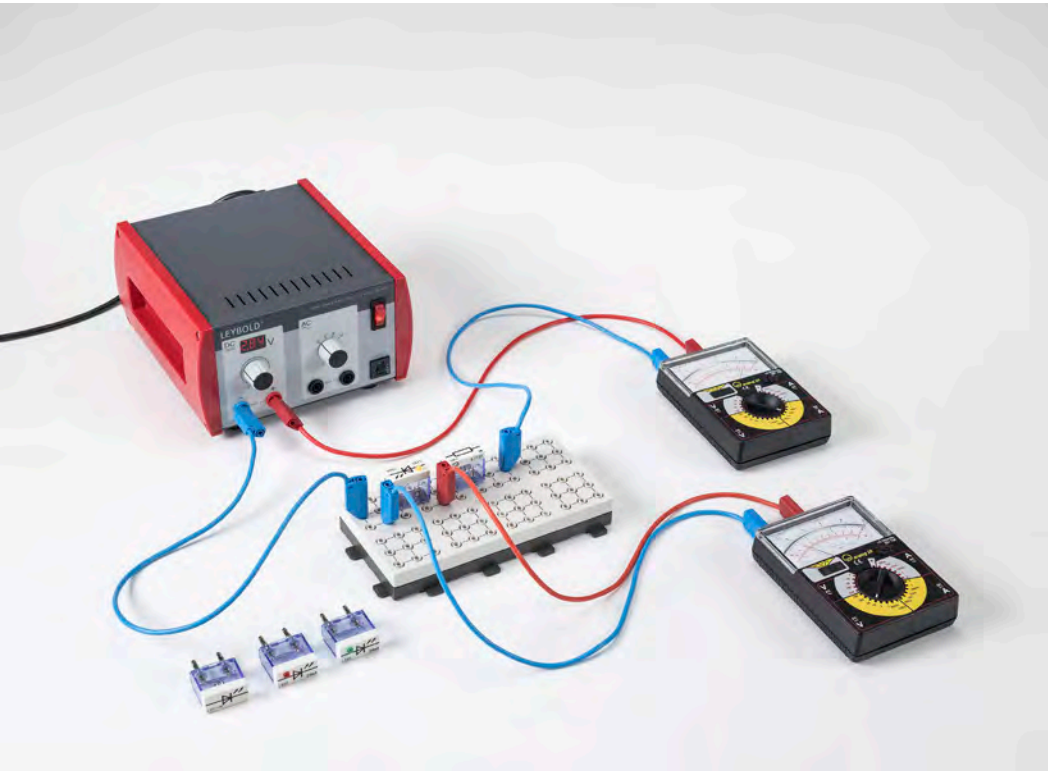
DIODES

P4.1.3.1
Recording the current–voltage characteristics of diodes

P4.1.3.2
Recording the current–voltage characteristics of Zener diodes (Z-diodes)

P4.1.3.3
Recording the current–voltage characteristics of light-emitting diodes (LED)

P4.1.3.4
Recording the current–voltage characteristics of diodes with CASSY

P4.1.3.5
Recording the current–voltage characteristics of Zener diodes (Z-diodes) with CASSY

P4.1.3.6
Recording the current–voltage characteristics of light-emitting diodes (LED) with CASSY

Cat. No.	Description	P4.1.3.1	P4.1.3.2	P4.1.3.3	P4.1.3.4	P4.1.3.5	P4.1.3.6
576 81	Plug-in board safety socket, 20/10	1	1	1	1	1	1
578 51	Diode 1N 4007, STE 2/19	1			1		
578 50	Diode, AA 118, germanium, STE 2/19	1			1		
577 32	Resistor 100 Ohm, STE 2/19	1	1	1	1	1	1
521 487	AC/DC power supply PRO 0…12 V/3 A	1	1	1			
531 120	Multimeter LDanalog 20	2	2	2			
500 621	Safety connecting lead 50 cm, red	2	2	2	2	2	2
500 622	Safety connecting lead 50 cm, blue	2	2	2	2	2	2
500 642	Safety connecting lead, 100 cm, blue	1	1	1			
578 55	Zener diode 6.2, STE 2/19		1			1	
578 54	Zener diode, 9.1 V, STE 2/19		1			1	
578 57	Light emitting diode green, STE 2/19			1			1
578 47	Light emitting diode, yellow, STE 2/19			1			1
578 48	Light emitting diode red, STE 2/19			1			1
578 49	Infrared diode, lateral, STE 2/19			1			1
524 013	Sensor-CASSY 2				1	1	1
524 220	CASSY Lab 2				1	1	1
500 644	Safety connecting lead, 100 cm, black				1	1	1
	additionally required: PC with Windows XP/Vista/7/8/10 (x86 or x64)				1	1	1
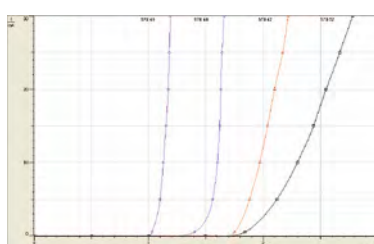
Virtually all aspects of electronic circuit technology rely on semiconductor components. The semiconductor diodes are among the simplest of these. They consist of a semiconductor crystal in which an n-conducting zone is adjacent to a p-conducting zone. Capture of the charge carriers, i.e. the electrons in the n-conducting and the "holes" in the p-conducting zones, forms a low-conductivity zone at the junction called the depletion layer. The size of this zone is increased when electrons or holes are removed from the depletion layer by an external electric field with a certain orientation. The direction of this electric field is called the reverse direction. Reversing the electric field drives the respective charge carriers into the depletion layer, allowing current to flow more easily through the diode.

In the experiments P4.1.3.1 and P4.1.3.4, the current-voltage characteristics of an Si-diode (silicon diode) and a Ge-diode (germanium diode) are measured and graphed manually point by point or with CASSY. The aim is to compare the current in the reverse direction and the threshold voltage as the most important specifications of the two diodes

The objective of the experiments P4.1.3.2 and P4.1.3.5 is to measure the current-voltage characteristic of a zener or Z-diode. Here, special attention is paid to the breakdown voltage in the reverse direction, as when this voltage level is reached the current rises abruptly. The current is due to charge carriers in the depletion layer, which, when accelerated by the applied voltage, ionize additional atoms of the semiconductor through collision.

The experiments P4.1.3.3 and P4.1.3.6 compare the characteristics of infrared, red, yellow and green light-emitting diodes.

Recording the current–voltage characteristics of light-emitting diodes (LED) (P4.1.3.3)

CASSY®

DIODE CIRCUITS

P4.1.4.1
Rectifying AC voltage using diodes

P4.1.4.2
Voltage-limiting with a Z-diode

P4.1.4.3
Testing polarity with light-emitting diodes

P4.1.4.4
Rectifying AC voltage using diodes with CASSY
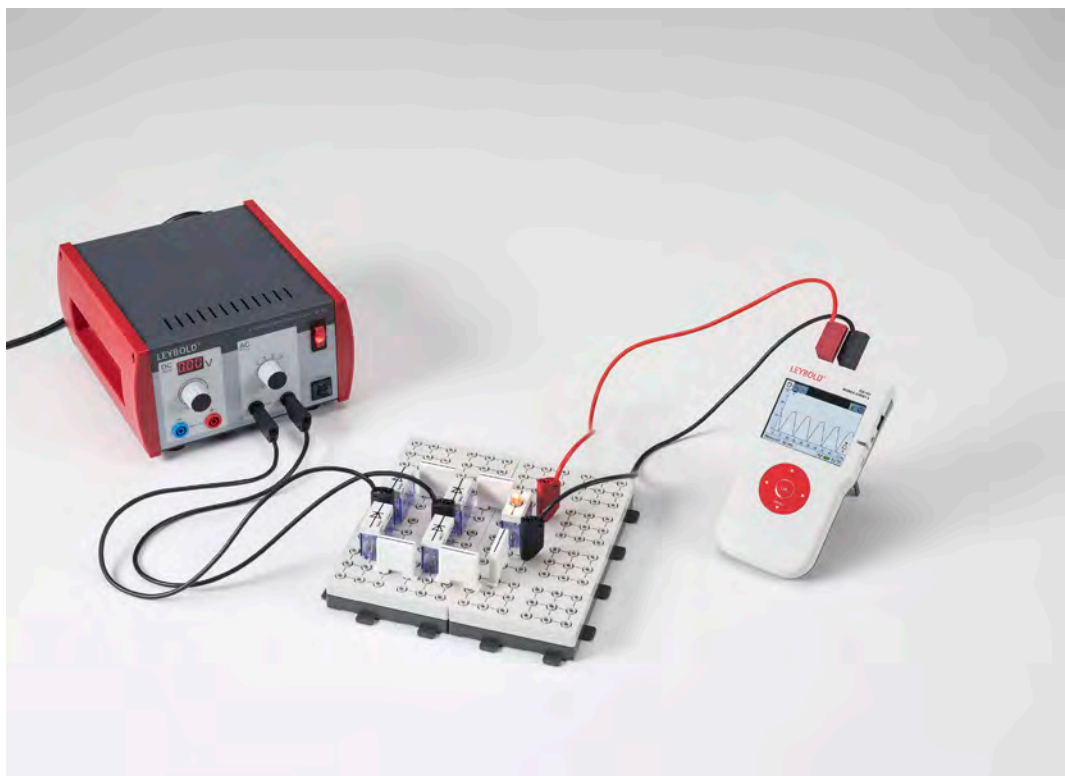
Rectifying AC voltage using diodes with CASSY (P4.1.4.4)

Cat. No.	Description	P4.1.4.1	P4.1.4.2	P4.1.4.3	P4.1.4.4
576 81	Plug-in board safety socket, 20/10	2	1	1	2
578 51	Diode 1N 4007, STE 2/19	4			4
579 06	Lamp holder, E10, top, STE 2/19	1	1		1
505 08	Bulbs, 12 V/3 W, E10, set of 10	1	1		1
501 48	Bridging plugs STE 2/19, set of 10	1			1
521 487	AC/DC power supply PRO 0...12 V/3 A	1	1	1	1
575 302	Oscilloscope 30 MHz, digital, PT1265	1			
575 24	Screened cable, BNC/4 mm	1			
531 120	Multimeter LDanalog 20	1	2	2	
500 621	Safety connecting lead 50 cm, red	1	3	3	1
500 622	Safety connecting lead 50 cm, blue	1	3	3	
500 624	Safety connecting lead 50 cm, black	2			3
578 55	Zener diode 6.2, STE 2/19		1		
577 42	Resistor, 680 Ω, STE 2/19		1	1	
578 57	Light emitting diode green, STE 2/19			1	
578 48	Light emitting diode red, STE 2/19			1	
524 005W	Mobile-CASSY 2 WiFi				1

Diodes, zener diodes (or Z-diodes) and light-emitting diodes are used today in virtually every electronic circuit.

The experiments P4.1.4.1 and P4.1.4.4 explore the function of half-wave and full-wave rectifiers in the rectification of AC voltages. The half-wave rectifier assembled using a single diode blocks the first half-wave of every AC cycle and conducts only the second half-wave (assuming the diode is connected with the corresponding polarity). The full-wave rectifier, assembled using four diodes in a bridge configuration, uses both half-waves of the AC voltage. In experiment P4.1.4.4 the computer-based system CASSY is used to record the voltages.

The experiment P4.1.4.2 demonstrates how a Z-diode can be used to protect against voltage surges. As long as the applied voltage is below the breakdown voltage U_Z of the Z-diode, the Z-diode acts as an insulator and the voltage U is unchanged. At voltages above U_Z, the current flowing through the Z-diode is so high that U is limited to U_Z.

The aim of the experiment P4.1.4.3 is to assemble a circuit for testing the polarity of a voltage using a green and a red light emitting diode (LED). The circuit is tested with both DC and AC voltage.

Recording the characteristics of a transistor (P4.1.5.2)

Cat. No.	Description	P4.1.5.1	P4.1.5.2	P4.1.5.3	P4.1.5.4	P4.1.5.5
576 81	Plug-in board safety socket, 20/10	1	2	3	1	1
578 67	Transistor BD 137, NPN, e.b., STE 4/50	1	1		1	
578 68	Transistor BD 138, PNP, e.b., STE 4/50	1				
577 32	Resistor 100 Ohm, STE 2/19	1		1		
521 487	AC/DC power supply PRO 0...12 V/3 A	1	1	1		
531 120	Multimeter LDanalog 20	2	3	2		
500 621	Safety connecting lead 50 cm, red	2	4	3	1	3
500 622	Safety connecting lead 50 cm, blue	3	4	3	2	3
577 44	Resistor 1 kOhm, STE 2/19		1	1		
577 64	Resistor, 47 kΩ, STE 2/19		1	1		
577 90	Potentiometer 220 Ohm, STE 4/50		1	1		
577 92	Potentiometer, 1 kΩ, STE 4/50		1	1		
501 48	Bridging plugs STE 2/19, set of 10		1	2		
578 772	Transistor (field effect), J112			1		1
578 51	Diode 1N 4007, STE 2/19			1		
521 210	Transformer 6/12 V			1		
575 302	Oscilloscope 30 MHz, digital, PT1265			1		
575 24	Screened cable, BNC/4 mm			2		
577 56	Resistor 10 kOhm, STE 2/19				1	1
578 31	Capacitor, 0.1 µF, STE 2/19				1	1
524 013	Sensor-CASSY 2				1	1
524 011USB	Power-CASSY USB				1	1
524 220	CASSY Lab 2				1	1
500 611	Safety connecting lead, 25 cm, red				1	
500 612	Safety connecting lead, 25 cm, blue				1	
	additionally required: PC with Windows XP/Vista/7/8/10 (x86 or x64)				1	1

Transistors are among the most important semiconductor components in electronic circuit technology. We distinguish between bipolar transistors, in which the electrons and holes are both involved in conducting current, and field-effect transistors, in which the current is carried by only one type of charge carriers. The electrodes of a bipolar transistor are called the emitter, the base and the collector. The transistor consists of a total of three n-conducting and p-conducting layers, in the order npn or pnp. The base layer, located in the middle, is so thin that charge carriers originating at one junction can cross to the other junction. In field-effect transistors, the conductivity of the current-carrying channel is changed using an electrical field, without applying power. The element which generates this field is called the gate. The input electrode of a field-effect transistor is known as the source, and the output electrode is called the drain.

The experiment P4.1.5.1 examines the principle of the bipolar transistor and compares it with a diode. Here, the difference between an npn and a pnp transistor is explicitly investigated.

The experiments P4.1.5.2 and P4.1.5.4 examine the properties of an npn transistor on the basis of its characteristics. This experiment measures the input characteristic, i.e. the base current I_B as a function of the base-emitter voltage U_{BE}, the output characteristic, i.e. the collector current I_C as a function of the collector-emitter voltage U_{CE} at a constant base current I_B and the collector current I_C as a function of the base current I_B at a constant collector-emitter voltage U_{CE}.

In the experiments P4.1.5.3 and P4.1.5.5, the characteristic of a field-effect transistor, i.e. the drain current I_D, is recorded and diagrammed as a function of the voltage U_{DS} between the drain and source at a constant gate voltage U_G.

TRANSISTOR CIRCUITS

P4.1.6.1
The transistor as an amplifier

P4.1.6.2
The transistor as a switch

P4.1.6.3
The transistor as a sine-wave generator
(oscillator)

P4.1.6.4
The transistor as a function generator

P4.1.6.5
The field-effect transistor as an
amplifier

P4.1.6.6
The field-effect transistor as a switch

The field-effect transistor as an amplifier (P4.1.6.5)

Cat. No.	Description	P4.1.6.1	P4.1.6.2	P4.1.6.3	P4.1.6.4	P4.1.6.5	P4.1.6.6
576 81	Plug-in board safety socket, 20/10	3	2	3	3	3	2
578 67	Transistor BD 137, NPN, e.b., STE 4/50	1	1				
577 44	Resistor 1 kOhm, STE 2/19	1	1	2			
577 56	Resistor 10 kOhm, STE 2/19	1		3		1	1
577 64	Resistor, 47 kΩ, STE 2/19	1		2			1
577 80	Variable resistor, 10 kΩ, STE 2/19	1	1				
577 82	Variable resistor 47 kOhm, STE 2/19	1					
578 38	Capacitor (electrolytic), 47 µF, STE 2/19	1				1	
578 39	Capacitor (electrolytic) 100 µF, STE 2/19	1					
578 40	Capacitor (electrolytic) 470 µF, STE 2/19	1			1		
501 48	Bridging plugs STE 2/19, set of 10	1	1	1	1	1	1
522 621	Function generator S 12	1				1	1
521 487	AC/DC power supply PRO 0...12 V/3 A	1	1	1	1	1	1
575 302	Oscilloscope 30 MHz, digital, PT1265	1		1	1	1	1
575 24	Screened cable, BNC/4 mm	2		2	2	2	2
500 621	Safety connecting lead 50 cm, red	2	3	2	1	2	3
500 622	Safety connecting lead 50 cm, blue	2	3	3	1	2	3
578 02	Photoresistor LDR 05, STE 2/19		1				
578 06	PTC probe, 30 Ω, STE 2/19		1				
579 06	Lamp holder, E10, top, STE 2/19		1		2		
505 08	Bulbs, 12 V/3 W, E10, set of 10		1				
579 13	Toggle switch STE 2/19		1				
579 38	Heating element 100 Ohm, 2 W, STE 2/50		1				
531 120	Multimeter LDanalog 20		2	1		1	1
578 76	Transistor, BC 140, NPN, emitter bottom, STE 4/50			2	2		
577 58	Resistor, 15 kΩ, STE 2/19			2	2	1	
577 68	Resistor, 100 kΩ, STE 2/19			2		1	
577 81	Variable resistor, 4.7 kΩ, STE 2/19			2			
578 22	Capacitor, 100 pF, STE 2/19			2			
578 23	Capacitor, 220 pF, STE 2/19			2			
578 35	Capacitor, 1 µF, STE 2/19			2		2	
578 16	Capacitor, 4.7 µF, STE 2/19			2			
577 46	Resistor, 1.5 kΩ, STE 2/19				2		
578 41	Capacitor (electrolytic), 220 µF, bipolar, STE 2/19				1		

Cat. No.	Description	P4.1.6.1	P4.1.6.2	P4.1.6.3	P4.1.6.4	P4.1.6.5	P4.1.6.6
578 13	Capacitor, 0.22 µF, STE 2/19				1		
578 33	Capacitor, 0.47 µF, STE 2/19				1		
578 51	Diode 1N 4007, STE 2/19				2		
505 191	Bulbs, 15 V/2 W, E10, set of 5				1		
500 624	Safety connecting lead 50 cm, black				1	1	
578 772	Transistor (field effect), J112					1	1
577 61	Resistor, 33 kΩ, STE 2/19					1	
577 657	Resistor, 68 kΩ, STE 2/19					1	
577 76	Resistor, 1 MΩ, STE 2/19					1	
578 36	Capacitor, 2.2 µF, STE 2/19					1	
577 92	Potentiometer, 1 kΩ, STE 4/50						1

Transistor circuits are investigated on the basis of a number of examples. These include the basic connections of a transistor as an amplifier, the transistor as a light-dependent or temperature-dependent electronic switch, the Wien bridge oscillator as an example of a sine-wave generator, the astable multivibrator, basic circuits with field-effect transistors as amplifiers as well as the field-effect transistor as a low-frequency switch.

In the experiment P4.1.6.1 a bipolar transistor is investigated in the common emitter configuration. The adjustment of the operating point and the dependency of the amplification on the emitter resistance are treated.

In the experiment P4.1.6.2 a bipolar transistor is operated as a switch. By means of the high base current, the transistor is operated in saturation and its properties are investigated.

In the experiment P4.1.6.3 a sine-wave generator is set up using a Wien bridge oscillator and a two-stage amplifier. The operating parameters and circuit properties are investigated.

In the experiment P4.1.6.4 an astable multi-vibrator is constructed from two bipolar transistors, and the influences of the components on the frequency and the duty cycle of the vibrations are investigated.

In the experiment P4.1.6.5 a field-effect transistor is investigated as an amplifier in the source configuration and gate configuration, and the properties of the circuits are determined in greater detail.

In experiment P4.1.6.6 a field-effect transistor is operated as a switch. The switch-on resistance for various bias voltages and the signal damping during switching are investigated.
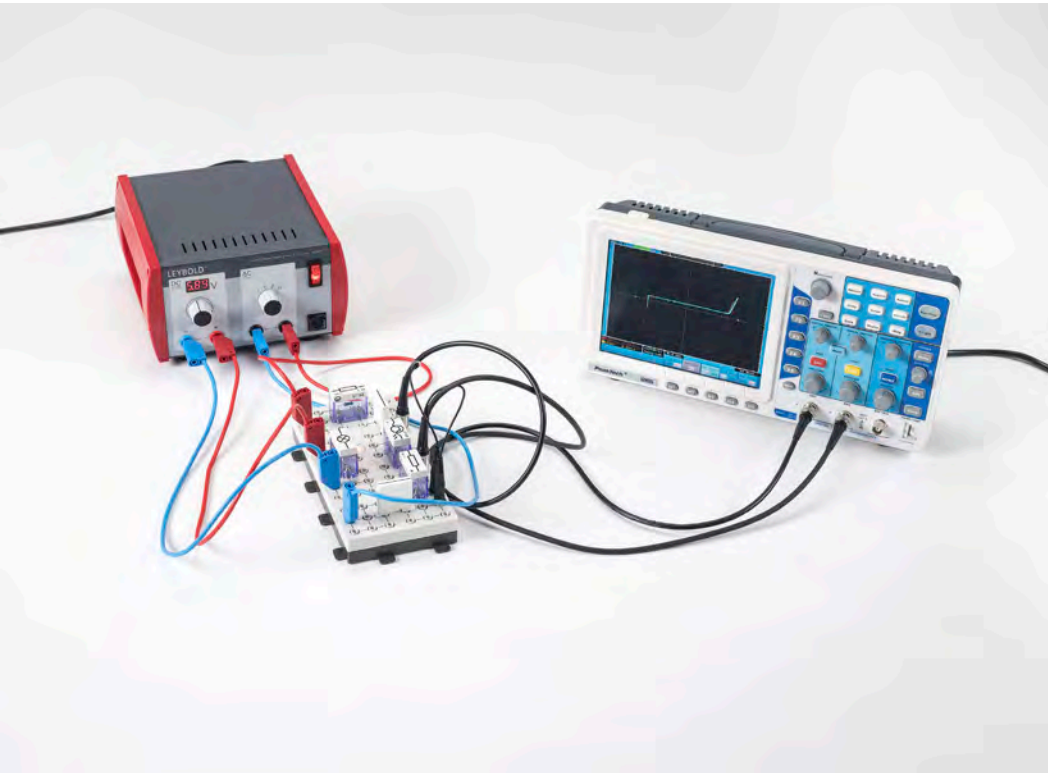
OPTOELECTRONICS

P4.1.7.1
Recording the characteristics of a phototransistor connected as a photodiode

P4.1.7.2
Assembling a purely optical transmission line

Recording the characteristics of a phototransistor connected as a photodiode (P4.1.7.1)

Cat. No.	Description	P4.1.7.1	P4.1.7.2
576 81	Plug-in board safety socket, 20/10	1	3
578 61	Phototransistor, lateral, STE 2/19	1	1
577 32	Resistor 100 Ohm, STE 2/19	1	
577 56	Resistor 10 kOhm, STE 2/19	1	3
579 05	Lamp holder E10, lateral, STE 2/19	1	
505 08	Bulbs, 12 V/3 W, E10, set of 10	1	
501 48	Bridging plugs STE 2/19, set of 10	1	1
521 487	AC/DC power supply PRO 0...12 V/3 A	1	
575 302	Oscilloscope 30 MHz, digital, PT1265	1	
575 24	Screened cable, BNC/4 mm	2	
500 621	Safety connecting lead 50 cm, red	2	2
500 622	Safety connecting lead 50 cm, blue	2	2
578 57	Light emitting diode green, STE 2/19		1
578 58	Light emitting diode, red, lateral, STE 2/19		1
578 68	Transistor BD 138, PNP, e.b., STE 4/50		1
578 85	Operational amplifier, LM 741, STE 4/50		1
577 28	Resistor 47 Ohm, STE 2/19		1
577 40	Resistor 470 Ohm, STE 2/19		1
577 44	Resistor 1 kOhm, STE 2/19		1
577 48	Resistor, 2.2 kΩ, STE 2/19		1
577 64	Resistor, 47 kΩ, STE 2/19		1
578 16	Capacitor, 4.7 µF, STE 2/19		2
578 39	Capacitor (electrolytic) 100 µF, STE 2/19		1
578 40	Capacitor (electrolytic) 470 µF, STE 2/19		1
521 536	DC Power Supply 2 x 0...16 V/2 x 0...5 A		1
522 621	Function generator S 12		1
579 29	Earphone		1
500 98	Safety adapter sockets, black, set of 6		1
500 614	Safety connecting lead, 25 cm, black		4
500 624	Safety connecting lead 50 cm, black		1

Optoelectronics deals with the application of the interactions between light and electrical charge carriers in optical and electronic devices. Optoelectronic arrangements consist of a light-emitting, a light-transmitting and a light-sensitive element. The light beam is controlled electrically.

The subject of the experiment P4.1.7.1 is a phototransistor without base terminal connection used as a photodiode. The current-voltage characteristics are displayed on an oscilloscope for the unilluminated, weakly illuminated and fully illuminated states. It is revealed that the characteristic of the fully illuminated photodiode is comparable with that of a Z-diode, while no conducting-state behavior can be observed in the unilluminated state.

The experiment P4.1.7.2 demonstrates optical transmission of the electrical signals of a function generator to a loudspeaker. The signals modulate the light intensity of an LED by varying the on-state current; the light is transmitted to the base of a phototransistor via a flexible light waveguide. The phototransistor is connected in series to the speaker, so that the signals are transmitted to the loudspeaker.

OPERATIONAL AMPLIFIER CIRCUITS

P4.2.2.1
Unconnected operational amplifier (comparator)

P4.2.2.2
Inverting operational amplifier

P4.2.2.3
Non-inverting operational amplifier

P4.2.2.4
Adder and subtracter

P4.2.2.5
Differentiator and integrator
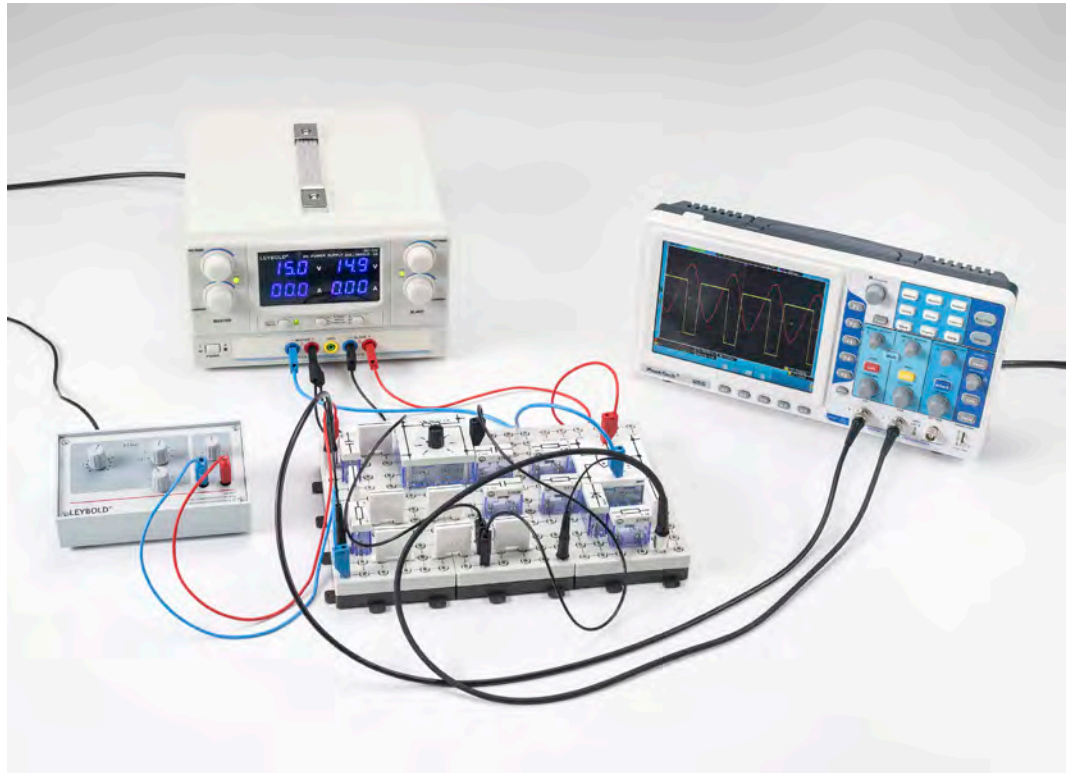
Unconnected operational amplifier (comparator) (P4.2.2.1)

Cat. No.	Description	P4.2.2.1	P4.2.2.2	P4.2.2.3	P4.2.2.4	P4.2.2.5
576 81	Plug-in board safety socket, 20/10	3	2	2	3	2
578 85	Operational amplifier, LM 741, STE 4/50	1	1	1	1	1
577 56	Resistor 10 kOhm, STE 2/19	1	2	2	2	1
577 61	Resistor, 33 kΩ, STE 2/19	2	1		1	
577 62	Resistor, 39 kΩ, STE 2/19	1				
577 68	Resistor, 100 kΩ, STE 2/19	1	1		4	1
577 74	Resistor, 470 kΩ, STE 2/19	1				
577 96	Potentiometer, 100 kΩ, STE 4/50	2	1			1
578 26	Capacitor, 2.2 nF, STE 2/19	2				1
578 28	Capacitor, 10 nF, STE 2/19	1				1
578 51	Diode 1N 4007, STE 2/19	1				
501 48	Bridging plugs STE 2/19, set of 10	1	1	1	1	1
522 621	Function generator S 12	1	1	1		1
521 536	DC Power Supply 2 x 0...16 V/2 x 0...5 A	1	1	1	1	1
575 302	Oscilloscope 30 MHz, digital, PT1265	1	1	1		1
575 24	Screened cable, BNC/4 mm	2	2	2		2
500 98	Safety adapter sockets, black, set of 6	1	1	1	1	1
500 614	Safety connecting lead, 25 cm, black	3	1	2	1	2
500 621	Safety connecting lead 50 cm, red	2	3	3	3	2
500 622	Safety connecting lead 50 cm, blue	2	3	3	3	2
500 624	Safety connecting lead 50 cm, black	1	1	1	1	1
577 44	Resistor 1 kOhm, STE 2/19		1		1	1
577 50	Resistor, 3.3 kΩ, STE 2/19		1			
577 52	Resistor 4.7 kOhm, STE 2/19		1	1		1
577 64	Resistor, 47 kΩ, STE 2/19		2			
577 80	Variable resistor, 10 kΩ, STE 2/19		1	1		
531 120	Multimeter LDanalog 20		1	1	1	
577 32	Resistor 100 Ohm, STE 2/19			1		
577 40	Resistor 470 Ohm, STE 2/19			1	1	
577 46	Resistor, 1.5 kΩ, STE 2/19			1	1	
577 48	Resistor, 2.2 kΩ, STE 2/19			1		

Cat. No.	Description	P4.2.2.1	P4.2.2.2	P4.2.2.3	P4.2.2.4	P4.2.2.5
577 58	Resistor, 15 kΩ, STE 2/19			1		
577 38	Resistor, 330 Ω, STE 2/19				1	
577 60	Resistor, 22 kΩ, STE 2/19				1	
577 76	Resistor, 1 MΩ, STE 2/19					1
578 15	Capacitor, 1 µF, STE 2/19					1
578 16	Capacitor, 4.7 µF, STE 2/19					1
578 76	Transistor, BC 140, NPN, emitter bottom, STE 4/50					1

The operational amplifier is an important analogue component in modern electronics. Originally designed as a calculating component for analogue computers, it has been introduced into an extremely wide range of applications as an amplifier.

The experiment P4.2.2.1 shows that the unconnected operational amplifier overdrives for even the slightest voltage differential at the inputs. It generates a maximum output signal with a sign corresponding to that of the input-voltage differential.

In the experiments P4.2.2.2 and 4.2.2.3, the output of the operational amplifier is fed back to the inverting and non-inverting inputs via resistor R_2. The initial input signal applied via resistor R_1 is amplified in the inverting operational amplifier by the factor

$$V = -\frac{R_2}{R_1}$$

and in the non-inverting module by the factor

$$V = \frac{R_2}{R_1} + 1$$

The experiment P4.2.2.4 demonstrates the addition of multiple input signals and the subtraction of input signals.

The aim of the experiment P4.2.2.5 is to use the operational amplifier as a differentiator and an integrator. For this purpose, a capacitor is connected to the input resp. the feedback loop of the operational amplifier. The output signals of the differentiator are proportional to the change in the input signals, and those of the integrator are proportional to the integral of the input signals.

De Morgan's laws (P4.5.1.2)

SIMPLE COMBINATIONS

P4.5.1.1
AND, OR, XOR, and NAND operations with two variables

P4.5.1.2
De Morgan's laws

P4.5.1.3
Operations with three variables
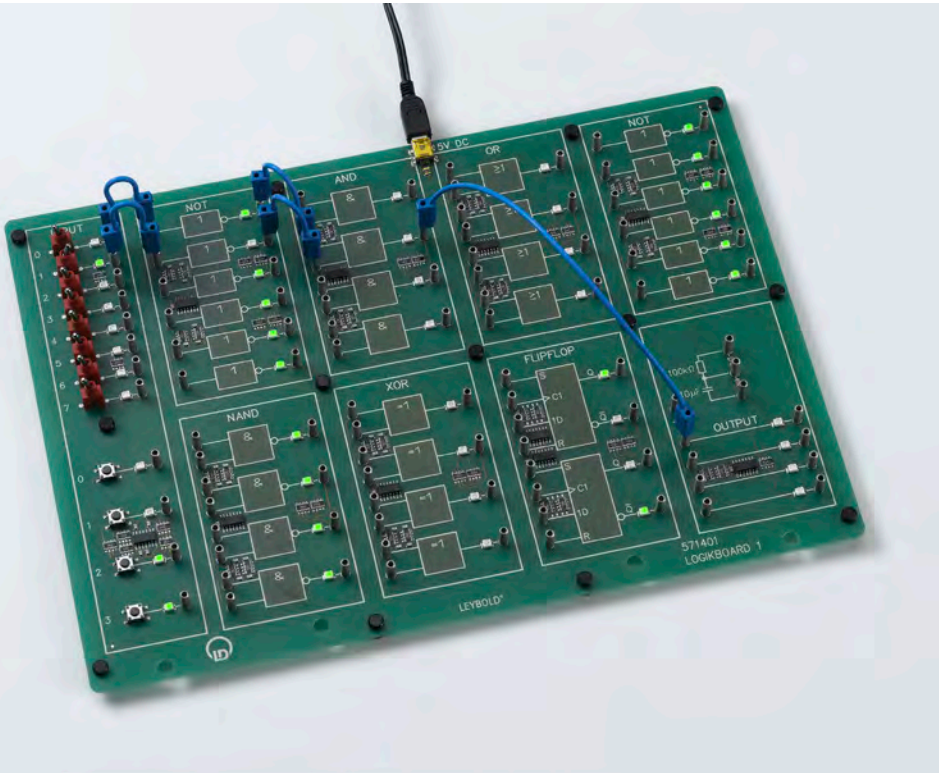
Cat. No.	Description	P4.5.1.1–3
571 4011	Logic board 1	1

Digital devices are built on the simple concept of repeated application of just a few basic circuits. Operations using these circuits are governed by the rules of Boolean algebra, sometimes also called "logic algebra" when applied to digital circuit technology.

The experiment P4.5.1.1 introduces all operations with one or two variables used in digital technology. The aim is to verify the laws which apply in Boolean algebra, i.e. those describing commutation, idempotents, absorption and negation.

The experiment P4.5.1.2 demonstrates de Morgan's laws in practical application. Not(And(A,B)) = Or(Not(A);Not(B))

The object of the experiment P4.5.1.3 is to verify the associative and distributive laws through experiment when operating three variables.

LOGIC CIRCUITS

P4.5.2.1
AND, NAND, OR and XOR operations with four variables

P4.5.2.3
Multiplexers and demultiplexers

P4.5.2.4
Adders

P4.5.2.5
Flipflops

P4.5.2.6
Counters

P4.5.2.7
Shift registers
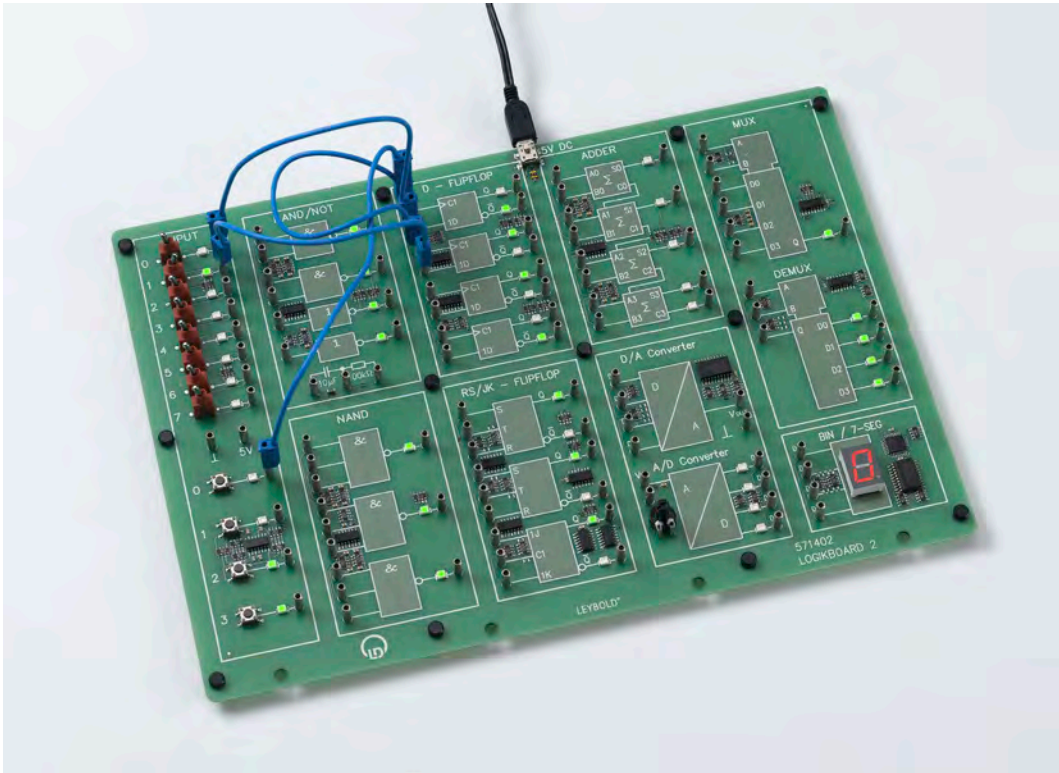
Flipflops (P4.5.2.5)

Cat. No.	Description	P4.5.2.1	P4.5.2.3–7
571 4011	Logic board 1	1	
571 4021	Logic board 2		1

A combinatorial circuit performs operations such that the output variables are only determined by the input variables, but not by past states. A sequential circuit is additionally able to store the states of individual variables. The output variables also depend on the result of preceding events, which is represented by the switching state of flipflops.

As an approach to the structure of complex combinatorial circuits, the experiment P4.5.2.1 applies the understanding of basic operations previously learned to the logical operation of four inputs.

The experiment P4.5.2.3 demonstrates how a multiplexer is used to switch multiple inputs onto a single output and a demultiplexer distributes the signals of a single input line to multiple output lines.

The experiment P4.5.2.4 investigates discrete and complex adders as key components of a computer.

The aim of the experiment P4.5.2.5 is to study the function of flipflops. It deals with the various demands on the behavior of these fundamental components of sequential circuits, which are required for assembling RS, D and JK flipflops.

The experiment P4.5.2.6 is showing the properties of counters in different configurations.

The experiment P4.5.2.7 investigates the shift register as a working block of a deserializer.

ANALOG INPUTS AND OUTPUTS

P4.5.3.1
DA and AD Converter
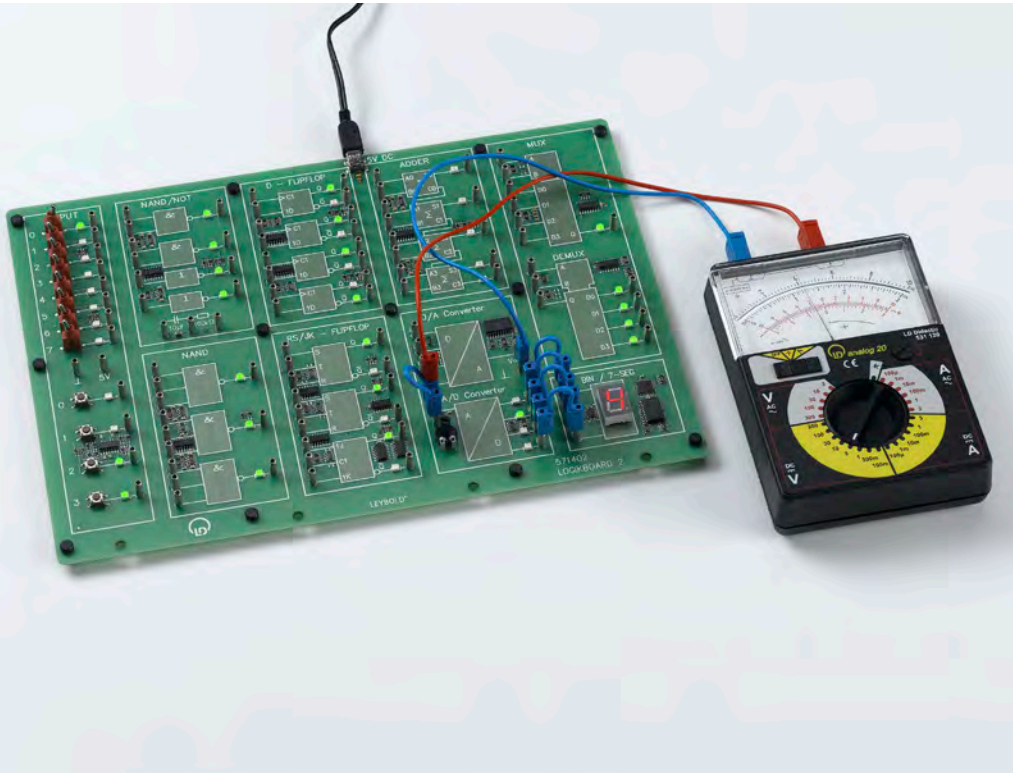
DA and AD Converter (P4.5.3.1)

Cat. No.	Description	P4.5.3.1
571 4021	Logic board 2	1
531 120	Multimeter LDanalog 20	1

Interfacing digital circuitry to the often analog world requires the use of A/D and D/A converters. In this process, continuous signals are converted into discrete, digital signals so that they can be processed further afterwards. Transfer characteristics are inverstigated.

The experiment P4.5.3.1 shows the function of analog to digital conversion and digital to analog conversion.

P5.5.1.1
Determining the radiant flux density and the luminous intensity
of a halogen lamp
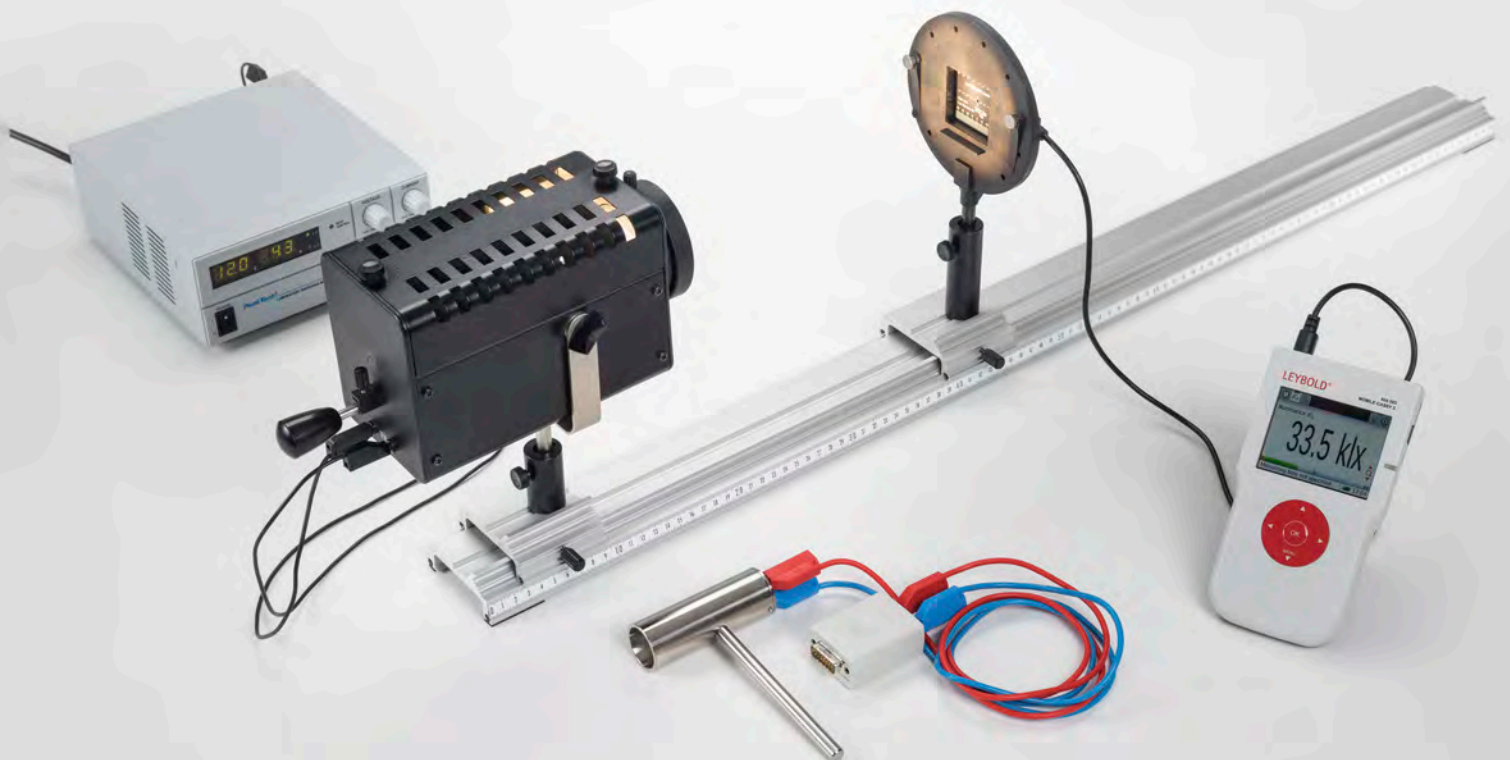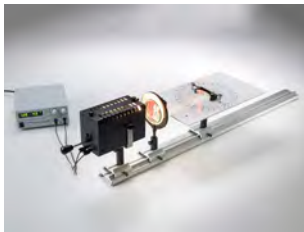
P5 OPTICS

P5 OPTICS
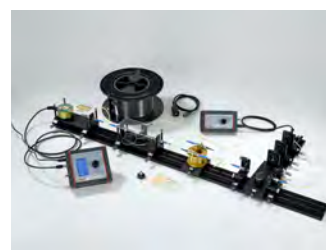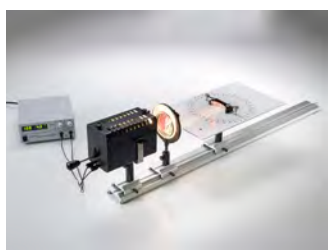
Reflection of light at straight and curved mirrors (P5.1.1.1)

REFLECTION, REFRACTION

P5.1.1.1
Reflection of light at straight and curved mirrors

P5.1.1.2
Refraction of light at straight surfaces and investigation of ray paths in prisms and lenses

Cat. No.	Description	P5.1.1.1-2
463 52	Optical disc	1
450 641	Halogen lamp 12 V, 50/100W	1
450 681	Halogen bulb 12 V/50 W, G6.35	1
726 890	DC-High Current Power Supply 1...32 V/0...20 A	1
463 51	Diaphragm with 5 slits	1
460 08	Lens in frame, f=150 mm	1
460 310	Optical bench, S1 profile, 1 m	1
460 311	Clamp rider with clamp 45/65	2
460 3112	Clamp rider with clamp 75/65	1
300 40	Stand rod, 10 cm, 12 mm diam.	1
500 624	Safety connecting lead 50 cm, black	2

Refraction of light at straight surfaces and investigation of ray paths in prisms and lenses (P5.1.1.2)

Frequently, the propagation of light can be adequately described simply by the ray path. Examples of this are the ray paths of light in mirrors, in lenses and in prisms using sectional models.

The experiment P5.1.1.1 examines how a mirror image is formed by reflection at a plane mirror and demonstrates the reversibility of the ray path. The law of reflection is experimentally validated:

$$\alpha = \beta$$

α: angle of incidence, β: angle of reflection

Further experiment objectives deal with the reflection of a parallel light beam in the focal point of a concave mirror, the existence of a virtual focal point for reflection in a convex mirror, the relationship between focal length and bending radius of the curved mirror and the creation of real and virtual images for reflection at a curved mirror

The experiment P5.1.1.2 deals with the change of direction when light passes from one medium into another. The law of refraction discovered by W. Snell is quantitatively verified:

$$\frac{\sin\alpha}{\sin\beta} = \frac{n_2}{n_1}$$

α: angle of incidence, β: angle of refraction,

n_1: refractive index of medium 1 (here air),

n_2: refractive index of medium 2 (here glass)

This experiment topic also studies total reflection at the transition from a medium with a greater refractive index to one with a lesser refractive index, the concentration of a parallel light beam at the focal point of a collecting lens, the existence of a virtual focal point when a parallel light beam passes through a dispersing lens, the creation of real and virtual images when imaging with lenses and the ray path through a prism.

LEYBOLD®

LAWS OF IMAGING

P5.1.2.1
Determining the focal lengths at collecting and dispersing lenses using collimated light

P5.1.2.2
Determining the focal lengths at collecting lenses through autocollimation

P5.1.2.3
Determining the focal lengths at collecting lenses using Bessel's method

P5.1.2.4
Verifying the imaging laws with a collecting lens

Verifying the imaging laws with a collecting lens (P5.1.2.4)

Cat. No.	Description	P5.1.2.1	P5.1.2.2	P5.1.2.3-4
450 60	Lamp housing with cable	1	1	1
450 511	Bulbs, 6 V/30 W, E14, set of 2	1	1	1
460 20	Condenser with diaphragm holder	1	1	1
521 210	Transformer 6/12 V	1	1	1
460 02	Lens in frame, f=50 mm	1		1
460 03	Lens in frame, f=100 mm	1		1
460 04	Lens in frame, f=200 mm	1		
460 06	Lens in frame, f=-100 mm	1		
441 53	Screen, translucent	1		1
460 310	Optical bench, S1 profile, 1 m	1	1	1
460 311	Clamp rider with clamp 45/65	2	2	2
460 312	Clamp rider with clamp 45/35	1	1	1
311 78	Tape measure 2 m / 1 mm	1	1	1
460 08	Lens in frame, f=150 mm		1	
460 09	Lens in frame, f=300 mm		1	
461 66	Objects for investigating images, pair		1	1
460 28	Plane mirror, 14 cm x 9 cm, with ball joint		1	

The focal lengths of lenses are determined by a variety of means. The basis for these are the laws of imaging.

In the experiment P5.1.2.1, an observation screen is set up parallel to the optical axis so that the path of a parallel light beam can be observed on the screen after passing through a collecting or dispersing lens. The focal length is determined directly as the distance between the lens and the focal point

In autocollimation, experiment P5.1.2.2 a parallel light beam is reflected by a mirror behind a lens so that the image of an object is viewed right next to that object. The distance d between the object and the lens is varied until the object and its image are exactly the same size. At this point, the focal length is

$$f = d$$

In the Bessel method, experiment P5.1.2.3, the object and the observation screen are set up at a fixed overall distance s apart. Between these points there are two lens positions x_1 and x_2 at which a sharply focused image of the object is produced on the observation screen. From the lens laws, we can derive the following relationship for the focal length

$$f = \frac{1}{4} \cdot \left(s - \frac{\left(x_1 - x_2 \right)^2}{s} \right)$$

In the experiment P5.1.2.4, the object height G, the object width g, the image height B and the image width b are measured directly for a collecting lens in order to confirm the lens laws. The focal length can be calculated using the formula:

$$f = \frac{g \cdot b}{g + b}$$

Spherical aberration in lens imaging (P5.1.3.1)

IMAGE DISTORTION

P5.1.3.1
Spherical aberration in lens imaging

P5.1.3.2
Astigmatism and curvature of image field in lens imaging

P5.1.3.3
Lens imaging distortions (barrel and cushion) and coma

P5.1.3.4
Chromatic aberration in lens imaging

Cat. No.	Description	P5.1.3.1	P5.1.3.2	P5.1.3.3	P5.1.3.4
450 60	Lamp housing with cable	1	1	1	1
450 511	Bulbs, 6 V/30 W, E14, set of 2	1	1	1	1
460 20	Condenser with diaphragm holder	1	1	1	1
521 210	Transformer 6/12 V	1	1	1	1
461 61	Diaphragms for spherical aberration, pair	1			
461 66	Objects for investigating images, pair	1	1	1	
460 08	Lens in frame, f=150 mm	1	1	1	1
460 26	Iris diaphragm	1	1		1
441 53	Screen, translucent	1	1	1	1
460 310	Optical bench, S1 profile, 1 m	1	1	1	1
460 311	Clamp rider with clamp 45/65	2	2	2	2
460 312	Clamp rider with clamp 45/35	2	2	2	2
460 02	Lens in frame, f=50 mm			1	
467 95	Colour filter set, primary				1

A spherical lens only images a point into an ideal point when the imaging ray traces intersect the optical axis at small angles, and the angle of incidence and angle of refraction are also small when the ray passes through the lens. As this condition is only fulfilled to a limited extent in practice, optical aberrations like coma are unavoidable.

The experiments P5.1.3.1 and P5.1.3.2 deal with aberrations of image sharpness. In a ray path parallel to the optical axis, paraxial rays are united at a different distance from abaxial rays. This effect, known as "spherical aberration", is particularly apparent in lenses with sharp curvatures. Astigmatism and curvature of field may be observed when imaging long objects with narrow light beams. The focal plane is in reality a curved surface, so that the image on the observation screen becomes increasingly fuzzy toward the edges when the middle is sharply focused. Astigmatism is the phenomenon whereby a tightly restricted light beam does not produce a point-type image, but rather two lines which are perpendicular to each other with a finite spacing with respect to the axis.

The experiment P5.1.3.3 explores aberrations of scale. Blocking light rays in front of the lens causes a barrel-shaped distortion, i. e. a reduction in the imaging scale with increasing object size. Screening behind the lens results in cushion-type aberrations. "Coma" is the term for one-sided, plume-like or blob-like distortion of the image when imaged by a beam of light passing through the lens at an oblique angle.

The experiment P5.1.3.4 examines chromatic aberrations. These are caused by a change in the refractive index with the wavelength, and are thus unavoidable when not working with non-monochromatic light.
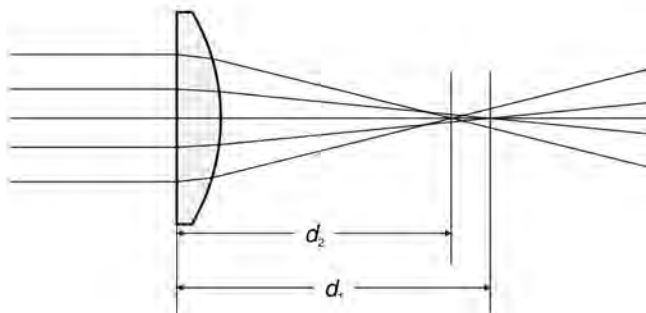
Intersections of paraxial and abaxial rays (P5.1.3.1)

OPTICAL INSTRUMENTS

P5.1.4.1
Magnifier and microscope

P5.1.4.2
Kepler's telescope and
Galileo's telescope

Magnifier and microscope (P5.1.4.1)

Cat. No.	Description	P5.1.4.1	P5.1.4.2
450 60	Lamp housing with cable	1	
450 511	Bulbs, 6 V/30 W, E14, set of 2	1	
460 20	Condenser with diaphragm holder	1	
521 210	Transformer 6/12 V	1	
460 22	Holder with spring clips	1	
311 091	Glass scale 50 mm	1	
460 02	Lens in frame, f=50 mm	1	1
460 03	Lens in frame, f=100 mm	1	1
460 08	Lens in frame, f=150 mm	1	
460 04	Lens in frame, f=200 mm	1	1
460 310	Optical bench, S1 profile, 1 m	1	1
460 311	Clamp rider with clamp 45/65	2	
460 312	Clamp rider with clamp 45/35	4	2
441 53	Screen, translucent	1	
311 78	Tape measure 2 m / 1 mm	1	
460 05	Lens in frame, f=500 mm		1
460 06	Lens in frame, f=-100 mm		1
311 22	Vertical rule		1
300 11	Saddle base		1

The magnifier, the microscope and the telescope are introduced as optical instruments which primarily increase the angle of vision. The design principle of each of these instruments is reproduced on the optical bench. For quantitative conclusions, the common definition of magnification is used:

$$V = \frac{\tan \psi}{\tan \varphi}$$

ψ: angle of vision with instrument

φ: angle of vision without instrument

In the experiment P5.1.4.1, small objects are observed from a short distance. First, a collecting lens is used as a magnifier. Then, a microscope in its simplest form is assembled using two collecting lenses. The first lens, the objective, produces a real, magnified and inverted intermediate image. The second lens, the ocular (or eyepiece) is used as a magnifier to view this intermediate image. For the total magnification of the microscope, the following applies:

$$V_M = V_{ob} \cdot V_{oc}$$

V_{ob}: imaging scale of objective

V_{oc}: imaging scale of ocular

Here, V_{oc} corresponds to the magnification of the magnifier.

$$V_{oc} = \frac{s_0}{f_{oc}}$$

s_0: clear field of vision

f_{oc}: focal length of ocular

The aim of the experiment P5.1.4.2 is to observe distant objects using a telescope. The objective and the ocular of a telescope are arranged so that the back focal point of the objective coincides with the front focal point of the ocular. A distinction is made between the Galilean telescope, which uses a dispersing lens as an ocular and produces an erect image, and the Kepler telescope, which produces an inverted image because its ocular is a collecting lens. In both cases, the total magnification can be determined as:

$$V_T = \frac{f_{ob}}{|f_{oc}|}$$

f_{ob}: focal length of objective

f_{oc}: focal length of ocular

Ray path through the Kepler telescope (P5.1.4.2)

Determining the refractive index and dispersion of liquids (P5.2.1.2)

REFRACTIVE INDEX AND DISPERSION

P5.2.1.1
Determining the refractive index and dispersion of flint glass and crown glass

P5.2.1.2
Determining the refractive index and dispersion of liquids

Cat. No.	Description	P5.2.1.1	P5.2.1.2
465 22	Prism, crown glass	1	
465 32	Prism, flint glass	1	
460 25	Prism table	1	1
460 22	Holder with spring clips	1	1
450 60	Lamp housing with cable	1	1
450 511	Bulbs, 6 V/30 W, E14, set of 2	1	1
460 20	Condenser with diaphragm holder	1	1
521 210	Transformer 6/12 V	1	1
468 03	Light filter, red	1	1
468 07	Light filter, yellow-green	1	1
468 11	Light filter, blue with violet	1	1
460 08	Lens in frame, f=150 mm	1	1
460 310	Optical bench, S1 profile, 1 m	1	1
460 311	Clamp rider with clamp 45/65	1	1
460 312	Clamp rider with clamp 45/35	3	3
311 78	Tape measure 2 m / 1 mm	1	1
465 52	Hollow prism		1
665 002	Funnel		1
675 2100	Toluene, 250 ml		1
675 0410	Turpentine oil, rectified, 250 ml		1
675 4760	Cinnamic ethylester, 100 ml		1

Dispersion is the term for the fact that the refractive index n is different for different-colored light. Often, dispersion also refers to the quantity $dn/d\lambda$, i.e. the quotient of the change in the refractive index dn and the change in the wavelength $d\lambda$.

In the experiment P5.2.1.1, the angle of minimum deviation ϑ is determined for a flint glass and a crown glass prism at the same refracting angle ε. This enables determination of the refractive index of the respective prism material according to the formula

$$n = \frac{\sin\frac{1}{2}(\varepsilon + \varphi)}{\sin\frac{1}{2}\varepsilon}$$

The measurement is conducted for several different wavelengths, so that the dispersion can also be quantitatively measured.

In the experiment P5.2.1.2, an analogous setup is used to investigate dispersion in liquids. Toluol, turpentine oil, cinnamic ether, alcohol and water are each filled into a hollow prism in turn, and the differences in the refractive index and dispersion are observed.
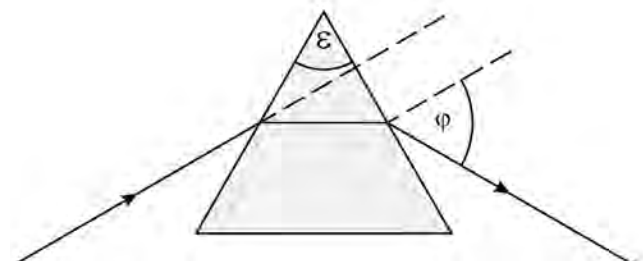
Ray path through a prism (P5.2.1.1)

COLOR MIXING

P5.2.3.2
Demonstration of additive color mixing

P5.2.3.3
Demonstration of subtractive color mixing

Demonstration of additive color mixing (P5.2.3.2)

Cat. No.	Description	P5.2.3.2	P5.2.3.3
459 098	Triple LED lamp	1	
459 095	Plug-in power supply USB 5 V DC (A socket)	1	1
459 096	Cable USB (USB Type A - Mini-USB)	1	1
460 03	Lens in frame, f=100 mm	1	1
460 22	Holder with spring clips	1	1
688 045	Sliding diaphragms, set of 6	1	
467 95	Colour filter set, primary	1	1
467 96	Colour filter set, secondary	1	1
467 97	Triple colour filter	1	
441 53	Screen, translucent	1	1
460 310	Optical bench, S1 profile, 1 m	1	1
460 311	Clamp rider with clamp 45/65	1	1
460 312	Clamp rider with clamp 45/35	2	3
460 313	Clamp rider with fixing column	1	1
459 094	LED lamp		1
460 02	Lens in frame, f=50 mm		1
311 78	Tape measure 2 m / 1 mm		1

The colour recognition of the human eye is determined by three types of light receptor cones in the retina. Comparison of the different colours (wavelength ranges) of the visible spectrum with the sensitivity of the different types of cone reveals division into the primary colours: red, green and blue. Combinations of two primary colours result in the secondary colours: cyan, magenta and yellow. Therefore secondary colour filters absorb the third primary colour. A combination of all three primary colours results in white.

In experiment P5.2.3.2 several colour filters (red, green, blue) are placed next to each other in front of a lamp with 3 light sources and in the image on a screen the overlap of these primary colours show additive colour mixing.

In experiment P5.2.3.3 subtractive colour mixing is shown by placing colour filters (yellow, magenta, cyan) partially overlapping in the light beam of a lamp.
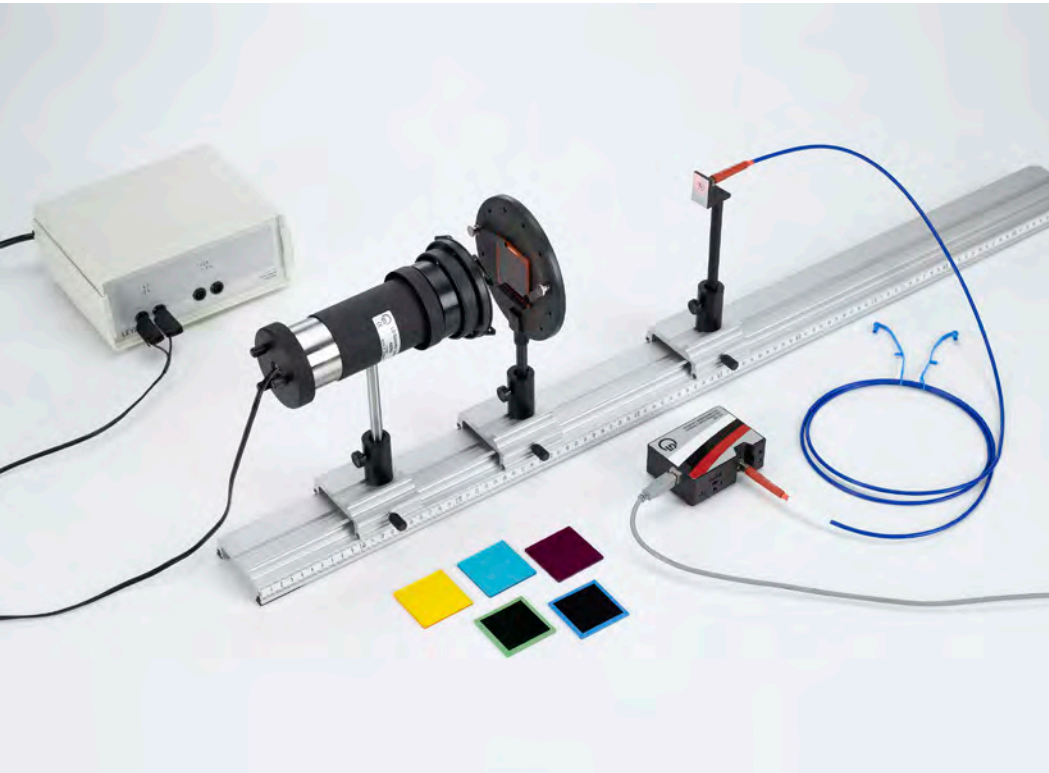
ABSORPTION SPECTRA

P5.2.4.3
Absorption spectra of tinted glass samples – Recording and evaluating with a spectrophotometer

P5.2.4.4
Absorption and fluorescence spectra of coloured liquids – Recording and evaluating with a spectrophotometer

P5.2.4.5
Absorption spectra of PMMA optical waveguide – Recording and evaluating with a spectrophotometer

Absorption spectra of tinted glass samples - Recording and evaluating with a spectrophotometer (P5.2.4.3)

Cat. No.	Description	P5.2.4.3	P5.2.4.4	P5.2.4.5
467 96	Colour filter set, secondary	1		
468 01	Light filter, dark red	1		
468 09	Light filter, blue-green	1		
468 11	Light filter, blue with violet	1	1	
460 22	Holder with spring clips	1	1	
450 60	Lamp housing with cable	1	1	
450 511	Bulbs, 6 V/30 W, E14, set of 2	1	1	
460 20	Condenser with diaphragm holder	1	1	
521 210	Transformer 6/12 V	1	1	
467 251	Compact spectrometer, physics (spectral photometer)	1	1	1
460 251	Fibre holder	1	1	1
460 310	Optical bench, S1 profile, 1 m	1	1	
460 311	Clamp rider with clamp 45/65	3	4	
477 14	Plate glass cell (cuvette), 50 x 50 x 20 mm		1	
460 25	Prism table		1	
300 11	Saddle base		1	2
300 40	Stand rod, 10 cm, 12 mm diam.		1	
301 01	Leybold multiclamp		1	
604 5672	Double microspatula, steel, 150 mm		1	
672 0110	Fluoresceine, 25 g		1	
451 17	Lamp socket, E27, Euro plug			1
505 302	Halogen Bulb 230 V/ 46 W, E27			1
579 44	Light waveguide, set of 2			1
	additionally required: PC with Windows XP/Vista/7/8/10 (x86 or x64)	1	1	1

The colors we perceive when looking through colored glass or liquids are created by the transmitted component of the spectral colors.

In the experiment P5.2.4.3, the light from an incandescent light bulb passing through coloured pieces of glass is recorded with a spectrometer and compared with the continuous spectrum of the lamp light. The original, continuous spectrum with the continuum of spectral colors disappears. All that remains is a band with the colour components of the filter. The transmission coefficient and the optical density of the coloured pieces of glass are calculated.

In the experiment P5.2.4.4, the light from an incandescent light bulb passing through a coloured liquid is recorded using a spectrometer. The fluorescence of the coloured liquid is recorded under a right angle. A blue filter is used to clearly separate fluorescence and light scattering. Both, absorption and fluorescence spectra are compared with the continuous spectrum of the lamp light.

In the experiment P5.2.4.5, light passing through an optical fibre is recorded by a compact spectrometer. The higher order overtones of molecular oscillations create spectral ranges of high absorption, leaving ranges of high transmission in between, the so called „optical windows".
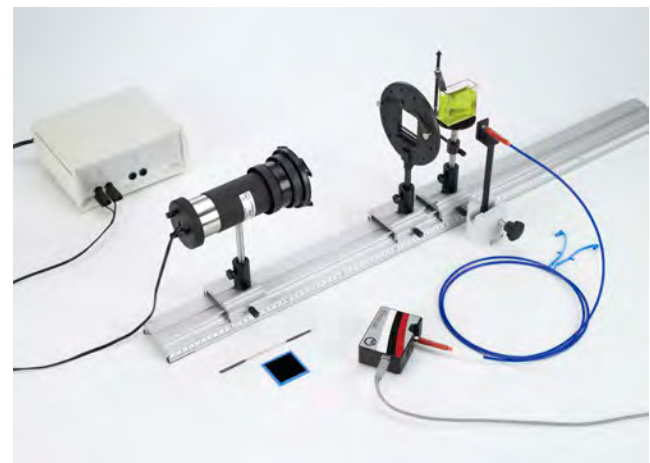
Absorption and fluorescence spectra of coloured liquids (P5.2.4.4)

REFLECTION SPECTRA

P5.2.5.1
Reflection spectra of different materials - Recording and evaluating with a spectrophotometer
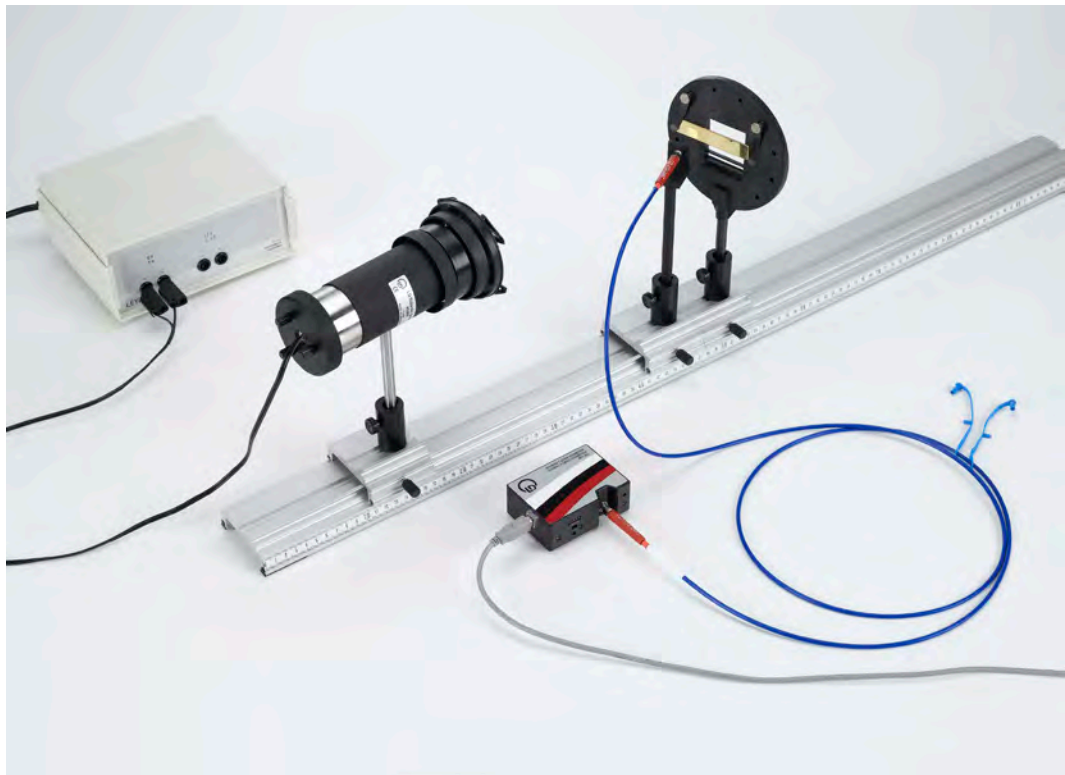
Reflection spectra of different materials - Recording and evaluating with a spectrophotometer (P5.2.5.1)

Cat. No.	Description	P5.2.5.1
567 06	Conductors/insulators, set of 6	1
460 22	Holder with spring clips	1
450 60	Lamp housing with cable	1
450 511	Bulbs, 6 V/30 W, E14, set of 2	1
460 20	Condenser with diaphragm holder	1
521 210	Transformer 6/12 V	1
467 251	Compact spectrometer, physics (spectral photometer)	1
460 251	Fibre holder	1
460 310	Optical bench, S1 profile, 1 m	1
460 311	Clamp rider with clamp 45/65	3
	additionally required: PC with Windows XP/Vista/7/8/10 (x86 or x64)	1

The colors we perceive of opaque objects are induced by the reflected com-ponent of the spectral colors.

In the experiment P5.2.5.1, the light from an incandescent light bulb reflected by different materials is recorded using a spectrometer. By comparison with the reflection from a sheet of white paper (scattered light), the reflection coefficient can be calculated.
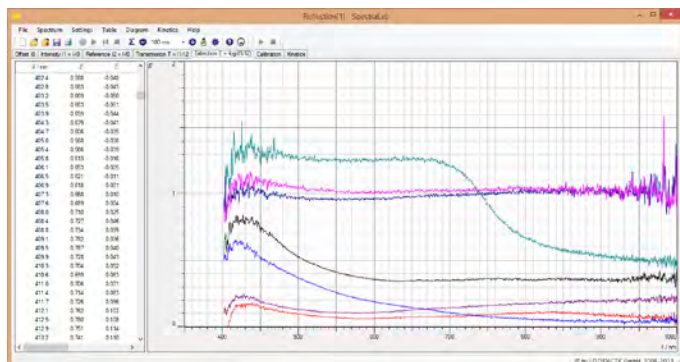
Reflectivity of different materials against the wavelength (P5.2.5.1)

Diffraction at a double slit and multiple slits (P5.3.1.2)

DIFFRACTION

P5.3.1.1
Diffraction at a slit, at a post and at a circular iris diaphragm

P5.3.1.2
Diffraction at a double slit and multiple slits

P5.3.1.3
Diffraction at one- and two-dimensional gratings

Cat. No.	Description	P5.3.1.1	P5.3.1.2	P5.3.1.3
469 91	Diaphragm with 3 single slits	1		
469 96	Diaphragm with 3 diffraction holes	1		
469 97	Diaphragm with 3 diffraction objects	1		
460 22	Holder with spring clips	1	1	1
471 830	He-Ne Laser, linearly polarised	1	1	1
460 01	Lens in frame, f=5 mm	1	1	1
460 02	Lens in frame, f=50 mm	1	1	1
460 32	Optical bench with standardised profile, 1 m	1	1	1
460 370	Optics rider, 60/34	4	4	4
441 53	Screen, translucent	1	1	1
300 11	Saddle base	1	1	1
469 84	Diaphragm with 3 double slits of different slit widths		1	
469 85	Diaphragm with 4 double slits of different slit spacing		1	
469 86	Diaphragm with 5 multiple slits with different slit numbers		1	
469 87	Diaphragm with 3 gratings			1
469 88	Diaphragm with 2 wire-mesh gratings			1

The experiment P5.3.1.1 looks at the intensity minima for diffraction at a slit. Their angles ϑ_k with respect to the optical axis for a slit of the width b is given by the relationship

$$\sin\varphi_k = k \cdot \frac{\lambda}{b} \, (k = 1;\ 2;\ 3;\dots)$$

λ: **wavelength of the light**

In accordance with Babinet's theorem, diffraction at a post produces similar results. In the case of diffraction at a circular iris diaphragm with the radius r, concentric diffraction rings may be observed; their intensity minima can be found at the angles ϑ_k using the relationship

$$\sin\varphi_k = k \cdot \frac{\lambda}{r} \quad (k = 0.610;\ 1.116;\ 1.619;\dots)$$

The experiment P5.3.1.2 explores diffraction at a double slit. The constructive interference of secondary waves from the first slit with secondary waves from the second slit produces intensity maxima; at a given distance d between slit midpoints, the angles ϑ_n of these maxima are specified by

$$\sin\varphi_n = n \cdot \frac{\lambda}{d} \quad (n = 0;\ 1;\ 2;\dots)$$

The intensities of the various maxima are not constant, as the effect of diffraction at a single slit is superimposed on the diffraction at a double slit. In the case of diffraction at more than two slits with equal spacings d, the positions of the interference maxima remain the same. Between any two maxima, we can also detect N-2 secondary maxima; their intensities decrease for a fixed slit width b and increasing number of slits N.

The experiment P5.3.1.3 investigates diffraction at a line grating and a crossed grating. We can consider the crossed grating as consisting of two line gratings arranged at right angles to each other. The diffraction maxima are points at the "nodes" of a straight, square matrix pattern.
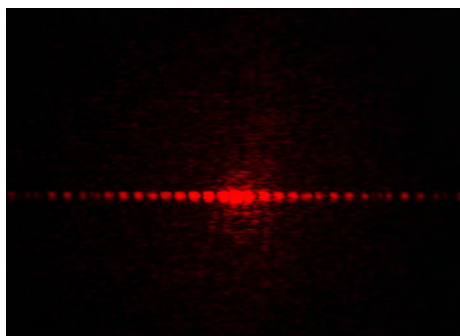
Interference pattern of experiment on the screen (P5.3.1.2)

DIFFRACTION

P5.3.1.4
Diffraction at a single slit –
Recording and evaluating with CASSY

P5.3.1.5
Diffraction at a double slit and
multiple slits – Recording and
evaluating with CASSY
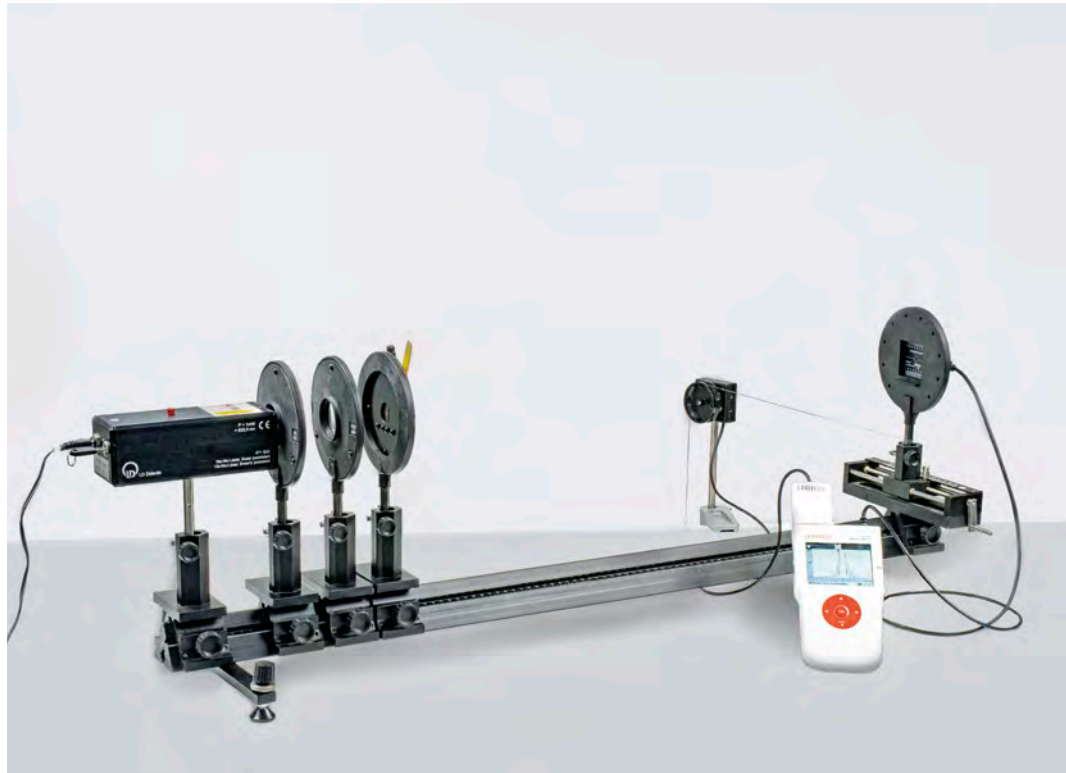
Diffraction at a single slit – Recording and evaluating with CASSY (P5.3.1.4)

Cat. No.	Description	P5.3.1.4	P5.3.1.5
460 14	Adjustable slit	1	
471 830	He-Ne Laser, linearly polarised	1	1
460 22	Holder with spring clips	1	2
460 01	Lens in frame, f=5 mm	1	1
460 02	Lens in frame, f=50 mm	1	1
460 33	Optical bench with standardised profile, 2 m	1	1
460 374	Optics rider, 90/50	4	4
460 383	Sliding rider, 90/50	1	1
524 005W	Mobile-CASSY 2 WiFi	1	1
524 220	CASSY Lab 2	1	1
524 444	Lux Sensor M	1	1
524 082	Rotary motion sensor S	1	1
301 07	Simple bench clamp	1	1
309 48	Fishing line	1	1
342 63	Weight 50 g	1	1
469 84	Diaphragm with 3 double slits of different slit widths		1
469 85	Diaphragm with 4 double slits of different slit spacing		1
469 86	Diaphragm with 5 multiple slits with different slit numbers		1
	additionally required: PC with Windows XP/Vista/7/8/10 (x86 or x64)	1	1

A photoelement with a narrow light opening is used to measure the diffraction intensities; this sensor can be moved perpendicularly to the optical axis on the optical bench, and its lateral position can be measured using a displacement transducer.

The experiment P5.3.1.4 investigates diffraction at slit of variable width. The recorded measured values for the intensity I are compared with the results of a model calculation for small diffraction angles ϑ which uses the slit width b as a parameter:

$$I \propto \left(\frac{\sin\left(\frac{\pi b}{\lambda}\varphi\right)}{\frac{\pi b}{\lambda}\varphi} \right)^2 \text{ where } \varphi = \frac{s}{L}$$

λ: wavelength of the light

s: lateral shift of photoelement

L: distance between object and photoelement

The experiment P5.3.1.5 explores diffraction at multiple slits. In the model calculation performed for comparison purposes, the slit width b and the slit spacing d are both used as parameters.

$$I \propto \left(\frac{\sin\left(\frac{\pi b}{\lambda}\varphi\right)}{\frac{\pi b}{\lambda}\varphi} \right)^2 \cdot \left(\frac{\sin\left(\frac{N\pi d}{\lambda}\varphi\right)}{\sin\left(\frac{\pi d}{\lambda}\varphi\right)} \right)^2$$

N: number of illuminated slits

DIFFRACTION

P5.3.1.9
Investigation of the spatial coherence of an extended light source

Investigation of the spatial coherence of an extended light source (P5.3.1.9)

Cat. No.	Description	P5.3.1.9
451 062	Spectral lamp, Hg 100	1
451 16	Housing for spectral lamps	1
451 30	Universal choke, 230 V, 50 Hz	1
460 32	Optical bench with standardised profile, 1 m	1
460 370	Optics rider, 60/34	2
460 373	Optics rider, 60/50	1
460 374	Optics rider, 90/50	3
468 07	Light filter, yellow-green	1
460 22	Holder with spring clips	2
688 045	Sliding diaphragms, set of 6	1
460 14	Adjustable slit	1
469 85	Diaphragm with 4 double slits of different slit spacing	1
460 02	Lens in frame, f=50 mm	1
460 135	Ocular with scale	1

A photoelement with a narrow light opening is used to measure the diffraction intensities; this sensor can be moved perpendicularly to the optical axis on the optical bench, and its lateral position can be measured using a displacement transducer. The measured values are recorded and evaluated using the software CASSY Lab.

The experiment P5.3.1.9 explores the condition for spatial coherence. The light source is a single slit of variable width illuminated by a Hg spectral lamp. Combined with a filter this results in a monochromatic light source with variable width a. At a distance L double slits of different distances of the slits g (and fixed slit width b) are illuminated. For each distance g the width a of the adjustable single slit is determined where the interference pattern after the double slit vanishes. Then, the coherence condition is no longer fulfilled.

TWO–BEAM INTERFERENCE

P5.3.2.1
Interference at a Fresnel's mirror
with an He-Ne laser

P5.3.2.2
Lloyd's mirror experiment
with an He-Ne laser

P5.3.2.3
Interference at Fresnel's biprism
with an He-Ne laser

Interference at a Fresnel's mirror with an He-Ne laser (P5.3.2.1)

Cat. No.	Description	P5.3.2.1–2	P5.3.2.3
471 830	He-Ne Laser, linearly polarised	1	1
471 05	Fresnel's mirror, adjustable	1	
460 01	Lens in frame, f=5 mm	1	1
460 04	Lens in frame, f=200 mm	1	1
460 32	Optical bench with standardised profile, 1 m	1	1
460 370	Optics rider, 60/34	3	3
460 373	Optics rider, 60/50	1	1
441 53	Screen, translucent	1	1
300 11	Saddle base	1	1
311 53	Vernier callipers	1	1
311 78	Tape measure 2 m / 1 mm	1	1
471 09	Fresnel biprism		1
460 25	Prism table		1

In these experiments, two coherent light sources are generated by recreating three experiments of great historical significance. In each of these experiments, the respective wavelength λ of the light used is determined by the distance d between two interference lines and the distance a of the (virtual) light sources. At a sufficiently great distance L between the (virtual) light sources and the projection screen, the relationship

$$\lambda = a \cdot \frac{d}{L}$$

obtains. The determination of the quantity a depends on the respective experiment setup.

In 1821, A. Fresnel used two mirrors inclined with respect to one another to create two virtual light sources positioned close together, which, being coherent, interfered with each other – P5.3.2.1.

In 1839, *H. Lloyd* demonstrated that a second, virtual light source coherent with the first can be created by reflection in a mirror. He observed interference phenomena between direct and reflected light – P5.3.2.2.

Coherent light sources can also be produced using a Fresnel biprism, first demonstrated in 1826 (P5.3.2.3). Refraction in both halves of the prism results in two virtual images, which are closer together the smaller the prism angle is.
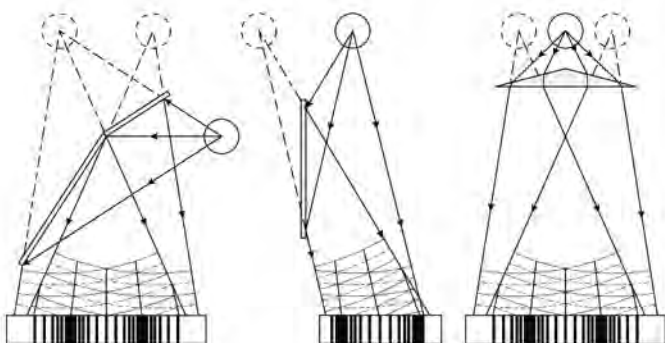
Fresnel mirror - Lloyd mirror - Biprism (P5.3.2.1-3)

Newton's rings in transmitted and reflected white light (P5.3.3.2)

NEWTON'S RINGS

P5.3.3.1
Newton's Rings in transmitted monochromatic light

P5.3.3.2
Newton's rings in transmitted and reflected white light

Cat. No.	Description	P5.3.3.1	P5.3.3.2
471 111	Glass plates for Newton's rings	1	1
460 03	Lens in frame, f=100 mm	2	
460 26	Iris diaphragm	1	
460 22	Holder with spring clips	1	
460 32	Optical bench with standardised profile, 1 m	1	1
460 370	Optics rider, 60/34	6	5
451 111	Spectral lamp, Na	1	
451 062	Spectral lamp, Hg 100	1	
451 16	Housing for spectral lamps	1	
451 30	Universal choke, 230 V, 50 Hz	1	
468 30	Light filter, yellow	1	
468 31	Light filter, green	1	
468 32	Light filter, blue	1	
441 53	Screen, translucent	1	
300 11	Saddle base	1	
460 04	Lens in frame, f=200 mm		2
460 373	Optics rider, 60/50		1
460 380	Cantilever arm		1
471 88	Beam splitter		2
450 641	Halogen lamp 12 V, 50/100W		1
450 63	Halogen bulb 12 V/100 W, G6.35		1
726 890	DC-High Current Power Supply 1...32 V/0...20 A		1
500 624	Safety connecting lead 50 cm, black		2

Newton's rings are produced using an arrangement in which a convex lens with an extremely slight curvature is touching a glass plate, so that an air wedge with a spherically curved boundary surface is formed. When this configuration is illuminated with a vertically incident, parallel light beam, concentric interference rings (the Newton's rings) are formed around the point of contact between the two glass surfaces both in reflection and in transmitted light. For the path difference of the interfering partial beams, the thickness d of the air wedge is the defining factor; this distance is not in a linear relation to the distance r from the point of contact:

$$d = \frac{r^2}{2R}$$

R: bending radius of convex lens

In the experiment P5.3.3.1, the Newton's rings are investigated with mono-chromatic, transmitted light. At a known wavelength λ, the bending radius R is determined from the radii r_n of the interference rings. Here, the relationship for constructive interference is:

$$d = n \cdot \frac{\lambda}{2} \quad \text{where} \quad n = 0,\ 1,\ 2,\ \ldots$$

Thus, for the radii of the bright interference rings, we can say:

$$r_n^2 = n \cdot R \cdot \lambda \quad \text{where} \quad n = 0,\ 1,\ 2,\ \ldots$$

In the experiment P5.3.3.2, the Newton's rings are studied both in reflection and in transmitted light. As the partial beams in the air wedge are shifted in phase by $\lambda/2$ for each reflection at the glass surfaces, the interference conditions for reflection and transmitted light are complementary. The radii r_n of the bright interference lines calculated for transmitted light using the equations above correspond precisely to the radii of the dark rings in reflection. In particular, the center of the Newton's rings is bright in transmitted light and dark in reflection. As white light is used, the interference rings are bordered by colored fringes.

MICHELSON INTERFEROMETER

P5.3.4.1
Setting up a Michelson interferometer on the laser optics base plate

P5.3.4.2
Determining the wavelength of the light of an He-Ne laser using a Michelson interferometer

Setting up a Michelson interferometer on the laser optics base plate (P5.3.4.1)

Cat. No.	Description	P5.3.4.1	P5.3.4.2
473 40	Laser optics base plate	1	1
471 830	He-Ne Laser, linearly polarised	1	1
473 411	Laser mount	1	1
473 421	Optics base	4	5
473 432	Beam divider, 50 %	1	1
473 431	Holder for beam divider	1	1
473 461	Planar mirror with fine adjustment	2	2
473 471	Spherical lens, f = 2.7 mm	1	1
441 53	Screen, translucent	1	1
300 11	Saddle base	1	1
311 02	Metal rule, 1 m	1	1
473 48	Fine adjustment mechanism		1

In a Michelson interferometer, an optical element divides a coherent light beam into two parts. The component beams travel different paths, are reflected into each other and finally recombined. As the two component beams have a fixed phase relationship with respect to each other, interference patterns can occur when they are superposed on each other. A change in the optical path length of one component beam alters the phase relation, and thus the interference pattern as well. Thus, given a constant refractive index, a change in the interference pattern can be used to determine a change in the geometric path. When the geometric path is unchanged, then this configuration can be used to investigate changes in the refractive index due to variations e.g. in pressure, temperature and density.

In the experiment P5.3.4.1, the Michelson interferometer is assembled on the vibration-proof laser optics base plate. This setup is ideal for demonstrating the effects of mechanical shocks and air streaking.

In the experiment P5.3.4.2, the wavelength of an He-Ne laser is determined from the change in the interference pattern when moving an interferometer mirror using the shifting distance Δs of the mirror. During this shift, the interference lines on the observation screen move. In evaluation, either the interference maxima or interference minima passing a fixed point on the screen while the plane mirror is shifted are counted. For the wavelength λ, the following equation applies:

$$\lambda = 2 \cdot \frac{\Delta s}{Z}$$

Z: number of intensity maxima or minima counted
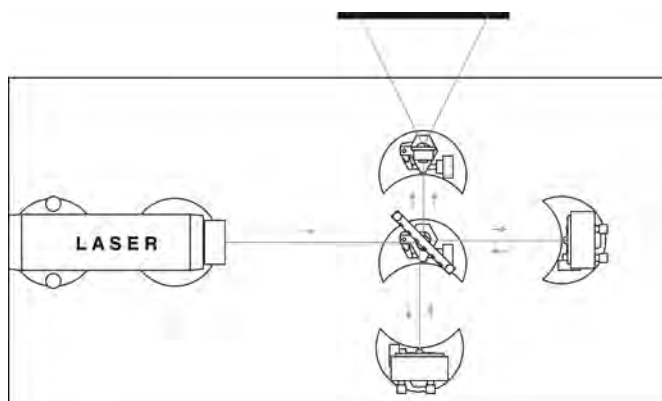
Setup of the Michelson interferometer (P5.3.4.1)

MICHELSON INTERFEROMETER

P5.3.4.3
Determining the wavelength of the light of an He-Ne laser using a Michelson interferometer - Set-up on the optical bench

P5.3.4.4
Determination of the coherence time and the line width of spectral lines with the Michelson interferometer

P5.3.4.5
Investigation of the pressure induced line broadening using a Michelson interferometer

P5.3.4.6
Determination of the line splitting of two spectral lines using a Michelson interferometer

Determination of the coherence time and the line width of spectral lines with the Michelson interferometer (P5.3.4.4)

Cat. No.	Description	P5.3.4.3	P5.3.4.4	P5.3.4.5	P5.3.4.6
471 830	He-Ne Laser, linearly polarised	1			
460 32	Optical bench with standardised profile, 1 m	1	1	1	1
460 373	Optics rider, 60/50	1	1	1	1
460 374	Optics rider, 90/50	5	7	7	7
471 88	Beam splitter	1	1	1	1
473 461	Planar mirror with fine adjustment	2	2	2	2
460 380	Cantilever arm	1	1	1	1
460 01	Lens in frame, f=5 mm	1			
473 48	Fine adjustment mechanism	1	1	1	1
441 53	Screen, translucent	1	1	1	1
300 11	Saddle base	1	1	1	1
311 02	Metal rule, 1 m	1			
451 062	Spectral lamp, Hg 100		1	1	1
451 16	Housing for spectral lamps		1	1	1
451 30	Universal choke, 230 V, 50 Hz		1	1	1
460 26	Iris diaphragm		2	2	2
468 07	Light filter, yellow-green		1	1	
460 22	Holder with spring clips		1	1	1
451 15	High pressure mercury lamp			1	
451 19	Lamp socket, E 27, multi-pin connector			1	
468 30	Light filter, yellow				1

Temporal coherence can be investigated by means of a Michelson interferometer. The maximum time difference Δt during which interference can be observed is called the coherence time. The coherence length is defined as the distance Δs_C the light travels in the coherence time. Typical coherence lengths are a few microns in incandescent lamps, some millimeters in spectral lamps and many meters in lasers. In addition, the coherence time Δt_C is connected to the spectral width $\Delta \nu$ or $\Delta \lambda$ of the light source:

$$\Delta \nu = \frac{1}{\Delta t_C} \quad \text{or} \quad \Delta \lambda = \frac{1}{c} \cdot \frac{\lambda_0^2}{\Delta t_C}$$

In the experiment P5.3.4.3, the Michelson interferometer is assembled on the optical bench. The wavelength of an He-Ne laser is determined from the change in the interference pattern when moving an interferometer mirror using the shifting distance Δs of the mirror.

In the experiment P5.3.4.4 the wavelength λ of the green spectral line of a Hg spectral lamp is determined. To measure the coherence length the positions of the movable plane mirror are measured where interference can barely be seen. From the difference in path length the coherence length Δs_C, the coherence time Δt_C and the line width $\Delta \nu$ of the spectral line are determined.

In experiment P5.3.4.5 the coherence lengths and spectral widths of the green spectral line of a Hg spectral lamp and a high pressure mercury lamp are determined and the results are compared. The higher pressure in the high pressure mercury lamp leads to a significant broadening of the spectral line causing a shorter coherence length.

In the experiment P5.3.4.6 the mean wavelength λ and the line splitting $\Delta \lambda$ of the yellow line doublet is determined. For two different proximate wavelengths λ_1 and λ_2 the coherent superposition of two beams leads to a beating: At distinct path length differences the contrast between bright and dark rings of the interference pattern is big while for other path length differences the contrast vanishes completely.

OTHER TYPES OF INTERFEROMETERS

P5.3.5.1
Setting up a Mach-Zehnder interferometer on the laser optics base plate

P5.3.5.2
Measuring the refractive index of air with a Mach-Zehnder interferometer

Measuring the refractive index of air with a Mach-Zehnder interferometer (P5.3.5.2)

Cat. No.	Description	P5.3.5.1	P5.3.5.2
473 40	Laser optics base plate	1	1
471 830	He-Ne Laser, linearly polarised	1	1
473 411	Laser mount	1	1
473 421	Optics base	5	6
473 431	Holder for beam divider	2	2
473 432	Beam divider, 50 %	2	2
473 461	Planar mirror with fine adjustment	2	2
473 471	Spherical lens, f = 2.7 mm	1	1
441 53	Screen, translucent	1	1
300 11	Saddle base	1	1
311 02	Metal rule, 1 m	1	1
473 485	Evacuable chamber		1
375 58	Hand vacuum pump		1
667 186	Vacuum rubber tubing, 8 mm diam.		1
604 520	Connector with nipple		1
300 02	Stand base, V-shaped, small		1
666 555	Universal clamp 0...80 mm		1

In a Mach-Zehnder interferometer, an optical element divides a coherent light beam into two parts. The component beams are deflected by mirrors and finally recombined. As the two partial beams have a fixed phase relationship with respect to each other, interference patterns can occur when they are superposed on each other. A change in the optical path length of one component beam alters the phase relation, and consequently the interference pattern as well. As the component beams are not reflected into each other, but rather travel separate paths, these experiments are easier to comprehend and didactically more effective than experiments with the Michelson interferometer. However, the Mach-Zehnder interferometer is more difficult to adjust.

In the experiment P5.3.5.1, the Mach-Zehnder interferometer is assembled on the vibration-proof laser optics base plate.

In the experiment P5.3.5.2, the refractive index of air is determined. To achieve this, an evacuable chamber is placed in the path of one component beam of the Mach-Zehnder interferometer. Slowly evacuating the chamber alters the optical path length of the respective component beam.
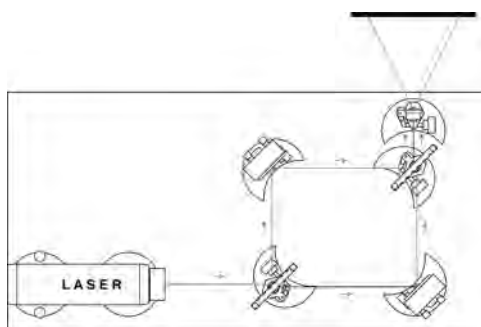
Setting up a Mach-Zehnder interferometer on the laser optics base plate (P5.3.5.1)

OTHER TYPES OF INTERFEROMETERS

P5.3.5.3
Determining the wavelength of the light of an He-Ne laser using a Fabry-Perot interferometer

Determining the wavelength of the light of an He-Ne laser using a Fabry-Perot interferometer (P5.3.5.3)

Cat. No.	Description	P5.3.5.3
473 40	Laser optics base plate	1
471 830	He-Ne Laser, linearly polarised	1
473 411	Laser mount	1
473 421	Optics base	5
473 432	Beam divider, 50 %	2
473 431	Holder for beam divider	2
473 461	Planar mirror with fine adjustment	1
473 48	Fine adjustment mechanism	1
473 471	Spherical lens, f = 2.7 mm	1
441 53	Screen, translucent	1
300 11	Saddle base	1
311 02	Metal rule, 1 m	1

Besides the Michelson and Mach-Zender interferometers, more geometries can be used to split a light beam in two parts and let them overlap afterwards. One with particular practical use is the Fabry-Perot interferometer.

In the experiment P5.3.5.3 the mirrors on the laser base plate are arranged to set up a Fabry-Perot interferometer with two parallel mirrors in line. The first semi-transparent mirror splits the light beam, while the second fully reflective mirror reflects the light back to overlap with the first reflected beam. Moving the second mirror will change the length of the resonator, thus changing the interference pattern and enables the measurement of the laser wavelength.

WHITE-LIGHT REFLECTION HOLOGRAPHY

P5.3.6.1
Creating white-light reflection holograms on the laser optics base plate

Creating white-light reflection holograms on the laser optics base plate (P5.3.6.1)

Cat. No.	Description	P5.3.6.1
473 40	Laser optics base plate	1
471 830	He-Ne Laser, linearly polarised	1
473 411	Laser mount	1
473 421	Optics base	3
473 441	Film holder	1
473 451	Object holder	1
473 471	Spherical lens, f = 2.7 mm	1
311 02	Metal rule, 1 m	1
663 615	Socket strip for earthed plugs, 5-way	1
313 27	Hand-held stop-watch, 60s/0.2s	1
649 11	Storage trays, 86 x 86 x 26, set of 6	1
661 234	Polyethylene bottle	3
667 016	Scissors, 200 mm, pointed	1
473 448	Holography film, 3000 lines/mm	1
473 446	Darkroom accessories	1
473 444	Photographic chemicals	1
671 8910	Iron(III) nitrate-9-hydrate, 250 g	1
672 4910	Potassium bromide, 100 g	1

In creating white-light reflection holograms, a broadened laser beam passes through a film and illuminates an object placed behind the film. Light is reflected from the surface of the object back onto the film, where it is superposed with the light waves of the original laser beam. The film consists of a light sensitive emulsion of sufficient thickness. Interference creates standing waves within the film, i.e. a series of numerous nodes and antinodes at a distance of $\lambda/4$ apart. The film is exposed in the planes of the anti-nodes but not in the nodes. Semitransparent layers of metallic silver are formed at the exposed areas. To reconstruct the image, the finished hologram is illuminated with white light – the laser is not required. The light waves reflected by the semitransparent layers are superposed on each other in such a way that they have the same properties as the waves originally reflected by the object. The observer sees at three-dimensional image of the object. Light beams originating at different layers only reinforce each other when they are in phase. The in-phase condition is only fulfilled for a certain wavelength, which allows the image to be reconstructed using white light.

The object of the experiment P5.3.6.1 is to create white-light reflection holograms. This process uses a protection class 2 laser, so as to minimize the risk of eye damage for the experimenter. Both amplitude and phase holograms can be created simply by varying the photochemical processing of the exposed film.
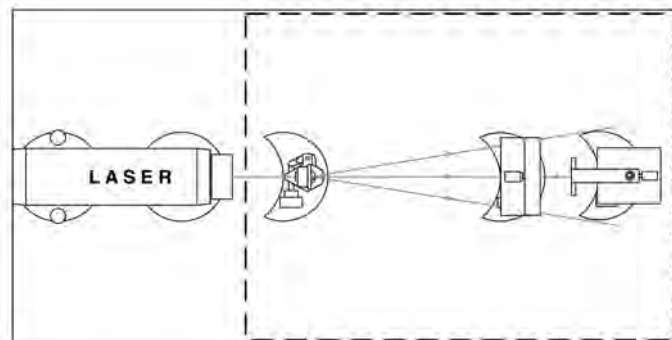
Experiment setup for creating white-light reflection holograms (P5.3.6.1)

Creating transmission holograms on the laser optics base plate (P5.3.7.1)

TRANSMISSION HOLOGRAPHY

P5.3.7.1
Creating transmission holograms on the laser optics base plate

Cat. No.	Description	P5.3.7.1
473 40	Laser optics base plate	1
471 830	He-Ne Laser, linearly polarised	1
473 411	Laser mount	1
473 421	Optics base	5
473 432	Beam divider, 50 %	1
473 431	Holder for beam divider	1
473 441	Film holder	1
473 451	Object holder	1
473 471	Spherical lens, f = 2.7 mm	2
311 02	Metal rule, 1 m	1
663 615	Socket strip for earthed plugs, 5-way	1
313 27	Hand-held stop-watch, 60s/0.2s	1
649 11	Storage trays, 86 x 86 x 26, set of 6	1
661 234	Polyethylene bottle	3
667 016	Scissors, 200 mm, pointed	1
473 448	Holography film, 3000 lines/mm	1
473 446	Darkroom accessories	1
473 444	Photographic chemicals	1
671 8910	Iron(III) nitrate-9-hydrate, 250 g	1
672 4910	Potassium bromide, 100 g	1

In creating transmission holograms, a laser beam is split into an object beam and a reference beam, and then broadened. The object beam illuminates an object and is reflected. The reflected light is focused onto a film together with the reference beam, which is coherent with the object beam. The film records an irregular interference pattern which shows no apparent similarity with the object in question. To reconstruct the hologram, a light beam which corresponds to the reference beam is diffracted at the amplitude hologram in such a way that the diffracted waves are practically identical to the object waves. In reconstructing a phase hologram the phase shift of the reference waves is exploited. In both cases, the observer sees a three-dimensional image of the object.

The object of the experiment P5.3.7.1 is to create transmission holograms and subsequently reconstruct them. This process uses a protection class 2 laser, so as to minimize the risk of eye damage for the experimenter. Both amplitude and phase holograms can be created simply by varying the photochemical processing of the exposed film.
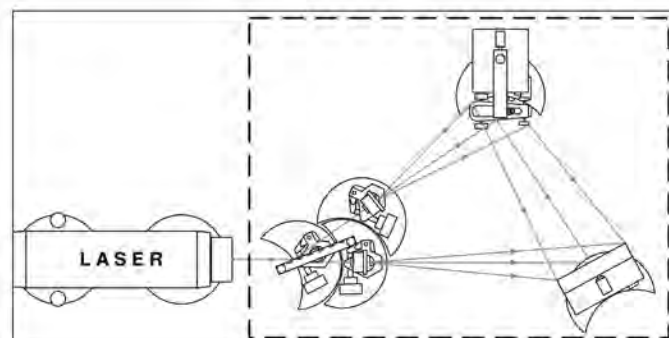
Experiment setup for creating transmission holograms (P5.3.7.1)

BASIC EXPERIMENTS

P5.4.1.1
Polarization of light through reflection at a glass plate

P5.4.1.2
Fresnel's laws of reflection

P5.4.1.3
Polarization of light through scattering in an emulsion

P5.4.1.4
Malus' law

Fresnel's laws of reflection (P5.4.1.2)

The fact that light can be polarized is important evidence of the transversal nature of light waves. Natural light is unpolarized. It consists of mutually independent, unordered waves, each of which has a specific polarization state. Polarization of light is the selection of waves having a specific polarization state.

In the experiment P5.4.1.1, unpolarized light is reflected at a glass surface. When we view this through an analyzer, we see that the reflected light as at least partially polarized. The greatest polarization is observed when reflection occurs at the polarizing angle (Brewster angle) α_p. The relationship

$$\tan\alpha_p = n$$

gives us the refractive index n of the glass.

Closer observation leads to Fresnel's laws of reflection, which describe the ratio of reflected to incident amplitude for different directions of polarization. These laws are quantitatively verified in the experiment P5.4.1.2.

The experiment P5.4.1.3 demonstrates that unpolarized light can also be polarized through scattering in an emulsion, e. g. diluted milk, and that polarized light is not scattered uniformly in all directions.

The aim of the experiment P5.4.1.4 is to derive Malus's law: when linearly polarized light falls on an analyzer, the intensity of the transmitted light is

$$I = I_0 \cdot \cos^2 \varphi$$

I_0: intensity of incident light

φ: angle between direction of polarization and analyzer

Cat. No.	Description	P5.4.1.1	P5.4.1.2	P5.4.1.3	P5.4.1.4
477 33	Cuvette made of optical glass 45 x 12,5 x 102,5 mm	1	1	1	
460 25	Prism table	1	1	1	
450 641	Halogen lamp 12 V, 50/100W	1	1		1
450 63	Halogen bulb 12 V/100 W, G6.35	1	1		1
450 66	Picture slider	1	1		1
726 890	DC-High Current Power Supply 1...32 V/0...20 A	1	1		1
460 26	Iris diaphragm	1	1	1	1
472 401	Polarisation filter	2	2	2	2
460 03	Lens in frame, f=100 mm	1	1		1
441 53	Screen, translucent	1			
460 317	Optical bench, S1 profile, 0.5 m	2	2		
460 3151	Swivel joint with protactor scale and clamp	1	1		
460 311	Clamp rider with clamp 45/65	2	1	1	1
460 312	Clamp rider with clamp 45/35	4	6	5	5
500 624	Safety connecting lead 50 cm, black	2	2		2
460 08	Lens in frame, f=150 mm		1		
578 62	Solar cell, STE 2/19		1		1
460 21	Holder for plug-in elements		1		1
531 183	Digital multimeter 3340		1		1
500 98	Safety adapter sockets, black, set of 6		1		1
500 621	Safety connecting lead 50 cm, red		1		1
500 622	Safety connecting lead 50 cm, blue		1		1
450 60	Lamp housing with cable			1	
450 511	Bulbs, 6 V/30 W, E14, set of 2			1	
460 20	Condenser with diaphragm holder			1	
521 210	Transformer 6/12 V			1	
460 04	Lens in frame, f=200 mm			1	
460 310	Optical bench, S1 profile, 1 m			1	1

Fresnel's laws of reflection (P5.4.1.2)

BIREFRINGENCE

P5.4.2.1
Birefringence and polarization with calcareous spar

P5.4.2.2
Quarter-wavelength and half-wavelength plate

P5.4.2.3
Photoelasticity: Investigating the distribution of strains in mechanically stressed bodies

Quarter-wavelength and half-wavelength plate (P5.4.2.2)

Cat. No.	Description	P5.4.2.1	P5.4.2.2	P5.4.2.3
472 02	Calcite crystal, birefringent	1		
460 25	Prism table	1		1
460 26	Iris diaphragm	1		1
472 401	Polarisation filter	1	2	2
460 02	Lens in frame, f=50 mm	1		
460 06	Lens in frame, f=-100 mm	1		
441 53	Screen, translucent	1	1	1
460 310	Optical bench, S1 profile, 1 m	1	1	1
460 311	Clamp rider with clamp 45/65	2	2	1
460 312	Clamp rider with clamp 45/35	5	5	8
450 641	Halogen lamp 12 V, 50/100W	1	1	1
450 63	Halogen bulb 12 V/100 W, G6.35	1	1	1
450 66	Picture slider	1	1	1
726 890	DC-High Current Power Supply 1...32 V/0...20 A	1	1	1
500 624	Safety connecting lead 50 cm, black	2	2	2
472 601	Quarter-wavelength plate, 140 nm		2	2
472 59	Half-wavelength plate		1	
468 30	Light filter, yellow		1	
578 62	Solar cell, STE 2/19		1	
460 21	Holder for plug-in elements		1	
531 183	Digital multimeter 3340		1	
500 98	Safety adapter sockets, black, set of 6		1	
500 621	Safety connecting lead 50 cm, red		1	
500 622	Safety connecting lead 50 cm, blue		1	
471 95	Photoelastic models, set of 4			1
460 08	Lens in frame, f=150 mm			2
300 11	Saddle base			1

The validity of Snell's law of refraction is based on the premise that light propagates in the refracting medium at the same velocity in all directions. In birefringent media, this condition is only fulfilled for the ordinary component of the light beam (the ordinary ray); the law of refraction does not apply for the extraordinary ray.

The experiment P5.4.2.1 looks at birefringence of calcite (Iceland spar). We can observe that the two component rays formed in the crystal are linearly polarized, and that the directions of polarization are perpendicular to each other.

The experiment P5.4.2.2 investigates the properties of $\lambda/4$ and $\lambda/2$ plates and explains these in terms of their birefringence; it further demonstrates that the names for these plates refer to the path difference between the ordinary and the extraordinary rays through the plates.

In the experiment P5.4.2.3, the magnitude and direction of mechanical stresses in transparent plastic models are determined. The plastic models become optically birefringent when subjected to mechanical stress. Thus, the stresses in the models can be revealed using polarization-optical methods. For example, the plastic models are illuminated in a setup consisting of a polarizer and analyzer arranged at right angles. The stressed points in the plastic models polarize the light elliptically. Thus, the stressed points appear as bright spots in the field of view. In another configuration, the plastic models are illuminated with circularly polarized light and observed using a quarter-wavelength plate and an analyzer. Here too, the stressed points appear as bright spots in the field of view.
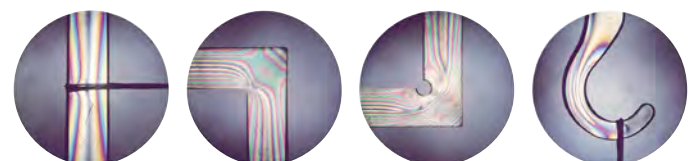
Photoelasticity: Investigating the distribution of strains in mechanically stressed bodies (P5.4.2.3)

OPTICAL ACTIVITY, POLARIMETRY

P5.4.3.1
Rotation of the plane of polarization with quartz

P5.4.3.2
Rotation of the plane of polarization with sugar solutions

P5.4.3.3
Building a half-shadow polarimeter with discrete elements

P5.4.3.4
Determining the concentration of sugar solutions with a standard commercial polarimeter

Rotation of the plane of polarization with sugar solutions (P5.4.3.2)

Cat. No.	Description	P5.4.3.1	P5.4.3.2	P5.4.3.3	P5.4.3.4
472 621	Quartz, parallel	1			
472 641	Quartz, right-handed	1			
472 651	Quartz, left-handed	1			
460 22	Holder with spring clips	1		1	
450 641	Halogen lamp 12 V, 50/100W	1	1	1	
450 63	Halogen bulb 12 V/100 W, G6.35	1	1	1	
450 66	Picture slider	1	1	1	
726 890	DC-High Current Power Supply 1...32 V/0...20 A	1	1	1	
468 30	Light filter, yellow	1		1	
472 401	Polarisation filter	2	2	2	
460 03	Lens in frame, f=100 mm	1	1	1	
441 53	Screen, translucent	1	1	1	
460 310	Optical bench, S1 profile, 1 m	1	1	1	
460 311	Clamp rider with clamp 45/65	2	2	2	
460 312	Clamp rider with clamp 45/35	4	4	5	
500 624	Safety connecting lead 50 cm, black	2	2	2	
477 33	Cuvette made of optical glass 45 x 12,5 x 102,5 mm		1		
460 25	Prism table		1	1	
468 03	Light filter, red		1		
468 07	Light filter, yellow-green		1		
468 11	Light filter, blue with violet		1		
666 963	Spoon-ended spatula, stainless steel, 120 mm		1	1	1
674 6050	D(+)-Sucrose, 100 g		1	1	1
688 107	Polarizing foils 38 mm Ø, set of 2			1	
688 109	Set of 100 slides cover slip 5 x 5 cm			1	
477 31	Cuvette made of optical glass 40 x 20 x 104 mm			1	
657 591	Polarimeter				1
664 111	Beaker, DURAN, 100 ml, tall				1
OHC R221	Compact Balance CR221, 220 g : 0.1 g				1

Optical activity is the property of some substances of rotating the plane of linearly polarized light as it passes through the material. The angle of optical rotation is measured using a device called a polarimeter.

The experiment P5.4.3.1 studies the optical activity of crystals, in this case a quartz crystal. Depending on the direction of intersection with respect to the optical axis, the quartz rotates the light clockwise ("right-handed") or counter-clockwise ("left-handed"). The angle of optical rotation is strongly dependent on the wavelength of the light; therefore a yellow filter is used.

The experiment P5.4.3.2 investigates the optical activity of a sugar solution. For a given cuvette length d, the angles of optical rotation α of optically active solutions are proportional to the concentration c of the solution.

$$\alpha = [\alpha] \cdot c \cdot d$$

$[\alpha]$: rotational effect of the optically active solution

The object of the experiment P5.4.3.3 is to assemble a half-shadow polarimeter from discrete components. The two main elements are a polarizer and an analyzer, between which the optically active substance is placed. Half the field of view is covered by an additional, polarizing foil, of which the direction of polarization is rotated slightly with respect to the first. This facilitates measuring the angle of optical rotation.

In the experiment P5.4.3.4, the concentrations of sugar solutions are measured using a standard commercial polarimeter and compared with the values determined by weighing.

Determining the concentration of sugar solutions with a standard commercial polarimeter (P5.4.3.4)

Investigating the Kerr effect in nitrobenzene (P5.4.4.1)

KERR EFFECT

P5.4.4.1
Investigating the Kerr effect in nitrobenzene

Cat. No.	Description	P5.4.4.1
473 31	Kerr cell	1
450 641	Halogen lamp 12 V, 50/100W	1
450 63	Halogen bulb 12 V/100 W, G6.35	1
450 66	Picture slider	1
468 03	Light filter, red	1
468 05	Light filter, yellow	1
468 07	Light filter, yellow-green	1
468 11	Light filter, blue with violet	1
472 401	Polarisation filter	2
460 03	Lens in frame, f=100 mm	1
460 25	Prism table	1
441 53	Screen, translucent	1
460 32	Optical bench with standardised profile, 1 m	1
460 373	Optics rider, 60/50	6
726 890	DC-High Current Power Supply 1...32 V/0...20 A	1
521 70	High-voltage power supply, 10 kV	1
501 051	Cable for high voltages, 1.5 m	2
500 624	Safety connecting lead 50 cm, black	2
673 9410	Nitrobenzene, 250 ml	1

In 1875, *J. Kerr* discovered that electrical fields cause birefringence in isotropic substances. The birefringence increases quadratically with the electric field strength. For reasons of symmetry, the optical axis of birefringence lies in the direction of the electric field. The normal refractive index of the substance is changed to n_e for the direction of oscillation parallel to the applied field, and to n_o for the direction of oscillation perpendicular to it. The experiment results in the relationship

$$n_e - n_o = K \cdot \lambda \cdot E^2$$

K: Kerr constant

λ: wavelength of light used

E: electic field strength

The experiment P5.4.4.1 demonstrates the Kerr effect for nitrobenzol, as the Kerr constant is particularly great for this material. The liquid is filled into a small glass vessel in which a suitable plate capacitor is mounted. The arrangement is placed between two polarization filters arranged at right angles, and illuminated with a linearly polarized light beam. The field of view is dark when no electric field is applied. When an electric field is applied, the field of view brightens, as the light beam gets elliptically polarized when passing through the birefringent liquid.

POCKELS EFFECT

P5.4.5.1
Demonstrating the Pockels effect in a conoscopic beam path

P5.4.5.2
Pockels effect: transmitting information using modulated light

Demonstrating the Pockels effect in a conoscopic beam path (P5.4.5.1)

Cat. No.	Description	P5.4.5.1	P5.4.5.2
472 90	Pockels cell	1	1
521 70	High-voltage power supply, 10 kV	1	1
471 830	He-Ne Laser, linearly polarised	1	1
460 01	Lens in frame, f=5 mm	1	
460 02	Lens in frame, f=50 mm	1	
472 401	Polarisation filter	1	1
460 32	Optical bench with standardised profile, 1 m	1	1
460 370	Optics rider, 60/34	5	4
441 53	Screen, translucent	1	
300 11	Saddle base	1	1
500 604	Safety connecting lead, 10 cm, black	1	
500 641	Safety connecting lead, 100 cm, red	1	3
500 642	Safety connecting lead, 100 cm, blue	1	3
522 621	Function generator S 12		1
578 62	Solar cell, STE 2/19		1
460 21	Holder for plug-in elements		1
532 20	AC/DC amplifier 30 W		1
587 08	Broad-band speaker		1
500 98	Safety adapter sockets, black, set of 6		1
500 622	Safety connecting lead 50 cm, blue		2

The occurrence of birefringence and the alteration of existing birefringence in an electrical field as a linear function of the electric field strength is known as the Pockels effect. In terms of the visible phenomena, it is related to the Kerr effect. However, due to its linear dependency on the electric field strength, the Pockels effect can only occur in crystals without an inversion center, for reasons of symmetry.

The experiment P5.4.5.1 demonstrates the Pockels effect in a lithium niobate crystal placed in a conoscopic beam path. The crystal is illuminated with a divergent, linearly polarized light beam, and the transmitted light is viewed behind a perpendicular analyzer. The optical axis of the crystal, which is birefringent even when no electric field is applied, is parallel to the incident and exit surfaces; as a result, the interference pattern consists of two sets of hyperbolas which are rotated 90° with respect to each other. The bright lines of the interference pattern are due to light rays for which the difference Δ between the optical paths of the extraordinary and ordinary rays is an integral multiple of the wavelength λ. The Pockels effect alters the difference of the main refractive indices, $n_o - n_e$, and consequently the position of the interference lines. When the so-called half-wave voltage U_l is applied, Δ changes by one half wavelength. The dark interference lines move to the position of the bright lines, and vice versa. The process is repeated each time the voltage is increased by U_λ.

The experiment P5.4.5.2 shows how the Pockels cell can be used to transmit audio-frequency signals. The output signal of a function generator with an amplitude of several volts is superposed on a DC voltage which is applied to the crystal of the Pockels cell. The intensity of the light transmitted by the Pockels cell is modulated by the superposed frequency. The received signal is output to a speaker via an amplifier and thus made audible.

Faraday effect: determining Verdet's constant for flint glass as a function of the wavelength (P5.4.6.1)

FARADAY EFFECT

P5.4.6.1
Faraday effect: determining Verdet's constant for flint glass as a function of the wavelength

Cat. No.	Description	P5.4.6.1
560 482	Flint glass block with holder	1
460 381	Rider base with thread	1
562 11	U-core with yoke	1
560 31	Bored pole pieces, pair	1
562 13	Coil, 250 turns	2
450 641	Halogen lamp 12 V, 50/100W	1
450 63	Halogen bulb 12 V/100 W, G6.35	1
450 66	Picture slider	1
468 05	Light filter, yellow	1
468 09	Light filter, blue-green	1
468 11	Light filter, blue with violet	1
468 13	Light filter, violet	1
460 02	Lens in frame, f=50 mm	1
472 401	Polarisation filter	2
441 53	Screen, translucent	1
460 32	Optical bench with standardised profile, 1 m	1
460 373	Optics rider, 60/50	5
521 551	AC/DC power supply 0...24 V/0...10 A	1
726 890	DC-High Current Power Supply 1...32 V/0...20 A	1
524 005W	Mobile-CASSY 2 WiFi	1
524 0381	Combi B sensor S	1
501 11	Extension cable, 15 pin	1
300 02	Stand base, V-shaped, small	1
300 41	Stand rod, 25 cm, 12 mm Ø	1
301 01	Leybold multiclamp	1
500 622	Safety connecting lead 50 cm, blue	1
500 624	Safety connecting lead 50 cm, black	2
500 641	Safety connecting lead, 100 cm, red	1
500 642	Safety connecting lead, 100 cm, blue	1

Transparent isotropic materials become optically active in a magnetic field; in other words, the plane of polarization of linearly polarized light rotates when passing through the material. *M. Faraday* discovered this effect in 1845 while seeking a relationship between magnetic and optical phenomena. The angle of optical rotation of the plane of polarization is proportional to the illuminated length s and the magnetic field B.

$$\Delta\varphi = V \cdot B \cdot s$$

The proportionality constant V is known as Verdet's constant, and depends on the wavelength λ of the light and the dispersion.

$$V = \frac{e}{2mc^2} \cdot \lambda \cdot \frac{dn}{d\lambda}$$

For flint glass, the following equation approximately obtains:

$$\frac{dn}{d\lambda} = \frac{1{,}8 \cdot 10^{-14} \mathrm{m}^2}{\lambda^3}$$

In the experiment P5.4.6.1, the magnetic field is initially calibrated with reference to the current through the electromagnets using a magnetic field probe, and then the Faraday effect in a flint glass square is investigated. To improve measuring accuracy, the magnetic field is reversed each time and twice the angle of optical rotation is measured. The proportionality between the angle of optical rotation and the magnetic field and the decrease of Verdet's constant with the wavelength λ are verified.

CASSY®

QUANTITIES AND MEASURING METHODS OF LIGHTING ENGINEERING

P5.5.1.1
Determining the radiant flux density and the luminous intensity of a halogen lamp

P5.5.1.2
Determining the luminous intensity as a function of the distance from the light source – Measuring with Mobile-CASSY

P5.5.1.3
Verifying Lambert's law of radiation

Verifying Lambert's law of radiation (P5.5.1.3)

Cat. No.	Description	P5.5.1.1	P5.5.1.2	P5.5.1.3
450 641	Halogen lamp 12 V, 50/100W	1		1
450 63	Halogen bulb 12 V/100 W, G6.35	1		1
450 66	Picture slider	1		
468 03	Light filter, red	1		
726 890	DC-High Current Power Supply 1...32 V/0...20 A	1		1
524 005W	Mobile-CASSY 2 WiFi	1	1	1
557 36	Moll's thermopile	1		1
524 0401	µV sensor S	1		1
524 444	Lux Sensor M	1	1	
460 03	Lens in frame, f=100 mm	1		1
460 22	Holder with spring clips	1	1	1
460 310	Optical bench, S1 profile, 1 m	1	1	
460 311	Clamp rider with clamp 45/65	1	1	1
460 3112	Clamp rider with clamp 75/65	1		1
500 98	Safety adapter sockets, black, set of 6	1		1
500 624	Safety connecting lead 50 cm, black	2		2
500 641	Safety connecting lead, 100 cm, red	1		1
500 642	Safety connecting lead, 100 cm, blue	1		1
450 60	Lamp housing with cable		1	
450 511	Bulbs, 6 V/30 W, E14, set of 2		1	
521 210	Transformer 6/12 V		1	
460 312	Clamp rider with clamp 45/35		1	2
450 681	Halogen bulb 12 V/50 W, G6.35			1
460 26	Iris diaphragm			1
460 317	Optical bench, S1 profile, 0.5 m			2
460 3151	Swivel joint with protactor scale and clamp			1

There are two types of physical quantities used to characterize the brightness of light sources: quantities which refer to the physics of radiation, which describe the energy radiation in terms of measurements, and quantities related to lighting engineering, which describe the subjectively perceived brightness under consideration of the spectral sensitivity of the human eye. The first group includes the irradiance E_e, which is the radiated power per unit of area Φ_e. The corresponding unit of measure is watts per square meter. The comparable quantity in lighting engineering is illuminance E, i. e. the emitted luminous flux per unit of area Φ, and it is measured in lumens per square meter, or lux for short.

In the experiment P5.5.1.1, the irradiance is measured using the Moll's thermopile, and the luminous flux is measured using a luxmeter. The luxmeter is matched to the spectral sensitivity of the human eye $V(\lambda)$ by means of a filter placed in front of the photoelement. A halogen lamp serves as the light source. From its spectrum, most of the visible light is screened out using a color filter; subsequently, a heat filter is used to absorb the infrared component of the radiation

The experiment P5.5.1.2 demonstrates that the luminous intensity is proportional to the square of the distance between a point-type light source and the illuminated surface

The aim of the experiment P5.5.1.3 is to investigate the angular distribution of the reflected radiation from a diffusely reflecting surface, e.g. matte white paper. To the observer, the surface appears uniformly bright; however, the apparent surface area varies with the cosine of the viewing angle. The dependency of the luminous intensity is described by Lambert's law of radiation:

$$E_e(\phi) = E_e(0) \cdot \cos\phi$$

Determining the luminous intensity as a function of the distance from the light source - Measuring with Mobile-CASSY (P5.5.1.2)

CASSY®

LAWS OF RADIATION

P5.5.2.1
Stefan-Boltzmann law: measuring the radiant intensity of a „black body" as a function of temperature

P5.5.2.2
Stefan-Boltzmann law: measuring the radiant intensity of a „black body" as a function of temperature - Recording and evaluating with CASSY

P5.5.2.3
Confirming the laws of radiation with Leslie's cube

Stefan-Boltzmann law: measuring the radiant intensity of a „black body" as a function of temperature (P5.5.2.1)

Cat. No.	Description	P5.5.2.1	P5.5.2.2	P5.5.2.3
555 81	Electric oven for tubes, 230 V	1	1	
389 43	Black body accessory	1	1	
502 061	Safety connecting box, with earth	1	1	
555 84	Support for electric oven	1	1	1
524 005W	Mobile-CASSY 2 WiFi	1		1
529 676	Temperature probe, NiCr-Ni, 1.5 mm, type K	1	1	1
524 0401	µV sensor S	1	1	1
557 36	Moll's thermopile	1	1	1
460 310	Optical bench, S1 profile, 1 m	1	1	1
460 311	Clamp rider with clamp 45/65	2	2	
460 3113	Clamp rider with clamp 105/65	2	2	2
460 380	Cantilever arm	1	1	
666 555	Universal clamp 0...80 mm	1	1	
500 98	Safety adapter sockets, black, set of 6	1	1	1
500 641	Safety connecting lead, 100 cm, red	1	1	1
500 642	Safety connecting lead, 100 cm, blue	1	1	1
388 181	Immersion pump	1*	1*	
521 231	Low-voltage power supply 3/6/9/12 V	1*	1*	
667 194	Silicone tubing 7 mm Ø, 1 m	1*	1*	
604 3131	Wide-mouthed can 10 l	1*	1*	
524 013	Sensor-CASSY 2		1	
524 220	CASSY Lab 2		1	
524 0673	NiCr-Ni adapter S, type K		1	
389 261	Leslie's cube with stirrer			1
301 01	Leybold multiclamp			1
303 25	Immersion heater			1
664 117	Beaker, DURAN, 1000 ml, tall			1
665 009	Funnel PP 75 mm Ø			1
	additionally required: PC with Windows XP/Vista/7/8/10 (x86 or x64)		1	

* additionally recommended

The total radiated power M_B of a black body increases in proportion to the fourth power of its absolute temperature T (Stefan-Boltzmann's law).

$$M_B = \sigma \cdot T^4$$

$\sigma = 5.67 \cdot 10^{-8}$ W m^{-2} K^{-4}: (Stefan-Boltzmann's constant)

For all other bodies, the radiated power M is less than that of the black body, and depends on the properties of the surface of the body. The emittance of the body is described by the relationship

$$\varepsilon = \frac{M}{M_B}$$

M: radiated power of body

In the two experiments P5.5.2.1 and P5.5.2.2, a cylindrical electric oven with a burnished brass cylinder is used as a "black body". The brass cylinder is heated in the oven to the desired temperature between 300 and 750 K. A thermocouple is used to measure the temperature. A water-coolable screen is positioned in front of the oven to ensure that the setup essentially measures only the temperature of the burnished brass cylinder. The measurement is conducted using a Moll's thermopile; its output voltage provides a relative measure of the radiated power M. The thermopile can be connected via the µV sensor, either to Mobile-CASSY or to the CASSY computer interface device. In the former case, the measurement must by carried out manually, point by point; the latter configuration enables computer-assisted measuring and evaluation. The aim of the evaluation is to confirm Stefan-Boltzmann's law.

The experiment P5.5.2.3 uses a radiation cube according to Leslie ("Leslie's cube"). This cube has four different face surfaces (metallic matte, metallic shiny, black finish and white finish), which can be heated from the inside to almost 100 °C by filling the cube with boiling water. The heat radiated by each of the surfaces is measured as a function of the falling temperature. The aim of the evaluation is to compare the emittances of the cube faces.
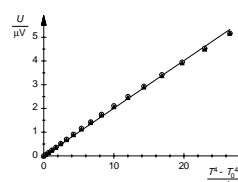
Stefan-Boltzmann law: measuring the radiant intensity of a "black body" as a function of temperature (P5.5.2.1)

LAWS OF RADIATION

P5.5.2.4
The Wien's displacement law –
spectral recording of the
black body radiation
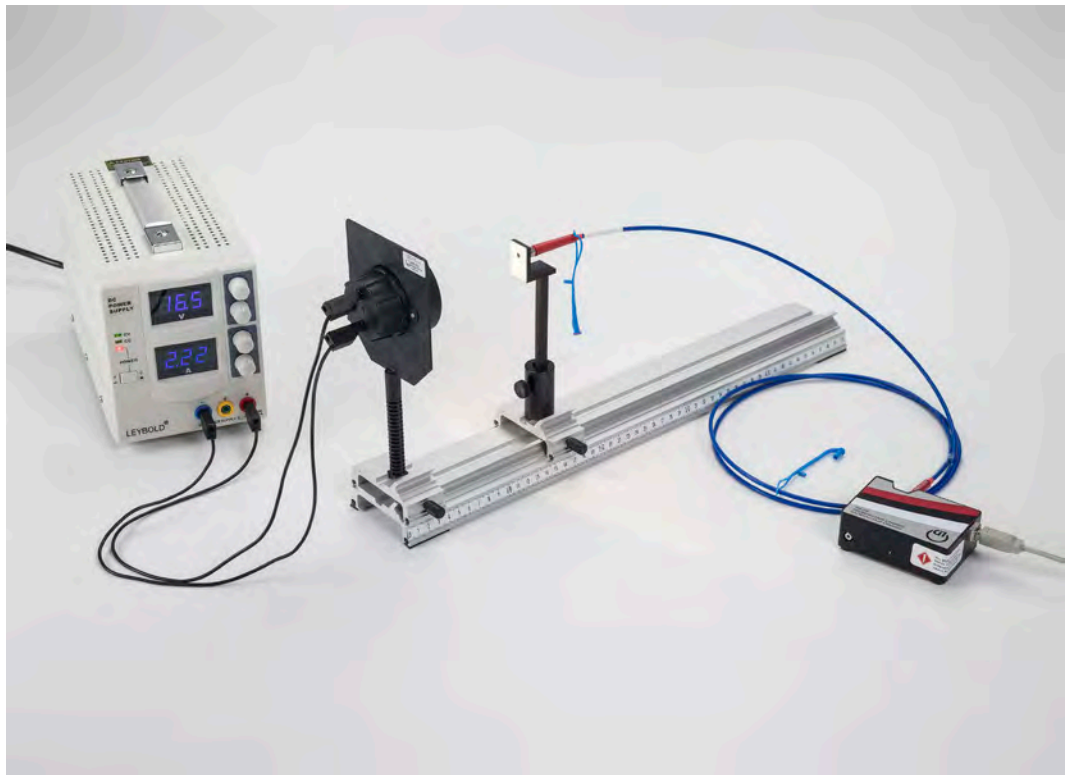
The Wien's displacement law – spectral recording of the black body radiation (P5.5.2.4)

Cat. No.	Description	P5.5.2.4
467 251	Compact spectrometer, physics (spectral photometer)	1
460 251	Fibre holder	1
459 032	Halogen lamp,12 V/20 W	1
521 546	DC Power Supply 0...16 V/0...5 A	1
460 317	Optical bench, S1 profile, 0.5 m	1
460 311	Clamp rider with clamp 45/65	1
460 313	Clamp rider with fixing column	1
501 451	Connecting leads, 19 A, 50 cm, black, pair	1
	additionally required: PC with Windows XP/Vista/7/8/10 (x86 or x64)	1

In the experiment P5.5.2.4 an incandescent lamp, an electric conductor is heated by an electric current causing it to glow. The emitted spectrum is continuous and can be described with Planck's radiation formula. The radiation maximum of the radiation shifts with increasing temperature T according to Wien's displacement law

$$\lambda_{max} = 2.9 \cdot 10^{-3} \text{ m·K} / T$$

toward smaller wavelengths; at the same time the maximum value of the radiation increases. At the temperatures attained by normal incandescent lamps, about 2300 to 2900 K, the radiation maximum lies in the infrared spectral range. Halogen lamps reach a somewhat higher operating temperature of about 3000 K.

This experiment will record the spectra of a halogen lamp at different power levels. The specification for color temperature at 12 V nominal voltage allows the wavelength dependency of spectrometer sensitivity to be determined and thus permits a corrected display for the course of spectra intensity. Subsequently voltage will be applied to a halogen lamp then reduced in steps. The lamp's color temperature at each voltage step will be determined by adapting a suitable fit function.
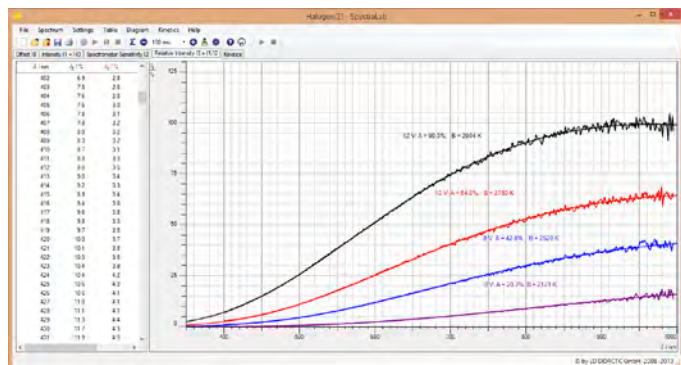
Spectral emission of a light bulb at different temperatures (P5.5.2.4)

MEASUREMENT ACCORDING TO FOUCAULT/MICHELSON

P5.6.1.1
Determining the velocity of light by means of the rotating-mirror method according to Foucault and Michelson - Measuring the image shift as a function of the rotational speed of the mirror

Determining the velocity of light by means of the rotating-mirror method according to Foucault and Michelson - Measuring the image shift as a function of the rotational speed of the mirror (P5.6.1.1)

Cat. No.	Description	P5.6.1.1
476 40	Rotary mirror	1
471 830	He-Ne Laser, linearly polarised	1
463 20	Front-silvered mirror	1
460 12	Lens in frame, f=5 m	1
471 88	Beam splitter	1
460 22	Holder with spring clips	1
311 091	Glass scale 50 mm	1
521 40	Variable transformer, 0...250 V	1
575 302	Oscilloscope 30 MHz, digital, PT1265	1
559 921	Semiconductor detector	1
501 02	BNC cable, 1 m	1
501 10	BNC adapter, straight	1
300 41	Stand rod, 25 cm, 12 mm Ø	1
300 42	Stand rod, 47 cm, 12 mm diam.	1
300 44	Stand rod, 100 cm, 12 mm diam.	1
300 01	Stand base, V-shaped, large	1
300 02	Stand base, V-shaped, small	4
300 11	Saddle base	1
301 01	Leybold multiclamp	2
301 09	Bosshead S	1
311 02	Metal rule, 1 m	1

Measurement of the velocity of light by means of the rotary mirror method utilizes a concept first proposed by *L. Foucault* in 1850 and perfected by *A. A. Michelson* in 1878. In the variation utilized here, a laser beam is deviated into a fixed end mirror located next to the light source via a rotating mirror. The end mirror reflects the light so that it returns along the same path when the rotary mirror is at rest. Part of the returning light is imaged on a scale using a beam divider. A lens images the light source on the end mirror and focuses the image of the light source from the mirror on the scale. The main beam between the lens and the end mirror is parallel to the axis of the lens, as the rotary mirror is set up in the focal point of the lens.

Once the rotary mirror is turning at a high frequency ν, the shift Δx of the image on the scale is observed. In the period

$$\Delta t = \frac{2a}{c}$$

which the light requires to travel to the rotary mirror and back to the end mirror, the rotary mirror turns by the angle

$$\Delta\alpha = 2\pi v \cdot \Delta t$$

Thus, the image shift is

$$\Delta x = 2\Delta\alpha \cdot a$$

The velocity of light can then be calculated as

$$c = 8\pi \cdot a^2 \cdot \frac{v}{\Delta x}$$

To determine the velocity of light in experiment P5.6.1.1, the image shift is measured as a function of the speed of the mirror.
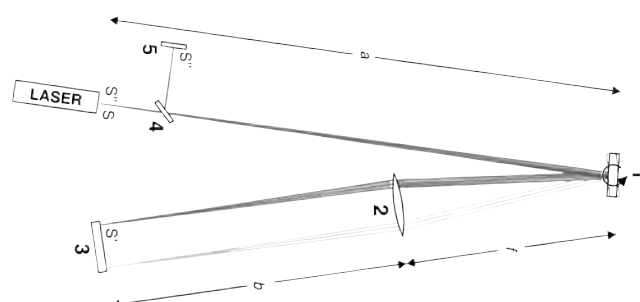
Schematic diagram of the velocity of light by means of the rotating-mirror method according to Foucault and Michelson - Measuring the image shift as a function of the rotational speed of the mirror (P5.6.1.1)

MEASURING WITH SHORT LIGHT PULSES

P5.6.2.1
Determining the velocity of light in air from the path and transit time of a short light pulse
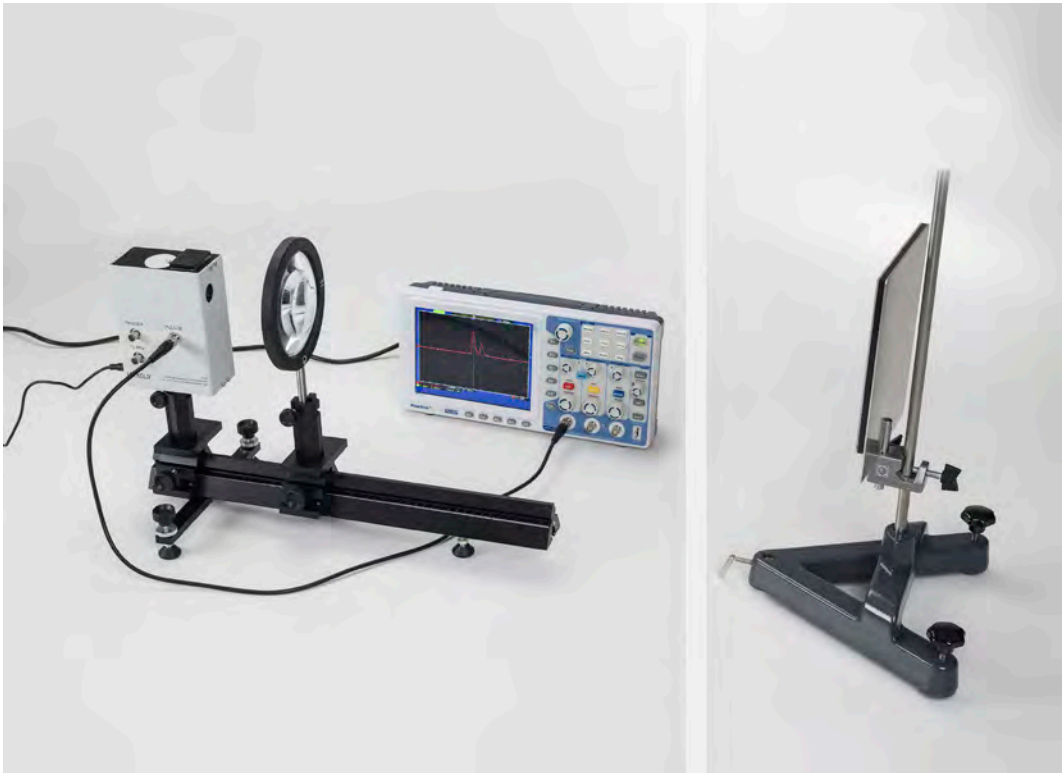
Determining the velocity of light in air from the path and transit time of a short light pulse (P5.6.2.1)

Cat. No.	Description	P5.6.2.1
476 50	Light velocity measuring instrument	1
460 10	Lens in frame, f=200 mm	1
460 335	Optical bench with standardised profile, 0.5 m	1
460 374	Optics rider, 90/50	2
575 302	Oscilloscope 30 MHz, digital, PT1265	1
501 02	BNC cable, 1 m	3
311 02	Metal rule, 1 m	1
300 01	Stand base, V-shaped, large	1
300 44	Stand rod, 100 cm, 12 mm diam.	1
301 01	Leybold multiclamp	1

The light velocity measuring instrument emits pulses of light with a pulse width of about 20 ns. After traversing a known measuring distance in both directions, the light pulses are converted into voltage pulses for observation on the oscilloscope.

In the experiment P5.6.2.1, the path of the light pulses is varied once, and the change in the transit time is measured with the oscilloscope. The velocity of light can then be calculated as quotient of the change in the transit distance and the change in the transit time. Alternatively, the total transit time of the light pulses can be measured in absolute terms using a reference pulse. In this case, the velocity of light can be calculated as quotient of the transit distance and the transit time. A quartz-controlled oscilloscope signal can be displayed on the instrument simultaneously with the measuring pulse in order to calibrate timing. Time measurement is then independent of the time base of the oscilloscope.
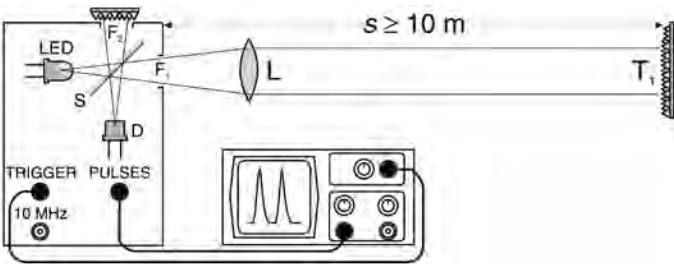
Schematic diagram of light velocity measurement with short light pulses (P5.6.2.1)

Determining the velocity of light in various materials (P5.6.3.2)

Cat. No.	Description	P5.6.3.1	P5.6.3.2
476 301	Light transmitter and receiver	1	1
575 302	Oscilloscope 30 MHz, digital, PT1265	1	1
460 08	Lens in frame, f=150 mm	1	1
300 11	Saddle base	2	4
311 02	Metal rule, 1 m	1	1
476 35	Tube with 2 end windows		1
476 34	Transparent plastic block		1*
477 32	Cuvette made of optical glass 45 x 12.5 x 52.5 mm		1*
460 25	Prism table		1*
671 9720	Ethanol, denaturated, 1 l		1*
672 1210	Glycerin, 99 %, 250 ml		1*

* additionally recommended

In determining the velocity of light with an electronically modulated signal, a light emitting diode which pulses at a frequency of 60 MHz is used as the light transmitter. The receiver is a photodiode which converts the light signal into a 60 MHz AC voltage. A connecting lead transmits a reference signal to the receiver which is synchronized with the transmitted signal and in phase with it at the start of the measurement. The receiver is then moved by the measuring distance Δs, so that the received signal is phase-shifted by the additional transit time Δt of the light signal.

$$\Delta\varphi = 2\pi \cdot f_1 \cdot \Delta t \quad \text{where } f_1 = 60 \text{ MHz}$$

Alternatively, a medium with a greater index of refraction can be placed in the beam path. The apparent transit time to be measured is increased by means of an electronic "trick". The received signal and the reference signal are each mixed (multiplied) with a 59.9 MHz signal before being fed through a frequency filter which only passes the low frequency components with the differential frequency $f_1 - f_2 = 0.1$ MHz. This mixing has no effect on the phase shift; however, this phase shift is now for a transit time $\Delta t'$ increased by a factor of

$$\frac{f_1}{f_1 - f_2} = 600$$

In the experiment P5.6.3.1, the apparent transit time $\Delta t'$ is measured as a function of the measuring distance Δs, and the velocity of light in the air is calculated according to the formula

$$c = \frac{\Delta s}{\Delta t'} \cdot \frac{f_1}{f_1 - f_2}$$

The experiment P5.6.3.2 determines the velocity of light in various propagation media. In the way of accessories, this experiment requires a tube 1 m long with two end windows, suitable for filling with water, a glass cell 5 cm wide for other liquids and an acrylic glass body 5 cm wide.

Determining the velocity of light using a periodical light signal at a short measuring distance (P5.6.3.1)

LEYBOLD®

MEASURING WITH AN ELECTRONICALLY MODULATED SIGNAL

P5.6.3.3
Determining the velocity of light using a periodical light signal at a short measuring distance – measuring with the laser motion sensor S and CASSY

P5.6.3.4
Determining the velocity of light for different propagation media – measuring with the laser motion sensor S and CASSY

Determining the velocity of light using a periodical light signal at a short measuring distance - measuring with the laser motion sensor S and CASSY (P5.6.3.3)

Cat. No.	Description	P5.6.3.3	P5.6.3.4
524 013	Sensor-CASSY 2	1	1
524 220	CASSY Lab 2	1	1
524 073	Laser motion sensor S	1	1
337 116	End buffers, pair	1	1
311 02	Metal rule, 1 m	1	
477 32	Cuvette made of optical glass 45 x 12.5 x 52.5 mm		1
476 34	Transparent plastic block		1
	additionally required: PC with Windows XP/Vista/7/8/10 (x86 or x64)	1	1

Modern distance meters use a periodically modulated laser beam for the measurement. They determine the phase shift between the emitted and the reflected modulated laser beam and, with the modulation frequency being known, obtain the time-of-flight t of the light on its path to and back from the reflector. Only afterwards do the distance meters calculate the distance with the aid of the known velocity of light.

In the experment P5.6.3.3, the laser motion sensor S is used as a time-of-flight meter because it is also capable of outputting the time-of-flight t directly. The proportionality between the distance and the time-of-flight of light is confirmed, and the velocity of light is calculated.

In the experiment P5.6.3.4 water and acrylic glass of thickness d are held into the path of the beam, and then the resulting increase of the time-of-flight Δt is measured. With the velocity of light c in air measured in the experiment P5.6.3.3, the velocity of light c_M in matter can now be determined:

$$c_M = 2d\left(\frac{2d}{c} + \Delta t\right) = \frac{1}{\frac{1}{c} + \frac{\Delta t}{2d}}$$

Finally, the refractive index n is determined according to

$$n = \frac{c}{c_M} = c \cdot \left(\frac{1}{c} + \frac{\Delta t}{2d}\right) = 1 + \frac{c}{2d \cdot \Delta t}$$
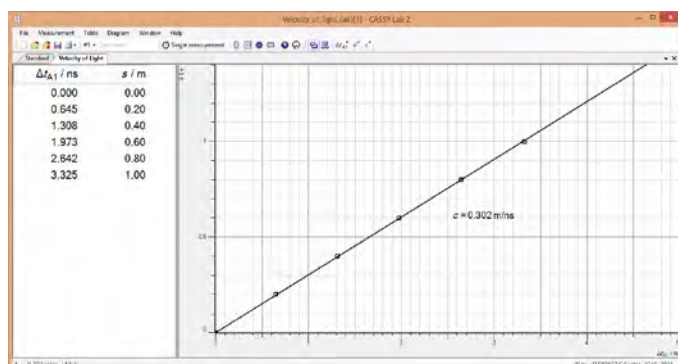
Transit times of light at different distances (P5.6.3.3)

PRISM SPECTROMETER

P5.7.1.1
Measuring the line spectra of inert gases and metal vapors using a prism spectrometer

Measuring the line spectra of inert gases and metal vapors using a prism spectrometer (P5.7.1.1)

Cat. No.	Description	P5.7.1.1
467 231	Spectrometer with goniometer	1
451 031	Spectral lamp, He	1
451 041	Spectral lamp, Cd	1
451 16	Housing for spectral lamps	1
451 30	Universal choke, 230 V, 50 Hz	1
300 02	Stand base, V-shaped, small	1
451 011	Spectral lamp, Ne	1*
451 071	Spectral lamp, Hg-Cd	1*
451 081	Spectral lamp, Tl	1*
451 111	Spectral lamp, Na	1*

*additionally recommended

To assemble the prism spectrometer, a flint glass prism is placed on the prism table of a goniometer. The light of the light source to be studied passes divergently through a collimator and is incident on the prism as a parallel light beam. The arrangement exploits the wavelength-dependency of the refractive index of the prism glass: the light is refracted and each wavelength is deviated by a different angle. The deviated beams are observed using a telescope focused on infinity which is mounted on a pivot-mounted arm; this allows the position of the telescope to be determined to within a minute of arc. The refractive index is not linearly dependent on the wavelength; thus, the spectrometer must be calibrated. This is done using e.g. an He spectral lamp, as its spectral lines are known and distributed over the entire visible range.

In the experiment P5.7.1.1, the spectrometer is used to observe the spectral lines of inert gases and metal vapors which have been excited to luminance. To identify the initially "unknown" spectral lines, the angles of deviation are measured and then converted to the corresponding wavelength using the calibration curve. *Note:* as an alternative to the prism spectrometer, the goniometer can also be used to set up a grating spectrometer (see P5.7.2.1).
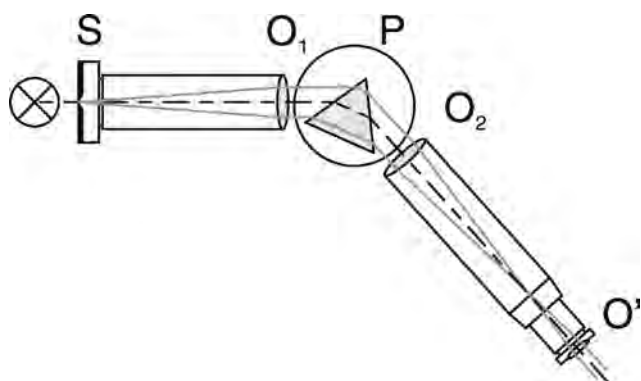
Ray path in a grating prism spectrometer (P5.7.1.1)

GRATING SPECTROMETER

P5.7.2.1
Measuring the line spectra of
inert gases and metal vapors
using a grating spectrometer

Measuring the line spectra of inert gases and metal vapors using a grating spectrometer (P5.7.2.1)

Cat. No.	Description	P5.7.2.1
467 231	Spectrometer with goniometer	1
471 23	Ruled grating, 6000/cm (Rowland)	1
451 031	Spectral lamp, He	1
451 111	Spectral lamp, Na	1
451 16	Housing for spectral lamps	1
451 30	Universal choke, 230 V, 50 Hz	1
300 02	Stand base, V-shaped, small	1
451 011	Spectral lamp, Ne	1*
451 041	Spectral lamp, Cd	1*
451 071	Spectral lamp, Hg-Cd	1*
451 081	Spectral lamp, Tl	1*

* additionally recommended

To create a grating spectrometer, a copy of a Rowland grating is mounted on the prism table of the goniometer in place of the prism. The ray path in the grating spectrometer is essentially analogous to that of the prism spectrometer (see P 5.7.1.1). However, in this configuration the deviation of the rays by the grating is proportional to the wavelength:

$$\sin \Delta\alpha = n \cdot g \cdot \lambda$$

n: diffraction order

g: grating constant

λ: wavelength

$\Delta\alpha$: angel of deviation of nth-order spectral line

Consequently, the wavelengths of the observed spectral lines can be calculated directly from the measured angles of deviation.

In the experiment P5.7.2.1, the grating spectrometer is used to observe the spectral lines of inert gases and metal vapors which have been excited to luminance. To identify the initially "unknown" spectral lines, the angles of deviation are measured and then converted to the corresponding wavelength. The resolution of the grating spectrometer is sufficient to determine the distance between the two yellow sodium D-lines $\lambda(D_1) - \lambda(D_2) = 0{,}60$ nm with an accuracy of 0.10 nm. However, this high resolution is achieved at the cost of a loss of intensity, as a significant part of the radiation is lost in the undiffracted zero order and the rest is distributed over multiple diffraction orders on both sides of the zero order.
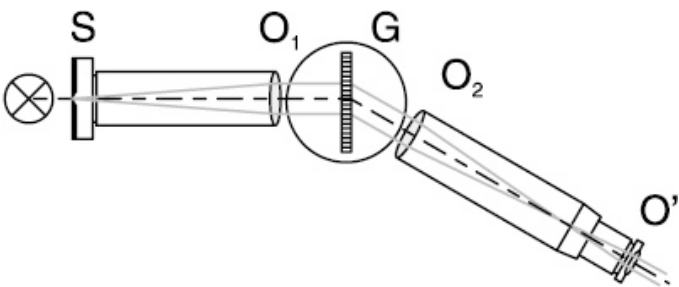
Ray path in a grating spectrometer (P5.7.2.1)

GRATING SPECTROMETER

P5.7.2.4
Determining the grating constant of a holographic grating with an He-Ne-Laser

P5.7.2.5
Investigating the spectrum of a xenon lamp with a holographic grating
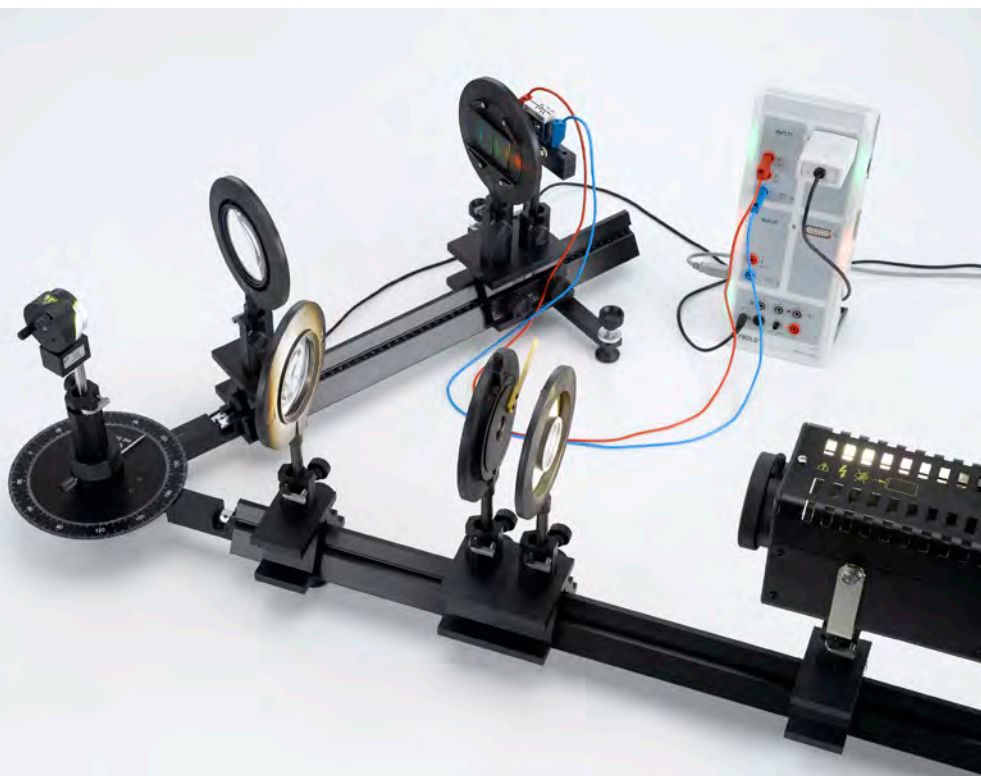
Investigating the spectrum of a xenon lamp with a holographic grating (P5.7.2.5)

Cat. No.	Description	P5.7.2.4	P5.7.2.5
471 830	He-Ne Laser, linearly polarised	1	
460 01	Lens in frame, f=5 mm	1	
460 08	Lens in frame, f=150 mm	1	1
460 09	Lens in frame, f=300 mm	1	1
471 27	Holographic grating in frame	1	1
441 531	Screen	1	1
460 335	Optical bench with standardised profile, 0.5 m	1	1
460 32	Optical bench with standardised profile, 1 m	1	1
460 341	Swivel joint with circular scale	1	1
460 374	Optics rider, 90/50	5	6
450 80	Xenon lamp		1
450 83	Power supply unit for xenon lamp		1
460 02	Lens in frame, f=50 mm		1
460 14	Adjustable slit		1
460 21	Holder for plug-in elements		1
460 22	Holder with spring clips		1
461 62	Set of 2 slit diaphragms		1
578 62	Solar cell, STE 2/19		1
524 013	Sensor-CASSY 2		1
524 220	CASSY Lab 2		1
524 082	Rotary motion sensor S		1
460 382	Tilting rider, 90/50		1
501 25	Connecting lead, 32 A, 50 cm, red		1
501 26	Connecting lead, 32 A, 50 cm, blue		1
501 46	Connecting leads 19 A, 100 cm, red/blue, pair		1
	additionally required: PC with Windows XP/Vista/7/8/10 (x86 or x64)		1

To assemble a grating spectrometer with very high resolution and high efficiency a holographic reflection grating with 24000 lines/cm is used. The loss of intensity is small compared to a transmission grating.

In the experiment P5.7.2.4 the grating constant of the holographic reflection grating is determined for different values of the angle of incidence. The light source used is a He-Ne-Laser with the wavelength $\lambda = 632.8$ nm. The best value is achieved for the special case where angle of incidence and angle of diffraction are the same, the so called Littrow condition.

In the experiment P5.7.2.5 the spectrum of a xenon lamp is investigated. The diffraction pattern behind the holographic grating is recorded by varying the position of a screen or a photocell. The corresponding diffraction angle is read of the circular scale of the rail connector or measured by a rotary motion sensor. It is revealed that the spectrum of the lamp which appears white to the eye consists of a variety of different spectral lines.

OPTICAL APPLICATIONS

P5.8.3.1
Optical interferometer
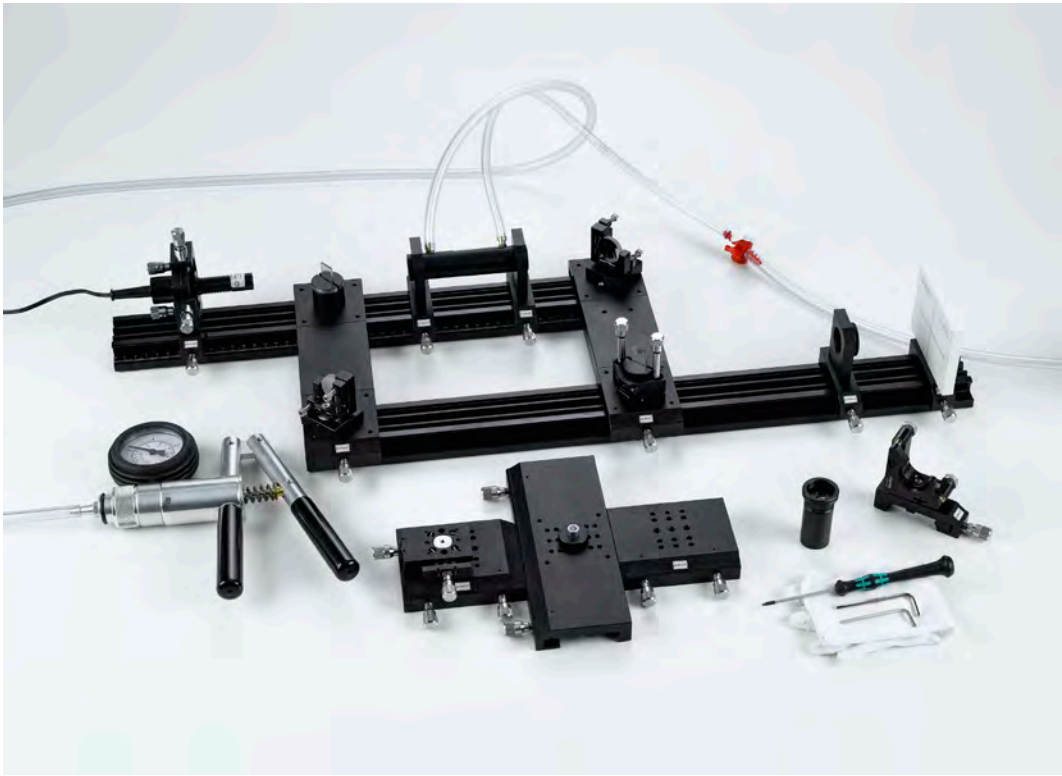
Optical interferometer (P5.8.3.1)

Cat. No.	Description	P5.8.3.1
474 5220	Biconcave Lens f = -10 mm, C25 mount	1
474 5264	Beam expander 2.7x	1
474 169	Gas Cuvette Assembly	1
474 171	Mach Zehnder Beam Combining Assembly	1
474 174	Mach-Zehnder Beam Splitting Assembly	1
474 5457	Screen with rider	1
474 5418	Diode Laser Module 532 nm	1
474 5441	Profile Rail, 300 mm	2
474 5442	Profile rail 500 mm	1
474 5449	Angle Joint, Cross Piece	1
474 209	Mounting Plate C25 with Carrier 20 mm	3
474 2112	Adjustment holder, 4 axes, with stop angle	1
474 213	Adjustment Holder 1 inch, left	1
474 251	Transport and Storage Box #01	2
474 7210	LIT: Optical Interferometer	1

While the Michelson interferometer is mainly used to determine the movement of a reflecting object in a nm scale, the Mach-Zehnder interferometer investigates transparent objects and is particularly useful for studying liquid or gas dynamics. Since the Mach-Zehnder is a unidirectional interferometer it is especially useful for measurements where the samples have to be traversed only once or in one direction.

Within the frame of the experiment P5.8.3.1 both, a Michelson- and a Mach-Zehnder interferometer will be realized. The former demonstrates the principle generation of interference patterns and the use of fringe counting in metrology. The latter uses the interference pattern to visualize changes of the index of refraction as a result of changes in physical properties of gasses, like pressure or composition.

LASER BASICS

P5.8.5.3
Emission & absorption /
Optical pumping
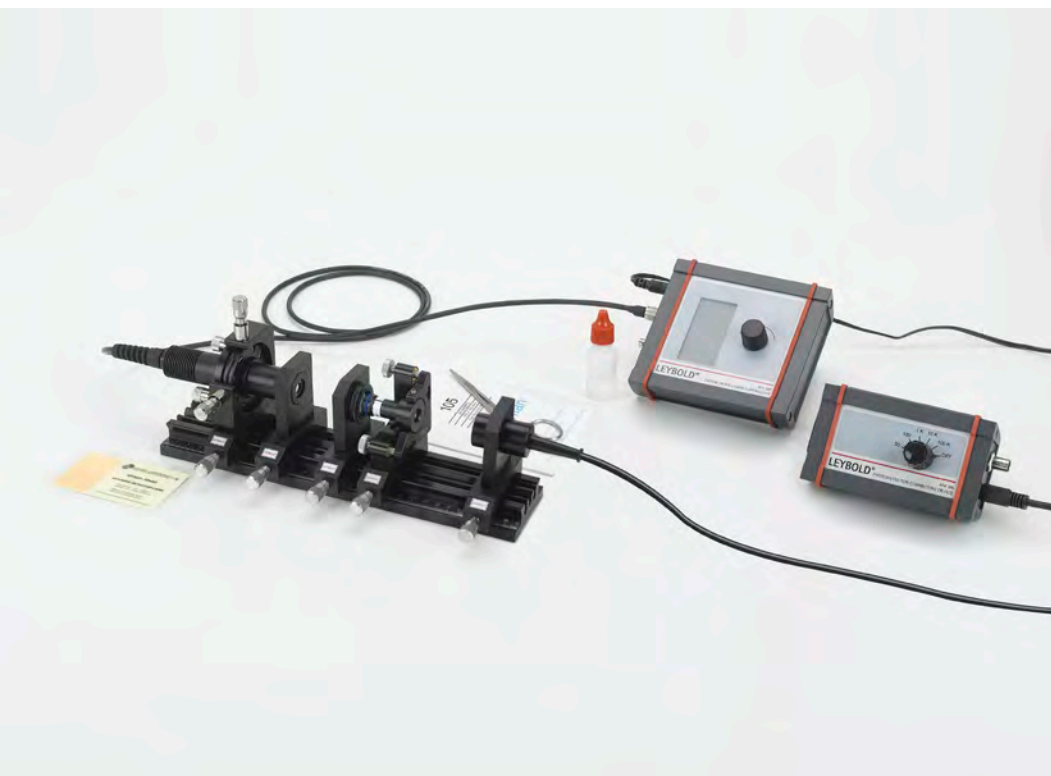
Emission & absorption / Optical pumping (P5.8.5.3)

Cat. No.	Description	P5.8.5.3
474 1032	Collimating optics on carrier, aspherical	1
474 104	Focussing Optics, f = 60 mm	1
474 5310	Crystal in holder Nd:YAG 1064 nm	1
474 113	Laser Mirror Adjustment Holder, left	1
474 137	Spatial filter with adjustable iris	1
474 5453	Crossed Hair Target in C25 mount	1
468 74	Filter infrared	1
474 107	Filter Plate Holder	1
474 4025	IR converter screen 800 - 1400 nm	1
474 306	Photodetector signal conditioning box	1
474 108	SiPIN photodetector	1
531 183	Digital multimeter 3340	1
575 24	Screened cable, BNC/4 mm	1
474 302	Controller for Diode Laser	1
474 1021	Single Mode Diode Laser Head with Adjust	1
474 5442	Profile rail 500 mm	1
474 122	Optics cleaning set	1
671 9700	Ethanol, absolute, 250 ml	1
474 251	Transport and Storage Box #01	1
474 7102	LIT: Emission & Absorption/Opt. Pumping	1
474 5464	Oscilloscope, Dual Channel, Digital	1*
501 06	HF-Cable, BNC-BNC, 1.5 m	1*
501 061	HF-Cable, BNC-Mini BNC, 1.5 m	1*
474 611	Laser safety goggles 808 and 1064 nm	2*

* additionally recommended

The experiment P5.8.5.3 introduces to optical pumping as well as emission and absorption. Due to the pumping process spontaneous and stimulated emission is generated. The emission is temporarily as well spectroscopical measured and analyzed. The tuning of the emission wavelength of the pump diode laser due to the temperature allows the recording of the absorption spectrum. From the timely decay of the fluorescence light the lifetime of the excited state is measured and the Einstein coefficient for stimulated emission calculated.

LEYBOLD®

LASER BASICS

P5.8.5.4
Fabry Perot resonator
– Fabry Perot mode analyzer
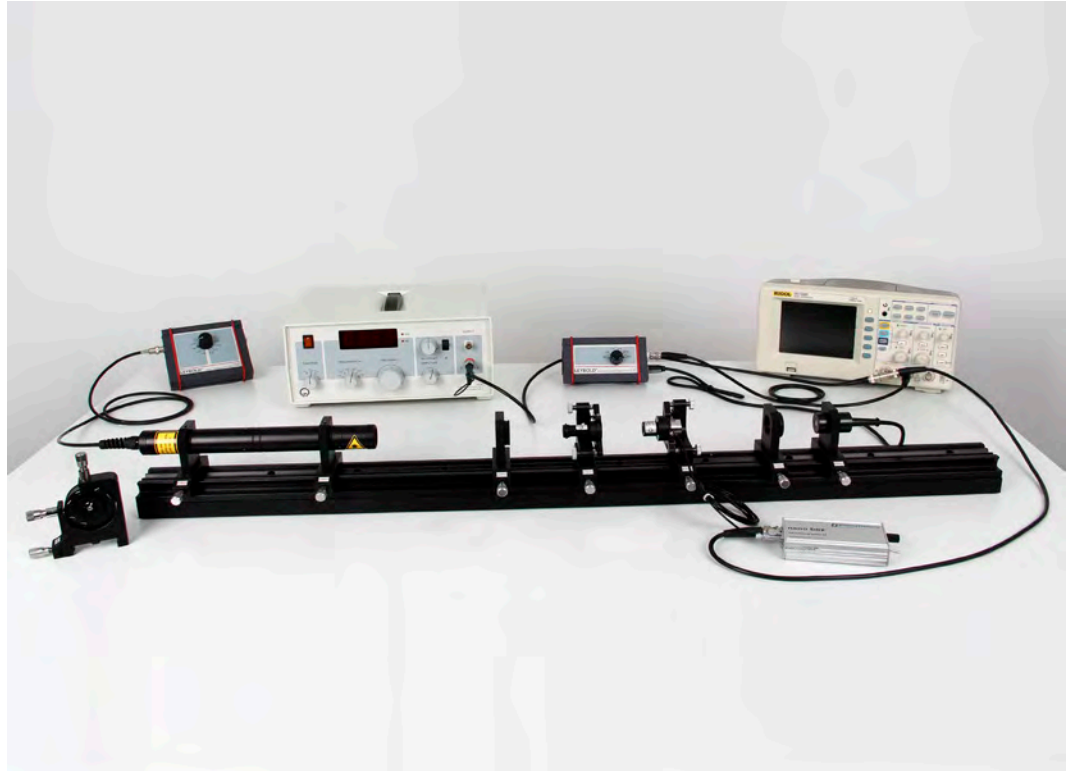
Fabry Perot resonator – Fabry Perot mode analyzer (P5.8.5.4)

Cat. No.	Description	P5.8.5.4
474 104	Focussing Optics, f = 60 mm	1
474 1404	Lens f = 150 mm, C25 Mount and Plate	1
474 140	Beam expander lens, adjustment holder	1
474 5213	Achromat f = 20 mm, C25 mount	1
474 5234	Laser Mirror, flat, M16 mount	1
474 5235	Laser Mirror, R = 75 mm, M16 Mount	1
474 5236	Laser Mirror, R = 100 mm, M16 Mount	1
474 5237	Laser Mirror, flat, M12 Mount	1
474 5238	Laser Mirror, R = 75 mm, M12 Mount	1
474 5239	Laser Mirror, R = 100 mm, M12 Mount	1
474 113	Laser Mirror Adjustment Holder, left	1
474 317	Piezo Actuator Controller	1
474 139	Piezo Element with Adjustment Holder	1
522 561	Function generator P	1
501 02	BNC cable, 1 m	2
501 091	BNC T adapter	1
575 24	Screened cable, BNC/4 mm	1
474 306	Photodetector signal conditioning box	1
474 108	SiPIN photodetector	1
474 5464	Oscilloscope, Dual Channel, Digital	1
474 303	HeNe Laser High Voltage supply, adjustable	1
474 5421	HeNe Pilot Laser Ø 30 mm	1
474 5445	Profile Rail 1000 mm	1
474 210	Mounting plate Ø 30 mm, carrier 20 mm	2
474 122	Optics cleaning set	1
671 9700	Ethanol, absolute, 250 ml	1
474 251	Transport and Storage Box #01	2
474 7103	LIT: Fabry Perot Resonator	1
471 828	Adjustment goggles for He-Ne-laser	2*

*additionally recommended

A Fabry Perot resonator is formed by two mirrors aligned parallel to each other. The resulting cavity changes transparency when the distance of the mirrors is changed by a multiple of half the wavelength. Scanning the length of the cavity creates a high resolution spectrometer.

Experiment P5.8.5.4 shows an open frame scanning Fabry Perot. As scanner a Piezo element and as probe a two mode Helium Neon laser is used. The mode spectrum of the Helium Neon laser is displayed on an oscilloscope and the characteristic parameter like finesse, free spectral range, resolution and contrast are measured and discussed. Additional components for beam expansion are used to investigate the effect of technical Finesse. Additional mirrors are used to show the difference of a plane and confocal Fabry Perot arrangement.

LASER BASICS

P5.8.5.5
Helium Neon laser
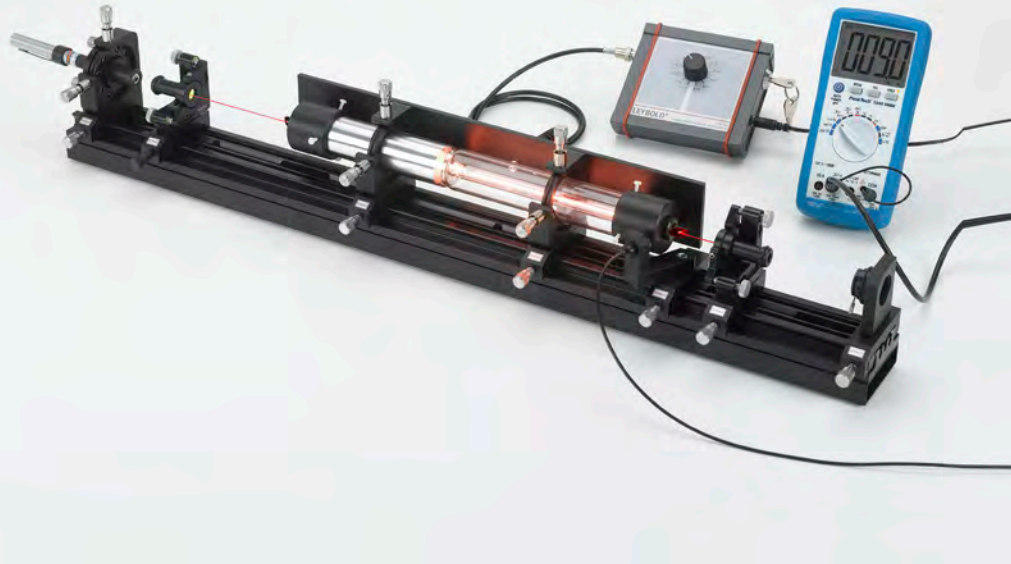
Helium Neon laser (P5.8.5.5)

Cat. No.	Description	P5.8.5.5
474 5242	Laser Mirror OC 632, flat, M16 Mount	1
474 5243	Laser Mirror VIS 700, M16 Mount	1
474 5244	Laser Mirror VIS 1000, M16 Mount	1
474 5246	Laser Mirror, flat, M16 Mount	1
474 113	Laser Mirror Adjustment Holder, left	1
474 114	Laser Mirror Adjustment Holder, right	1
474 126	Littrow prism with adjustment holder	1
474 141	Single Mode Etalon, Adjustmend Holder	1
474 142	Birefringent tuner	1
474 137	Spatial filter with adjustable iris	1
474 1082	Module G (SiPIN) photodetector on swivel arm	1
531 183	Digital multimeter 3340	1
575 24	Screened cable, BNC/4 mm	1
501 10	BNC adapter, straight	1
474 303	HeNe Laser High Voltage supply, adjustable	1
474 127	Main Laser Tube with XY-Adjustment	1
474 5422	Pilot laser 532 nm (green)	1
474 5445	Profile Rail 1000 mm	1
474 122	Optics cleaning set	1
671 9700	Ethanol, absolute, 250 ml	1
474 251	Transport and Storage Box #01	2
474 7104	LIT: HeNe Laser	1
474 5245	Laser Mirror IR 713, M16 Mount	2*
474 4025	IR converter screen 800 - 1400 nm	1*
471 828	Adjustment goggles for He-Ne-laser	2*

* additionally recommended

The experiment P5.8.5.5 realises a Helium Neon laser from basic parts. The open frame cavity allows the variation of parameters to measure the beam profile for different cavity mirror configurations and distances. The laser tube is equipped with a Brewster's window on both sides allowing the study of polarisation and losses. Optionally, a Littrow prism selects other wavelengths than the main laser line at 632 nm, especially the orange line at 611 nm. Further line tuning is demonstrated by means of the optional birefringent tuner. 4 different lines can be demonstrated by this element. An etalon is used to obtain the single mode operation of the Helium Neon laser.

SOLID STATE LASER

P5.8.6.1
Diode laser

Diode laser (P5.8.6.1)

Cat. No.	Description	P5.8.6.1
474 5266	Collimating cylindrical lens f = 20 mm	1
474 5267	Collimating cylindrical lens f = 80 mm	1
474 1032	Collimating optics on carrier, aspherical	1
474 5310	Crystal in holder Nd:YAG 1064 nm	1
474 113	Laser Mirror Adjustment Holder, left	1
474 112	Polarisation Analyzer	1
474 5453	Crossed Hair Target in C25 mount	1
474 4025	IR converter screen 800 - 1400 nm	1
474 306	Photodetector signal conditioning box	1
474 108	SiPIN photodetector	1
531 183	Digital multimeter 3340	1
575 24	Screened cable, BNC/4 mm	1
474 302	Controller for Diode Laser	1
474 1012	Diode Laser Head, Dual Axes Rotary Mount	1
474 5442	Profile rail 500 mm	1
474 209	Mounting Plate C25 with Carrier 20 mm	2
474 122	Optics cleaning set	1
671 9700	Ethanol, absolute, 250 ml	1
474 251	Transport and Storage Box #01	1
474 7105	LIT: Diode Laser	1
474 5464	Oscilloscope, Dual Channel, Digital	1*
501 06	HF-Cable, BNC-BNC, 1.5 m	1*
501 061	HF-Cable, BNC-Mini BNC, 1.5 m	1*
474 611	Laser safety goggles 808 and 1064 nm	2*

* additionally recommended

The goal of the experiment P5.8.6.1 is the study of the properties of a laser diode, i.e. the characteristic parameters like the output power and wavelength as function of the temperature. In a next step the spatial intensity distribution is measured. The more or less elliptical beam is formed by means of two cylindrical lenses into an almost circular beam.

Frequency doubling, 1064 nm -> 532 nm (P5.8.6.3)

SOLID STATE LASER

P5.8.6.2
Diode laser pumped
Nd:YAG laser

P5.8.6.3
Frequency doubling,
1064 nm -> 532 nm

P5.8.6.4
Frequency doubling,
1320 nm -> 660 nm
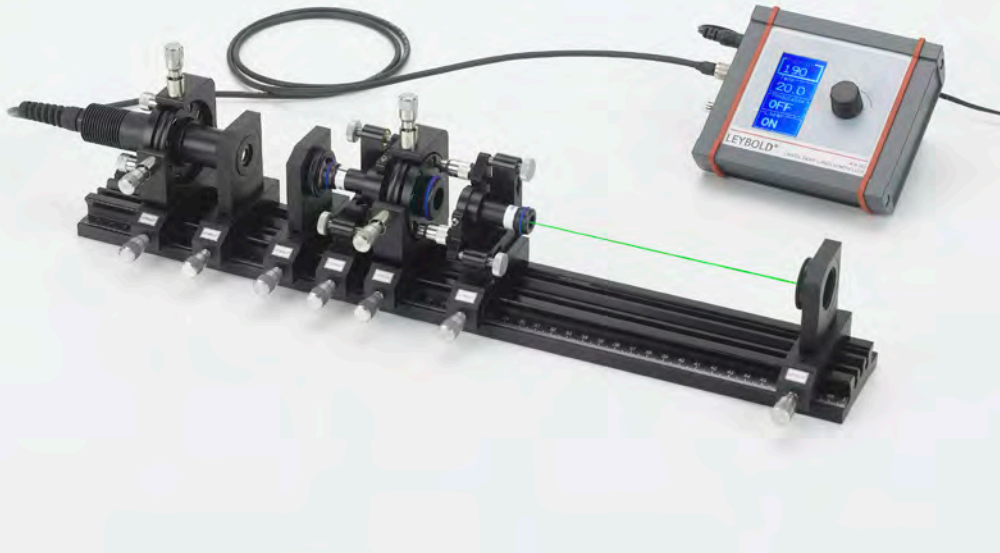
Cat. No.	Description	P5.8.6.2	P5.8.6.3	P5.8.6.4
474 1032	Collimating optics on carrier, aspherical	1	1	1
474 104	Focussing Optics, f = 60 mm	1	1	1
474 5310	Crystal in holder Nd:YAG 1064 nm	1	1	
474 5311	Laser mirror in holder SHG 100	1	1	
474 113	Laser Mirror Adjustment Holder, left	1	1	1
474 114	Laser Mirror Adjustment Holder, right	1	1	1
474 5453	Crossed Hair Target in C25 mount	1	1	1
474 107	Filter Plate Holder	1	1	1
468 74	Filter infrared	1	1	1
474 4025	IR converter screen 800 - 1400 nm	1	1	1
474 306	Photodetector signal conditioning box	1	1	1
474 108	SiPIN photodetector	1	1	
474 5464	Oscilloscope, Dual Channel, Digital	1	1	1
501 06	HF-Cable, BNC-BNC, 1.5 m	1	1	1
501 061	HF-Cable, BNC-Mini BNC, 1.5 m	1	1	1
474 302	Controller for Diode Laser	1	1	1
474 102	Diode Laser Head with Adjustment Holder	1	1	1
474 5442	Profile rail 500 mm	1	1	1
474 122	Optics cleaning set	1	1	1
671 9700	Ethanol, absolute, 250 ml	1	1	1
474 251	Transport and Storage Box #01	1	1	1
474 7106	LIT: DPSSL	1	1	1
474 611	Laser safety goggles 808 and 1064 nm	2*	2*	2*
474 109	KTP Crystal with Adjustment Holder, green		1	
468 77	Light filter green		1	
474 137	Spatial filter with adjustable iris		1*	1*
474 1094	KTP Crystal with Adjustment Holder, red			1
474 5240	Nd:YAG rod 1.3 µm in mirror holder			1
474 5241	Mirror SHG 1.3 µm			1
474 5290	Infrared barrier filter KG5			1
474 1081	Modul G InGaAs photodetector			1

* additionally recommended

Experiment P5.8.6.2 builds a diode pumped Nd:YAG laser ground up. First the pump diode laser is characterized. Then the process of optical pumping and the emitted spontaneous fluorescence are analysed spectrally and temporally by modulation and changing the wavelength of the pump laser leading to the Einstein coefficients. In a third step the laser operation is initiated by adding the second cavity mirror. The laser threshold and efficiency are determined and by modulating the pump laser diode the so called spiking effect demonstrated. By changing the length of the laser cavity the stability criterion is verified.

Experiment P5.8.6.3 enhances the basic set-up of the diode pumped Nd:YAG laser (P5.8.6.2) by a KTP crystal module placed into the laser cavity leading to a frequency doubled green (532 nm) visible output. By adding the optional adjustable iris the transverse mode structure can be controlled for various TEM structures down to TEM00.

Experiment P5.8.6.4 is a variation of P5.8.6.3, but using differently coated mirrors and differently cut KTP, the Nd:YAG laser operates at 1320 nm and the frequency doubled visible light is red at a wavelength of 660 nm.

OPTICAL FIBRES

P5.8.7.1
Fibre laser

Fibre laser (P5.8.7.1)

Cat. No.	Description	P5.8.7.1
474 104	Focussing Optics, f = 60 mm	1
474 5308	Bandpass filter 1.5 µm in C25	1
474 190	Fused WDM Coupler 980/1550 nm	1
474 191	Fibre collimator with ST connector, left	1
474 192	Fibre collimator with ST connector, right	1
474 194	ST coupler in C25 mounted	1
474 1898	Erbium Doped Fibre Module 8 m	1
474 246	Output coupling module	1
474 5293	SM Fibre 100 m on drum, ST connector	1
474 5296	Fibre Patch Cable ST/ST, Length 0.25 m	3
474 5297	Fibre Patch Cable ST/ST, Length 1 m	1
474 4025	IR converter screen 800 - 1400 nm	1
474 306	Photodetector signal conditioning box	1
474 108	SiPIN photodetector	1
474 1084	InGaAs Photodetector	1
474 5464	Oscilloscope, Dual Channel, Digital	1
501 06	HF-Cable, BNC-BNC, 1.5 m	1
501 061	HF-Cable, BNC-Mini BNC, 1.5 m	1
474 302	Controller for Diode Laser	1
474 5426	Diode laser module, ST fibre connector	1
474 5442	Profile rail 500 mm	1
474 5444	Profile rail 1000 mm	1
474 209	Mounting Plate C25 with Carrier 20 mm	1
474 251	Transport and Storage Box #01	2
474 7110	LIT: Fibre Laser	1
474 189	Erbium doped fibre 2 m module, ST connect	1*
474 1894	Erbium Doped Fibre Module 4 m	1*
474 1896	Erbium Doped Fibre Module 16 m	1*
474 5278	Passive mode locker module 1.5 µm	1*
474 5279	Optical isolator 1.5 µm	1*
474 611	Laser safety goggles 808 and 1064 nm	2*

* additionally recommended

In the experiment P5.8.7.1, an Erbium doped fibre is used as active material. Connected to a pump laser, the fluorescence from the erbium fiber is analysed. Before the laser operation at 1.5 µm is studied, the lifetime of the exited state is measured. To form a ring laser a WDM is used to couple the pump light into the fibre and to close the laser ring structure. The ring is opened where a thin glass plate couples a small fraction of the clockwise (cw) and counter clockwise (ccw) laser modes towards a detector.

OPTICAL FIBRES

P5.8.7.3
Glass fibre optics

Glass fibre optics (P5.8.7.3)

Cat. No.	Description	P5.8.7.3
474 1036	Collimating Optics on Carrier	1
474 151	Coupling Optics, XY- Adjustment Holder	1
474 152	Bare Fibre Holder with Translation Stage	1
474 154	Bare Fibre Holder on Rotation Stage	1
474 5227	Optical Glass Fibre 1000 m, multimode	1
474 6420	Optical Fibre Cleaver and Breaker	1
474 6421	Adjustable Plastic Cover Stripper	1
474 4025	IR converter screen 800 - 1400 nm	1
474 306	Photodetector signal conditioning box	1
474 216	Si PIN Photodetector for Swivel Unit, Mounting Plate C25	1
474 5464	Oscilloscope, Dual Channel, Digital	1
501 06	HF-Cable, BNC-BNC, 1.5 m	1
501 061	HF-Cable, BNC-Mini BNC, 1.5 m	1
474 302	Controller for Diode Laser	1
474 1022	Diode Laser Head with Adjustment Holder	1
474 5442	Profile rail 500 mm	1
474 251	Transport and Storage Box #01	1
474 7119	LIT: Glass Fibre Optics	1
474 5226	Optical Glass Fibre 1000 m, monomode	1*
474 5295	Optical Glass Fibre 5000 m, multimode	1*
474 611	Laser safety goggles 808 and 1064 nm	2*

* additionally recommended

Experiment P5.8.7.3 introduces to glass fibre optics. Within this experiment the diode laser itself will be characterised with respect to its output power as function of its temperature and injection current. The spatial intensity distribution is measured by means of the provided rotation stage. Cutting and preparing the fibre is part of the practical training. The light of the diode laser is coupled into the fibre by means of adjustable microscope objectives. The coupling efficiency is monitored with the photodetector detecting the light coming out at the end of the fibre.

The intensity distribution of the light emerging at the end of the fibre is measured and the numerical aperture determined.

By modulating the diode laser by means of the provided microprocessor controlled device the time of flight inside the fibre will be measured. From the results either the length of the fibre or the speed of light is calculated.

TECHNICAL APPLICATIONS

P5.8.8.4
Laser Doppler anemometer

Laser Doppler anemometer (P5.8.8.4)

Cat. No.	Description	P5.8.8.4
474 104	Focussing Optics, f = 60 mm	2
474 107	Filter Plate Holder	1
474 187	LDA Beam Splitting Assembly	1
474 1876	LDA Beam Deflection and Focussing	1
474 188	Ultrasonic particle seeder	1
474 315	Ultrasonic Particle Nebuliser	1
474 194	ST coupler in C25 mounted	1
474 5350	Patch cable ST-ST 600 µm	1
474 3314	Photodetektor Modul 400-1100 nm	1
474 5464	Oscilloscope, Dual Channel, Digital	1
501 06	HF-Cable, BNC-BNC, 1.5 m	1
501 061	HF-Cable, BNC-Mini BNC, 1.5 m	1
474 128	Diode laser module	1
474 5442	Profile rail 500 mm	1
474 209	Mounting Plate C25 with Carrier 20 mm	1
474 251	Transport and Storage Box #01	2
474 7115	LIT: Laser Doppler Anemometer	1
471 828	Adjustment goggles for He-Ne-laser	2*

* additionally recommended

Laser Doppler anemometry is a non-contact optical measurement method to obtain the velocity of a flow (liquid, gas). In the experiment P5.8.8.4 a laser Doppler anemometer is assembled. Among other things, this method is used for the calibration of flow sensors. A laser beam is split into two parts. Focused back to one spot, the laser beams create an interference pattern. Particles in the fluid flow move through the bright and dark zones of the pattern and the scattered light is modulated according to the speed of the particle.

Alternatively, the same setup can be explained in terms of Doppler shifted light. In this experiment, water droplets inside an air stream are used as the scattering particles. The water droplets are too small to stick to surfaces nearby and to wet them. They will just evaporate or bounce off due to surface tension.
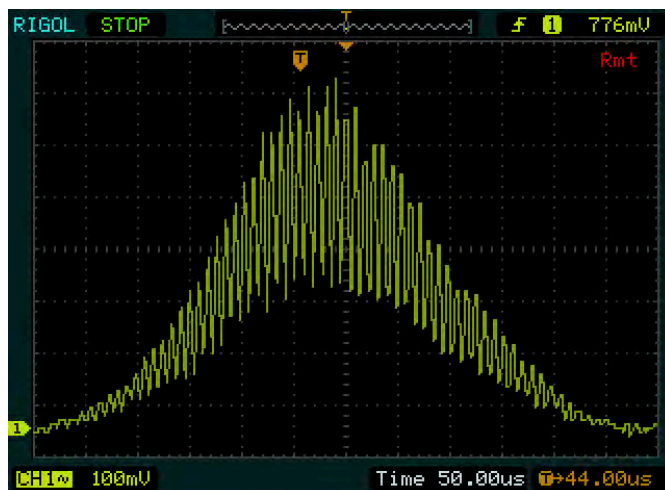
Oscilloscope signal of a water droplet passing throught the interference zone (P5.8.8.4)
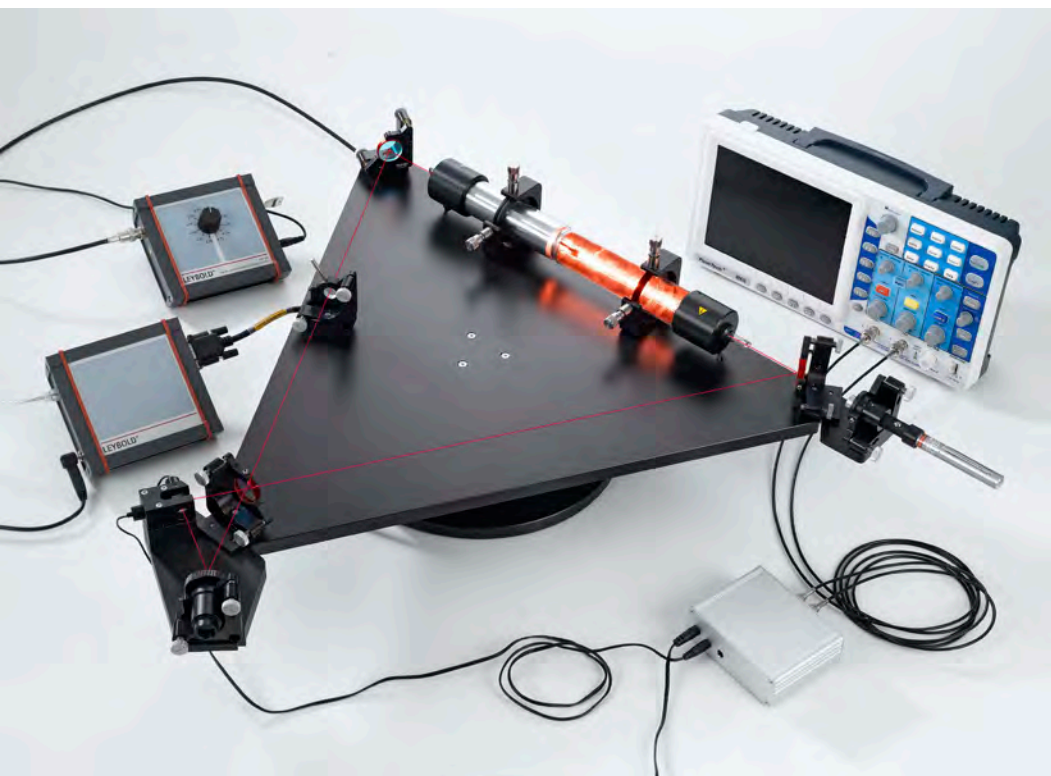
HeNe laser gyroscope (P5.8.8.5)

Cat. No.	Description	P5.8.8.5
474 159	Gyroscope base plate	1
474 160	Rotation Unit	1
474 330	Stepper Motor Controller, 1 Axis, USB	1
474 407	Fringe Detection Unit	1
474 308	Photodetector Preamplifier	1
474 311	Fringe Up and Down Counter	1
474 346	Plug-in power supply 12 V - 2.5 A	1
474 5464	Oscilloscope, Dual Channel, Digital	1
501 061	HF-Cable, BNC-Mini BNC, 1.5 m	4
728 950	USB port isolator	1
474 303	HeNe Laser High Voltage supply, adjustable	1
474 5423	Alignment laser 532 nm	1
474 122	Optics cleaning set	1
671 9700	Ethanol, absolute, 250 ml	1
474 7116	LIT: HeNe Laser Gyroscope	1
	additionally required: PC with Windows 7 or higher	1

Experiment P5.8.8.5 shows the basics of a laser gyroscope. Laser gyroscopes are used, for example, in aircraft to support navigation. A three-mirror mono mode HeNe ring laser is set up; using a green pilot laser adjusting the mirrors is made easy. Both CW and CCW light beams are coupled out of the resonator and fed into an interferometer, creating interference patterns. Rotating this laser, the CW and CCW cavity length is no longer equal due to special relativity, and mixing both light rays will generate a beat frequency in the kHz range. This way the absolute rotation of the laser can be measured.

This is not a Sagnac style interferometer, having the laser medium inside the moving system creates a much more sensitive setup with beat frequency instead of the phase shift of a rotating Sagnac interferometer.
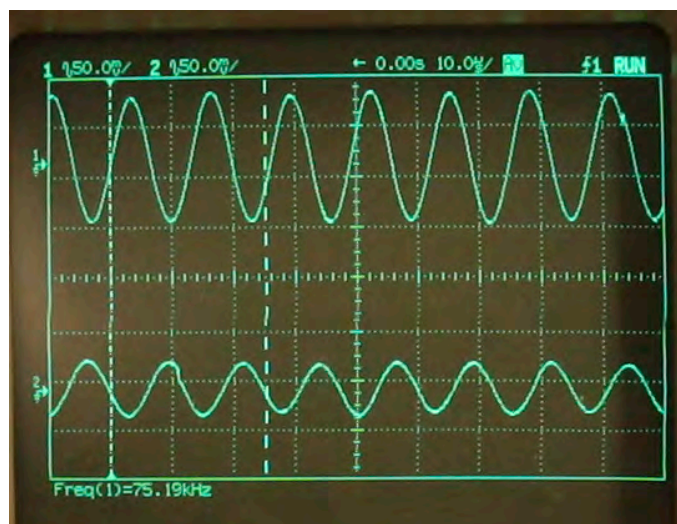
Output signal of the photodiodes during rotation (P5.8.8.5)

P6.2.7.4
Measuring the Zeeman splitting of the red cadmium line
as a function of the magnetic field - spectrocopy using a
Fabry–Perot etalon

For more information on this experiment, go to page 206.

P6 ATOMIC AND NUCLEAR PHYSICS

P6 ATOMIC AND NUCLEAR PHYSICS

MILLIKAN EXPERIMENT

P6.1.2.1
Determining the electric unit charge according to Millikan and verifying the charge quantification - Measuring the suspension voltage and the falling speed

P6.1.2.2
Determining the electric unit charge according to Millikan and verifying the charge quantification - Measuring the rising and falling speed

P6.1.2.3
Determining the electric unit charge according to Millikan and verifying the charge quantification - Measuring the suspension voltage and the falling speed with CASSY

P6.1.2.4
Determining the electric unit charge according to Millikan and verifying the charge quantification - Measuring the rising and falling speed with CASSY

Determining the electric unit charge according to Millikan and verifying the charge quantification - Measuring the suspension voltage and the falling speed (P6.1.2.1)

Cat. No.	Description	P6.1.2.1	P6.1.2.2	P6.1.2.3	P6.1.2.4
559 412	Millikan apparatus	1	1	1	1
559 421	Millikan supply unit	1	1	1	1
575 471	Counter S	1	2		
501 46	Connecting leads 19 A, 100 cm, red/blue, pair	2	3	3	3
501 461	Connecting leads 19 A, 100 cm, black, pair	1	1	1	1
524 013	Sensor-CASSY 2			1	1
524 220	CASSY Lab 2			1	1
524 034	Timer box			1	1
500 421	Connecting lead 19 A, 50 cm, red				1
	additionally required: PC with Windows XP/Vista/7/8/10 (x86 or x64)			1	1

With his famous oil-drop method, *R. A. Millikan* succeeded in demonstrating the quantum nature of minute amounts of electricity in 1910. He caused charged oil droplets to be suspended in the vertical electric field of a plate capacitor and, on the basis of the radius r and the electric field E, determined the charge q of a suspended droplet:

$$q = \frac{4\pi}{3} \cdot r^3 \cdot \frac{\rho \cdot g}{E}$$

ρ: density of oil

g: gravitational acceleratiom

He discovered that q only occurs as a whole multiple of an electron charge e. His experiments are produced here in two variations.

In the variation P6.1.2.1 and P6.1.2.3, the electric field

$$E = \frac{U}{d}$$

d: plate spacing

is calculated from the voltage U at the plate capacitor at which the observed oil droplet just begins to hover. The constant falling velocity v_1 of the droplet when the electric field is switched off is subsequently measured to determine the radius. From the equilibrium between the force of gravity and Stokes friction, we derive the equation

$$\frac{4\pi}{3} \cdot r^3 \cdot \rho \cdot g = 6\pi \cdot r \cdot \eta \cdot v_1$$

η: viscosity

In the variant P6.1.2.2 and P6.1.2.4, the oil droplets are observed which are not precisely suspended, but which rise with a low velocity v_2. The following applies for these droplets:

$$q \cdot \frac{U}{d} = \frac{4\pi}{3} \cdot r^3 \cdot \rho \cdot g + 6\pi \cdot r \cdot \eta \cdot v_2$$

Additionally, the falling speed v_1 is measured, as in the variant P6.1.2.1 and P6.1.2.3. The measuring accuracy for the charge q can be increased by causing the oil droplet under study to rise and fall over a given distance several times in succession and measuring the total rise and fall times.
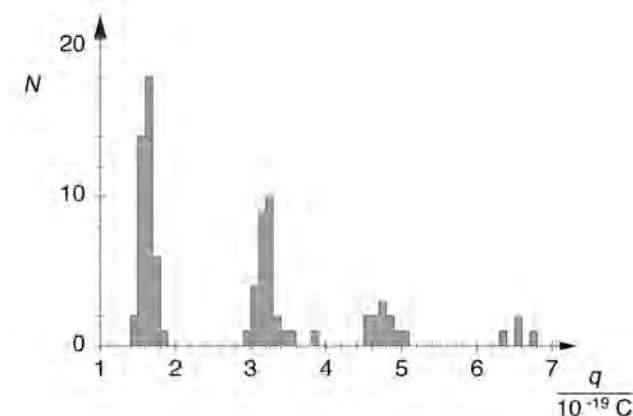
The histogram reveals the qantum nature of the change (P6.1.2.1-4)

LEYBOLD®

CASSY®

SPECIFIC ELECTRON CHARGE

P6.1.3.1
Determining the specific charge of the electron

Determining the specific charge of the electron (P6.1.3.1)

Cat. No.	Description	P6.1.3.1
555 571	Fine beam tube	1
555 581	Helmholtz coils with holder and measuring device for fine beam tube	1
531 120	Multimeter LDanalog 20	2
521 651	Tube power supply 0...500 V	1
521 546	DC Power Supply 0...16 V/0...5 A	1
311 78	Tape measure 2 m / 1 mm	1
500 614	Safety connecting lead, 25 cm, black	3
500 624	Safety connecting lead 50 cm, black	3
500 644	Safety connecting lead, 100 cm, black	7
524 005W	Mobile-CASSY 2 WiFi	1*
524 0382	Axial B sensor S, ±1000 mT	1*
501 11	Extension cable, 15 pin	1*

* additionally recommended

The mass m_e of the electron is extremely difficult to determine in an experiment. It is much easier to determine the specific charge of the electron

$$\varepsilon = \frac{e}{m_e}$$

from which we can calculate the mass m_e for a given electron charge e.

In the experiment P6.1.3.1, a tightly bundled electron beam is diverted into a closed circular path using a homogeneous magnetic field in order to determine the specific electron charge. The magnetic field B which diverts the electrons into the path with the given radius r is determined as a function of the acceleration voltage U. The Lorentz force caused by the magnetic field acts as a centripetal force. It depends on the velocity of the electrons, which in turn is determined by the acceleration voltage. The specific electron charge can thus be determined from the measurement quantities U, B and r according to the formula

$$\frac{e}{m_e} = 2 \cdot \frac{U}{B^2 \cdot r^2}$$
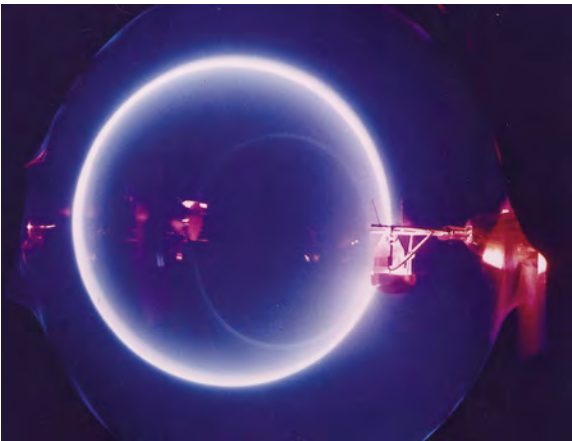
Circular electron path in fine beam tube (P6.1.3.1)

CASSY®

PLANCK'S CONSTANT

P6.1.4.2
Determining Planck's constant
- Separation of wavelengths with
a straight-view prism on the
optical bench

P6.1.4.3
Determining Planck's constant
- Selection of wavelengths using
interference filters on the
optical bench

Determining Planck's constant - Selection of wavelengths using interference filters on the optical bench (P6.1.4.3)

Cat. No.	Description	P6.1.4.2	P6.1.4.3
558 77	Photocell for determining Planck's constant	1	1
558 791	Holder for photocell	1	1
460 317	Optical bench, S1 profile, 0.5 m	2	1
460 3151	Swivel joint with protactor scale and clamp	1	
460 311	Clamp rider with clamp 45/65	2	1
460 3112	Clamp rider with clamp 75/65	5	4
460 02	Lens in frame, f=50 mm	1	
460 08	Lens in frame, f=150 mm	2	
461 62	Set of 2 slit diaphragms	1	
460 22	Holder with spring clips	1	
460 14	Adjustable slit	1	
466 05	Direct vision prism	1	
466 04	Holder for direct vision prism	1	
451 15	High pressure mercury lamp	1	1
451 195	Power supply unit for high-pressure mercury lamp	1	1
532 14	Electrometer amplifier	1	1
562 791	Plug-in power supply, 12 V AC	1	1
578 22	Capacitor, 100 pF, STE 2/19	1	1
579 10	Push button (NO), STE 2/19	1	1
590 011	Clamping plug	2	2
531 120	Multimeter LDanalog 20	1	1
501 10	BNC adapter, straight	1	1
501 09	BNC/4-mm plug adapter, single-pole	1	1
340 89	Coupling plug 4 mm	1	1
502 04	Distribution box with earthing socket	1	1
501 45	Connecting lead 19 A, 50 cm, red/blue, pair	1	1
500 440	Connecting lead, 19 A, 100 cm, yellow/green	2	2
468 41	Holder for interference filters		1
468 401	Interference filter, 578 nm		1
468 402	Interference filter, 546 nm		1
468 403	Interference filter, 436 nm		1

Cat. No.	Description	P6.1.4.2	P6.1.4.3
468 406	Interference filter, 365 nm		1
460 03	Lens in frame, f=100 mm		1
460 26	Iris diaphragm		1
468 404	Interference filter, 405 nm		1*

When light with the frequency ν falls on the cathode of a photocell, electrons are released. Some of the electrons reach the anode where they generate a current in the external circuit, which is compensated to zero by applying a voltage with opposite sign $U = -U_0$. The applicable relationship

$$e \cdot U_0 = h \cdot \nu - W \quad W: \text{electronic work function}$$

was first used by *R. A. Millikan* to determine Planck's constant h.

In determining Planck's constant using the photoelectric effect, it must be ensured that only the light of a single spectral line of the high-pressure mercury vapour lamp falls on the cathode of the photocell at any one time. As an alternative to a prism, it is also possible to use narrow-band interference filters to select the wavelength. This simplifies the subsequent optical arrangement, and it is no longer necessary to darken the experiment room. Also, the intensity of the light incident on the cathode can be easily varied using an iris diaphragm.

To determine Planck's quantum constant, the photoelectric effect is used in experiments P6.1.4.2 and P6.1.4.3. It must be ensured that only the light of a single spectral line of the high-pressure mercury vapour lamp falls on the cathode of the photocell at any one time. In experiment P6.1.4.2, the separation of the individual spectral lines is achieved by a straight–sight prism, whereas in experiment P6.1.4.3, this is done by using interferential filters. In both experiments A capacitor is connected between the cathode and the anode of the photocell which is charged by the anode current, thus generating the opposing voltage U. As soon as the opposing voltage reaches the value $-U_0$, the anode current is zero and the charging of the capacitor is finished. U_0 is measured without applying a current by means of an electrometer amplifier.

Note for P6.1.4.2 and P6.1.4.3: The opposing voltage U can alternatively be tapped from a DC voltage source. The I-measuring amplifier *D* is recommended for sensitive measurements of the anode current (see P6.1.4.4).

PLANCK'S CONSTANT

P6.1.4.4
Determining Planck's constant
- Recording the current-voltage
characteristics, selection of
wavelengths using interference
filters on the optical bench

Determining Planck's constant - Recording the current-voltage characteristics, selection of wavelengths using interference filters on the optical bench (P6.1.4.4)

Cat. No.	Description	P6.1.4.4
558 77	Photocell for determining Planck's constant	1
558 791	Holder for photocell	1
460 335	Optical bench with standardised profile, 0.5 m	1
460 374	Optics rider, 90/50	2
460 375	Optics rider, 120/50	3
558 792	Filter wheel with diaphragm	1
468 401	Interference filter, 578 nm	1
468 402	Interference filter, 546 nm	1
468 403	Interference filter, 436 nm	1
468 404	Interference filter, 405 nm	1
468 406	Interference filter, 365 nm	1
460 03	Lens in frame, f=100 mm	1
460 26	Iris diaphragm	1
451 15	High pressure mercury lamp	1
451 195	Power supply unit for high-pressure mercury lamp	1
532 00	I-measuring amplifier D	1
524 013	Sensor-CASSY 2	1
524 220	CASSY Lab 2	1
576 81	Plug-in board safety socket, 20/10	2
576 86	Monocell holder STE 2/50	3
685 48	Mono cell 1.5 V (IEC R20)	3
577 93	Potentiometer, 1 kΩ, 10-turn, STE 4/50	1
579 13	Toggle switch STE 2/19	1
501 48	Bridging plugs STE 2/19, set of 10	1
500 621	Safety connecting lead 50 cm, red	2
500 622	Safety connecting lead 50 cm, blue	2
500 644	Safety connecting lead, 100 cm, black	1
	additionally required: PC with Windows XP/Vista/7/8/10 (x86 or x64)	1

When light with the frequency ν falls on the cathode of a photocell, electrons are released. Some of the electrons reach the anode where they generate a current in the external circuit, which is compensated to zero by applying a voltage with opposite sign $U = -U_0$. The applicable relationship

$$e \cdot U_0 = h \cdot \nu - W \quad W: \text{electronic work function}$$

was first used by *R. A. Millikan* to determine Planck's constant *h*.

In determining Planck's constant using the photoelectric effect, it must be ensured that only the light of a single spectral line of the high-pressure mercury vapour lamp falls on the cathode of the photocell at any one time. As an alternative to a prism, it is also possible to use narrow-band interference filters to select the wavelength. This simplifies the subsequent optical arrangement, and it is no longer necessary to darken the experiment room. Also, the intensity of the light incident on the cathode can be easily varied using an iris diaphragm.

In the experiment P6.1.4.4 one of the emission lines from a mercury gas discharge lamp is selected by interference filters and focused onto the photocathode. The countervoltage of the anode is varied and the resulting current is measured with high sensitivity. The variation of the characteristic curves under irradiation with different wavelengths leads to the determination of Planck's constant *h*.
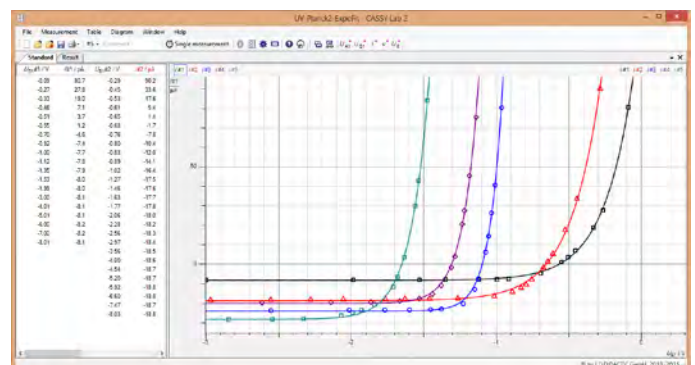
Current-voltage characteristics of the photocell (P6.1.4.4)

CASSY®

Diffraction of electrons at a polycrystalline lattice (Debye-Scherrer diffraction) (P6.1.5.1)

DUAL NATURE OF WAVE AND PARTICLE

P6.1.5.1
Diffraction of electrons at a polycrystalline lattice (Debye-Scherrer diffraction)

P6.1.5.2
Optical analogy to electron diffraction at a polycrystalline lattice

Cat. No.	Description	P6.1.5.1	P6.1.5.2
555 626	Electron diffraction tube	1	
555 600	Tube stand	1	
521 70	High-voltage power supply, 10 kV	1	
311 54	Precision vernier callipers	1	
500 611	Safety connecting lead, 25 cm, red	1	
500 621	Safety connecting lead 50 cm, red	1	
500 641	Safety connecting lead, 100 cm, red	1	
500 642	Safety connecting lead, 100 cm, blue	1	
500 644	Safety connecting lead, 100 cm, black	2	
555 629	Cross grating, 5000/cm, rotatable		1
450 641	Halogen lamp 12 V, 50/100W		1
450 63	Halogen bulb 12 V/100 W, G6.35		1
450 66	Picture slider		1
726 890	DC-High Current Power Supply 1...32 V/0...20 A		1
460 03	Lens in frame, f=100 mm		1
460 22	Holder with spring clips		1
441 53	Screen, translucent		1
311 78	Tape measure 2 m / 1 mm		1
460 310	Optical bench, S1 profile, 1 m		1
460 311	Clamp rider with clamp 45/65		2
460 312	Clamp rider with clamp 45/35		3
500 624	Safety connecting lead 50 cm, black		2
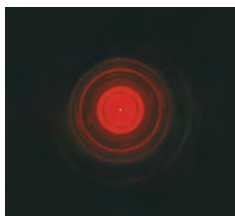
In 1924, *L. de Broglie* first hypothesized that particles could have wave properties in addition to their familiar particle properties, and that their wavelength depends on the linear momentum p

$$\lambda = \frac{h}{p} \qquad h: \text{Planck's constant}$$

His conjecture was confirmed in 1927 by the experiments of *C. Davisson* and *L. Germer* on the diffraction of electrons at crystalline structures.

The experiment P6.1.5.1 demonstrates diffraction of electrons at polycrystalline graphite. As in the Debye-Scherrer method with x-rays, we observe diffraction rings in the direction of radiation which surround a central spot on a screen. These are caused by the diffraction of electrons at the lattice planes of microcrystals which fulfill the Bragg condition

$$2 \cdot d \cdot \sin \vartheta = n \cdot \lambda$$

ϑ: angular aperture of diffraction ring

d: spacing of lattice planes

As the graphite structure contains two lattice-plane spacings, two diffraction rings in the first order are observed. The electron wavelength

$$\lambda = \frac{h}{\sqrt{2 \cdot m_e \cdot e \cdot U}}$$

m_e: mass of electron, e: elementary charge

is determined by the acceleration voltage U, so that for the angular aperture of the diffraction rings we can say

$$\sin \vartheta \propto \frac{1}{\sqrt{U}}$$

The experiment P6.1.5.2 illustrates the Debye-Scherrer method used in the electron diffraction tube by means of visible light. Here, parallel, monochromatic light passes through a rotating cross grating. The diffraction pattern of the cross grating at rest, consisting of spots of light arranged around the central beam in a network-like pattern, is deformed by rotation into rings arranged concentrically around the central spot. By using different colour filters the dependence of the ring diameters on the wavelength of the light can be shown.

Optical analogon of Debye-Scherrer diffraction (P6.1.5.2)

LEYBOLD®

197

BALMER SERIES OF HYDROGEN

P6.2.1.1
Determining the wavelengths H_a, H_β and H_γ from the Balmer series of hydrogen

P6.2.1.2
Observing the Balmer series of hydrogen using a prism spectrometer

P6.2.1.4
Observing the Balmer series of hydrogen using a compact spectrometer
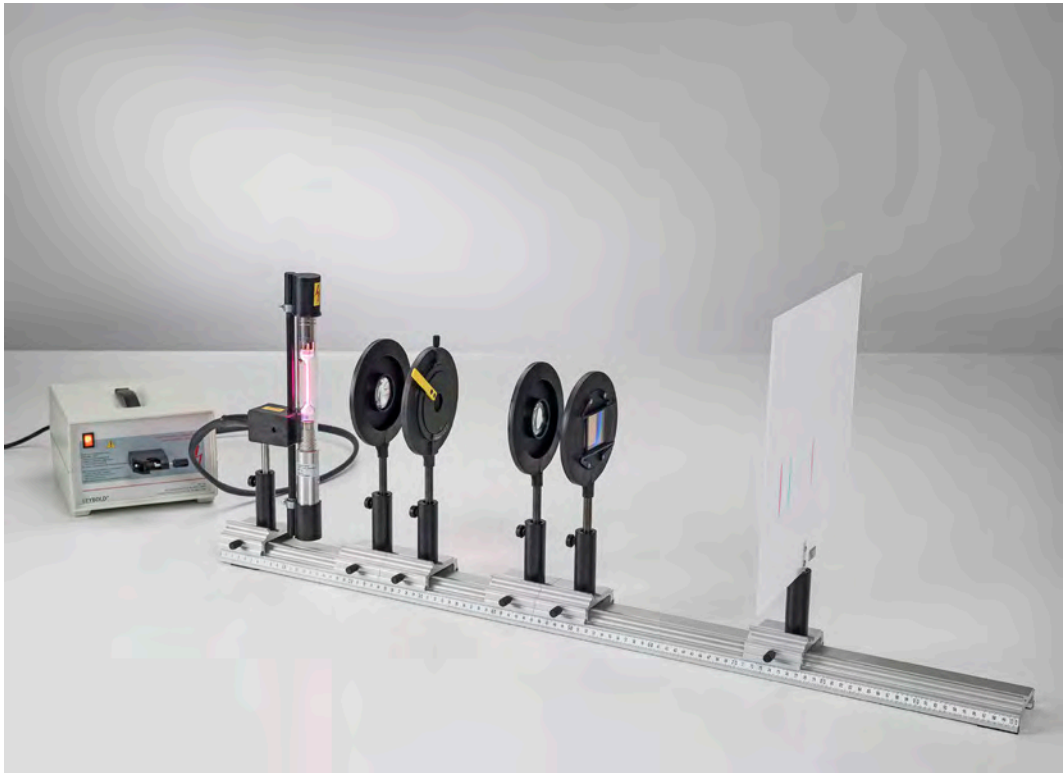
Determining the wavelengths H_a, H_β and H_γ from the Balmer series of hydrogen (P6.2.1.1)

Cat. No.	Description	P6.2.1.1	P6.2.1.2	P6.2.1.4
451 13	Balmer lamp	1	1	1
451 141	Power supply unit for Balmer lamp	1	1	1
471 23	Ruled grating, 6000/cm (Rowland)	1		
311 78	Tape measure 2 m / 1 mm	1		
460 02	Lens in frame, f=50 mm	1		
460 03	Lens in frame, f=100 mm	1		
460 14	Adjustable slit	1		
460 22	Holder with spring clips	1		
441 53	Screen, translucent	1		
460 310	Optical bench, S1 profile, 1 m	1		
460 3112	Clamp rider with clamp 75/65	6		
467 231	Spectrometer with goniometer		1	
467 251	Compact spectrometer, physics (spectral photometer)			1
460 251	Fibre holder			1
300 11	Saddle base			1
	additionally required: PC with Windows XP/Vista/7/8/10 (x86 or x64)			1

In the visible range, the emission spectrum of atomic hydrogen has four lines, H_α, H_β, H_γ and H_δ; this sequence continues into the ultraviolet range to form a complete series. In 1885, *Balmer* empirically worked out a formula for the frequencies of this series

$$\nu = R_\infty \cdot \left(\frac{1}{2^2} - \frac{1}{m^2} \right), \quad m: 3, 4, 5, \ldots$$

R_∞: $3.2899 \cdot 10^{15}$ s^{-1} : Rydberg constant

which could later be explained using Bohr's model of the atom.

In the experiment P6.2.1.1, the emission spectrum is excited using a Balmer lamp filled with water vapor, in which an electric discharge splits the water molecules into an excited hydrogen atom and a hydroxyl group. The wavelengths of the lines H_α, H_β and H_γ are determined using a high-resolution grating. In the first diffraction order of the grating, we can find the following relationship between the wavelength λ and the angle of observation ϑ:

$$\lambda = d \cdot \sin \vartheta$$

d: grating constant

The measured values are compared with the values calculated according to the Balmer formula.

In the experiment P6.2.1.2 the Balmer series is studied by means of a prism spectroscope (complete device).

In the experiment P6.2.1.4 the Balmer series is studied by means of a computer attached compact spectrometer. The optical adjustment is extremely simple, just placing the optical fiber close to the discharge lamp. As a result you get the complete infrared and visible range of the emission spectrum.

Emission spectrum of atomic hydrogen (P6.2.1.4)

Observing the splitting of the Balmer series on deuterated hydrogen (isotope splitting) – Observing the line splitting with a telescope setup (P6.2.1.5)

BALMER SERIES OF HYDROGEN

P6.2.1.5
Observing the splitting of the Balmer series on deuterated hydrogen (isotope splitting) – Observing the line splitting with a telescope setup

Cat. No.	Description	P6.2.1.5
451 41	Balmer lamp, deuterated	1
451 141	Power supply unit for Balmer lamp	1
460 02	Lens in frame, f=50 mm	1
460 08	Lens in frame, f=150 mm	1
460 09	Lens in frame, f=300 mm	1
460 14	Adjustable slit	1
471 27	Holographic grating in frame	1
460 135	Ocular with scale	1
460 32	Optical bench with standardised profile, 1 m	1
460 335	Optical bench with standardised profile, 0.5 m	1
460 341	Swivel joint with circular scale	1
460 374	Optics rider, 90/50	6

The Balmer series of the hydrogen atom is given by the electron transitions to the second energy level (principal quantum number n=2) from higher states (m: 3, 4, 5,...). The wavelength of the emitted photons is given by

$$\frac{c}{\lambda} = R \left(\frac{1}{n^2} - \frac{1}{m^2} \right) \quad R = \text{Rydberg constant}$$

Here, one assumes that the mass of the nucleus is much bigger than the mass of the electron. For a more exact calculation, the Rydberg constant has to be corrected employing the reduced mass. Therefore, the Rydberg constants RH for hydrogen and RD for the isotope deuterium whose nucleus consists of a proton and a neutron differ. The spectral lines of the Balmer series of deuterium are shifted to somewhat smaller wavelengths compared to the spectral lines of hydrogen. This effect is called isotopic shift.

In the experiment P6.2.1.5 the Balmer series is studied by means of a high resolution spectrometer setup. A holographic grating with the grating constant g is used. The wavelength splitting is calculated from the angle β of the 1. order maximum and the angle splitting Δβ:

$$\Delta\lambda = g \cdot \cos\beta \cdot \Delta\beta$$

EMISSION AND ABSORPTION SPECTRA

P6.2.2.1
Displaying the spectral lines of inert gases and metal vapors

P6.2.2.2
Qualitative investigation of the absorption spectrum of sodium
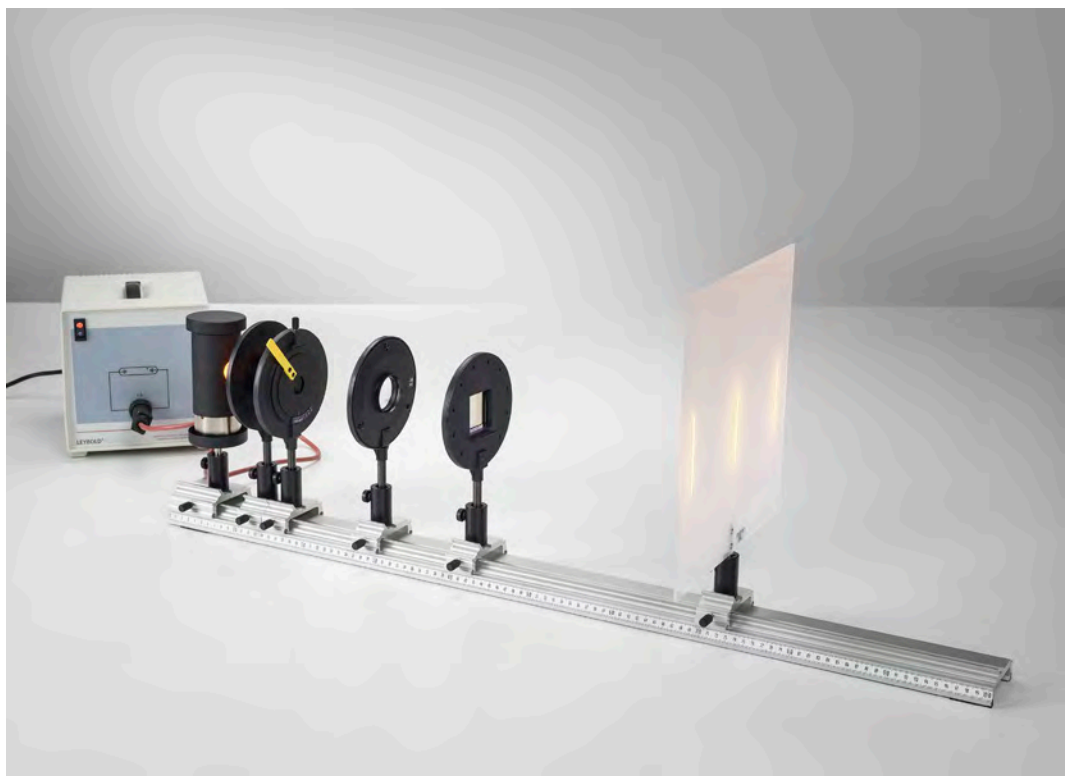
Displaying the spectral lines of inert gases and metal vapors (P6.2.2.1)

Cat. No.	Description	P6.2.2.1	P6.2.2.2
451 011	Spectral lamp, Ne	1	
451 041	Spectral lamp, Cd	1	
451 062	Spectral lamp, Hg 100	1	
451 111	Spectral lamp, Na	1	1
451 16	Housing for spectral lamps	1	1
451 30	Universal choke, 230 V, 50 Hz	1	1
471 23	Ruled grating, 6000/cm (Rowland)	1	
311 78	Tape measure 2 m / 1 mm	1	
460 02	Lens in frame, f=50 mm	1	
460 03	Lens in frame, f=100 mm	1	
460 14	Adjustable slit	1	
460 22	Holder with spring clips	1	
441 53	Screen, translucent	1	1
460 310	Optical bench, S1 profile, 1 m	1	
460 311	Clamp rider with clamp 45/65	1	
460 312	Clamp rider with clamp 45/35	5	
450 60	Lamp housing with cable		1
450 511	Bulbs, 6 V/30 W, E14, set of 2		1
521 210	Transformer 6/12 V		1
300 02	Stand base, V-shaped, small		2
300 11	Saddle base		1
300 42	Stand rod, 47 cm, 12 mm diam.		2
666 711	Butane gas burner		1
666 712ET3	Butane cartridge, 190 g, set of 3		1
301 01	Leybold multiclamp		2
666 962	Double-ended spatula, stainless steel, 150 mm		1
673 0840	Magnesia rods, 25 pieces		1
673 5700	Sodium chloride 250 g		1

When an electron in the shell of an atom or atomic ion drops from an excited state with the energy E_2 to a state of lower energy E_1, it can emit a photon with the frequency

$$\nu = \frac{E_2 - E_1}{h}$$

h: Planck's constant

In the opposite case, a photon with the same frequency is absorbed. As the energies E_1 and E_2 can only assume discrete values, the photons are only emitted and absorbed at discrete frequencies. The totality of the frequencies which occur is referred to as the spectrum of the atom. The positions of the spectral lines are characteristic of the corresponding element.

The experiment P6.2.2.1 disperses the emission spectra of metal vapors and inert gases (mercury, sodium, cadmium and neon) using a high-resolution grating and projects these on the screen for comparison purposes.

In the experiment P6.2.2.2, the flame of a Bunsen burner is alternately illuminated with white light and sodium light and observed on a screen. When sodium is burned in the flame, a dark shadow appears on the screen when illuminating with sodium light. From this it is possible to conclude that the light emitted by a sodium lamp is absorbed by the sodium vapor, and that the same atomic components are involved in both absorption and emission.

Qualitative investigation of the absorption spectrum of sodium (P6.2.2.2)

Investigating the spectrum of a high pressure mercury lamp (P6.2.2.3)

EMISSION AND ABSORPTION SPECTRA

P6.2.2.3
Investigating the spectrum of a high pressure mercury lamp

Cat. No.	Description	P6.2.2.3
451 15	High pressure mercury lamp	1
451 195	Power supply unit for high-pressure mercury lamp	1
460 02	Lens in frame, f=50 mm	1
460 08	Lens in frame, f=150 mm	1
460 09	Lens in frame, f=300 mm	1
460 14	Adjustable slit	1
471 27	Holographic grating in frame	1
441 531	Screen	1
460 135	Ocular with scale	1
460 335	Optical bench with standardised profile, 0.5 m	1
460 32	Optical bench with standardised profile, 1 m	1
460 341	Swivel joint with circular scale	1
460 373	Optics rider, 60/50	1
460 374	Optics rider, 90/50	4
460 382	Tilting rider, 90/50	1

Spectral lines arise by the transistion of electrons from higher to lower energy states in the shell of excited atoms. The wavelength of the emitted light depends on this energy difference:

$$\Delta E = h \cdot \nu = \frac{h \cdot c}{\lambda}$$

The multiple energy states in the term scheme of mercury results in a large number of lines with different intensities (transition probabilities). These lines can be observed in the visible range respectively measured in the near UV range.

In the experiment P6.2.2.3 the spectral lines of a high pressure mercury lamp are investigated with a high-resolution spectrometer assembly using a holographic grating. The grating works in reflection, leading to a high intensity of the lines. Different lines are observed and their wavelengths determined, especially the yellow, green, blue, violet and also the ultraviolet line. Some lines are investigated closely, e.g. the yellow double line, and the splitting of the wavelengths is determined.

EMISSION AND ABSORPTION SPECTRA

P6.2.2.4
Recording the emission spectra of flame colouration

P6.2.2.5
Recording Fraunhofer lines with a compact spectrometer

P6.2.2.6
Recording the spectra of gas discharge lamps with a compact spectrometer

Recording the emission spectra of flame colouration (P6.2.2.4)

Cat. No.	Description	P6.2.2.4	P6.2.2.5	P6.2.2.6
467 251	Compact spectrometer, physics (spectral photometer)	1	1	1
460 251	Fibre holder	1	1*	1
300 11	Saddle base	1	1*	1
666 711	Butane gas burner	1		
666 712ET3	Butane cartridge, 190 g, set of 3	1		
666 731	Gas igniter, mechanical	1		
673 0840	Magnesia rods, 25 pieces	1		
604 5681	Powder spatula, steel, 150 mm	1		
667 089	Spotting tile	1		
661 088	Salts for flame tests, set of 9	1		
674 6950	Hydrochloric acid, 0.1 mol/l, 500 ml	1		
467 63	Spectral tube, Hg (with Ar)			1
467 67	Spectral tube, He			1
467 68	Spectral tube, Ar			1
467 69	Spectral tube, Ne			1
467 81	Holder for spectral tubes			1
521 70	High-voltage power supply, 10 kV			1
536 251	Measuring resistor, 100 kΩ			1
300 02	Stand base, V-shaped, small			1
300 40	Stand rod, 10 cm, 12 mm diam.			1
301 01	Leybold multiclamp			1
500 621	Safety connecting lead 50 cm, red			1
500 622	Safety connecting lead 50 cm, blue			1
500 611	Safety connecting lead, 25 cm, red			1
500 610	Safety connecting lead, 25 cm, yellow/green			1
	additionally required: PC with Windows XP/Vista/7/8/10 (x86 or x64)	1	1	1

* additionally recommended

When an electron in the shell of an atom or atomic ion drops from an excited state with the energy E_2 to a state of lower energy E_1, it can emit a photon with the frequency

$$\nu = \frac{E_2 - E_1}{h}$$

h: Planck's constant

In the opposite case, a photon with the same frequency is absorbed. As the energies E_1 and E_2 can only assume discrete values, the photons are only emitted and absorbed at discrete frequencies. The totality of the frequencies which occur is referred to as the spectrum of the atom. The positions of the spectral lines are characteristic of the corresponding element.

Spectral lines arise by the transistion of electrons from higher to lower energy states in the shell excited atoms. The wavelength of the emitted light depends on this energy difference:

$$\Delta E = h \cdot \nu = \frac{h \cdot c}{\lambda}$$

In the experiment P6.2.2.4 flame tests with metal salts are performed. A compact spectrometer at the USB port of a PC enables the easy recording of such transient processes and analyses the different emission lines. In contrast to classical observation with the eye, the spectrometer records also lines in the IR region, identifying potassium for example.

In the experiment P6.2.2.5 Fraunhofer absorption lines in the solar spectrum are recorded with a compact spectrometer. The presence of several elements in the solar photosphere is shown.

Experiment P6.2.2.6 records the spectra of gas discharge lamps using a compact spectrometer, which allows a very easy access to optical spectroscopy of gases.
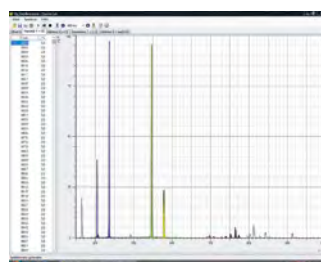
Spectra of gas discharge lamps (P6.2.2.6)

Franck-Hertz experiment with mercury - Recording with the oscilloscope (P6.2.4.1)

FRANCK–HERTZ EXPERIMENT

P6.2.4.1
Franck-Hertz experiment with mercury - Recording with the oscilloscope

P6.2.4.2
Franck-Hertz experiment with mercury - Recording and evaluation with CASSY

Cat. No.	Description	P6.2.4.1	P6.2.4.2
555 854	Hg Franck–Hertz tube	1	1
555 864	Socket for Hg Franck-Hertz tube, with DIN connector	1	1
555 81	Electric oven for tubes, 230 V	1	1
555 880	Franck-Hertz supply unit	1	1
666 193	Temperature probe, NiCr-Ni, 1.5 mm	1	1
575 304	Digital storage oscilloscope 70 MHz two-channel	1	
575 24	Screened cable, BNC/4 mm	2	
524 013	Sensor-CASSY 2		1
524 220	CASSY Lab 2		1
501 46	Connecting leads 19 A, 100 cm, red/blue, pair		2
	additionally required: PC with Windows XP/Vista/7/8/10 (x86 or x64)		1

In 1914, *J. Franck* and *G. Hertz* reported observing discontinuous energy emission when electrons passed through mercury vapor, and the resulting emission of the ultraviolet spectral line (λ = 254 nm) of mercury. A few months later, Niels Bohr recognized that their experiment supported his model of the atom.

This experiment is offered in two variations, experiments P6.2.4.1 and P6.2.4.2, which differ only in the means of recording and evaluating the measurement data. The mercury atoms are enclosed in a tetrode with cathode, grid-type control electrode, acceleration grid and target electrode. The control grid ensures a virtually constant emission current of the cathode. An opposing voltage is applied between the acceleration grid and the target electrode. When the acceleration voltage U between the cathode and the acceleration grid is increased, the target current I corresponds closely to the tube characteristic once it rises above the opposing voltage. As soon as the electrons acquire sufficient kinetic energy to excite the mercury atoms through inelastic collisions, the electrons can no longer reach the target, and the target current drops. At this acceleration voltage, the excitation zone is directly in front of the excitation grid. When the acceleration voltage is increased further, the excitation zone moves toward the cathode, the electrons can again accumulate energy on their way to the grid and the target current again increases. Finally, the electrons can excite the mercury atoms once more, the target current drops again, and so forth. The $I(U)$ characteristic thus demonstrates periodic variations, whereby the distance between the minima ΔU = 4.9 V corresponds to the excitation energy of the mercury atoms from the ground state $^1S_0$ to the first $^3P_1$ state.
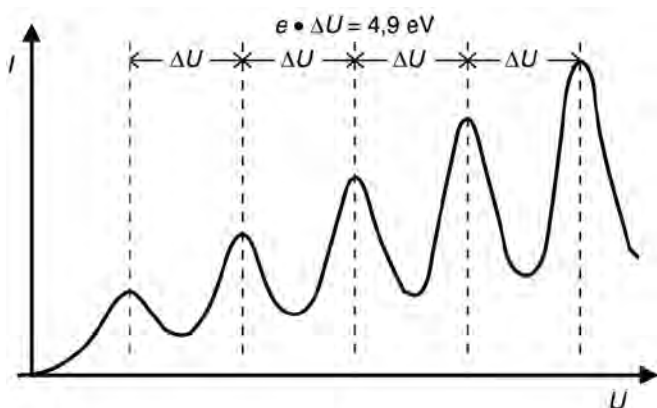
Franck-Hertz curve for mercury (P6.2.4.1)

CASSY®

FRANCK–HERTZ EXPERIMENT

P6.2.4.3
Franck-Hertz experiment with neon
- Recording with the oscilloscope

P6.2.4.4
Franck-Hertz experiment with neon
- Recording and evaluation
with CASSY

Franck-Hertz experiment with neon - Recording and evaluation with CASSY (P6.2.4.4)

Cat. No.	Description	P6.2.4.3	P6.2.4.4
555 870	Ne Franck-Hertz tube	1	1
555 871	Holder with socket and screen	1	1
555 872	Connecting cable for Ne Franck-Hertz tube	1	1
555 880	Franck-Hertz supply unit	1	1
575 304	Digital storage oscilloscope 70 MHz two-channel	1	
575 24	Screened cable, BNC/4 mm	2	
524 013	Sensor-CASSY 2		1
524 220	CASSY Lab 2		1
501 46	Connecting leads 19 A, 100 cm, red/blue, pair		2
	additionally required: PC with Windows XP/Vista/7/8/10 (x86 or x64)		1

When neon atoms are excited by means of inelastic electron collision at a gas pressure of approx. 10 hPa, excitation is most likely to occur to states which are 18.7 eV above the ground state. The de-excitation of these states can occur indirectly via intermediate states, with the emission of photons. In this process, the photons have a wavelength in the visible range between red and green. The emitted light can thus be observed with the naked eye and e.g. measured using the school spectroscope Kirchhoff/Bunsen (467 112).

The Franck-Hertz experiment with neon is offered in two variations, experiments P6.2.4.3 and P6.2.4.4, which differ only in the means of recording and evaluating the measurement data. In both variations, the neon atoms are enclosed in a glass tube with four electrodes: the cathode K, the grid-type control electrode G_1, the acceleration grid G_2 and the target electrode A. Like the Franck-Hertz experiment with mercury, the acceleration voltage U is continuously increased and the current I of the electrons which are able to overcome the opposing voltage between G_2 and A and reach the target is measured. The target current is always lowest when the kinetic energy directly in front of grid G_2 is just sufficient for collision excitation of the neon atoms, and increases again with the acceleration voltage. We can observe clearly separated luminous red layers between grids G_1 and G_2; their number increases with the voltage. These are zones of high excitation density, in which the excited atoms emit light in the visible spectrum.
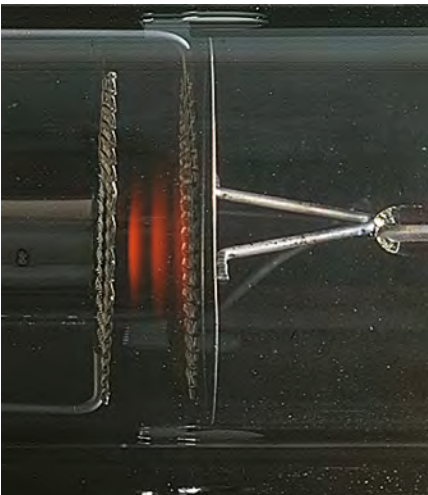
Luminous layers between control electrode and acceleration grid (P6.2.4.3-4)

CASSY®

ELECTRON SPIN RESONANCE

P6.2.6.2
Electron spin resonance at DPPH
– determinig the magnetic field as a function of the resonance frequency

P6.2.6.3
Resonance absorption of a passive RF oscillator circuit

Electron spin resonance at DPPH - determinig the magnetic field as a function of the resonance frequency (P6.2.6.2)

Cat. No.	Description	P6.2.6.2	P6.2.6.3
514 55	ESR basic unit	1	1
514 571	ESR supply unit	1	1
555 604	Pair of Helmholtz coils	1	
575 304	Digital storage oscilloscope 70 MHz two-channel	1	1
501 02	BNC cable, 1 m	2	
300 11	Saddle base	3	2
501 20	Connecting lead, 32 A, 25 cm, red	1	
501 25	Connecting lead, 32 A, 50 cm, red	1	
501 26	Connecting lead, 32 A, 50 cm, blue	1	
531 120	Multimeter LDanalog 20		1
575 24	Screened cable, BNC/4 mm		1
501 644	Two-way adapters, black, set of 6		1
590 13	Stand rod with bore holes		1

The magnetic moment of the unpaired electron with the total angular momentum j in a magnetic field assumes the discrete energy states

$$E_m = -g_j \cdot \mu_B \cdot m \cdot B \quad \text{where} \quad m = -j, -j+1, \ldots, j$$

$$\mu_B = 9.274 \cdot 10^{-24} \; \frac{J}{T} : \text{ Bohr's magneton}$$

g_j: g factor

When a high-frequency magnetic field with the frequency ν is applied perpendicularly to the first magnetic field, it excites transitions between the adjacent energy states when these fulfill the resonance condition

$$h \cdot \nu = E_{m+1} - E_m$$

h: Planck's constant

This fact is the basis for electron spin resonance, in which the resonance signal is detected using radio-frequency technology. The electrons can often be regarded as free electrons. The g-factor then deviates only slightly from that of the free electron ($g = 2.0023$), and the resonance frequency ν in a magnetic field of 1 mT is about 27.8 MHz. The actual aim of electron spin resonance is to investigate the internal magnetic fields of the sample substance, which are generated by the magnetic moments of the adjacent electrons and nuclei.

The experiment P6.2.6.2 verifies electron spin resonance in diphenylpicryl-hydrazyl (DPPH). DPPH is a radical, in which a free electron is present in a nitrogen atom. In the experiment, the magnetic field B which fulfills the resonance condition the resonance frequencies ν can be set in a continuous range from 13 to 130 MHz. The aim of the evaluation is to determine the g factor.

The object of the experiment P6.2.6.3 is to verify resonance absorption using a passive oscillator circuit.
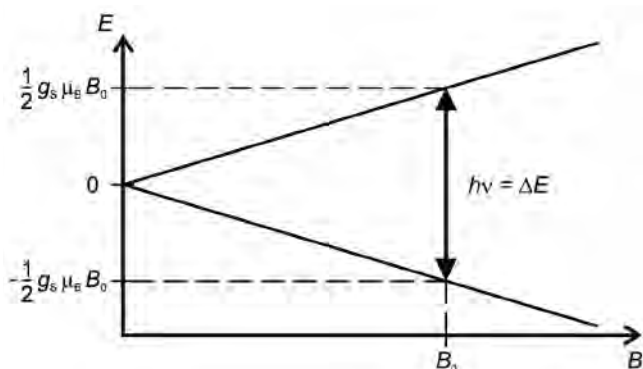
Diagram of resonance condition of free electrons (P6.2.6.2)

NORMAL ZEEMAN EFFECT

P6.2.7.3
Observing the normal Zeeman effect in transverse and longitudinal configuration - spectroscopy using a Fabry-Perot etalon

P6.2.7.4
Measuring the Zeeman splitting of the red cadmium line as a function of the magnetic field - spectroscopy using a Fabry-Perot etalon

Observing the normal Zeeman effect in transverse and longitudinal configuration - spectroscopy using a Fabry-Perot etalon (P6.2.7.3)

Cat. No.	Description	P6.2.7.3	P6.2.7.4
451 12	Spectral lamp, Cd, with holding plate	1	1
451 30	Universal choke, 230 V, 50 Hz	1	1
562 11	U-core with yoke	1	1
562 131	Coil, 480 turns, 10 A	2	2
560 315	Pole pieces with large bore, pair	1	1
521 551	AC/DC power supply 0...24 V/0...10 A	1	1
471 221	Fabry-Perot etalon mirror, in holder	1	1
460 08	Lens in frame, f=150 mm	2	2
472 601	Quarter-wavelength plate, 140 nm	1	
472 401	Polarisation filter	1	
468 41	Holder for interference filters	1	1
468 400	Interference filter, 644 nm	1	1
460 135	Ocular with scale	1	1
460 32	Optical bench with standardised profile, 1 m	1	1
460 381	Rider base with thread	1	1
460 373	Optics rider, 60/50	7	5
501 30	Connecting lead, 32 A, 100 cm, red	1	1
501 31	Connecting lead, 32 A, 100 cm, blue	2	2
662 1584	WEBCAM with USB 1080p		1
688 801	Stand rod with photo thread 1/4", 10 x 112.5 mm		1
460 374	Optics rider, 90/50		1
524 005W	Mobile-CASSY 2 WiFi		1
524 0381	Combi B sensor S		1
501 11	Extension cable, 15 pin		1
300 02	Stand base, V-shaped, small		1
300 42	Stand rod, 47 cm, 12 mm diam.		1
301 01	Leybold multiclamp		1
	additionally required: PC with Windows XP/Vista/7/8/10 (x86 or x64)		1

The Zeeman effect is the name for the splitting of atomic energy levels in an external magnetic field and, as a consequence, the splitting of the transitions between the levels. The effect was predicted by *H. A. Lorentz* in 1895 and experimentally confirmed by *P. Zeeman* one year later. In the red spectral line of cadmium (λ = 643.8 nm), Zeeman observed a line triplet perpendicular to the magnetic field and a line doublet parallel to the magnetic field, instead of just a single line. Later, even more complicated splits were discovered for other elements, and were collectively designated the anomalous Zeeman effect. It eventually became apparent that the normal Zeeman effect is the exception, as it only occurs at transitions between atomic levels with the total spin S = 0.

In the experiment P6.2.7.3, the Zeeman effect is observed at the red cadmium line perpendicular and parallel to the magnetic field, and the polarization state of the individual Zeeman components is determined. The observations are explained on the basis of the radiating characteristic of dipole radiation. The so-called π component corresponds to a Hertzian dipole oscillating parallel to the magnetic field, i.e. it cannot be observed parallel to the magnetic field and radiates linearly polarized light perpendicular to the magnetic field. Each of the two σ components corresponds to two dipoles oscillating perpendicular to each other with a phase differential of 90°. They radiate circularly polarized light in the direction of the magnetic field and linearly polarized light parallel to it.

In the experiment P6.2.7.4, the Zeeman splitting of the red cadmium line is measured as a function of the magnetic field B. The energy interval of the triplet components

$$\Delta E = \frac{h}{4\pi} \cdot \frac{e}{m_e} \cdot B$$

m_e: mass of electron, e: electron charge

h: Planck's constant

B: magnetic induction

is used to calculate the specific electron charge.
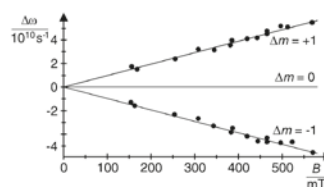
Zeeman splitting as a function of magnetic field (P6.2.7.2 + P6.2.7.4)

DETECTION OF X-RAYS

P6.3.1.1
Fluorescence of a luminescent screen due to X-rays

P6.3.1.2
X-ray photography: Exposure of film stock due to X-rays

P6.3.1.5
Investigation of an implant model

P6.3.1.6
Influence of a contrast medium on the absorption of X-rays

Investigation of an implant model (P6.3.1.5)

Cat. No.	Description	P6.3.1.1	P6.3.1.2	P6.3.1.5	P6.3.1.6
554 800	X-ray apparatus	1	1	1	1
554 861	X-ray tube, Mo	1	1	1	1
554 838	Film holder, X-ray		1	1	
554 895	X-ray film		1		
554 8391	Implant model			1	
554 839	Blood vessel model for contrast medium				1
602 023	Beaker, Boro 3.3, 150 ml, squat				1
602 295	Bottle brown glass wide treath with cap				1
602 783	Glass rod, 200 mm, diam. 6 mm				1
672 6610	Potassium iodide, 100 g				1

Soon after the discovery of X-rays by *W. C. Röntgen*, physicians began to exploit the ability of this radiation to pass through matter which is opaque to ordinary light for medical purposes. The technique of causing a luminescent screen to fluoresce with X-ray radiation is still used today for screen examinations, although image amplifiers are used additionally. The exposure of a film due to X-ray radiation is used both for medical diagnosis and materials testing, and is the basis for dosimetry with films.

The experiment P6.3.1.1 demonstrates the transillumination with X-rays using simple objects made of materials with different absorption characteristics. A luminescent screen of zinc-cadmium sulfate is used to detect X-rays; the atoms in this compound are excited by the absorption of X-rays and emit light quanta in the visible light range. This experiment investigates the effect of the emission current I of the X-ray tube on the brightness and the effect of the high voltage U on the contrast of the luminescent screen.

The experiment P6.3.1.2 records the transillumination of objects using X-ray film. Measuring the exposure time required to produce a certain degree of exposure permits quantitative conclusions regarding the intensity of the x-rays.

The experiment P6.3.1.5 demonstrates the use of radioscopy to detect hidden objects. A metal rod inside a block of wood is visually invisible, but can be seen by X-ray fluorescence and its dimensions measured.

The experiment P6.3.1.6 demonstrates the use of contrast medium. The radio-paque iodine solution is flowing through channels inside a plate and is clearly visible in the X-ray fluorescence image, but pure water is not.

Screen of the implant model (P6.3.1.5)

DETECTION OF X-RAYS

P6.3.1.3
Detecting X-rays using an ionization chamber

P6.3.1.4
Determining the ion dose rate of the X-ray tube with molydenum anode
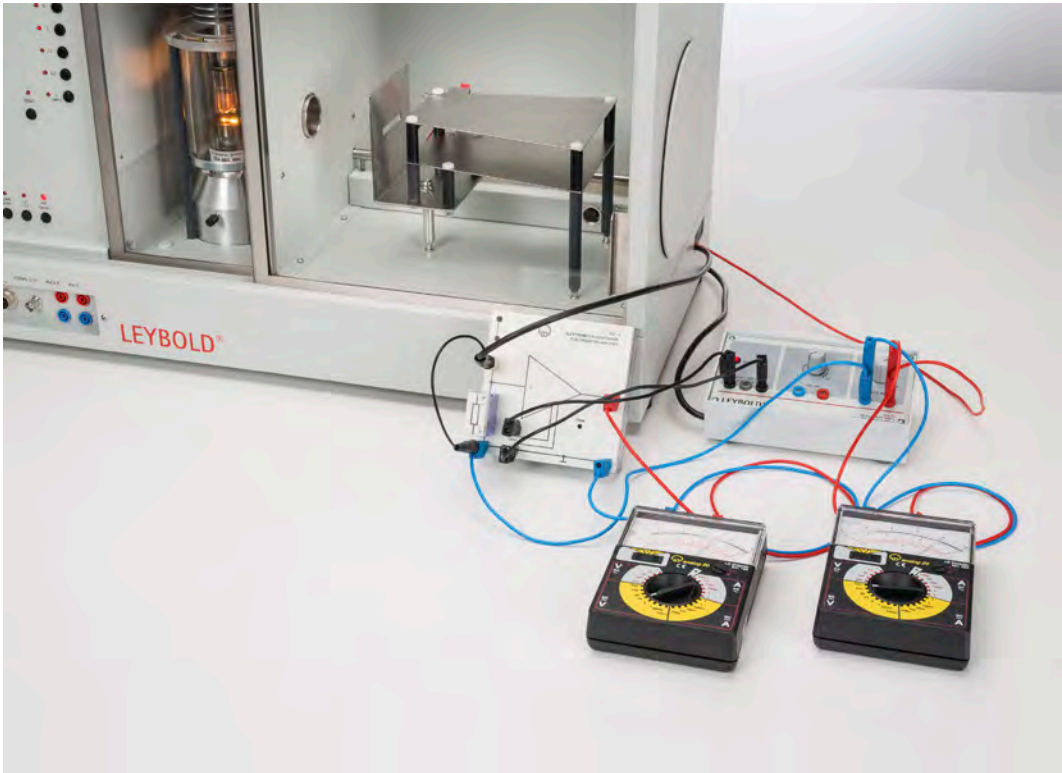
Detecting X-rays using an ionization chamber (P6.3.1.3)

Cat. No.	Description	P6.3.1.3-4
554 800	X-ray apparatus	1
554 861	X-ray tube, Mo	1
554 840	Plate capacitor, X-ray	1
522 27	Power supply, 450 V	1
532 14	Electrometer amplifier	1
577 02	Resistor, 1 GΩ, STE2/19	1
531 120	Multimeter LDanalog 20	2
575 24	Screened cable, BNC/4 mm	1
501 451	Connecting leads, 19 A, 50 cm, black, pair	1
501 46	Connecting leads 19 A, 100 cm, red/blue, pair	1
501 45	Connecting lead 19 A, 50 cm, red/blue, pair	2

As X-rays ionize gases, they can also be measured via the ionization current of an ionization chamber.

The aim of the experiments P6.3.1.3 and P6.3.1.4 is to detect X-rays using an ionization chamber. While experiment P6.3.1.3 focuses on the investigation of the saturation characteristics of the experimental setup, experiment P6.3.1.4 investigates the ion dose rate to quantify the effect of X-rays. The mean ion dose rate

$$\bar{J} = \frac{I_{ion}}{m}$$

is calculated from the ionization current I_{ion} which the X-radiation generates in the irradiated volume of air V, and the mass m of the irradiated air. The measurements are conducted for various emission currents I and high voltages U of the X-ray tube.
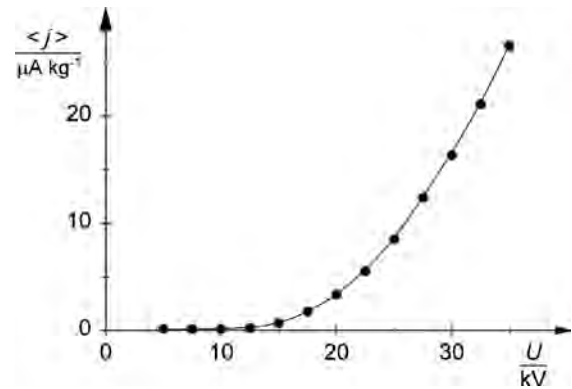
Mean ion dose rate j as a function of the tube high voltage U, I = 1.0 mA (P6.3.1.4)

Digital X-ray photography with the X-ray image sensor (P6.3.1.12)

DETECTION OF X–RAYS

P6.3.1.11
Digital X-ray photography with the computed tomography module

P6.3.1.12
Digital X-ray photography with the X-ray image sensor

Cat. No.	Description	P6.3.1.11	P6.3.1.12
554 800	X-ray apparatus	1	1
554 866	X-ray tube, Au	1	1
554 821	Computed tomography module	1	
554 838	Film holder, X-ray	1	
554 8382	Object holder X-ray 1	1	
554 834	Absorption accessory, X-ray	1	1
554 822	Test patterns, 2D	1	1
554 8281	X-ray image sensor		1
554 8291	Precision rail for X-ray image sensor		1
554 8292	Object holder X-ray 2		1
	additionally required: PC with Windows XP/Vista/7/8/10 (x86 or x64)	1	1

In X-ray radiography and image processing it is necessary to know the properties of the radiation source as well as the properties of the irradiated object. The minimum resolution in an image is determined by the size of the focal spot and the visbility of details in an image depends on the different attenuation properties of various materials and the radiation spectrum of the X-ray-source.

The experiment P6.3.1.11 measures the attenuation of X-rays through the quantitative analysis of a digital X-ray image on the computer, the contrast of a digital X-ray image as a function of the energy and intensity of x-radiation is measured and the resolution digital radiographs is determined using various test images.

The experiment P6.3.1.12 measures the attenuation of X-rays through the quantitative analysis of a digital X-ray image on the computer, the contrast of a digital X-ray image as a function of the energy and intensity of x-radiation is measured, the resolution digital radiographs is determined using various test images and the focal spot of the anode of the x-ray tube is measured by a simple geometric projection on the X-ray image sensor.
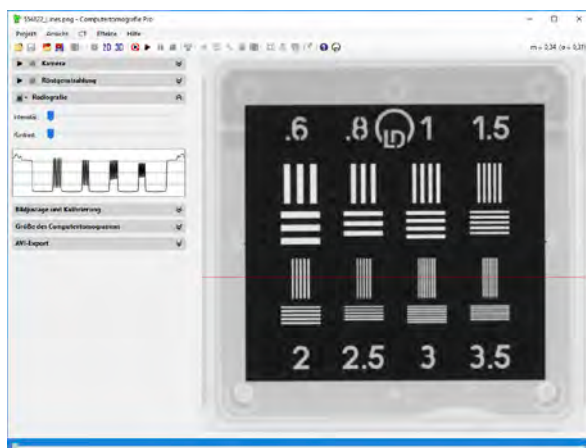
X-ray image of one of the testobjects (P6.3.1.12)

ATTENUATION OF X-RAYS

P6.3.2.1
Investigating the attenuation of X-rays as a function of the absorber material and absorber thickness

P6.3.2.2
Investigating the wavelength dependency of the attenuation coefficient

P6.3.2.3
Investigating the relationship between the attenuation coefficient and the atomic number Z

P6.3.2.4
Investigating the attenuation of X-rays as a function of distance
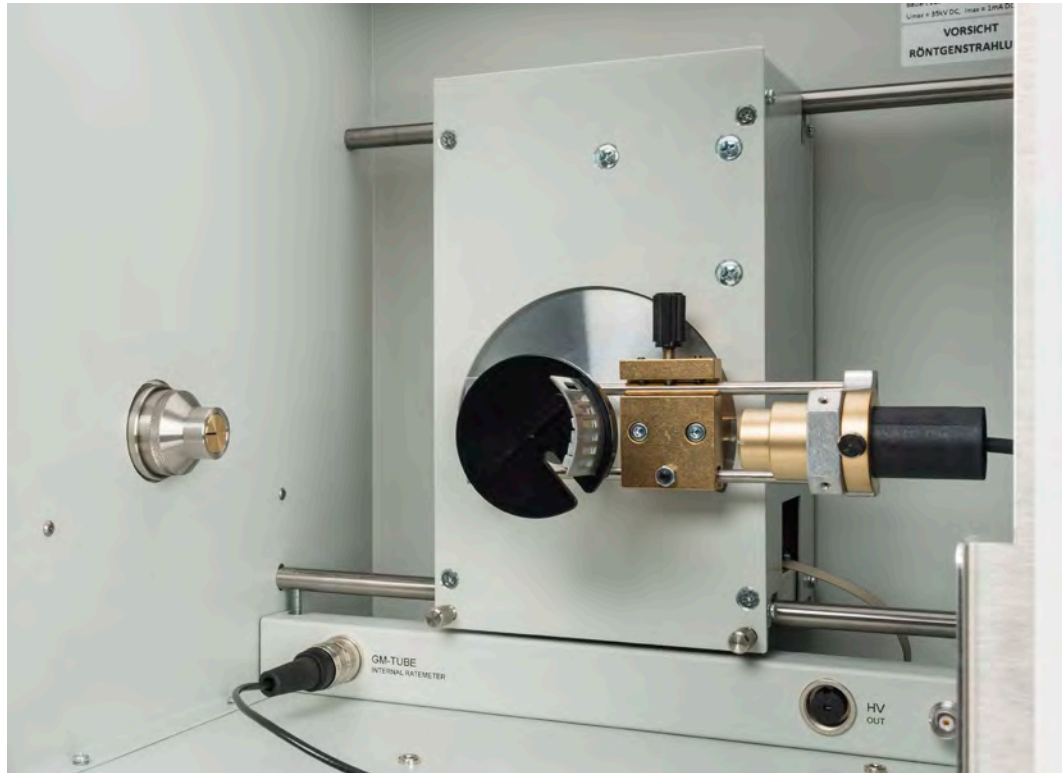
Investigating the attenuation of X-rays as a function of the absorber material and absorber thickness (P6.3.2.1)

Cat. No.	Description	P6.3.2.1	P6.3.2.2	P6.3.2.3	P6.3.2.4
554 800	X-ray apparatus	1	1	1	1
554 861	X-ray tube, Mo	1	1	1	
554 831	Goniometer	1	1	1	
559 01	End-window counter with cable for α, β, γ and X-rays	1	1	1	
554 834	Absorption accessory, X-ray	1			
554 78	NaCl crystal for Bragg reflection		1	1	
554 832	Set of absorber foils		1	1	
554 866	X-ray tube, Au				1
554 8281	X-ray image sensor				1
554 8291	Precision rail for X-ray image sensor				1
	additionally required: PC with Windows XP/Vista/7/8/10 (x86 or x64)	1			1

The attenuation of X-rays on passing through an absorber with the thickness d is described by Lambert's law for attenuation:

$$I = I_0 \cdot e^{-\mu d}$$

I_0: intensity of primary beam

I: transmitted intensity

Here, the attenuation is due to both absorption and scattering of the X-rays in the absorber. The linear attenuation coefficient μ depends on the material of the absorber and the wavelength λ of the X-rays. An absorption edge, i.e. an abrupt transition from an area of low absorption to one of high absorption, may be observed when the energy $h \cdot \nu$ of the X-ray quantum just exceeds the energy required to move an electron out of one of the inner electron shells of the absorber atoms.

The object of the experiment P6.3.2.1 is to confirm Lambert's law using aluminium and to determine the attenuation coefficients μ for six different absorber materials averaged over the entire spectrum of the X-ray apparatus.

The experiment P6.3.2.2 records the transmission curves

$$T(\lambda) = \frac{I(\lambda)}{I_0(\lambda)}$$

for various absorber materials. The aim of the evaluation is to confirm the λ^3 relationship of the attenuation coefficients for wavelengths outside of the absorption edges.

In the experiment P6.3.2.3, the attenuation coefficient μ(λ) of different absorber materials is determined for a wavelength λ which lies outside of the absorption edge. This experiment reveals that the attenuation coefficient is closely proportional to the fourth power of the atomic number Z of the absorbers.

In the experiment P6.3.2.4 the intensity of th X-radiation is measured at different distances from the X-ray tube. The inverse square distance law is confirmed.
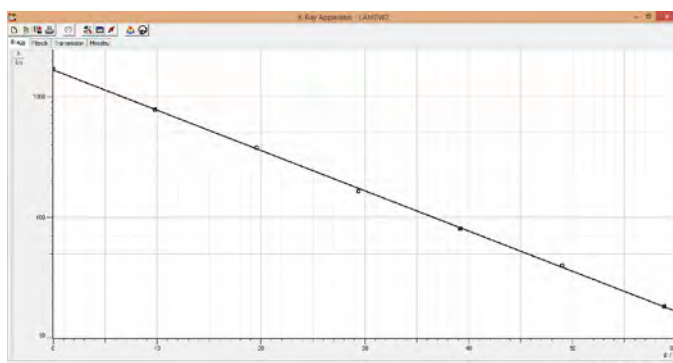
Investigating the attenuation of X-rays as a function of the absorber thickness (P6.3.2.1)

Investigating the energy spectrum of an X-ray tube as a function of the high voltage and the emission current (P6.3.3.2)
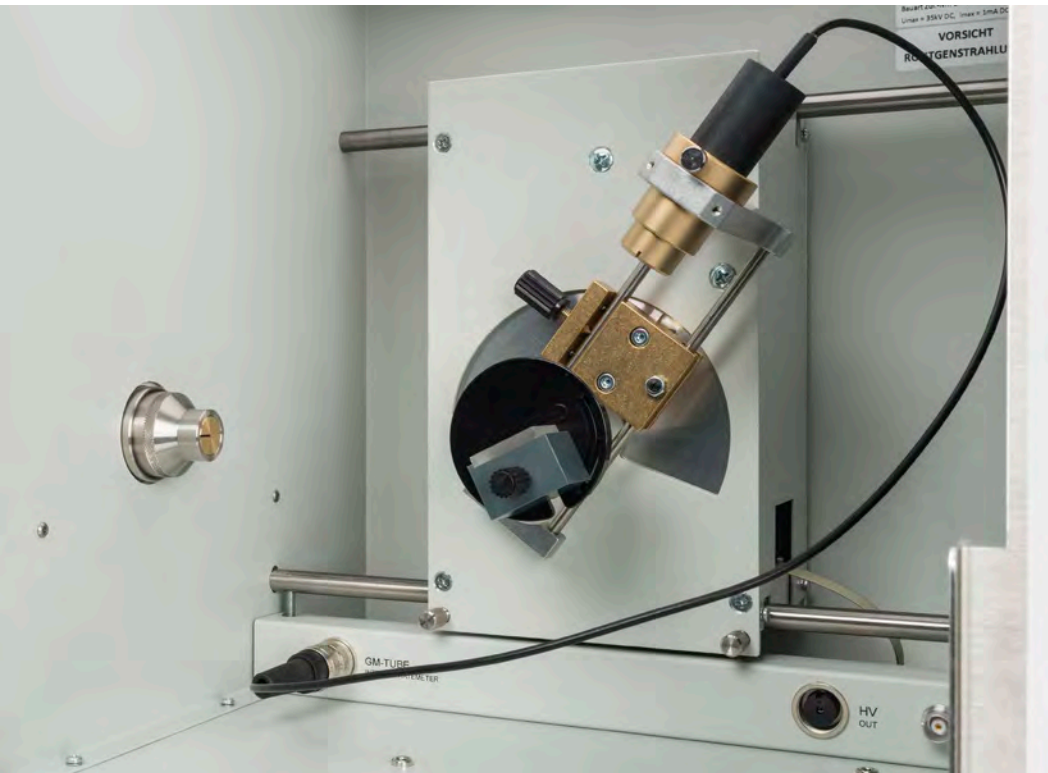
PHYSICS OF THE ATOMIC SHELL

P6.3.3.1
Bragg reflection: diffraction of X-rays at a monocrystal

P6.3.3.2
Investigating the energy spectrum of an X-ray tube as a function of the high voltage and the emission current

P6.3.3.3
Duane-Hunt relation and determination of Planck's constant

P6.3.3.5
Edge absorption: filtering X-rays

P6.3.3.6
Moseley's law and determination of the Rydberg constant

Cat. No.	Description	P6.3.3.1-3	P6.3.3.5	P6.3.3.6
554 801	X-ray apparatus, Mo, complete	1	1	1
559 01	End-window counter with cable for α, β, γ and X-rays	1	1	1
554 832	Set of absorber foils			1
	additionally required: PC with Windows XP/Vista/7/8/10 (x86 or x64)	1	1	*1*

The radiation of an X-ray tube consists of two components: continuous bremsstrahlung radiation is generated when fast electrons are decelerated in the anode. Characteristic radiation consisting of discrete lines is formed by electrons dropping to the inner shells of the atoms of the anode material from which electrons were liberated by collision.

To confirm the wave nature of X-rays, the experiment P6.3.3.1 investigates the diffraction of the characteristic K_α and K_β lines of the molybdenum anode at an NaCl monocrystal and explains these lines using Bragg's law of reflection.

The experiment P6.3.3.2 records the energy spectrum of the X-ray apparatus as a function of the high voltage and the emission current using a goniometer in the Bragg configuration. The aim is to investigate the spectral distribution of the continuum of bremsstrahlung radiation and the intensity of the characteristic lines.

The experiment P6.3.3.3 measures how the limit wavelength λ_{min} of the continuum of bremsstrahlung radiation depends on the high voltage U of the X-ray tube. When we apply the Duane-Hunt relationship

$$e \cdot U = h \cdot \frac{c}{\lambda_{min}}$$

e: electron charge
c: velocity of light

to the measurement data, we can derive Planck's constant h.

The object of the experiment P6.3.3.5 is to filter X-rays using the absorption edge of an absorber, i. e. the abrupt transition from an area of low absorption to one of high absorption.

The experiment P6.3.3.6 determines the wavelengths l_K of the absorption edges as as function of the atomic number Z. When we apply Moseley's law

$$\frac{1}{\lambda_K} = R \cdot (Z - \sigma)^2$$

to the measurement data we obtain the Rydberg constant R and the mean screening σ.
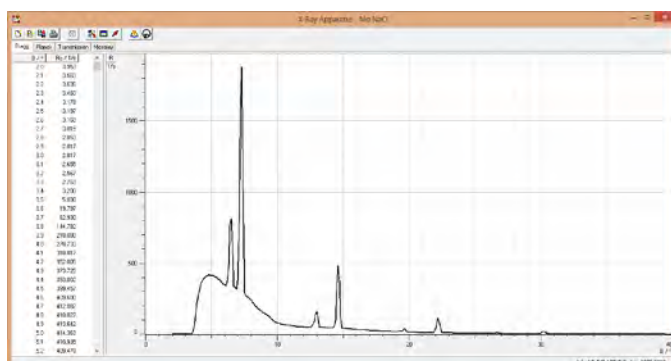
Bragg spectrum of a molybdenum anode (P6.3.3.1)

X-RAY ENERGY SPECTROSCOPY

P6.3.5.1
Recording and calibrating an X-ray energy spectrum

P6.3.5.2
Recording the energy spectrum of a molybdenum anode

P6.3.5.3
Recording the energy spectrum of a copper anode

P6.3.5.4
Investigation of the characteristic spectra as a function of the element's atomic number: K-lines

P6.3.5.5
Investigation of the characteristic spectra as a function of the element's atomic number: L-lines

P6.3.5.6
Energy-resolved Bragg reflection in different orders of diffraction

Recording and calibrating an X-ray energy spectrum (P6.3.5.1)

Cat. No.	Description	P6.3.5.1-2	P6.3.5.3	P6.3.5.4	P6.3.5.5	P6.3.5.6
554 800	X-ray apparatus	1	1	1	1	1
554 861	X-ray tube, Mo	1		1	1	
554 831	Goniometer	1	1	1	1	1
559 938	X-ray energy detector	1	1	1	1	1
524 013	Sensor-CASSY 2	1	1	1	1	1
524 220	CASSY Lab 2	1	1	1	1	1
524 058	MCA box	1	1	1	1	1
501 02	BNC cable, 1 m	1	1	1	1	1
554 862	X-ray tube, Cu		1			1
554 844	Set of targets for K-line fluorescence			1		
554 846	Set of targets for L-line fluorescence				1	
554 78	NaCl crystal for Bragg reflection					1
	additionally required:\nPC with Windows XP/Vista/7/8/10 (x86 or x64)	1	1	1	1	1

The X-ray energy detector enables recording of the energy spectrum of X-rays. The detector is a Peltier-cooled photodiode where in the incoming X-rays produce electron-hole pairs. The number of electron-hole pairs and thus the voltage pulse height after amplification is proportional to the X-ray energy. The pulse height analysis is carried out with CASSY used as a multichannel analyzer (MCA-Box), which is connected to a computer (PC).

The object of the experiment P6.3.5.1 is to record the X-ray fluorescence spectrum of a target and to use the known energies for calibration of the energy axis. The target is made of a zincplated steel and emits several fluorescent lines.

The experiments P6.3.5.2 and P6.3.5.3 use the calibrated detector to record emission spectra of either a molybdenum anode or a copper anode. The resulting spectrum shows the characteristic lines of the anode material and the bremsstrahlung continuum.

The experiment P6.3.5.4 demonstrates differences in the characteristic fluorescent K-lines (transitions to K-shell) within the X-ray spectra of different elements. These are used to confirm Moseley's law and show aspects of material analysis.

The experiment P6.3.5.5 shows similar characteristic fluorescent L-lines for heavier elements, demonstrating the X-ray emission from transitions to the L-shell.

In the experiment P6.3.5.6 using the X-ray energy detector in Bragg geometry it is possible to observe different X-ray energies simultaneously, because Bragg condition is fulfilled for different orders.
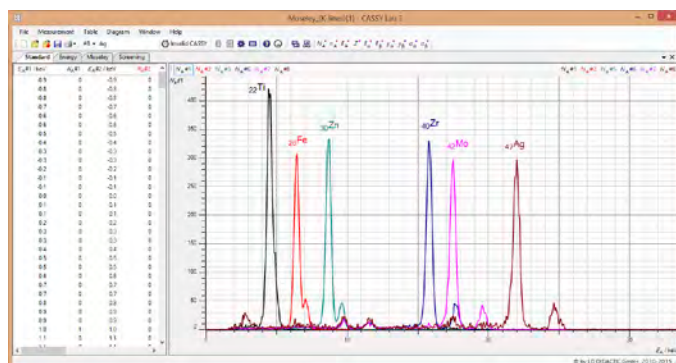
X-ray flourescence of different elements (P6.3.5.4/5)

Fine structure of the characteristic X-ray radiation of a molybdenum anode (P6.3.6.1)

STRUCTURE OF X-RAY SPECTRUMS

P6.3.6.1
Fine structure of the characteristic X-ray radiation of a molybdenum anode

P6.3.6.2
Fine structure of the characteristic X-ray radiation of a copper anode

P6.3.6.3
Fine structure of the characteristic X-ray radiation of an iron anode

P6.3.6.4
Fine structure of the characteristic X-ray radiation of a silver anode

P6.3.6.5
Fine structure of the characteristic X-ray radiation of a tungsten anode

P6.3.6.6
Determining the binding energy of individual subshells by selective excitation

P6.3.6.7
Fine structure of the characteristic X-ray radiation of a gold anode

Cat. No.	Description	P6.3.6.1	P6.3.6.2	P6.3.6.3	P6.3.6.4	P6.3.6.5-6	P6.3.6.7
554 800	X-ray apparatus	1	1	1	1	1	1
554 861	X-ray tube, Mo	1					
554 831	Goniometer	1	1	1	1	1	1
554 78	NaCl crystal for Bragg reflection	1			1		
559 01	End-window counter with cable for α, β, γ & X-rays	1	1	1	1	1	1
554 862	X-ray tube, Cu		1				
554 791	KBr crystal for Bragg reflection		1				
554 863	X-ray tube, Fe			1			
554 77	LiF crystal for Bragg reflection			1		1	1
554 865	X-ray tube, Ag				1		
554 864	X-ray tube, W					1	
554 866	X-ray tube, Au						1
	additionally required: PC with Windows XP/Vista/7/8/10 (x86 or x64)	1	1	1	1	1	1

The structure and fine-structure of X-ray spectra gives valuable Information on the position of the atomic energy levels. The systematics of X-ray transitions are presented. Starting with molybdenum and completed with other anode materials like copper and iron the K-shell transitions of light and medium elements are investigated.

In contrast to these materials the heavy elements like tungsten show characteristic emission from the L-shell with a lot of details, because the lower level of the transition consits of several sublevels which can also be selectively excited.

The experiment P6.3.6.1 investigates the X-ray spectrum of a molybdenum anode and the fine structure of the K_α line.

The experiments P6.3.6.2 and P6.3.6.3 observe the low-energy characteristic radiation from a copper or iron anode and the fine structure of the K_α line.

The experiment P6.3.6.4 observes the high-energy characteristic radiation of silver and the fine structure splitting due to spin-orbit coupling.

The experiment P6.3.6.5 demonstrates the fine structure of the tungsten L-lines. Due to the splitting of the energy levels there are approximately 11 transitions visible (L_α1-2, L_β1-4, L_γ1-3, L_l, L_v), which can be used to evaluate the position of the energy levels and to demonstrate allowed and forbidden transitions.

In addition to experiment P6.3.6.5, the experiment P6.3.6.6 measures directly the splitting of the L-shell. At a low acceleration voltage only the L3 level can be exited, with raising voltages transitions to L2 and later L1 become observable. The absolute binding energies of the L-sublevels can be measured directly.

The experiment P6.3.6.7 demonstrates the fine structure of the gold L-lines. Due to the splitting of the energy levels there are approximately 10 transitions visible (L_α1-2, L_β1-4, L_γ1-3, L_l, L_v), which can be used to evaluate the position of the energy levels and to demonstrate allowed and forbidden transitions.
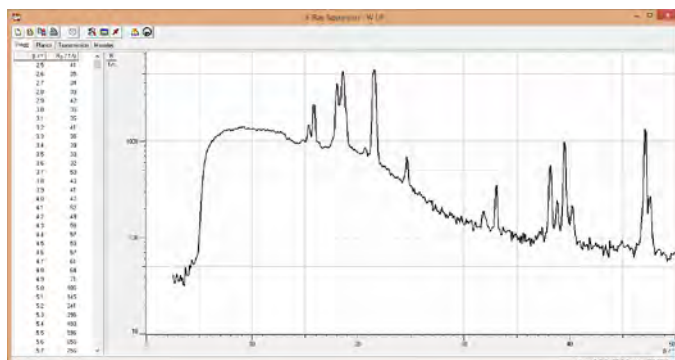
Bragg spectrum of the tungsten anode (P6.3.6.5)

STRUCTURE OF X-RAY SPECTRUMS

P6.3.6.11
High-resolution fine structure of the characteristic X-ray radiation of a molybdenum anode

P6.3.6.12
High-resolution fine structure of the characteristic X-ray radiation of a copper anode

P6.3.6.13
High-resolution fine structure of the characteristic X-ray radiation of an iron anode

P6.3.6.14
High-resolution fine structure of the characteristic X-ray radiation of a silver anode

P6.3.6.15
High-resolution fine structure of the characteristic X-ray radiation of a tungsten anode

P6.3.6.17
High-resolution fine structure of the characteristic X-ray radiation of a gold anode

High-resolution fine structure of the characteristic X-ray radiation of a molybdenum anode (P6.3.6.11)

Cat. No.	Description	P6.3.6.11	P6.3.6.12	P6.3.6.13	P6.3.6.14	P6.3.6.15	P6.3.6.17
554 800	X-ray apparatus	1	1	1	1	1	1
554 861	X-ray tube, Mo	1					
554 831	Goniometer	1	1	1	1	1	1
554 835	HD Accessory, X-ray	1	1	1	1	1	1
554 78	NaCl crystal for Bragg reflection	1			1		
559 01	End-window counter with cable for α, β, γ & X-rays	1	1	1	1	1	1
554 862	X-ray tube, Cu		1				
554 77	LiF crystal for Bragg reflection		1	1		1	1
554 863	X-ray tube, Fe			1			
554 865	X-ray tube, Ag				1		
554 864	X-ray tube, W					1	
554 866	X-ray tube, Au						1
	additionally required: PC with Windows XP/Vista/7/8/10 (x86 or x64)	1	1	1	1	1	1

The structure and fine-structure of X-ray spectra gives valuable Information on the position of the atomic energy levels. The systematics of X-ray transitions are presented. Starting with molybdenum and completed with other anode materials like copper and iron the K-shell transitions of light and medium elements are investigated.

In contrast to these materials the heavy elements like tungsten show characteristic emission from the L-shell with a lot of details, because the lower level of the transition consits of several sublevels which can also be selectively excited.

The resolution of the X-ray spectra can be improved by using narrower slits in the collimator and detector. In conjunction with a goniometer that can handle smaller step sizes, the fine structure of the X-ray spectra can be resolved in a lower diffraction order, which saves time and enables such measurements in a given time.

The use of slits of different widths also allows investigations of the intensity of the atomic line radiation compared to the intensity of the continuum due to bremsstrahlung of the electrons.

The experiment P6.3.6.11 investigates the high-resolution X-ray spectrum of a molybdenum anode and the fine structure of the K_a line.

The experiments P6.3.6.12 and P6.3.6.13 observe the low-energy characteristic radiation from a copper or iron anode and the high-resolution fine structure of the K_α line.

The experiment P6.3.6.14 observes the high-energy characteristic radiation of silver and the high-resolution fine structure splitting due to spin-orbit coupling.

The experiment P6.3.6.15 demonstrates the high-resolution fine structure of the tungsten L-lines. Due to the splitting of the energy levels there are approximately 10 transitions visible (L_α1-2, L_β1-5, L_γ1-3), which can be used to evaluate the position of the energy levels and to demonstrate allowed and forbidden transitions.

The experiment P6.3.6.17 demonstrates the fine structure of the gold L-lines. Due to the splitting of the energy levels there are approximately 10 transitions visible (L_α1-2, L_β1-4, L_γ1-3, L_l, L_v), which can be used to evaluate the position of the energy levels and to demonstrate allowed and forbidden transitions.
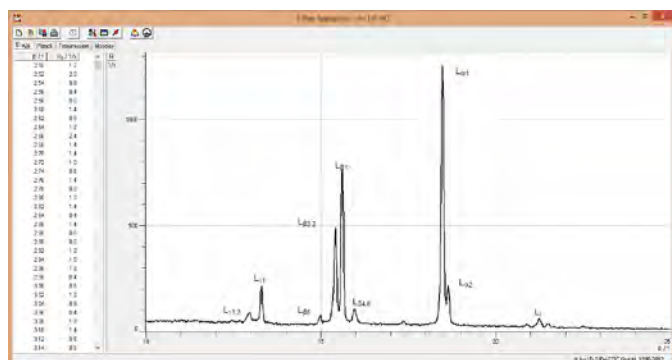
High resolution Bragg spectrum of a gold anode (P6.3.6.17)

Compton effect: Measurement the energy of the scattered photons as a function of the scattering angle (P6.3.7.2)

COMPTON EFFECT AT X–RAYS

P6.3.7.1
Compton effect: verifying the energy loss of the scattered X-ray quantum

P6.3.7.2
Compton effect: Measurement the energy of the scattered photons as a function of the scattering angle

Cat. No.	Description	P6.3.7.1	P6.3.7.2
554 800	X-ray apparatus	1	1
554 861	X-ray tube, Mo	1	1
554 831	Goniometer	1	1
559 01	End-window counter with cable for α, β, γ and X-rays	1	
554 836	Compton accessory, X-ray	1	
554 8371	Compton accessory, X-ray II		1
559 938	X-ray energy detector		1
524 013	Sensor-CASSY 2		1
524 058	MCA box		1
524 220	CASSY Lab 2		1
501 02	BNC cable, 1 m		1
	additionally required: PC with Windows XP/Vista/7/8/10 (x86 or x64)		1

At a time (early 1920's) when the particle nature of light (photons) suggested by the photoelectric effect was still being debated, the Compton experiment, the scattering of X-rays on weakly bound electrons, in 1923 gave another evidence of particle–like behaviour of X-rays in this process. Compton investigated the scattering of X-rays passing through matter. According to classical physics the frequency of the radiation should not be changed by the scattering process. However, *A. H. Compton* observed a frequency change for scattered X-rays. He interpreted this in the particle model as a collision of the X-ray photon and an electron of the scattering material. Assuming total energy and momentum to be conserved, energy is transferred from the photon to the electron, so the energy of the scattered photon depends on the scattering angle ϑ.

The experiment P6.3.7.1 verifies the Compton shift using the endwindow counter. The change of frequency or wavelength due to the scattering process is apparent as a change of the attenuation of an absorber, which is placed either in front of or behind the scattering body.

The object of the experiment P6.3.7.2 is to record directly the energy spectra of the scattered X-rays with the X-ray energy detector as a function of the scattering angle ϑ. The energy $E(\vartheta)$ of the scattered photons at different angles is determined and compared with the calculated energy obtained from conservation of energy and momentum by using the relativistic expression for the energy:

$$E(\vartheta) = \frac{E_0}{1 + \frac{E_0}{m \cdot c^2} \cdot (1 - \cos\vartheta)}$$

E_0: energy of the photon before the collision

m: mass of electron at rest

c: velocity of light
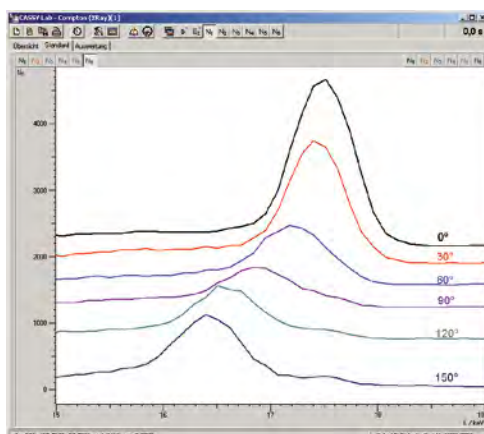
Energy shift of the scattered X-rays at different angeles (P6.3.7.2)

X-RAY TOMOGRAPHY

P6.3.8.1
Measurement and presentation of a computed tomogram with the computed tomography module

P6.3.8.2
Computed tomography of simple geometrical objects with the computed tomography module

P6.3.8.3
Medical basics of computed tomography with the computed tomography module

P6.3.8.4
Determining absorption coefficients and Hounsfield units with computed tomography with the computed tomography module

P6.3.8.5
Computed tomography of biological samples with the computed tomography module

Measurement and presentation of a computed tomogram with the computed tomography module (P6.3.8.1)

Cat. No.	Description	P6.3.8.1	P6.3.8.2–4	P6.3.8.5
554 800	X-ray apparatus	1	1	1
554 831	Goniometer	1	1	1
554 866	X-ray tube, Au	1	1	1
554 821	Computed tomography module	1	1	1
554 823	Phantom, 3D		1	
554 825	LEGO® adapter		1	
	additionally required: PC with Windows XP/Vista/7/8/10 (x86 or x64)	1	1	1

In 1972 the first computed tomographic scanner was built by Godfrey Hounsfield who, together with Allan Cormack, was awarded the Nobel Prize in Physiology or Medicine in 1979. The basic idea of computed tomography (CT) is the illumination of an object by X-rays from numerous different angles. Our educational X-ray apparatus allows the illumination of objects by X-rays. The resulting 2D-projections are visualised at the fluorescence screen or with the X-ray image sensor.

By turning an object using the built-in goniometer of the X-ray apparatus, and recording the 2D-projections from each angular step, the computer can reconstruct the object illuminated by X-rays. Our e-learning software visualises the back projection (necessary for reconstructing the computed tomography) concurrently with the scanning process. The 3D-model is then displayed on the PC screen.

Experiment P6.3.8.1 discusses the basics of computed tomography. The computed tomographies of simple geometrical objects are recorded and displayed.

Experiment P6.3.8.2 shows the CT of simple geometrical objects to demonstrate the basic properties and the resolution power of tomography.

Experiment P6.3.8.3 shows the CT of medical related objects to demonstrate the basic properties of tomography and to investigate possible problems with artefacts and image errors.

Experiment P6.3.8.4 analyses the absorption coefficient of water inside a plastic body to demonstrate the capabilities of CT in distinguishing different kinds of tissues and to calibrate Hounsfield units and it discusses hardening effects of the X-rays.

Experiment P6.3.8.5 analyses the CT of real biological specimens and applies to the results of the previous experiments.
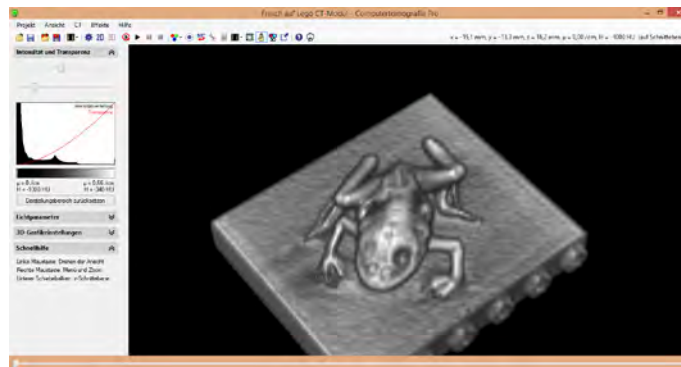
This small frog has a length of about 3.5 cm and was econstructed with a resolution of 0.3 mm (P6.3.8.5).
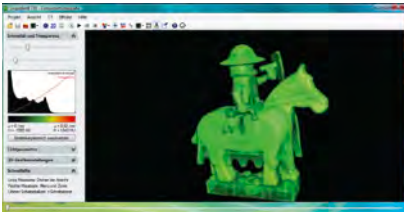
Computed tomography of a Lego figure (P6.3.8.2)

X–RAY TOMOGRAPHY

P6.3.8.11
Measurement and presentation of a computed tomogram with the X-ray image sensor

P6.3.8.12
Computed tomography of simple geometrical objects with the X-ray image sensor

P6.3.8.13
Medical basics of computed tomography with the X-ray image sensor

P6.3.8.14
Determining absorption coefficients and Hounsfield units with computed tomography with the X-ray image sensor

P6.3.8.15
Computed tomography of biological samples with the X-ray image sensor

Measurement and presentation of a computed tomogram with the X-ray image sensor (P6.3.8.11)

Cat. No.	Description	P6.3.8.11	P6.3.8.12–4	P6.3.8.15
554 800	X-ray apparatus	1	1	1
554 831	Goniometer	1	1	1
554 866	X-ray tube, Au	1	1	1
554 820P1	Computed Tomography Pro package	1	1	1
554 823	Phantom, 3D		1	
	additionally required: PC with Windows XP/Vista/7/8/10 (x86 or x64)	1	1	1

Experiment P6.3.8.11 discusses the basics of computed tomography. The computed tomographies of simple geometrical objects are recorded and displayed.

Experiment P6.3.8.12 shows the CT of simple geometrical objects to demonstrate the basic properties and the resolution power of tomography.

Experiment P6.3.8.13 shows the CT of medical related objects to demonstrate the basic properties of tomography and to investigate possible problems with artefacts and image errors.

Experiment P6.3.8.14 analyses the absorption coefficient of water inside a plastic body to demonstrate the capabilities of CT in distinguishing different kinds of tissues and to calibrate Hounsfield units and it discusses hardening effects of the X-rays.

Experiment P6.3.8.15 analyses the CT of real biological specimens and applies to the results of the previous experiments.
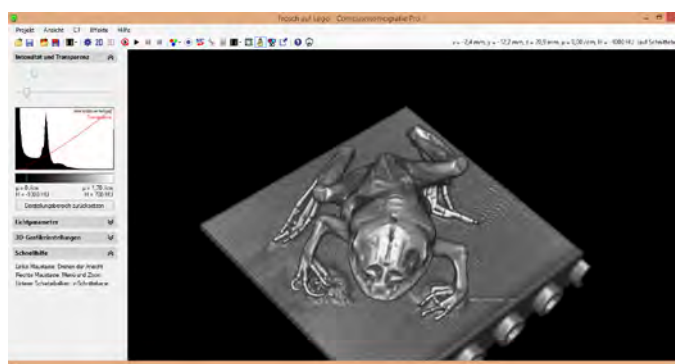
The same frog as shown on the previous page, but using the PRO image sensor the resolution is improved to 0.05 mm and the noise is significantly reduced (P6.3.8.15).
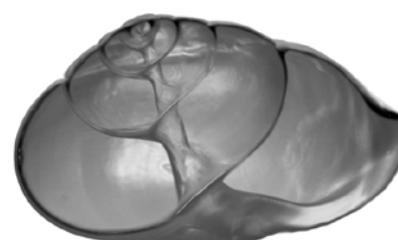
High-resolution computed tomograms of a snail shell

DETECTING RADIOACTIVITY

P6.4.1.4
Recording the characteristic of
a Geiger-Müller (end-window)
counter tube

Cat. No.	Description	P6.4.1.4
559 01	End-window counter with cable for α, β, γ</FONT> and X-rays	1
559 436	Ra 226 preparation, 5 kBq	1
524 005W	Mobile-CASSY 2 WiFi	1
524 440	GM adapter M	1
590 13	Stand rod with bore holes	1
591 21	Clip plug, large	1
532 16	Connecting rod	1
300 11	Saddle base	2

In 1895, *H. Becquerel* discovered radioactivity while investigating uranium salts. He found that these emitted a radiation which was capable of fogging light-sensitive photographic plates even through black paper. He also discovered that this radiation ionizes air and that it can be identified by this ionizing effect.

The experiment P6.4.1.4 records the count rate vs voltage characteristic of a Geiger-Müller counter tube. The count rate increases with the voltage for low voltage values, before reaching a saturation value (Plateau) which depends on the intensity or distance of the source.
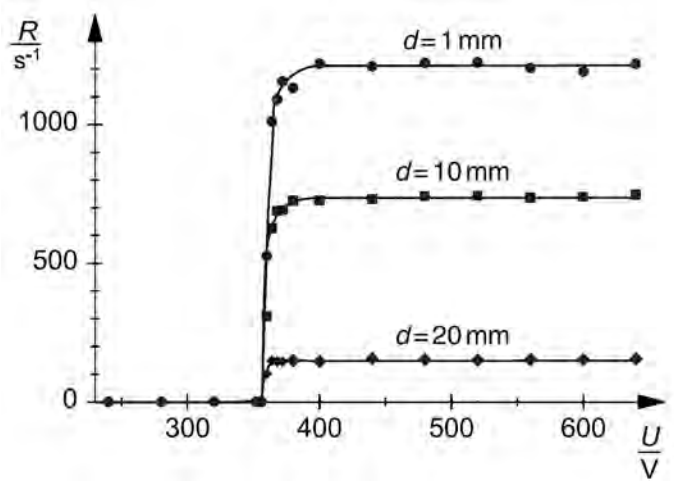
Characteristics of the counter tube (counting rate *R* as a function of the counter tube voltage *U*) at three different distances *d* between preparation and counter tube (P6.4.1.4).

WWW.LD-DIDACTIC.COM

CASSY®

POISSON DISTRIBUTION

P6.4.2.1
Statistical variations in determining counting rates

Statistical variations in determining counting rates (P6.4.2.1)

Cat. No.	Description	P6.4.2.1
524 013	Sensor-CASSY 2	1
524 220	CASSY Lab 2	1
524 0331	Geiger-Müller counter tube S	1
559 835	Radioactive preparations, set of 3	1
591 21	Clip plug, large	1
590 02	Small clip plug	1
532 16	Connecting rod	2
300 11	Saddle base	1*
587 07	Tweeter	1*
501 45	Connecting lead 19 A, 50 cm, red/blue, pair	1*
	additionally required: PC with Windows XP/Vista/7/8/10 (x86 or x64)	1

* additionally recommended

For each individual particle in a radioactive source, chance determines whether it will decay. The probability that any particular particle will decay in this time period is extremely low. The number of particles n which will decay over time Δt thus shows a Poisson distribution around the mean value µ. In other words, the probability that n decays will occur over a given time period Δt is

$$W_\mu(n) = \frac{\mu^n}{n!} e^{-\mu}$$

µ is proportional to the size of the preparation and the time Δt, and inversely proportional to the half-life $T_{1/2}$ of the radioactive decay.

Using the CASSY system, the experiment P6.4.2.1 determines multiple pulse counts n triggered in a Geiger-Müller counter tube by radioactive radiation over a selectable gate time Δt. After a total of N counting runs, the frequencies $h(n)$ are determined at which precisely n pulses were counted, and displayed as histograms. For comparision, the evaluation program calculates the mean value µ and the standard deviation

$$\sigma = \sqrt{\mu}$$

of the measured intensity distribution $h(n)$ as well as the Poisson distribution $w_\mu(N)$. For higher mean values µ the Poisson distribution develops into a Gaussian distribution.
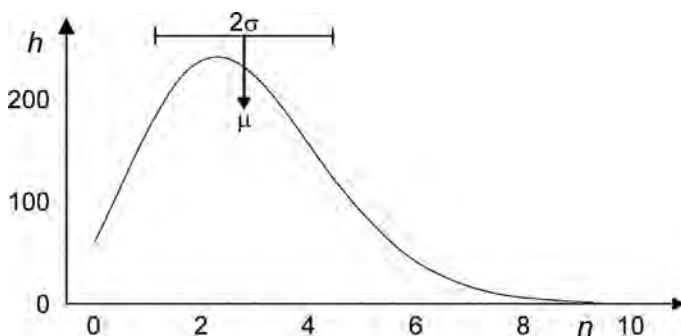
Measured and calculated Poisson distribution Histogram: $h(n)$, curve: $N \cdot wB(n)$ (P6.4.2.1)

LEYBOLD®
219
CASSY®

RADIOACTIVE DECAY AND HALF-LIFE

P6.4.3.3
Determining the half-life of Cs-137 - Point-by-point recording of a decay curve

P6.4.3.4
Determination of half-life of Cs-137 - Recording and evaluating the decay and production curve with CASSY

Determination of half-life of Cs-137 - Recording and evaluating the decay and production curve with CASSY (P6.4.3.4)

Cat. No.	Description	P6.4.3.3	P6.4.3.4
559 815OZ	Cs/Ba 137 m isotope generator 370 kBq	1	1
559 01	End-window counter with cable for α, β, γ and X-rays	1	
524 440	GM adapter M	1	
524 005W	Mobile-CASSY 2 WiFi	1	
300 02	Stand base, V-shaped, small	1	1
300 42	Stand rod, 47 cm, 12 mm diam.	1	1
301 01	Leybold multiclamp	2	4
666 555	Universal clamp 0...80 mm	2	4
664 043	Test tubes, Fiolax, 16 x 160 mm, set of 10	1	1
664 103	Beaker, DURAN, 250 ml, squat	1	1
524 013	Sensor-CASSY 2		1
524 220	CASSY Lab 2		1
524 0331	Geiger-Müller counter tube S		2
	additionally required: PC with Windows XP/Vista/7/8/10 (x86 or x64)		1

Decaying radioactivity after elution of Ba-137m (P6.4.3.4)

For the activity of a radioactive sample, we can say:

$$A(t) = \left| \frac{dN}{dt} \right|$$

Here, N is the number of radioactive nuclei at time t. It is not possible to predict when an individual atomic nucleus will decay. However, from the fact that all nuclei decay with the same probability, it follows that over the time interval dt, the number of radioactive nuclei will decrease by

$$dN = -\lambda \cdot N \cdot dt$$

λ: decay constant

Thus, for the number N, the law of radioactive decay applies:

$$N(t) = N_0 \cdot e^{-\lambda \cdot t}$$

N_0: number of radioactive nuclei at time $t = 0$

Among other things, this law states that after the half-life

$$t_{1/2} = \frac{\ln 2}{\lambda}$$

the number of radioactive nuclei will be reduced by half.

To determine the half-life of Ba-137m in the experiment P6.4.3.3, a plastic bottle with Cs-137 stored at salt is used. The metastable isotop Ba-137m arising from the β-decay is released by an eluation solution. The half-time amounts to 2.6 minutes approx.

In the experiment P6.4.3.4, a plastic bottle with radioactive Cs-137 is used. The Cs-137 continually decays into Ba-137m. The metastable isotop Ba-137m arising from the β-decay is selectively washed out by a syringe with eluation solution. The half-time amounts to 2.6 minutes approx.

Using two counter tubes, we can first observe the eluation transfer of radioactive Ba-137m out of the plastic bottle into the test tube. Inside the test tube, the Ba-137m will decay exponentially over time within a few minutes, at the same time, the activity of Ba-137m inside the plastic bottle will build up again. In the end, there is again a dynamic equilibrium of decay and production in the plastic bottle.

Confirming the inverse-square law of distance for β radiation (P6.4.4.3)

ATTENUATION OF α-, β- AND γ RADIATION

P6.4.4.2
Attenuation of β radiation when passing through matter

P6.4.4.3
Confirming the inverse-square law of distance for β radiation

P6.4.4.4
Absorption of γ radiation through matter

Cat. No.	Description	P6.4.4.2	P6.4.4.3	P6.4.4.4
559 835	Radioactive preparations, set of 3	1	1	
559 01	End-window counter with cable for α, β, γ and X-rays	1	1	1
575 471	Counter S	1	1	1
559 18	Holder with absorber foils	1		
590 02	Small clip plug	1	1	
591 21	Clip plug, large	1	1	
532 16	Connecting rod	2	2	
300 11	Saddle base	2	2	
460 97	Metal rule, 0.5 m		1	
559 845	Mixed nuclide preparation, α, β, γ			1
559 855	Co-60 preparation, 74 kBq			1
686 651	RAD experimental board			1
686 653	Holders for counter tube and preparation			1
686 657	Plastic clamps, span 1.2 cm, set of 3			1
686 660	Frame and 9 slides, set of			1
686 661	Lead slides, 50 x 50 x 2 mm, set of 8			1

High-energy α and β particles release only a part of their energy when they collide with an absorber atom. For this reason, many collisions are required to brake a particle completely. Its range R

$$R \propto \frac{E_0^2}{n \cdot Z}$$

depends on the initial energy E_0, the number density n and the atomic number Z of the absorber atoms. Low-energy α and β particles or γ radiation are braked to a certain fraction when passing through a specific absorber density dx, or are absorbed or scattered and thus disappear from the beam. As a result, the radiation intensity I decreases exponentially with the absorption distance x

$$I = I_0 \cdot e^{-\mu \cdot x} \quad \mu\text{: attenuation coefficient}$$

The experiment P6.4.4.2 examines the attenuation of β radiation from Sr-90 in aluminum as a function of the absorber thickness d. This experiment shows an exponential decrease in the intensity.

As a comparison, the absorber is removed in the experiment P6.4.4.3 and the distance between the β preparation and the counter tube is varied. As one might expect for a point-shaped radiation source, the following is a good approximation for the intensity:

$$I(d) \propto \frac{1}{d^2}$$

The experiment P6.4.4.4 examines the attenuation of γ radiation in matter. Here too, the decrease in intensity is a close approximation of an exponential function. The attenuation coefficient μ depends on the absorber material and the γ energy.

DEMONSTRATING PATHS OF PARTICLES

P6.5.1.1
Demonstrating the tracks of α particles in a Wilson cloud chamber

Demonstrating the tracks of α particles in a Wilson cloud chamber (P6.5.1.1)

Cat. No.	Description	P6.5.1.1
559 57	Wilson cloud chamber	1
559 596	Ra-226 radium source for Wilson chamber	1
450 60	Lamp housing with cable	1
450 511	Bulbs, 6 V/30 W, E14, set of 2	1
460 20	Condenser with diaphragm holder	1
522 27	Power supply, 450 V	1
521 210	Transformer 6/12 V	1
301 06	Bench clamp	1
300 11	Saddle base	1
501 46	Connecting leads 19 A, 100 cm, red/blue, pair	1
671 9720	Ethanol, denatured, 1 l	1

In a Wilson cloud chamber, a saturated mixture of air, water and alcohol vapor is briefly caused to assume a supersaturated state due to adiabatic expansion. The supersaturated vapor condenses rapidly around condensation seeds to form tiny mist droplets. Ions, which are formed e.g. through collisions of α particles and gas molecules in the cloud chamber, make particularly efficient condensations seeds.

In the experiment P6.5.1.1, the tracks of α particles are observed in a Wilson cloud chamber. Each time the pump is vigorously pressed, these tracks are visible as traces of droplets in oblique light for one to two seconds. An electric field in the chamber clears the space of residual ions.
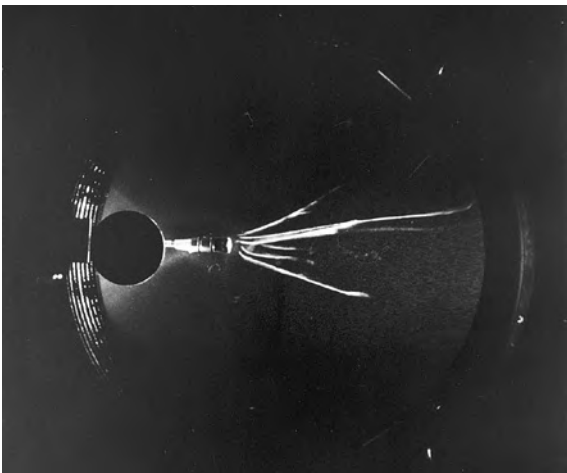
Droplet traces in the Wilson cloud chamber (P6.5.1.1)

Rutherford scattering: measuring the scattering rate as a function of the scattering angle and the atomic number (P6.5.2.1)

RUTHERFORD SCATTERING

P6.5.2.1
Rutherford scattering: measuring the scattering rate as a function of the scattering angle and the atomic number

Cat. No.	Description	P6.5.2.1
559 82OZ	Am-241 preparation, 330 kBq	1
559 56	Rutherford scattering chamber	1
559 52	Aluminium foil in frame	1
559 931	Discriminator preamplifier	1
562 791	Plug-in power supply, 12 V AC	1
575 471	Counter S	1
378 73	Rotary-vane vacuum pump S 1.5	1
378 005	T-piece, DN 16 KF	1
378 040	Centering ring (adapter) DN 10/16	1
378 045	Centering ring DN 16 KF	1
378 050	Clamping ring, DN 10/16 KF	2
378 771	Air inlet valve, DN 10 KF	1
378 031	Hose nozzle, DN 16 KF	1
667 186	Vacuum rubber tubing, 8 mm diam.	1
501 01	BNC cable, 0.25 m	1
575 24	Screened cable, BNC/4 mm	1

The fact that an atom is "mostly empty space" was confirmed by *Rutherford*, *Geiger* and *Marsden* in one of the most significant experiments in the history of physics. They caused a parallel beam of α particles to fall on an extremely thin sheet of gold leaf. They discovered that most of the α particles passed through the gold leaf virtually without deflection, and that only a few were deflected to a greater degree. From this, they concluded that atoms consist of a virtually massless extended shell, and a practically point-shaped massive nucleus.

The experiment P6.5.2.1 reproduces these observations using an Am-241 preparation in a vacuum chamber. The scattering rate $N(\vartheta)$ is measured as a function of the scattering angle ϑ using a semiconductor detector. As scattering materials, a sheet of gold leaf (Z = 80) and aluminum foil (Z = 13) are provided. The scattering rate confirms the relationship

$$N(\vartheta) \propto \frac{1}{\sin^4 \frac{\vartheta}{2}} \quad \text{and} \quad N(\vartheta) \propto Z^2$$
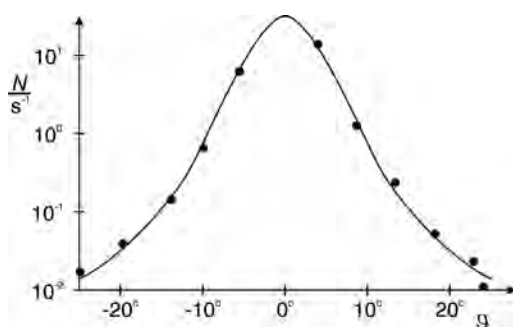
Scattering rate *N* as a function of the scattering angle ϑ (P6.5.2.1)

ATOMIC AND NUCLEAR PHYSICS
NUCLEAR PHYSICS

NUCLEAR MAGNETIC RESONANCE

P6.5.3.1
Nuclear magnetic resonance in polystyrene, glycerin and Teflon

Nuclear magnetic resonance in polystyrene, glycerin and Teflon (P6.5.3.1)

Cat. No.	Description	P6.5.3.1
514 602	NMR supply unit	1
514 606	NMR probe	1
562 11	U-core with yoke	1
562 131	Coil, 480 turns, 10 A	2
521 546	DC Power Supply 0...16 V/0...5 A	1
575 304	Digital storage oscilloscope 70 MHz two-channel	1
501 02	BNC cable, 1 m	2
500 622	Safety connecting lead 50 cm, blue	1
500 641	Safety connecting lead, 100 cm, red	1
500 642	Safety connecting lead, 100 cm, blue	1
524 005W	Mobile-CASSY 2 WiFi	1*
524 0381	Combi B sensor S	1*
501 11	Extension cable, 15 pin	1*

*additionally recommended
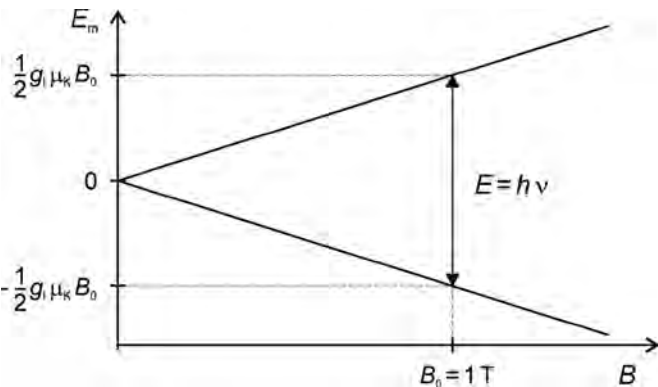
Diagram of resonance condition of hydrogen (P6.5.3.1)

The magnetic moment of the nucleus entailed by the nuclear spin I assumes the energy states

$$E_m = -g_I \cdot \mu_K \cdot m \cdot B \quad \text{with} \quad m = -I, \ -I+1, \ ..., \ I$$

$$\mu_K = 5.051 \cdot 10^{-27} \frac{J}{T}: \ \text{nuclear magneton}$$

g_I: g factor of nucleus

in a magnetic field B. When a high-frequency magnetic field with the frequency ν is applied perpendicularly to the first magnetic field, it excites transitions between the adjacent energy states when these fulfill the resonance condition

$$h \cdot \nu = E_{m+1} - E_m$$

h: Planck's constant

This fact is the basis for nuclear magnetic resonance, in which the resonance signal is detected using radio-frequency technology. For example, in a hydrogen nucleus the resonance frequency in a magnetic field of 1 T is about 42.5 MHz. The precise value depends on the chemical environment of the hydrogen atom, as in addition to the external magnetic field B the local internal field generated by atoms and nuclei in the near vicinity also acts on the hydrogen nucleus. The width of the resonance signal also depends on the structure of the substance under study.

The experiment P6.5.3.1 verifies nuclear magnetic resonance in polystyrene, glycerine and Teflon. The evaluation focuses on the position, width and intensity of the resonance lines.

Additionally, the relaxation time of the spin system can be observed by a beat frequency mesurement.

224   WWW.LD-DIDACTIC.COM

CASSY®

α spectroscopy of radioactive samples (P6.5.4.1)
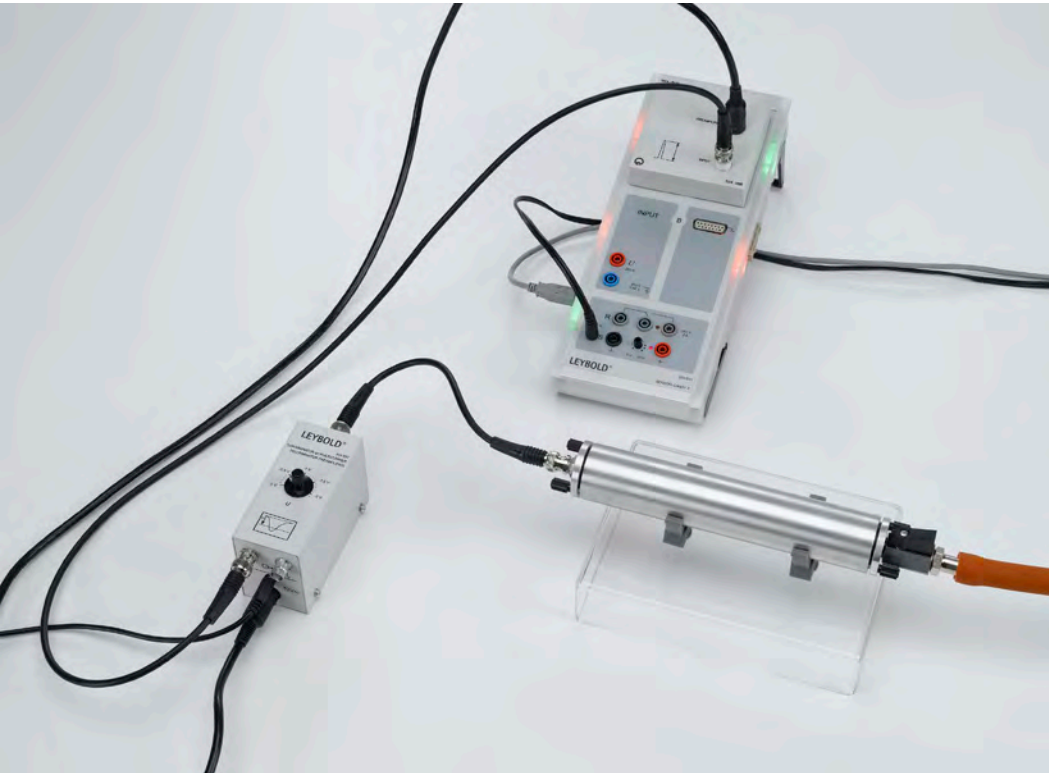
α SPECTROSCOPY

P6.5.4.1
α spectroscopy of radioactive samples

P6.5.4.2
Determining the energy loss of α radiation in air

P6.5.4.3
Determining the energy loss of α radiation in aluminum and in gold

P6.5.4.4
Determining age using a Ra-226 sample

P6.5.4.5
Fine structure of Am-241 α radiation

Cat. No.	Description	P6.5.4.1	P6.5.4.2	P6.5.4.3	P6.5.4.4	P6.5.4.5
559 565	Alpha spectroscopy chamber	1	1	1	1	1
559 921	Semiconductor detector	1	1	1	1	1
559 825	Am-241 preparation, open, 3.7 kBq	1	1	1		1
559 436	Ra 226 preparation, 5 kBq	1		1	1	
524 013	Sensor-CASSY 2	1	1	1	1	1
524 220	CASSY Lab 2	1	1	1	1	1
524 058	MCA box	1	1	1	1	1
559 931	Discriminator preamplifier	1	1	1	1	1
501 16	Multi-core cable, 6-pole, 1.5 m	1	1	1	1	1
501 02	BNC cable, 1 m	1	1	1	1	1
501 01	BNC cable, 0.25 m	1	1	1	1	1
378 73	Rotary-vane vacuum pump S 1.5	1	1	1	1	1
378 005	T-piece, DN 16 KF	1		1	1	1
378 040	Centering ring (adapter) DN 10/16	1		1	1	1
378 045	Centering ring DN 16 KF	1	3	1	1	1
378 050	Clamping ring, DN 10/16 KF	2	3	2	2	2
378 771	Air inlet valve, DN 10 KF	1		1	1	1
378 031	Hose nozzle, DN 16 KF	1	1	1	1	1
667 186	Vacuum rubber tubing, 8 mm diam.	1	1	1	1	1
575 302	Oscilloscope 30 MHz, digital, PT1265	1*				1*
378 015	Cross piece, DN 16 KF		1			
378 776	Variable leak valve, DN 16 KF		1			
378 510	Pointer manometer, DN 16 KF		1			
311 78	Tape measure 2 m / 1 mm		1			
559 521	Gold and aluminium foil in holder				1	
	additionally required: PC with Windows XP/Vista/7/8/10 (x86 or x64)	1	1	1	1	1

* additionally recommended

Up until about 1930, the energy of α rays was characterized in terms of their range in air. For example, a particle of 5.3 MeV (Po-210) has a range of 3.84 cm. Today, α energy spectra can be studied more precisely using semiconductor detectors. These detect discrete lines which correspond to the discrete excitation levels of the emitting nuclei.

The aim of the experiment P6.5.4.1 is to record and compare the α energy spectra of the two standard preparations Am-241 and Ra-226. To improve the measuring accuracy, the measurement is conducted in a vacuum chamber.

In the experiment P6.5.4.2, the energy E of α particles is measured as a function of the air pressure p in the vacuum chamber. The measurement data is used to determine the energy per unit of distance dE/dx which the α particles lose in the air. Here,

$$x = \frac{p}{p_0} \cdot x_0$$

x_0: actual distance

p_0: standard pressure

is the apparent distance between the preparation and the detector.

The experiment P6.5.4.3 determines the amount of energy of α particles lost per unit of distance in gold and aluminum as the quotient of the change in the energy ΔE and the thickness Δx of the metal foils.

In the experiment P6.5.4.4, the individual values of the decay chain of Ra-226 leading to the α energy spectrum are analyzed to determine the age of the Ra-226 preparation used here. The activities A_1 and A_2 of the decay chain "preceding" and "following" the longer-life isotope Pb-210 are used to determine the age of the sample from the relationship

$$A_2 = A_1 \cdot \left(1 - e^{-\frac{T}{\tau}} \right)$$

$\tau = 32.2$ a: liftime of Pb-210

The aim of the experiment P6.5.4.5 is to record the fine structure in the α spectrum of Am-241. An alpha decay can end in several excited states of the daughter nucleus, revealing nuclear excitation levels of the nucleus. Experimentally, this can be recorded using an unsealed radioactive source.

LEYBOLD®

CASSY®

γ SPECTROSCOPY

P6.5.5.1
Detecting γ radiation with a scintillation counter

P6.5.5.2
Recording and calibrating a γ spectrum

P6.5.5.3
Absorption of γ radiation

P6.5.5.4
Identifying and determining the activity of radioactive samples

P6.5.5.5
Recording a β spectrum with a scintillation counter

P6.5.5.6
Coincidence and γ–γ angular correlation in positron decay

P6.5.5.7
Coincidence at γ decay of cobalt

Absorption of γ radiation (P6.5.5.3)

Cat. No.	Description	P6.5.5.1	P6.5.5.2	P6.5.5.3	P6.5.5.4	P6.5.5.5	P6.5.5.6	P6.5.5.7
559 901	Scintillation counter	1	1	1	1	1	2	2
559 912	Detector output stage	1	1	1	1	1	2	2
521 68	High-voltage power supply, 1.5 kV	1	1	1	1	1	2	2
524 013	Sensor-CASSY 2	1	1	1	1	1	1	1
524 058	MCA box	1	1	1	1	1	2	2
524 220	CASSY Lab 2	1	1	1	1	1	1	1
300 42	Stand rod, 47 cm, 12 mm diam.	1	1	1		1	1	1
301 01	Leybold multiclamp	1	1	1		1	1	1
666 555	Universal clamp 0...80 mm	1	1	1		1	1	1
575 302	Oscilloscope 30 MHz, digital, PT1265	1*						
501 02	BNC cable, 1 m	1*						
559 94	Absorbers and targets, set			1		1		
672 5210	Potassium chloride, 250 g				4			
559 88	Marinelli beaker				2			
559 89	Scintillator shielding				1	1		
559 835	Radioactive preparations, set of 3		1	1		1		
559 845	Mixed nuclide preparation, α, β, γ	1					1	
559 855	Co-60 preparation, 74 kBq		1*	1*				1
559 865	Na-22 preparation, 74 kBq		1				1	
559 885	Calibrating preparation CS-137, 5 KBq				1			
559 891	Socket for scintillator shielding	1	1	1	1	1	1	1
	additionally required: PC with Windows XP/Vista/7/8/10 (x86 or x64)	1	1	1	1	1	1	1

*additionally recommended

γ-spectra recorded with the scintillation counter allow to identify different nuclei and give insight into fundamental aspects of nuclear physics and the interaction of radiation with matter, like compton scattering or photoeffect.

In the experiment P6.5.5.1, the output pulses of the scintillation counter are investigated using the oscilloscope and the MCA-Box with CASSY. The total absorption peak and the Compton distribution are identified in the pulse-amplitude distribution generated with monoenergetic γ radiation.

The aim of the experiment P6.5.5.2 is to record and compare the γ energy spectra of standard preparations. The total absorption peaks are used to calibrate the energy of the scintillation counter and to identify the preparations.

The experiment P6.5.5.3 examines the attenuation of γ radiation in various absorbers. The aim here is to show how the attenuation coefficient μ depends on the absorber material and the γ energy.

A Marinelli beaker is used in the experiment P6.5.5.4 for quantitative measurements of weak radioactive samples. This apparatus encloses the scintillator crystal virtually completely, ensuring a defined measurement geometry. Lead shielding considerably reduces the interfering background from the laboratory environment.

The experiment P6.5.5.5 records the continuous spectrum of a pure β emitter (Sr-90/Y-90) using the scintillation counter. To determine the energy loss dE/dx of the β particles in aluminum, aluminium absorbers of various thicknesses x are placed in the beam path between the preparation and the detector.

In the experiment P6.5.5.6, the spatial correlation of the two γ quanta in electron-positron pair annihilation is demonstrated. The conservation of momentum requires emission of the two quanta at an angle of 180°. Selective measurement of a coincidence spectrum leads to the suppression of non-correlated lines.

The experiment P6.5.5.7 shows the decay of Cobalt-60 in detail and proves the existence of a decay chain by coincidence measurements.

CASSY®

Quantitative observation of the Compton effect (P6.5.6.1)
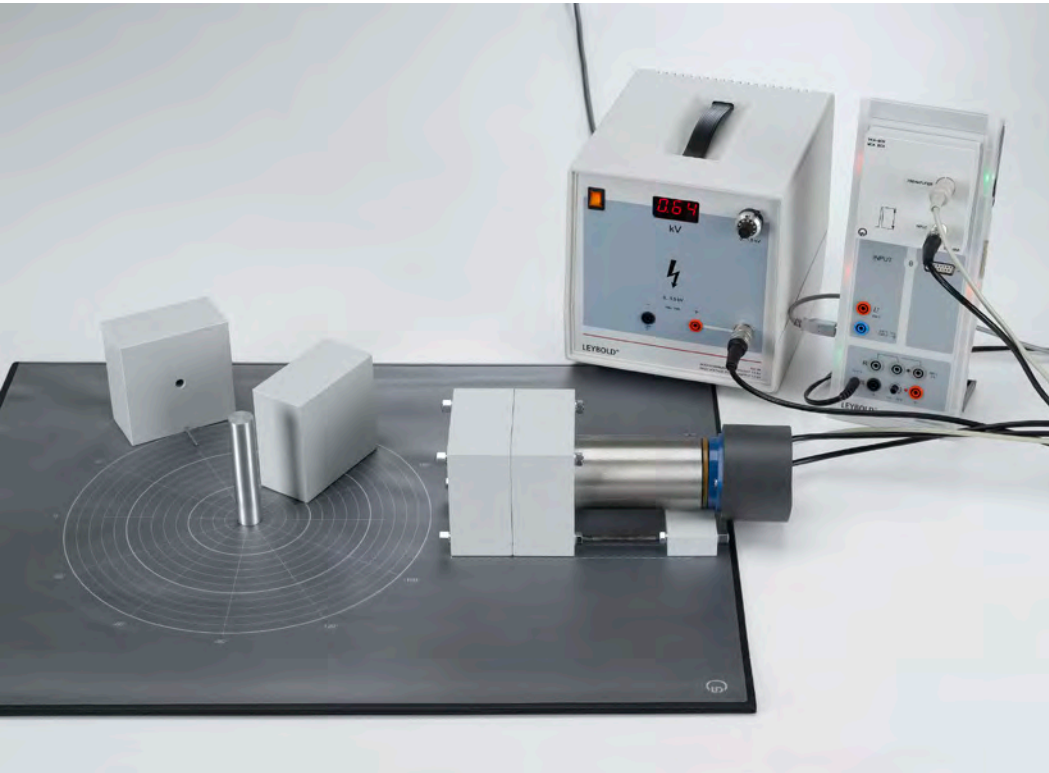
COMPTON EFFECT

P6.5.6.1
Quantitative observation of the Compton effect

Cat. No.	Description	P6.5.6.1
559 800	Equipment set for Compton scattering	1
559 809	Cs-137 preparation, 3.7 MBq	1
559 845	Mixed nuclide preparation, α, β, γ	1
559 901	Scintillation counter	1
559 912	Detector output stage	1
521 68	High-voltage power supply, 1.5 kV	1
524 013	Sensor-CASSY 2	1
524 058	MCA box	1
524 220	CASSY Lab 2	1
	additionally required: PC with Windows XP/Vista/7/8/10 (x86 or x64)	1

In the Compton effect, a photon transfers a part of its energy E_0 and its linear momentum

$$p_0 = \frac{E_0}{c}$$

c: speed of light in a vacuum

to a free electron by means of elastic collision. Here, the laws of conservation of energy and momentum apply just as for the collision of two bodies in mechanics. The energy

$$E(\vartheta) = \frac{E_0}{1 + \frac{E_0}{m \cdot c^2} \cdot (1 - \cos \vartheta)}$$

m: mass of electron at rest

and the linear momentum

$$p = \frac{E}{c}$$

of the scattered photon depend on the scattering angle ϑ. The effective cross-section depends on the scattering angle and is described by the *Klein-Nishina* formula:

$$\frac{d\sigma}{d\Omega} = \frac{1}{2} \cdot r_0^2 \cdot \frac{p^2}{p_0^2} \cdot \left(\frac{p_0}{p} + \frac{p}{p_0} - \sin^2 \vartheta \right)$$

r_0: $2.5 \cdot 10^{-15}$ m: classic electron radius

In the experiment P6.5.6.1, the Compton scattering of γ quanta with the energy E_0 = 667 keV at the quasi-free electrons of an aluminium scattering body is investigated. For each scattering angle ϑ, a calibrated scintillation counter records one γ spectrum with and one without aluminum scatterer as a function of the respective scattering angle. The further evaluation utilizes the total absorption peak of the differential spectrum. The position of this peak gives us the energy $E(\vartheta)$. Its integral counting rate $N(\vartheta)$ is compared with the calculated effective cross-section.
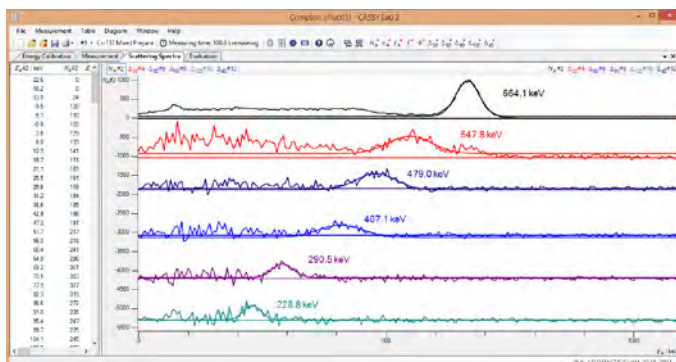
Energy shift of the Cs-137 line when scattered in different directions (P6.5.6.1)

CASSY®

PROPERTIES OF RADIATION PARTICLES

P6.5.7.1
Deflection of beta radiation in a magnetic field

Deflection of beta radiation in a magnetic field (P6.5.7.1)

Cat. No.	Description	P6.5.7.1
559 835	Radioactive preparations, set of 3	1
559 01	End-window counter with cable for α, β, γ and X-rays	1
575 471	Counter S	1
LDS 00001	Stopwatch, digital	1
521 391	AC/DC power supply 0...24 V/5 A	1
562 11	U-core with yoke	1
562 13	Coil, 250 turns	2
560 31	Bored pole pieces, pair	1
559 23	Swivelling clamp	1
559 18	Holder with absorber foils	1
300 11	Saddle base	1
300 41	Stand rod, 25 cm, 12 mm Ø	1
301 01	Leybold multiclamp	1
501 25	Connecting lead, 32 A, 50 cm, red	1
501 26	Connecting lead, 32 A, 50 cm, blue	2
524 005W	Mobile-CASSY 2 WiFi	1*
524 0381	Combi B sensor S	1*
501 11	Extension cable, 15 pin	1*

* additionally recommended

Historically, it was easy to see that there are different kinds of radioactive radiation. But to identify which particles were involved took some time. The behaviour of those particles in an magnetic field was and still is the most valuable tool to characterize charged particles.

In the experiment P6.5.7.1 β radiation passes through a magnetic field and the resulting angular distribution is recorded. From these data, the energy of the decay can be estimated.

QUANTUM OPTICS

P6.6.1.1
Quantum eraser
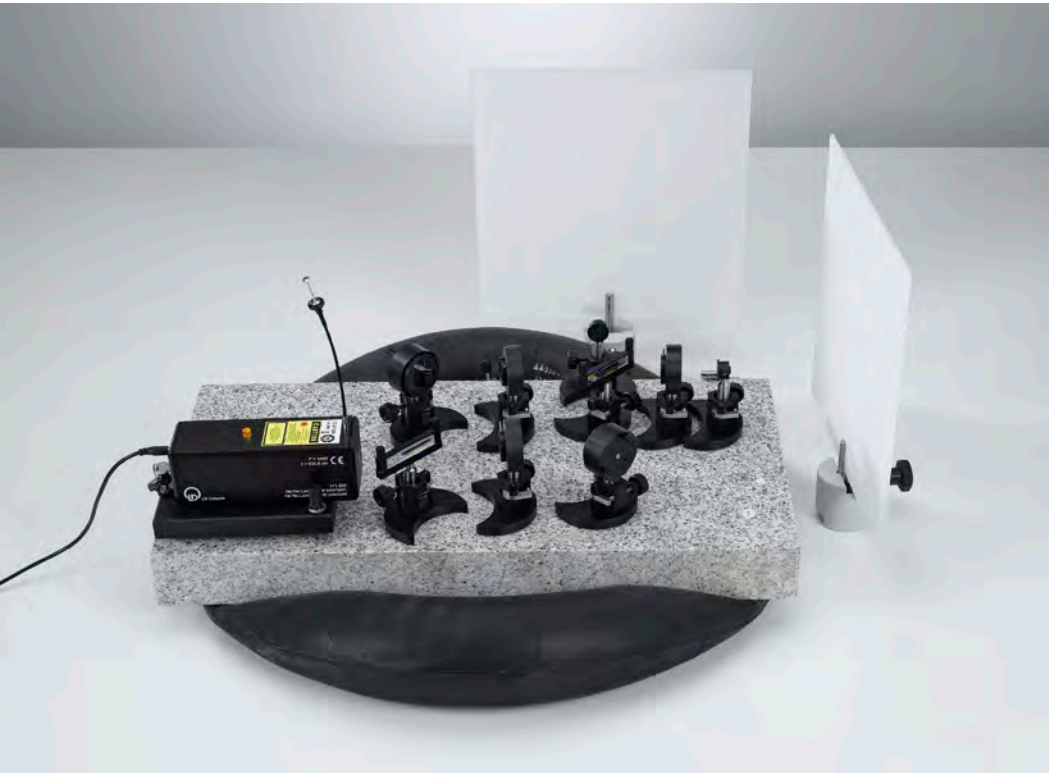
Quantum eraser (P6.6.1.1)

Cat. No.	Description	P6.6.1.1
473 40	Laser optics base plate	1
471 830	He-Ne Laser, linearly polarised	1
473 411	Laser mount	1
473 421	Optics base	9
473 431	Holder for beam divider	2
473 432	Beam divider, 50 %	2
473 461	Planar mirror with fine adjustment	2
473 471	Spherical lens, f = 2.7 mm	2
473 49	Polarising filter for laser optics base plate	3
441 53	Screen, translucent	2
300 11	Saddle base	2
311 02	Metal rule, 1 m	1

Quantum optics is a field of research in physics, dealing with the application of quantum mechanics to phenomena involving light and its interactions with matter.

A basic principle of quantum mechanics is complementarity: each quantum-mechanical object has both wave-like and particle-like properties. In the experiment P6.6.1.1 an analogue experiment to a quantum eraser is built up. It shows the complementarity of which-way information and interference.

PARTICLES

P6.6.2.1
Detection of Muons

Detection of Muons (P6.6.2.1)

Cat. No.	Description	P6.6.2.1
524 013	Sensor-CASSY 2	1
524 220	CASSY Lab 2	1
524 033	GM box	2
559 012	Pancake GM counter tube	2
300 11	Saddle base	1*
587 07	Tweeter	1*
501 45	Connecting lead 19 A, 50 cm, red/blue, pair	1*
	additionally required: PC with Windows XP/Vista/7/8/10 (x86 or x64)	1

* additionally recommended

The origin of high-energy particles is not only from radioactive decay of unstable nuclei on earth, they can also be found in the cosmic radiation. Such particles are an interesting topic on their own.

Experiment P6.6.2.1 uses the coincidence detection of two GM detectors to identifiy natural muons passing through this muon telescope. The specific properties of the muons can be shown this way and recording the muon flux over the day shows their origin is related to the sun.
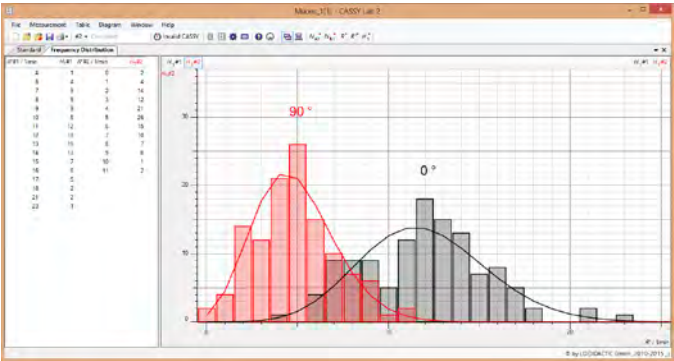
Count rate distribution for the muon detector oriented in different directions (P6.6.2.1)

P7 SOLID-STATE PHYSICS

P7 SOLID-STATE PHYSICS

Laue diagrams: investigating the lattice structure of monocrystals (P7.1.2.2)

X-RAY SCATTERING

P7.1.2.1
Bragg reflection: determining the lattice constants of monocrystals

P7.1.2.2
Laue diagrams: investigating the lattice structure of monocrystals

P7.1.2.3
Debye-Scherrer photography: determining the lattice plane spacings of polycrystalline powder samples

P7.1.2.4
Debye-Scherrer Scan: determining the lattice plane spacings of polycrystalline powder samples

Cat. No.	Description	P7.1.2.1	P7.1.2.2	P7.1.2.3	P7.1.2.4
554 800	X-ray apparatus	1	1	1	1
554 861	X-ray tube, Mo	1	1	1	
554 831	Goniometer	1			1
559 01	End-window counter with cable for α, β, γ and X-rays	1			1
554 77	LiF crystal for Bragg reflection	1			
554 78	NaCl crystal for Bragg reflection	1			
554 838	Film holder, X-ray		1	1	
554 895	X-ray film		1	1	
554 87	LiF crystal for Laue diagrams		1		
554 88	NaCl crystal for Laue diagrams		1		
667 091	Pestle 88 mm			1	1
667 092	Mortar porcelain 70 mm Ø			1	1
666 960	Powder spatula, stainless steel, 150 mm			1	1
311 54	Precision vernier callipers			1	
673 5700	Sodium chloride 250 g			1	1
673 0520	Lithium fluoride, analytically pure, 10 g			1	1
554 862	X-ray tube, Cu				1
554 842	Crystal powder holder				1
	additionally required: PC with Windows XP/Vista/7/8/10 (x86 or x64)	1			1

X-rays are an essential tool to determine the structure of crystals. The lattice planes inside a crystal are identified by their Miller idices h, k, l and reflect the X-rays only if the Laue or Bragg conditions are fulfilled. The distribution of reflexes allows to calculate the lattice constant and crystal structure of the investigated crystal.

In the experiment P7.1.2.1, the Bragg reflection of Mo-K_a radiation (λ = 71.080 pm) at NaCl and LiF monocrystals is used to determine the lattice constant. The K_β component of the X-ray radiation can be suppressed using a zirconium filter.

Laue diagrams from NaCl and LiF monocrystals are created in the experiment P7.1.2.2 using the bremsstrahlung of the X-ray apparatus as „white" X-radiation. The positions of the „multicolored" reflections on an X-ray film behind the crystal and their intensities can be used to determine the crystal structure and the lengths of the crystal axes through application of the *Laue* condition.

In the experiment P7.1.2.3, *Debye-Scherrer* photographs are produced by irradiating samples of a fine crystal powder with Mo-K_α radiation. Some of the randomly oriented crystallites conform to the *Bragg* condition and diffract X-rays into cones for which the aperture angles ϑ can be derived from a photograph. This experiment determines the lattice spacing corresponding to ϑ as well as its *Laue* indices h, k, l, and thus the lattice structure of the crystallite.

The experiment P7.1.2.4 records the *Debye-Scherrer* pattern with an end window counter instead of X-ray film. The diffracted reflections of a fine powder sample are recorded as a function of diffraction angle. The intensity peaks in the diffraction spectrum allow the calculation of the separations of adjacent lattice planes.
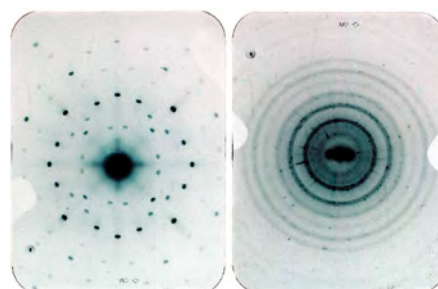
Laue diagram of NaCl and Debye-scherrer photograph of NaCl (P7.1.2.2 + P7.1.2.3)

LEYBOLD®

233

X–RAY SCATTERING

P7.1.2.5
Digital Laue diagrams: investigating the lattice structure of monocrystals

P7.1.2.6
Digital Debye-Scherrer photography: determining the lattice plane spacings of polycrystalline powder samples

Digital Laue diagrams: investigating the lattice structure of monocrystals (P7.1.2.5)

Cat. No.	Description	P7.1.2.5	P7.1.2.6
554 800	X-ray apparatus	1	1
554 866	X-ray tube, Au	1	
554 8281	X-ray image sensor	1	1
554 8282	Beam stop for X-ray image sensor	1	1
554 8291	Precision rail for X-ray image sensor	1	1
554 8383	Pinhole collimator with Laue crystals	1	1
554 861	X-ray tube, Mo		1
667 091	Pestle 88 mm		1
667 092	Mortar porcelain 70 mm Ø		1
666 960	Powder spatula, stainless steel, 150 mm		1
673 5700	Sodium chloride 250 g		1
673 0520	Lithium fluoride, analytically pure, 10 g		1
	additionally required: PC with Windows XP/Vista/7/8/10 (x86 or x64)	1	1
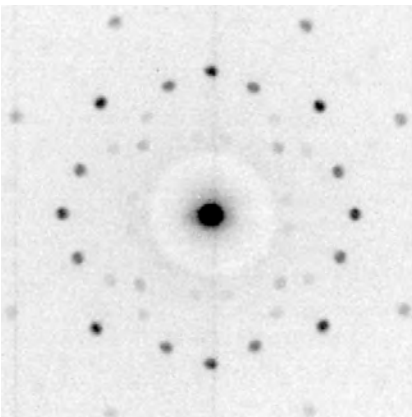
X-rays are an essential tool to determine the structure of crystals. The lattice planes inside a crystal are identified by their Miller idices *h, k, l* and reflect the X-rays only if the Laue or Bragg conditions are fulfilled. The distribution of reflexes allows to calculate the lattice constant and crystal structure of the investigated crystal.

To create *Laue* diagrams of NaCl and LiF monocrystals, the bremsstrahlung of the X-ray apparatus is used in the experiment P7.1.2.5 as a „white" spectrum of X-rays. The positions of the „multicolored" diffraction spots on an X-ray image sensor behind the crystal and their intensities can be used to determine the crystal structure and the dimensions of the unit cellthrough application of the *Laue* condition.

The X-ray image sensor allows capturing the *Laue* pattern in one minute (much faster than conventional film) and the digital evaluation eases the determination of the diffraction angles on the computer.

In the experiment P7.1.2.6, *Debye-Scherrer* photography are produced by irradiating samples of a fine crystal powder with Mo-K_a radiation. Some of the randomly oriented crystallites conform to the *Bragg* condition and diffract X-rays into cones for which the aperture angles ϑ can be derived from a photograph. This experiment determines the lattice spacing corresponding to ϑ as well as its *Laue* indices *h, k, l*, and thus the lattice structure of the crystallite.

The sensitive X-ray image sensor allows capturing the *Debye-Scherrer* pattern in one minute and the digital evaluation of the circle diameter and circle integral on the computer, if the powder sample has been carefully prepared and the diffracted rays have a correspondingly high intensity.

Laue diagram of NaCl (P7.1.2.5)

ELASTIC AND PLASTIC DEFORMATION

P7.1.4.1
Investigating the elastic and plastic extension of metal wires

P7.1.4.2
Investigating the elastic and plastic extension of metal wires - Recording and evaluating with CASSY

Investigating the elastic and plastic extension of metal wires - Recording and evaluating with CASSY (P7.1.4.2)

Cat. No.	Description	P7.1.4.1	P7.1.4.2
550 35	Copper resistance wire, 0.2 mm diam., 100 m	1	1
550 51	Iron resistance wire, 0.2 mm diameter, 100 m	1	1
342 63	Weight 50 g	18	
340 911	Pulley Ø 50 mm, plug-in	1	
381 331	Pointer for linear expansion	1	
340 82	Double scale	1	
314 04	Support clip, for plugging in	2	
301 07	Simple bench clamp	2	2
301 01	Leybold multiclamp	4	3
301 25	Support block	3	
301 26	Stand rod 25 cm, 10 mm Ø	3	2
301 27	Stand rod 50 cm, 10 mm Ø	1	
300 44	Stand rod, 100 cm, 12 mm diam.	1	1
524 005W	Mobile-CASSY 2 WiFi		1
524 042	Force sensor S, ±50 N		1
524 082	Rotary motion sensor S		1
311 78	Tape measure 2 m / 1 mm		1

The shape of a crystalline solid is altered when a force is applied. We speak of elastic behavior when the solid resumes its original form once the force ceases to act on it. When the force exceeds the elastic limit, the body is permanently deformed. This plastic behavior is caused by the migration of discontinuities in the crystal structure.

In the experiments P7.1.4.1 and P7.1.4.2, the extension of iron and copper wires is investigated by hanging weights from them. A precision pointer indicator or the rotary motion sensor S attached to a CASSY measures the change in length Δs, i. e. the extension

$$\varepsilon = \frac{\Delta s}{s}$$

s: length of wire

After each new tensile load

$$\sigma = \frac{F}{A}$$

F: weight of load pieces

A: wire cross-section

the students observe whether the pointer or the rotary motion sensor returns to the zero position when the strain is relieved, i.e. whether the strain is below the elasticity limit σ_ε. Graphing the measured values in a tension-extension diagram confirms the validity of Hooke's law

$$\sigma = E \cdot \varepsilon$$

E: modulus of elasticity

up to a proportionality limit σ_p.
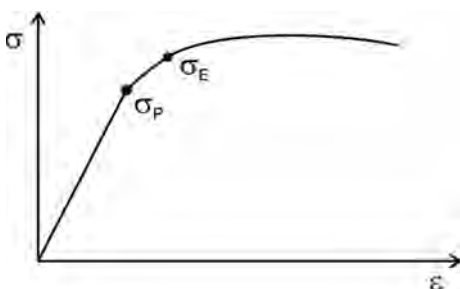
Load-extension diagram for a typical metal wire (P7.1.4.1)

Investigating the elastic and plastic extension of metal wires (P7.1.4.1)

LEYBOLD®

CASSY®

HALL EFFECT

P7.2.1.1
Investigating the Hall effect in silver

P7.2.1.2
Investigating the anomalous Hall effect in tungsten

Investigating the Hall effect in silver (P7.2.1.1)

Cat. No.	Description	P7.2.1.1	P7.2.1.2
586 81	Hall effect apparatus (silver)	1	
524 005W	Mobile-CASSY 2 WiFi	1	1
524 0381	Combi B sensor S	1	1
501 11	Extension cable, 15 pin	1	1
524 0401	µV sensor S	1	1
521 551	AC/DC power supply 0...24 V/0...10 A	1	1
726 890	DC-High Current Power Supply 1...32 V/0...20 A	1	1
562 11	U-core with yoke	1	1
560 31	Bored pole pieces, pair	1	1
562 13	Coil, 250 turns	2	2
300 41	Stand rod, 25 cm, 12 mm Ø	1	1
301 01	Leybold multiclamp	1	1
300 02	Stand base, V-shaped, small	1	1
500 442	Connecting lead 19 A, 100 cm, blue	1	1
501 46	Connecting leads 19 A, 100 cm, red/blue, pair	2	2
501 33	Connecting lead, 32 A, 100 cm, black	2	2
586 84	Hall effect apparatus (tungsten)		1

In the case of electrical conductors or semiconductors within a magnetic field B, through which a current I is flowing perpendicular to the magnetic field, the Hall effect results in an electric potential difference

$$U_H = R_H \cdot B \cdot I \cdot \frac{1}{d} \quad d: \text{thickness of sample}$$

The Hall coefficient

$$R_H = \frac{1}{e} \cdot \frac{p \cdot \mu_p^2 - n \cdot \mu_n^2}{\left(p \cdot \mu_p + n \cdot \mu_n\right)^2} \quad e: \text{elementary charge}$$

depends on the concentrations n and p of the electrons and holes as well as their mobilities μ_n and μ_p, and is thus a quantity which depends on the material and the temperature.

The experiments P7.2.1.1 and P7.2.1.2 determine the Hall coefficient R_H of two electrical conductors by measuring the Hall voltage U_H for various currents I as a function of the magnetic field B. A negative value is obtained for the Hall coefficient of silver, which indicates that the charge is being transported by electrons. A positive value is found as the Hall coefficient of tungsten. Consequently, the holes are mainly responsible for conduction in this metal.

HALL EFFECT

P7.2.1.3
Determining the density and mobility of charge carriers in n-Germanium

P7.2.1.4
Determining the density and mobility of charge carriers in p-Germanium

P7.2.1.5
Determining the band gap of germanium

Determining the density and mobility of charge carriers in p-Germanium (P7.2.1.4)

Cat. No.	Description	P7.2.1.3	P7.2.1.4	P7.2.1.5
586 850	Base unit for Hall effect	1	1	1
586 853	N-doped germanium on plug-in board	1		
562 11	U-core with yoke	1	1	
562 13	Coil, 250 turns	2	2	
560 31	Bored pole pieces, pair	1	1	
521 536	DC Power Supply 2 x 0...16 V/2 x 0...5 A	1	1	
521 546	DC Power Supply 0...16 V/0...5 A	1	1	2
524 005W	Mobile-CASSY 2 WiFi	1	1	1
524 220	CASSY Lab 2	1	1	1
524 438	Voltage sensor M, ±30 V	1	1	1
524 0381	Combi B sensor S	1	1	
501 11	Extension cable, 15 pin	1	1	
300 02	Stand base, V-shaped, small	1	1	1
300 41	Stand rod, 25 cm, 12 mm Ø	1	1	
301 01	Leybold multiclamp	1	1	
500 442	Connecting lead 19 A, 100 cm, blue	1	1	
501 46	Connecting leads 19 A, 100 cm, red/blue, pair	6	6	4
586 852	P-doped germanium on plug-in board		1	
586 851	Undoped germanium on plug-in board			1
	additionally required: PC with Windows XP/Vista/7/8/10 (x86 or x64)	1	1	1

The experiments P7.2.1.3 and P7.2.1.4 explore the temperature-dependency of the Hall voltage and the electrical conductivity

$$\sigma = e \cdot \left(p \cdot \mu_p + n \cdot \mu_n \right)$$

using doped germanium samples. The concentrations of the charge carriers and their mobilities are determined under the assuption that, depending on the doping, one of the concentrations n or p can be ignored.

In the experiment P7.2.1.5, the electrical conductivity of undoped germanium is measured as a function of the temperature to provide a comparison. The measurement data permits determination of the band gap between the valence band and the conduction band in germanium.
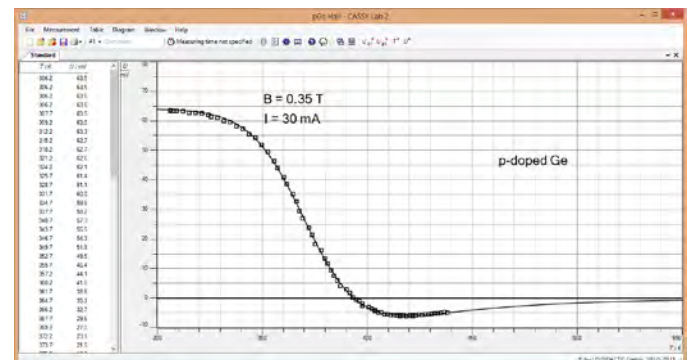
Hall voltage when heating up the p-Ge sample (P7.2.1.4)

ELECTRICAL CONDUCTIVITY IN SOLIDS

P7.2.2.1
Measuring the temperature-dependency of a noble-metal resistor

P7.2.2.2
Measuring the temperature-dependency of a semiconductor resistor
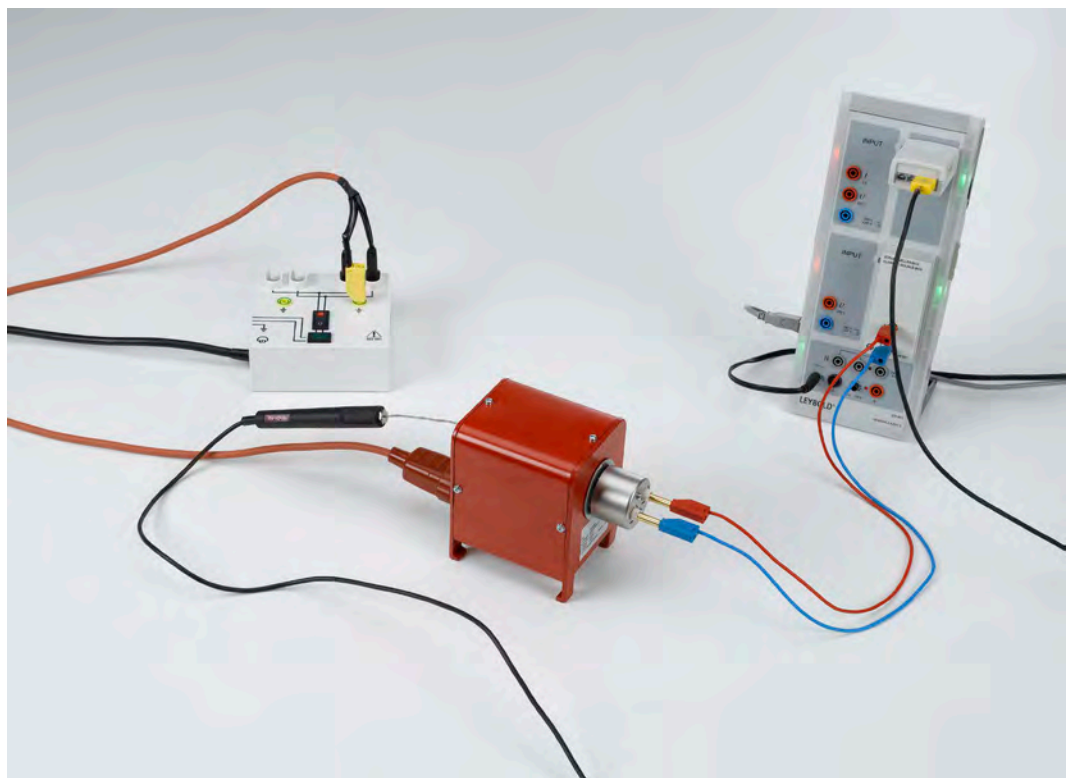
Measuring the temperature-dependency of a noble-metal resistor (P7.2.2.1)

Cat. No.	Description	P7.2.2.1	P7.2.2.2
586 80	Noble metal resistor	1	
555 81	Electric oven for tubes, 230 V	1	1
524 013	Sensor-CASSY 2	1	1
524 220	CASSY Lab 2	1	1
524 0673	NiCr-Ni adapter S, type K	1	1
529 676	Temperature probe, NiCr-Ni, 1.5 mm, type K	1	1
524 031	Current source box	1	1
502 061	Safety connecting box, with earth	1	1
500 614	Safety connecting lead, 25 cm, black	1	1
500 621	Safety connecting lead 50 cm, red	1	1
500 622	Safety connecting lead 50 cm, blue	1	1
586 821	Semiconductor resistor, 5 kΩ		1
	additionally required: PC with Windows XP/Vista/7/8/10 (x86 or x64)	1	1

The temperature-dependency of the specific resistance ρ is a simple test for models of electric conductivity of conductors and semiconductors. In electrical conductors, ρ increases with the temperature, as the collisions of the quasi-free electrons from the conduction band with the atoms of the conductor play an increasingly important role. In semiconductors, on the other hand, the specific resistance decreases as the temperature increases, as more and more electrons move from the valence band to the conduction band, thus contributing to the conductivity.

The experiments P7.2.2.1 and P7.2.2.2 measure the resistance values as a function of temperature using a Wheatstone bridge. The computer-assisted CASSY measured-value recording system is ideal for recording and evaluating the measurements. For the noble metal resistor, the relationship

$$R = R_\Theta \cdot \frac{T}{\Theta}$$

Θ = 240 K: *Debye* temperature of platinum

is verified with sufficient accuracy in the temperature range under study. For the semiconductor resistor, the evaluation reveals a dependency with the form

$$R \propto e^{\frac{\Delta E}{2kT}}$$

$$k = 1.38 \cdot 10^{-23} \frac{J}{K} : Boltzmann \text{ constant}$$

with the band spacing E = 0.5 eV.
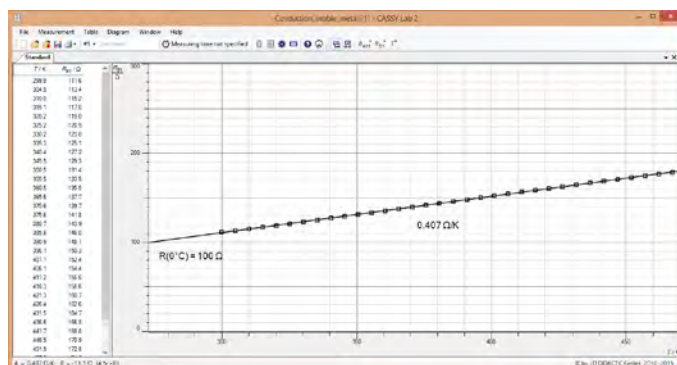
Resistance against temperature (P7.2.2.1)

CASSY®

Recording the current-voltage characteristics of a CdS photoresistor (P7.2.3.1)

PHOTOCONDUCTIVITY

P7.2.3.1
Recording the current-voltage characteristics of a CdS photoresistor
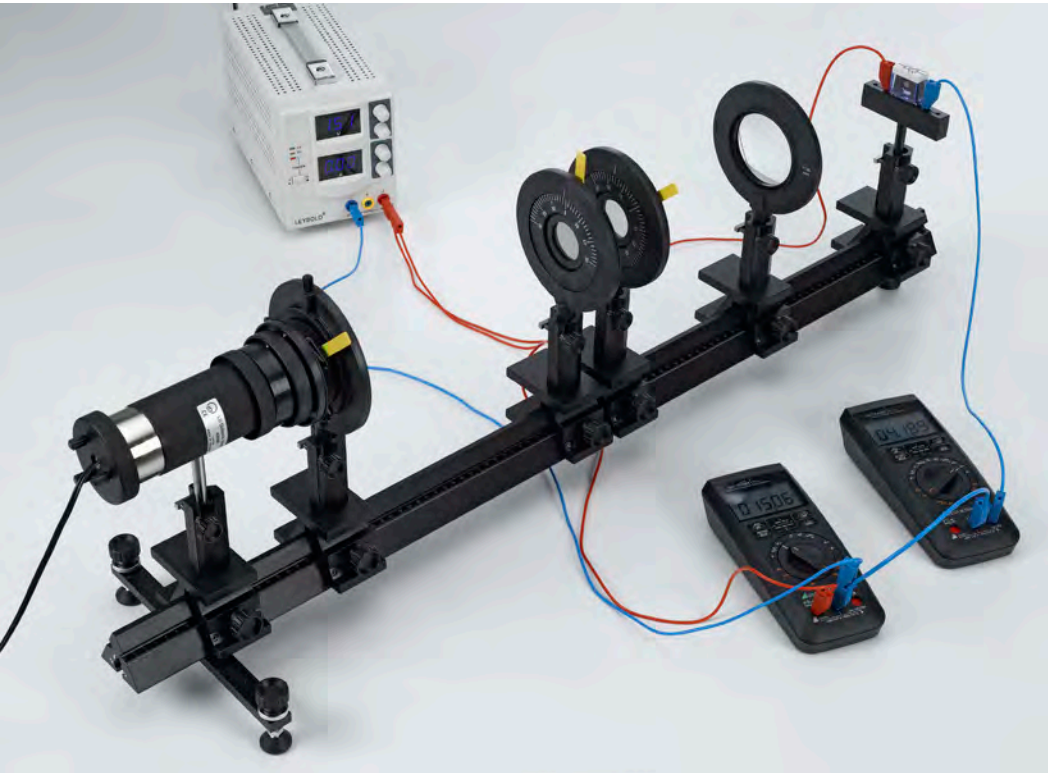
Cat. No.	Description	P7.2.3.1
578 02	Photoresistor LDR 05, STE 2/19	1
450 511	Bulbs, 6 V/30 W, E14, set of 2	1
450 60	Lamp housing with cable	1
460 20	Condenser with diaphragm holder	1
460 14	Adjustable slit	1
472 401	Polarisation filter	2
460 08	Lens in frame, f=150 mm	1
460 32	Optical bench with standardised profile, 1 m	1
460 374	Optics rider, 90/50	6
460 21	Holder for plug-in elements	1
521 546	DC Power Supply 0...16 V/0...5 A	1
521 210	Transformer 6/12 V	1
531 282	Multimeter Metrahit Pro	1
531 303	Multimeter Metrahit X-tra	1
500 422	Connecting lead 19 A, 50 cm, blue	1
501 46	Connecting leads 19 A, 100 cm, red/blue, pair	2

Photoconductivity is the phenomenon in which the electrical conductivity σ of a solid is increased through the absorption of light. In CdS, for example, the absorbed energy enables the transition of activator electrons to the conduction band and the reversal of the charges of traps, with the formation of electron holes in the valence band. When a voltage U is applied, a photocurrent I_{ph} flows.

The object of the experiment P7.2.3.1 is to determine the relationship between the photocurrent I_{ph} and the voltage U at a constant radiant flux Φ_e as well as between the photocurrent I_{ph} and the radiant flux Φ_e at a constant voltage U in the CdS photoresistor.

LUMINESCENCE

P7.2.4.1
Exciting luminescence through irraditaion with ultraviolet light and electrons

Exciting luminescence through irraditaion with ultraviolet light and electrons (P7.2.4.1)

Cat. No.	Description	P7.2.4.1
555 618	Luminescence tube	1
555 600	Tube stand	1
521 70	High-voltage power supply, 10 kV	1
451 15	High pressure mercury lamp	1
451 195	Power supply unit for high-pressure mercury lamp	1
469 79	Filter, ultra-violet	1
500 611	Safety connecting lead, 25 cm, red	1
500 621	Safety connecting lead 50 cm, red	1
500 641	Safety connecting lead, 100 cm, red	1
500 642	Safety connecting lead, 100 cm, blue	1
500 644	Safety connecting lead, 100 cm, black	2

Luminescence is the emission of light following the absorption of energy. This energy can be transmitted in the form of e.g. high-energy electrons or photons which have an energy greater than that of the emitted photons. Depending on the type of decay, we distinguish between fluorescence and phosphorescence. In fluorescence, the emission of photons fades exponentially very rapidly when excitation is switched off (i.e. about 10^{-8} s). Phosphorescence, on the other hand, can persist for several hours.

In the experiment P7.2.4.1, the luminescence of various solids following irradiation with ultraviolet light or electrons is demonstrated. These samples include yttrium vanadate doped with europium (red fluorescent), zinc silicate doped with manganese (green fluorescent) and barium magnesium aluminate doped with europium (blue fluorescent).

Note: It is possible to recognize individual emission lines within the band spectrum using a spectrometer.

Exciting luminescence through irraditaion with ultraviolet light and electrons (P7.2.4.1)

Seebeck effect: Determining the thermoelectric voltage as a function of the temperature differential (P7.2.5.1)

Cat. No.	Description	P7.2.5.1
557 01	Thermocouples, set	1
590 011	Clamping plug	2
524 005W	Mobile-CASSY 2 WiFi	1
524 0401	µV sensor S	1
382 34	Thermometer, -10...+110 °C/0.2 K	1
666 767	Hotplate, 1500 W, 180 mm Ø	1
664 104	Beaker, DURAN, 400 ml, squat	1

When two metal wires with different Fermi energies E_F touch, electrons move from one to the other. The metal with the lower electronic work function W_A emits electrons and becomes positive. The transfer does not stop until the contact voltage

$$U = \frac{W_{A,1} - W_{A,2}}{e}$$

e: elementary charge

is reached. If the wires are brought together in such a way that they touch at both ends, and if the two contact points have a temperature differential $T = T_1 - T_2$, an electrical potential, the thermoelectric voltage

$$U_T = U(T_1) - U(T_2)$$

is generated. Here, the differential thermoelectric voltage

$$\alpha = \frac{dU_T}{dT}$$

depends on the combination of the two metals.

In the experiment P7.2.5.1, the thermoelectric voltage U_T is measured as a function of the temperature differential T between the two contact points for thermocouples with the combinations iron/constantan, copper/constantan and chrome-nickel/constantan. One contact point is continuously maintained at room temperature, while the other is heated in a water bath. The differential thermoelectric voltage is determined by applying a best-fit straight line

$$U_T = \alpha \cdot T$$

to the measured values.
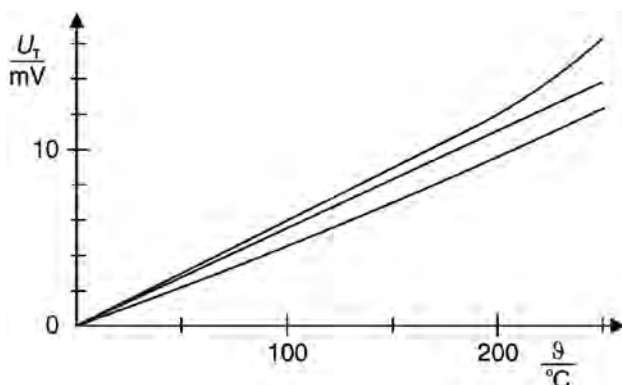
Thermoelectric voltage as a function of the temperature Top: chrome-nickel/constantan, Middle: iron/constantan, Bottom: cupper/constantan (P7.2.5.1)

SUPERCONDUCTIVITY

P7.2.6.1
Determining the transition temperature of a high-temperature superconductor

P7.2.6.2
Meissner-Ochsenfeld effect for a high-temperature superconductor
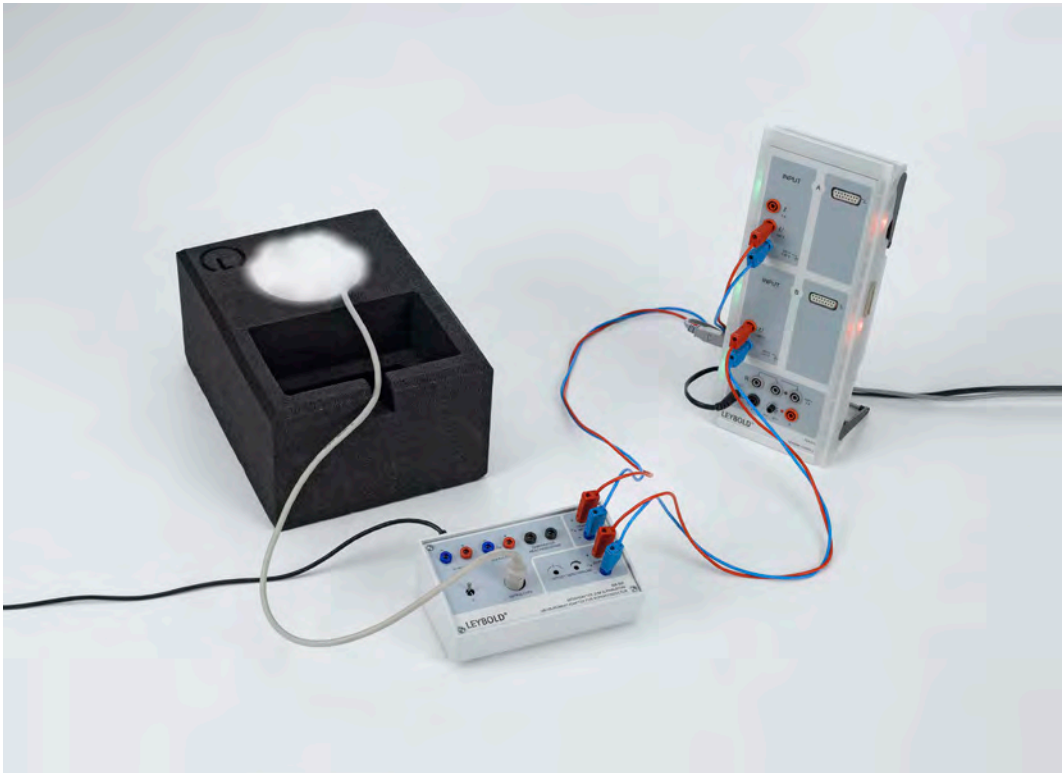
Determining the transition temperature of a high-temperature superconductor (P7.2.6.1)

Cat. No.	Description	P7.2.6.1	P7.2.6.2
667 553	Experiment kit Superconductor	1	
524 013	Sensor-CASSY 2	1	
524 220	CASSY Lab 2	1	
501 45	Connecting lead 19 A, 50 cm, red/blue, pair	2	
667 551	Meissner-Ochsenfeld effect, experiment kit		1
	additionally required: PC with Windows XP/Vista/7/8/10 (x86 or x64)	1	

In 1986, *K. A. Müller* and *J. G. Bednorz* succeeded in demonstrating that the compound $YBa_2Cu_3O_7$ becomes superconducting at temperatures far greater than any known up to that time. Since then, many high-temperature super-conductors have been found which can be cooled to their transition temperature using liquid nitrogen. Like all superconductors, high-temperature superconductors have no electrical resistance and demonstrate the phenomenon known as the Meissner-Ochsenfeld effect, in which magnetic fields are displaced out of the superconducting body.

The experiment P7.2.6.1 determines the transition temperature of the high-temperature superconductor $YBa_2Cu_3O_{7-x}$. For this purpose, the substance is cooled to below its critical temperature of $T_c = 92$ K using liquid nitrogen. In a four-point measurement setup, the voltage drop across the sample is measured as a function of the sample temperature using the computer-assisted measured value recording system CASSY.

In the experiment P7.2.6.2, the superconductivity of the $YBa_2Cu_3O_{7-x}$ body is verified with the aid of the Meissner-Ochsenfeld effect. A low-weight, high field-strength magnet placed on top of the sample begins to hover when the sample is cooled to below its critical temperature so that it becomes super-conducting and displaces the magnetic field of the permanent magnet.
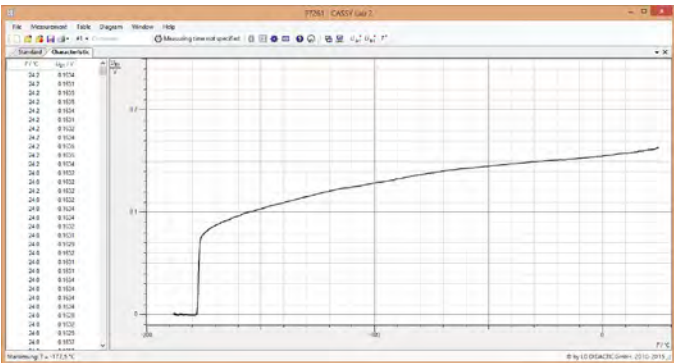
Determining the transition temperature of a high-temperature superconductor (P7.2.6.1)
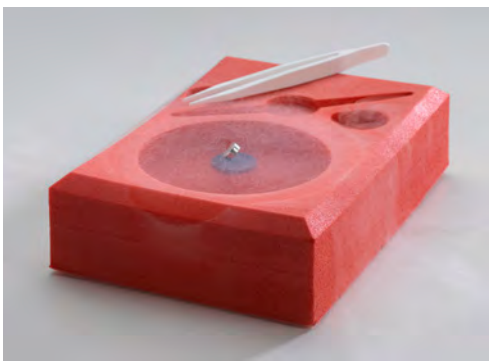
Meissner-Ochsenfeld effect for a high-temperature superconductor (P7.2.6.2)

CASSY®

WWW.LD-DIDACTIC.COM

Dia-, para- and ferromagnetic materials in an inhomogeneous magnetic field (P7.3.1.1)

DIA-, PARA- AND FERROMAGNETISM

P7.3.1.1
Dia-, para- and ferromagnetic materials in an inhomogeneous magnetic field

Cat. No.	Description	P7.3.1.1
560 41	Set of rods for para- and diamagnetism	1
562 11	U-core with yoke	1
562 13	Coil, 250 turns	2
560 31	Bored pole pieces, pair	1
521 391	AC/DC power supply 0...24 V/5 A	1
300 02	Stand base, V-shaped, small	1
300 41	Stand rod, 25 cm, 12 mm Ø	2
301 01	Leybold multiclamp	1
500 422	Connecting lead 19 A, 50 cm, blue	1
501 46	Connecting leads 19 A, 100 cm, red/blue, pair	1

Diamagnetism is the phenomenon in which an external magnetic field causes magnetization in a substance which is opposed to the applied magnetic field in accordance with Lenz's law. Thus, in an inhomogeneous magnetic field, a force acts on diamagnetic substances in the direction of decreasing magnetic field strength. Paramagnetic materials have permanent magnetic moments which are aligned by an external magnetic field. Magnetization occurs in the direction of the external field, so that these substances are attracted in the direction of increasing magnetic field strength. Ferromagnetic substances in magnetic fields assume a very high magnetization which is orders of magnitude greater than that of paramagnetic substances.

In the experiment P7.3.1.1, three 9 mm long rods with different magnetic behaviors are suspended in a strongly inhomogeneous magnetic field so that they can easily rotate, allowing them to be attracted or repelled by the magnetic field depending on their respective magnetic property.
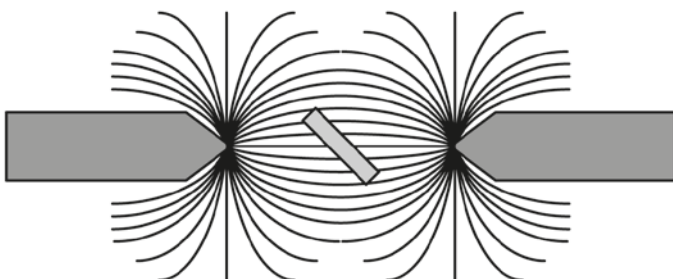
Placement of a sample in the magnetic field (P7.3.1.1)

FERROMAGNETIC HYSTERESIS

P7.3.2.1
Recording the initial magnetization curve and the hysteresis curve of a ferromagnet and iron

Recording the initial magnetization curve and the hysteresis curve of a ferromagnet and iron (P7.3.2.1)

Cat. No.	Description	P7.3.2.1
562 11	U-core with yoke	1
562 115	U-core with yoke, iron	1
562 121	Clamping device with spring clip	1
562 14	Coil, 500 turns	2
522 621	Function generator S 12	1
524 013	Sensor-CASSY 2	1
524 220	CASSY Lab 2	1
577 20	Resistor, 10 Ω, STE 2/19	1
576 81	Plug-in board safety socket, 20/10	1
500 624	Safety connecting lead 50 cm, black	1
500 644	Safety connecting lead, 100 cm, black	7
	additionally required: PC with Windows XP/Vista/7/8/10 (x86 or x64)	1

In a ferromagnet, the magnetic induction

$$B = \mu_r \cdot \mu_0 \cdot H$$

$$\mu_0 = 4\pi \cdot 10^{-7} \frac{Vs}{Am}: \text{ magnetic field constant}$$

reaches a saturation value B_s as the magnetic field H increases. The relative permiability μ_r of the ferromagnet depends on the magnetic field strength H, and also on the previous magnetic treatment of the ferromagnet. Thus, it is common to represent the magnetic induction B in the form of a hysteresis curve as a function of the rising and falling field strength H. The hysteresis curve differs from the magnetization curve, which begins at the origin of the coordinate system and can only be measured for completely demagnetized material.

In the experiment P7.3.2.1, a current I_1 in the primary coil of a transformer which increases (or decreases) linearly over time generates the magnetic field strength

$$H = \frac{N_1}{L} \cdot I_1$$

L: effective length of iron core

N_1: number of windings of primary coil

The corresponding magnetic induction value B is obtained through integration of the voltage U_2 induced in the secondary coil of a transformer:

$$B = \frac{1}{N_2 \cdot A} \cdot \int U_2 \cdot dt$$

A: cross-section of iron core

N_2: number of windings of secondary coil

The computer-assisted measurement system CASSY is used to control the current and to record and evaluate the measured values. The aim of the experiment is to determine the relative permeability μ_r in the magnetization curve and the hysteresis curve as a function of the magnetic field strength H.
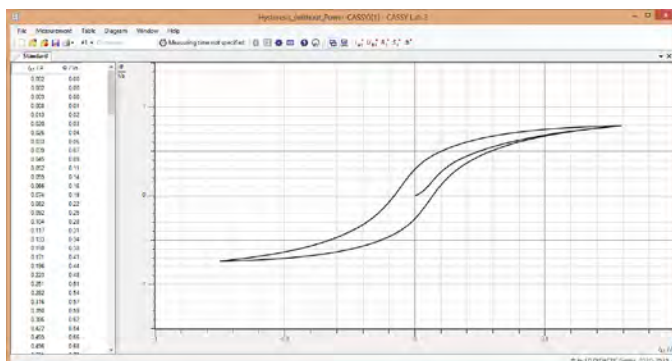
Magnetic flux in the iron core against the coil current (P7.3.2.1)

CASSY®

Application of X-ray fluorescence for the non-destructive analysis of the chemical composition (P7.5.1.1)

X–RAY FLUORESCENCE ANALYSIS

P7.5.1.1
Application of X-ray fluorescence for the non-destructive analysis of the chemical composition

P7.5.1.2
Determination of the chemical composition of a brass sample by X-ray fluorescence analysis

Cat. No.	Description	P7.5.1.1	P7.5.1.2
554 800	X-ray apparatus	1	1
554 861	X-ray tube, Mo	1	1
554 831	Goniometer	1	1
559 938	X-ray energy detector	1	1
554 848	Set of target alloys	1	1
524 013	Sensor-CASSY 2	1	1
524 220	CASSY Lab 2	1	1
524 058	MCA box	1	1
501 02	BNC cable, 1 m	1	1
554 844	Set of targets for K-line fluorescence		1
554 846	Set of targets for L-line fluorescence		1
	additionally required: PC with Windows XP/Vista/7/8/10 (x86 or x64)	1	1

X-ray fluorescence is a very useful tool for a non-destructive analysis of the chemical composition of a target alloy. When irradiating a sample with X-rays, all the different elements it contains emit characteristic X-rays due to fluorescence, which are fingerprints of every single element.

In the experiment P7.5.1.1, X-ray fluorescence is used to do qualitative analysis by identifying the substances in four alloy samples, made from chrome–nickel steel, two different kinds of brass and rare earth magnet.

In the experiment P7.5.1.2, the composition of one brass alloy is analysed quantitatively. The weight percentage of each component in the alloy is calculated from the strength of different fluorescence lines.
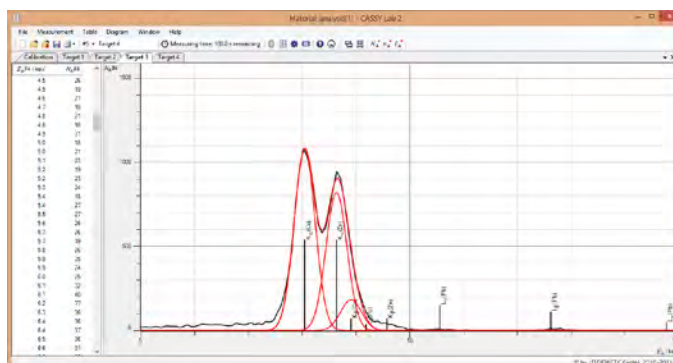
X-Ray fluorescence spectrum of a brass sample (P7.5.1.2)

CASSY®

P7.2.6.1
Determining the transition temperature of a high-temperature superconductor

For more information on this experiment, go to page 242.

P8 REGISTER

α, β, γ

3

A

B

C

D

M

N

O

P

P3.4.6.2
Measuring the earth's
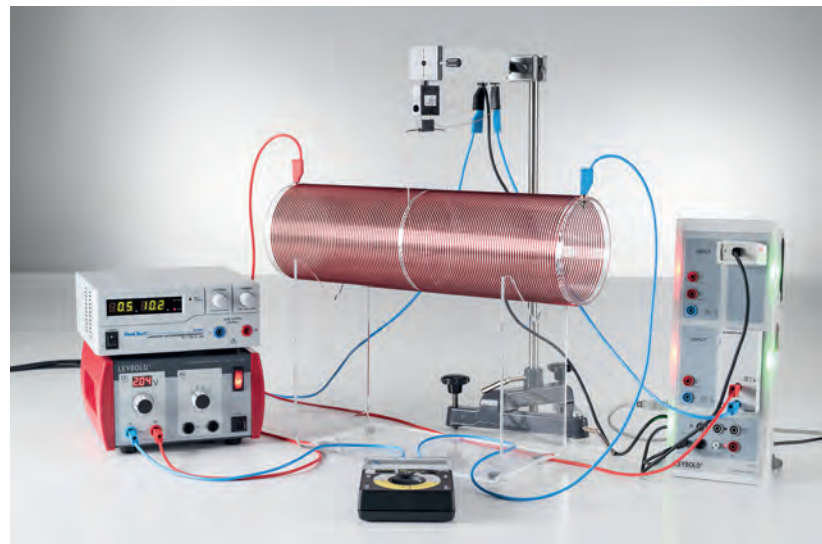magnetic field with
a rotating induction
coil and CASSY

CONTACT

GERMANY:

LD DIDACTIC GmbH
Leyboldstr. 1
50354 Huerth
Germany
Tel.: +49 2233 604 0
Fax: +49 2233 604 222
E-Mail: info@ld-didactic.de
www.ld-didactic.com

WWW.LD-DIDACTIC.COM

BRANDS OF THE LD DIDACTIC GROUP

LEYBOLD®   Feedback   ELWE® TECHNIK